SIMULTANEOUS HEAT AND MASS TRANSPORT WITH PHASE CHANGE IN INSULATED STRUCTURES

by

SHAHRYAR MOTAKEF

S.M. in Mechanical Engineering
Massachusetts Institute of Technology (1980)

S.B. in Mechanical Engineering
Massachusetts Institute of Technology (1978)

SUBMITTED TO THE DEPARTMENT OF MECHANICAL ENGINEERING
IN PARTIAL FULFILLMENT OF THE REQUIREMENTS
FOR THE DEGREE OF

DOCTOR OF PHILOSOPHY IN
MECHANICAL ENGINEERING

at the

MASSACHUSETTS INSTITUTE OF TECHNOLOGY

May 18, 1984

Signature of Author _____
Department of Mechanical Engineering
May 18, 1984

Certified by _____
Maher A. El-Masri
Thesis Supervisor

Accepted by _____
Warren M. Rohsenow
Chairman, Departmental Graduate Committee

SIMULTANEOUS HEAT AND MASS TRANSPORT WITH PHASE CHANGE IN INSULATED STRUCTURES

BY

SHAHRYAR MOTAKEF

Submitted to the Department of Mechanical Engineering on May 18, 1984 in partial fulfillment of the requirements for the degree of Doctor of Philosophy in Mechanical Engineering.

ABSTRACT

Simultaneous transport of heat and mass with phase change is of practical importance in applications such as the design of energy-efficient buildings.

An analytical model for the simultaneous transport of heat and mass with phase change in a porous slab subject to temperature and vapor-concentration differentials is developed. Closed-form solutions for temperature and concentration profiles are obtained by linearizing the governing differential equation in the two-phase zone. Those are matched to the imposed boundary conditions yielding complete solutions for two regimes; that where the liquid is mobile and the limiting case of pendular condensate. The analytical results are obtained for the cases of steady-state condensation, and quasi-steady transients associated with step changes in the boundary-conditions. The analytical solution compares favorably with the numerical results.

Liquid diffusion in fiberglass insulation was studied experimentally. The medium-properties which control liquid-diffusion in fibrous media are found to be fiber-radius, directional fiber-density, macroscopic void-fraction, tortuosity factor, orientation of the medium with respect to gravity, and the spatial-distribution of the void-fraction. The experimental results are found to agree satisfactorily with the model predictions.

Moisture migration and condensation in a typical wall-construction is investigated. It is found that the condensation rate depends on the climatic conditions, air-infiltration rates, and the location of the vapor-barrier, as well as the thermal and diffusive properties of the materials used in the wall-construction. Worst case scenarios indicate that in improperly designed wall structures moisture condensed during the cold-season may not evaporate completely during the warm-season. This will result in irreversible damage to the building shell.

Thesis Supervisor : Professor M. A. El-Masri

Thesis Committee Members: Professor W. M. Rohsenow
Professor B. B. Mikic
Professor S. Backer
Professor M.P. Cleary

To My Parents,

To Whom I Owe The Essential

ACKNOWLEDGMENTS

Praise be to the Lord who endowed me with the circumstances to begin and end this work.

The work presented in this manuscript was initiated by Professor El-Masri. Throughout the period of this research I have had the immense pleasure of working closely with him. I have greatly benefited, in more than one way, from this collaboration and would like to express to my deepest gratitudes.

My association with Professor W. M. Rohsenow both during this research and my tenure as his Teaching Assistant has significantly broadened my understanding of heat transfer. His suggestions and assistance are sincerely appreciated.

The intellectual acuteness of Professor B. B. Mikic was always the litmus test for any new ideas. I am thankful to him for his assistance.

The assistance of Professors S. Backer and M. P. Cleary is also appreciated.

I am greatly indebted to Professor H. M. Paynter who many years ago helped me develop my intellectual carreer. He has always been a source of intellectual stimulus and refreshing conversations.

I am also thankful to the students in the Heat Transfer Laboratory for the fruitful and joyful conversations I have had with them.

r

During the course of this work I have often failed to attend fully to my family and loved one. I am greatful to their patience and moral support.

This work was supported, in part, through funds supplied by M.I.T. and Owens-Corning Corporation to the Center for Energy Efficient Buildings and Systems. I wish to express my gratitude to the support of the Center.

TABLE OF CONTENTS

LIST OF FIGURES

NOMENCLATURE

Latin

C	Vapor concentration
C*	Saturation vapor concentration
D	Diffusivity
F	Cumulative frequency distribution
f	Frequency density distribution
Fo'	Fourier Number = $D_v L_w^2/t$
Fo''	Fourier Number = $D_l L_w^2/t$
Fo*	Fourier Number = $D_v L_T^2/t$
Fo**	Fourier Number = $D_l L_T^2/t$
g_1	Function defined in eq. [5.4.14]
g_2	Function defined in eq. [5.4.15]
h	Thickness of a layer in the fiberglass insulation
h_{fg}	Latent heat of condensation
h_{fs}	Latent heat of solidification
J	Flux
k	Thermal conductivity
k*	Permeability
L	Length
L_{ij}	Interaction coefficient
L_0	Distance of the closer boundary of the condensation-region from the hot reservoir
L_1	Distance of the farthest boundary of the condensation-region from the hot reservoir
L_T	Total length of the slab

L_w	Width of the condensation-region
Le	Lewis number
M	Ratio of vapor-diffusivity to liquid-diffusivity = D_v/D_l
n_i/N	Directional fiber density
N	Total number of fibers of unit length per unit volume
P	Pressure
Pe	Peclet number
(q/A)	Heat flux per unit area
r	Radial Coordinate
r_d	Hydraulic radius
r_f	Fiber radius
r_s	Equivalent suction-radius
r*	Equivalent diffusion-radius
S	Term defined in eq. [5.3.2.20]
t	Time
T	Temperature
T*	Temperature in the Condensation-region
u	Velocity
u_i	Boundary condition variable, eq. [2.5.15]
U	Velocity
(W/A)	Condensation rate per unit area
x	Length-scale in condensation-region
z	Length-scale in the slab

Greek

α	Liquid diffusivity

α	Ratio of two liquid-fluxes, eq. [2.4.42]
β	$\Delta T/T_r$
γ	h_{fg}/RT_r
γ	Contact angle
ϵ	Void fraction
ϵ_i	Directional void fraction
ϵ_T	Macroscopic void fraction
ζ	Non-dimensional distance
ξ	Non-dimensional distance
η	Dimensionless temperature
θ	Liquid-content
θ	Critical liquid-content
χ'	Latent heat transport coefficient
μ	Viscosity
ν	Kinematic viscosity
ρ	Density
ρ_e	Electric resistivity
σ	Surface tension
τ_i	Tortuousity factor
τ	Correction factor, eq. [2.5.14]
Γ	Condensation rate per unit volume
Λ	Ratio of two condensation rates, eq. [4.4.2]
Ψ	Stream function
Ω	Kossovitch number, eq. [2.3.12]
Φ	A variable, eq. [2.3.20]

Subscripts

c	Cold
h	Hot
f	Fluid
g	Gas
l	Liquid
s	Steady-state
t	Transient
v	Vapor
0	Variable associated with L_0
1	Variable associated with L_1

Superscripts

*	Variable evaluated in the condensation-region
—	Mean value
'	Variable associated with the condensation-region

There is no text material missing here.
Pages have been incorrectly numbered.

P. 18

CHAPTER 1

INTRODUCTION

In the last decade much attention has been focused on the inevitable decrease in the supply of cheap energy. It has, therefore, become imperative to take measures to reduce energy consumption without declines in the standard of living. In the past ten years many energy conservation schemes have been put into effect and significant savings have materialized. The building industry has been the latest newcomer to the area of energy-conservation. Buildings, especially residential buildings are constructed without any strong commitments to energy-efficiency. About one-third of the energy consumption in this country is used for sapce-heating. A small decrease in every building's energy consumption results in a significant decrease in the national oil-consumption.

Energy loss through the building-shell takes place through different mechanisms. The major mechanisms are air-infiltration and conduction through the walls. With the sources of heat-loss

known, the remedies seem to be clear. Added insulation decreases heat transfer through the walls, and a tighter building construction should decrease the air-infiltration paths. However, in existing structures the infiltration paths cannot be easily discovered, and even when discovered cannot be easily obstructed. On the other hand, insulation may be added to the building-shell at minimal cost. In the next generation of building structures, both infiltration and conduction problem may be overcome by such novel designs as earth-sheltered buildings. However, these novel designs must, before all else, overcome the psychological barriers in order to penterate the market place. This may not turn out to be any easy task, barring an explosive increase in the price of oil. The future trend in the construction of the enegy-efficient buildings seems to lie in product development and improvements in construction workmanship.

One of the major problems associated with energy-efficient buildings is vapor-condensation in the building-shell. This increases with increasing levels of humidity. Therefore, with the air-infiltration paths obstructed, the level of humidity in the building may increase to undesireable levels. Furthermore, in well insulated structures, a significant portion of the overall temperature drop occurs across the insulation. It will be shown that this increases the possibility of condensation in the insulation. Thus, in a well insulated and tight building the possibility of condensation in the building-shell is much more pronounced than in conventional buildings.

The condensation of vapor in building-shells is a multi-dimensional problem [1,2]. Its existence is undesireable primarily for three reasons:

- Condensation of moisture in building walls and its subsequent freezing constitutes a deteriorating factor in the materials' strength and service-life.

- Presence of moisture promotes certain chemical reactions which enhance the deterioration of building materials. Decay of wood, corrosion of metals (e.g. pipes, concrete reinforcements, etc.), and efflorescence on the masonary are examples of the harmful chemcial reactions promoted by the presence of condensed moisture [4,5].

-Studies of seasonal fuel utilization efficiency of residential heating systems reveal that excess capacity is a source of inefficiency [6,7,8]. Optimal sizing of appliances requires a better knowledge of heat loss characteristics of the building structure. There are two factors associated with the heat losses from building-shells as a result of vapor-condensation:

(i) The thermal conductivity of the building materials increases with increasing moisture-content. It is most likely that condensation occurs in the insulation, which is the most thermally-resistive element of a wall structure. The decrease in the thermal resistance of the insulation translates into higher rates of energy loss.

(ii) In most instances the water-vapor inside the building has been formed by the addition of heat to liquid-water. The high enthalpic vapor leaves the building and condenses within the wall strucutre, eventually releasing its enthalpy of phase-change to the outside ambient. As the level of vapor-concentration in the building is maintained above a certain level, energy must be consumed to convert liquid into water-vapor. This energy consumption is associated with condensation of vapor in the wall structure. It will be shown in this work, that the amount of energy lost in the

form of latent heat is of the same order of magnitude as the heat-loss by conduction through the wall.

Moisture is transported through the building shell by two mechanisms: air-infiltration and moisture-diffusion. Air-infiltration occurs in response to a pressure difference across the building walls. It has been observed that under adverse conditions condensation due to air-infiltration is many times larger than the amount of condensation caused by moisture diffusion [10]. Natural convection in porous materials has been investigated by some authors [11-15]. Attention is mainly focused on closed-form solutions with various boundary conditions. Burns et al. have investigated the effect of air-infiltration on natural convection heat transfer [15]. They model air leakage in the strucutre as discrete mass injections and removal at different positions on the boundary of natural convection cell. This investigation reveals that leakage due to cracks is capable of enhancing free convection, and hence, the total heat transfer across the wall. The effect of outside air-pressure and neighboring body effects on air-infiltration is studied in [16]. The results show that depending on the particular two body configuration a neighboring building can have a favorable or adverse effect on the infiltration rates. Relatively little information can be found in the literature regarding actual pressure-difference across the walls of buildings and their leakage characteristics. References [17-21] discuss different aspects of the problem. Model studies using bluff bodies in wind tunnels are reported in [22-24]. The effect of air-infiltration on moisture-transport and condensation in porous insulation is included in the model developed by Ogniewicz and Tien [25]. Their steady-state model incorporates the effect of infiltration through the dependence of the solution on the Peclet number. This study will be discussed in greater length later. Overall, much work needs to be done in this area in order to completely formulate and quantify the effects of infiltration

on heat losses through building-shells.

Moisture diffusion under non-isothermal conditions is controlled by the simultaneous flow of heat and water-vapor. Luikov [26] has extensively investigated the theory of simultaneous heat and mass transfer in capillary-porous materials. The general approach is to relate the flux of heat and mass to the coupled interaction of heat nad mass potentials. The phenomenon of coupled diffusion in capillary-porous materials is controlled by a system of three differential equations, where the three dependent variables are mass content, temperature and pressure [27]. The form of the system of equations is simplified by applying Onsager's reciprocal relations [28]. The solution of the system of equations depends on nine interaction coefficents. However, due to the symmetry of the equations and according to Onsager's relationship, only six interaction coefficients have to be measured empirically and related to the properties of the capillary-porous body.

The theory of simultaneous heat and mass diffusion is extensively applied to the science of soil-mechanics [29-37]. In the study of mositure and heat diffusion in soils, the pressure field may be considered to be uniform and ,hence, the system is reduced to two differential equations in terms of temperature and moisture-content fields [38]. The symmteric interaction coefficents have experimentally been found to be identical, in accordance with Onsager's postulate [29]. A fundamental contribution to the study of mositure and heat transfer in soils is made by Edlefsen and Anderson through a thermodynamic study of soil moisture [39]. Different approaches to the solution of the set of equations, with varying degrees of complexity, are reported in the literature [40-43]. Heat and mass transfer in capillary-porous bodies with evaporation/condensation [44-47], and thawing/freezing [48-52] have also been investigated. Heat and mass transfer in concrete has been the subject of exhaustive research. References [53,54] give an excellent report of the

theory and experimental evidence. Other studies of the subject can be found in [55-59].

Most studies in heat and mass transfer focus on hygroscopic liquid-contents. As the equations describing the phenomenon are complex, the solutions obtained are valid for a very restricted class of problems. Furthermore, as moisture-removal is a very energy-intensive technology, most studies are performed for drying-processes [60-62].

Water-vapor condensation within porous wall-insulations has been observed particularly when the temperature difference across the wall is large and the environment humid [63,64]. Vapor-barriers are theoretically capable of inhibiting the migration of vapor. However, cracks and holes, caused by faulty installation and aging, decrease the effectiveness of the barriers significantly. It has been obseved that for a .036% ratio of total hole area to barrier area the diffusive resistance of aluminium-sheet and PVC-foil decrease by 92% and 80%, respectively [65].

Internal condensation in structures has been investigated mostly by experimental observations. Wilson has experimentally studied the migration of moisture toward the inside of buildings in summer, and its subsequent condensation in the insulation [66]. Permyakov and Telegerion have qualitatively studied the main factors governing the moisture-state of buildings for different construction schemes and choice of materials [67]. These studies fail to provide any definite conclusions.

There have been few quantitative investigations of condensation in building structures [68-71]. Vos has studied condensation in roofs extensively. His model is one of the few that consider the mobility of the condensate in the medium. He hypothesizes a simple form of diffusivity for hygroscopic liquid-contents. His analytical results agree well with the

experimental findings.

Ogniewicz and Tien [25] have studied a steady-state one dimensional formulation of condensation in porous insulation. Their analytical model is one of the better formulations avialable in the literature. Their formulation has one serious draw-back, in the sense that it does not consider the diffusion of the condensate in the medium. In this work, the solution of the resulting equations is obtained numerically. Hence, the results cannot be generalized and only serve to show the parametric dependence of the width and location of the condensation region and the condensation rate on such parameters as the Peclet number and Biot number.

This work has three definitive objectives:

1- To develop a complete and comprehensive analytical model for simultaneous transport of vapor, liquid, and heat in one-dimensional porous media.

2- As the majority of building insulation used in this country is of fiberglass, to conduct a study of liquid-diffusion in the fiberglass insulation.

3- Study heat and mass transport in composite walls, and investigate the implications of the results to building-design.

This study is divided into eight chapters. Chapters 2-4 are devoted to the analytical study of simultaneous heat and mass transport in a porous slab. Case studies and illustrative examples are presented in some sections to underline the critical conclusions. The case studies are chosen so as to represent realistic and encounterable situations. Chapters 5 and 6 explain

the experimental investigation and modelling of liquid-diffusion in fibrous media. Chapter 7 is the synthesis of the analytical results with the experimental observations. Condensation associated with two different climatic conditions in a composite slab similar to a typical wall strucutre is investigated in chapter 7.

CHAPTER 2

HEAT AND MASS TRANSFER WITH PHASE CHANGE IN A POROUS SLAB: SPATIALLY - STEADY SOLUTIONS

2.1 INTRODUCTION

The simultaneous transport of heat and mass in porous media is an important phenomenon in many natural and industrial processes. A brief literature survey of the analytical and experimental works in this area was given in chapter 1. In this and the next chapter simultaneous transport of heat and mass with phase change in a porous slab is studied. In this chapter the spatially-steady solutions are investigated, whereas in chapter 3 the spatially-unsteady solutions are derived. In chapter 4 the special case of a porous slab with an impermeable boundary is discussed. The approach of this work departs from the tradition of starting with the Luikov equations. The relevant conservation equations are derived from the first principles. However, as the Luikov equations occupy a prominent position in the literature,

they are briefly discussed here. In general the flux of each species is contrtolled by the gradient of all existing potentials. The formulation of the process is complicated by the coupling between the fluxes and the driving potentials. The coupling is further increased when phase change occurs in the medium. This coupling involves the transformation of one transported species into another (e.g. vapor to liquid and vice versa), and the energy released from this process which couples into the the energy equation. A formulation based on the thermodynamics of irreversible processes has received considerable attention in the recent years. Although this formulation is systematic and the resulting equations are symmetric, the solution of the complete set of equations is not available. However, in this section the phenomenon of simultaneous heat and mass transport is studied from an alternate approach. The results obtained by this approach are simpler than the equations based on the thermodynamics of irreversible processes. However, they do retain all the important physical parameters. In this section, a description of the formulation based on the thermodynamics of irreversible processes , and the formulation used in this study will be given. The extensive discussion of the formulation and the solution methodology is given in section 2.2.

The formulation of simultaneous transport of species based on the thermodynamics of irreversible processes is due to Onsager [28]. However, the popularity of the approach is due to Luikov and his Russain co-workers [26,27]. Onsager stated a law which cannot be deduced from the classical laws of thermodynamics. His postulate is discussed here. Consider a set of driving potentials $\dot{P}_i$, i=1,..n, and a set of fluxes J_i, i=1,..n, where each flux is associated with a conjugate potential, such as heat and temperature. Then in a system of potentials the rate of entropy generation is:

$$\dot{S} = \sum_i J_i \dot{P}_i, \qquad [2.1.1]$$

where J_i and P_i are conjugate pairs. The flux of each species is controlled by the gradient of all potentials :

$$J_i = - L_{ij} \dot{P}_j. \qquad [2.1.2]$$

The L_{ij} term is the conductivity of flux i with respect to the potential gradient j. Equation [2.1.2] can be written in vector form:

$$[J] = [L] [\dot{P}] \qquad [2.1.3]$$

where $[J]$ = Vector of fluxes = $[J_1,\ldots,J_n]^T$

$[L]$ = Matrix of conductivities

$[\dot{P}]$ = Vector of Potential gradients = $[\dot{P}_1,\ldots,\dot{P}_n]^T$

Onsager's postulate states that once the flux-potential conjugate pairs are identified such that eq. [2.1.1] is satisfied, the matrix of conductivities, [L], is symmetric:

$$L_{ij} = L_{ji} \qquad i,j = 1,\ldots,n \qquad [2.1.4]$$

In simultaneous heat and mass transfer the following conjugate pair of fluxes and potential gradients are identified:

Potential	FLUX
Pressure	Mass Flux
Temperature	Heat Flux
Vapor-concentration	Vapor Flux
Liquid- Potential	Liquid Flux

The system of equations with the above conjugate pairs has become known as the Luikov equations [27].

The transport equations of the form:

$$J_i = -L_{ij} \dot{P}_j$$

are phenomenological in nature and require a suitable definition of the conductivity term, L_{ij}. In many situations, some of the conductivity terms are negligible. Hence, the system of equations [2.1.3] is greatly simplified. Nevertheless, the physical character of the remaining conductivities must be investigated and established.

In this study the equations describing heat and mass transfer are not written in the form of Luikov equations. Rather, the equations are developed from the basic principles. They are then modified to incorporate additional effects. In this manner, the discussion of the significance of the driving potentials and the coupling terms can be more illuminating. The flux- potential gradient relations used in this study are analogous to the phenomenological statements of eq. [2.1.1]. The difference between this approach and the Luikov formulation lies in the manner of presentation. Whereas in the Luikov formulation all equations are put forward at once, in this study the

equations are developed and studied in such a manner as to reduce the coupling between them.

Although, the transport equations of most species are of the form of eq. [2.1.2], historically, they have been referrred to as laws. They are defined in the following:

LAW	EQUATION	
Fourier	$(\dot{q}/A) = - k\nabla T$	[2.1.5(a)]
D'Arcy	$\vec{u} = -k^{*}\vec{\nabla}P$	[2.1.5(b)]
Fick	$\vec{J}_v = -D_v \vec{\nabla}C$	[2.1.5(c)]

The above terms are all defined in the nomenclature. Fourier's Law relates the flow of heat to the gradients in the temperature field. Vapor diffuses in response to the gradient of vapor-concentration. This is known as the Fick's law. D'Arcy's law relates the flux of a fluid in a porous medium saturated with the fluid to the gradients in the pressure field. D'Arcy's law can be extended to include flow in unsaturated porous media under surface tension forces by the introduction of a term equivalent to pressure, namely liquid potential. Furthermore, as liquid potential is a function of liquid-content, D'Arcy's law can be written as:

$$\vec{J}_l = -D_l(\theta)\,\vec{\nabla}\theta \qquad [2.1.6]$$

where D_l would be a properly defined liquid-diffusivity. The case under study is fully discussed in the next section. The

nature of the species' fluxes, phase change, and the coupling between the equations are discusses there. A solution methodology based on different regimes of liquid diffusivity is presented.

2.2 PROBLEM STATEMENT AND SOLUTION METHODOLOGY

Consider a porous medium which is permeable to the flow of heat, vapor and liquid. The medium seperates two reservoirs, each characterized by a value of temperature and vapor concentration. When the vapor concentration and/or temperature of the two reservoirs are unequal, a flux of vapor and/or heat is set up in the direction antiparallel to the potential gradient. Depending on relative values of the reservoir temperatures to the dew-point of the diffusing vapor, the vapor could undergo phase change and condense into liquid form over some region of the porous medium. It is also possible for the vapor to freeze. The analysis of this chapter is focused on the formation of liquid condensate. In section 2.8, the model will be extended to include the possibility of frost formation.

In Fig. 2.2.1 a situation where both liquid and solid condensate are formed in a porous slab is depicted. The two reservoirs are identified by (T_h, C_h), and (T_c, C_c) where

T_h = Temperature of the hot reservoir

T_c = Temperature of the cold reservoir

C_h = Vapor concentration of the hot reservoir

C_c = Vapor concentration of the cold reservoir,

and

$$T_h > T_c$$

$$C_h > C_c$$

A value of saturation vapor-concentration corresponds to every value of temperature, and is denoted by C^*. Relative humidity is defined as:

$$h_h = C_h/C^*(T=T_h) \leq 1$$

$$h_c = C_c/C^*(T=T_c) \leq 1$$

Heat flows from the "hot" reservoir to the "cold" one according to the Fourier's law. Vapor migration from the hot reservoir to the cold one is defined by Fick's law. At some point in the medium the diffusing vapor reaches its dew point and condenses. Heat released by condensation is conducted out of the condensation-region at steady state. The temperature at which the vapor condenses in the porous medium may be different from its dew-point due to the surface tension effects at the surface of the capillaries. This point is elaborated in the next section. Given that neither of the two reservoirs have a relative humidity value of 100%, the region of condensation is sandwiched between two dry regions.

As condensation occurs liquid drops are formed in the medium, and the fraction of medium voidage occupied by the

condensate increases with time. At some point the condensate begins to flow in response to the gradient in liquid-content potential. The liquid-flux is defined by the following phenomenological transport equation:

$$J_l = -D_l(\theta)\nabla\theta ,$$

where J_l = Liquid-flux vector

θ = Liquid Content = Volume of liquid/Void volume

$D_l(\theta)$ = Liquid diffusivity

The functionmal dependence of liquid diffusivity, $D_l(\theta)$, on liquid content depends on the geometry and structure of the porous medium. However, a certain typical behavior of liquid diffusivity for media with large values of void-fraction can be expected. At low values of liquid-content, such as in early stages of condensation, the liquid is dispersed in the medium and is held by surface tension forces at the nucleation sites in a pendular state. With a large fraction of the medium consisting of void-space the liquid drops are distant from eachother and do not coalesce to form a continuous liquid volume. In this state the isolated drops do not exhibit the tendency to diffuse. Beyond a critical value of the liquid-content, the liquid ceases to be disjoint drops and forms a continuous volume. At this stage liquid becomes responsive to gradients in liquid-content and migrates from the regions of higher liquid content to the drier regions. The movement of the liquid towards the drier regions and its subsequent evaportion at the borders of the wet

zone causes drastic departure from the case where the liquid is stationary. With regards to the behavior of condensate three regimes can be clearly identified: (a) the early period of quasi-steady increase of liquid content with no liquid motion, (b) unsteady diffusion of liquid towards the drier regions, (c) steady state liquid-content profile, where all condensed vapor leaves the two edges of the wet zone.

Liquid-flux can also be established in response to temperature gradient. The surface tension of most liquids decreases with increasing temperatures. Hence, a slug of liquid held in a porous medium, subject to a temperature gradient, by capillary forces feels a net force in the direction of positive temperature gradient, i.e. towards the colder side. This force propels the liquid slug towards the colder side. This mode of liquid transport is not discussed in this manuscript. Experimental observations indicate that the increase in surface tension forces, in a typical insulation arrangement, is much smaller than the variations in hydraulic conductivities of the medium. This is explained in more detail in Chapter 5.

The condensation of vapor can be considered to be simultaneously, a vapor sink, heat source, and liquid source. Hence, the energy equation, vapor diffusion equation, and liquid diffusion equation are all coupled through the condensation rate. The temperature values at the two sides of the condensation-region and the width of the condensation-region depend on the values of temperature and humidity of the two reservoirs. As the phenomenon under study is complex, the following solution methodology is proposed: Consider the wet-zone to be a domain of arbitrary length, L_w, and temperatures T_0, and T_1. By construction the humidity levels h_0 and h_1 are both 100%. The energy equation, vapor diffusion equation, and liquid content equation are solved simultaneously in the condensation-domain. The temperature and vapor-concentration profiles in the dry region are also obtained with the arbitrary

boundary condition of temperature at the condensation-zone edges. The three solutions are then matched to generate the unknown temperatures and the width of the condensation-zone. In this manner, the effects of coupling between the dry and wet zones is reduced. Heat and vapor transfer in the condensation-zone can be studied independently of the mobility level of the condensate. The effects of the liquid mobility are incoporated into the matching process.

2.3 HEAT AND VAPOR TRANSFER IN THE CONDENSATION REGION

Consider a porous medium of finite width, L_w, with boundary temperatures of T_0 and T_1, Fig 2.3.1. With $T_0 > T_1$, heat flows from the hot reservoir to the cold reservoir. The relative humidity at the two boundaries are 100%, and corresponding to T_0 and T_1 the vapor concentration at the boundaries are C^*_0 and C^*_1. Vapor flows against the gradient of vapor-concentration from x=0 to $x=L_w$. The vapor is at saturation concentration at the x=0 edge. Hence, as it travels through points of lower temperature condenses into liquid form. With condensation occuring throughout the region the vapor is at saturation concentration every where. The energy released by condensation is conducted out of the medium at $x=L_w$.

Consider a differential element of thickness x in the medium. The net heat-flux conducted out of the element is:

$$(\dot{q}/A)_{conduction} = -k(d^2T/dx^2)\,\Delta x \qquad [2.3.1]$$

Let W_i denote the rate of energy production per unit volume inside the element. At steady-state the total heat-flux conducted out of the element equals the energy generated iniside

it:

$$-k(d^2T/dx^2) = W_i \qquad [2.3.2]$$

Consider the same differential element again. According to Fick's Law the vapor-flux is given by

$$J_v = -D_v(dC^*/dx) \qquad [2.3.3]$$

where

D_v = Vapor diffusivity.

Then, the net vapor-flux diffusing into the element equals

$$\text{Vapor-flux in} = D_v(d^2C^*/dx^2)\,\Delta x \qquad [2.3.4]$$

At steady state the net vapor-flux into the element condenses into liquid. Let the condensation rate per unit volume be denoted by Γ, then:

$$D_v(d^2C^*/dx^2) = \Gamma \qquad [2.3.5]$$

The energy released by the condensation process is:

$$\dot{q}_{released} = \Gamma h_{fg} \qquad [2.3.6]$$

where

h_{fg} = latent heat of condensation

The heat source term in eq. [2.3.2] equals the heat released by condensation. Hence, eq. [2.3.2] may be written as:

$$k(d^2T/dx^2) + \Gamma h_{fg} = 0 \qquad [2.3.7]$$

Equations [2.3.5] and [2.3.7] are coupled through the condensation term. The two equations are collapsed into one by eliminating the condensation rate term:

$$\frac{d^2T}{dx^2} + \frac{h_{fg}\, D_v}{k} \frac{d^2C^*}{dx^2} = 0 \qquad [2.3.8]$$

Let the mean temeprature and concentration, and the temperature and concentration difference of the wet-zone be defined as

$$T_r' = (T_0+T_1)/2.$$

$$\Delta T' = T_0-T_1$$

$$C_r' = (C^*_0 + C^*_1)/2.$$

$$\Delta C' = C^*_0 - C^*_1 \qquad [2.3.9]$$

The independant varaible, x, and the dependant variables T and C^* are non-dimensionalized as:

$$\eta' = (T-T_r')/\Delta T'$$

$$\overline{C^*} = (C-C_r')/\Delta C'$$

$$\overline{x} = x/L_w \qquad [2.3.10]$$

Introducing the above non-dimensional varaibles into eq. [2.3.8] yields:

$$\frac{d^2\eta'}{d\bar{x}^2} + \frac{\Omega'}{Le\ \beta'} \frac{d^2C^*}{d\bar{x}^2} = 0 \qquad [2.3.11]$$

The non-dimensional groups that appear in the above are:

$$\beta' = \Delta T'/T_r'$$

$$Le\ [Lewis\ Number] = \alpha/D_v$$

$$\Omega'\ [Kossovitch\ Number] = (h_{fg}\Delta C'/\rho c_p T_r') \qquad [2.3.12]$$

The Kossovitch number scales latent heat to sensible heat, and the Lewis number is the ratio of thermal diffusivity to vapor diffusivity.

Equation [2.3.11] has two dependant variables: temperature and vapor saturation-concetration. In general, the vapor saturation-concentration in a porous medium is a function of temperature and the pore-size. The effect of pore-size on the depression of saturation pressure is investigated in [72]. For pore-sizes of order of angstrom the suppresion of the vapor pressure is considerable. As the typical medium under study does Not have such small pore-sizes, the vapor saturation concentration can be considered to be a unique function of temperature. Hence, eq. [2.3.11] is, in effect, a differential equation in dimensionless temperature only.

The functional dependence of saturation vapor-concentration on temperature is obtained through the Clausius-Clapeyron relationship. The Clausius-Clapeyron relation is derived from the Maxwell relations and links three quantities for two phases in equilibrium: the gradient of pressure with temperature, the latent heat, and the volumetric expansion corresponding to change of phase:

$$T(dP/dT) = (h_g - h_f)/(v_g - v_f) \qquad [2.3.13]$$

In the cases under study:

$$v_g >> v_f .$$

Recognizing that:

$$C^* = 1 / v_g \quad ,$$

eq. [2.3.13] can be written as:

$$\frac{dP}{dT} = \frac{h_{fg}\, C^*}{T^2} \qquad [2.3.14]$$

A further assumption, relating pressure to temperature is required to transform eq.[2.3.14] into a unique functional relationship between vapor-concentration and temperature. This is provided by approximating the vapor as a perfect gas. It, then, obeys the perfect gas law:

$$P = C^* R T \qquad [2.3.15]$$

Differentiating the above with respect to temperature and subsituting into eq. [2.3.14] yields:

$$\frac{dC^*}{dT} = \frac{h_{fg}\, C^*}{R\, T^2} - \frac{C^*}{T} , \qquad [2.3.16]$$

which to a good approximation is:

$$\frac{dC^*}{dT} = \frac{h_{fg}\, C^*}{R\, T^2} \qquad [2.3.17]$$

The above can be integrated with some reference value

$$C'^*_r = C^*(T=T_r')$$

to yield:

$$\frac{C^*}{C'^*_r} = \exp\left[\frac{h_{fg}}{RT_r'}\left[1 - \frac{T_r'}{T_r}\right]\right] \qquad [2.3.18]$$

Let

$$\gamma' = h_{fg}/(R\ T_r'), \qquad [2.3.19]$$

then, with the definitions of eq. [2.3.12]:

$$C^*/C^*_r{}' = \exp(\Phi)$$

where $$\Phi = \frac{\gamma'^2\ \beta'\ \eta'}{1 + \beta'\ \eta'} \qquad [2.3.20]$$

Substituting the above into eq. [2.3.11] yields the energy differential equation in η':

$$\left[1 + \frac{\Omega' \gamma'}{Le} (1+\beta' \eta')^{-2} \exp[\Phi]\right] \frac{d^2 \eta'}{d\bar{x}^2} +$$

$$\left[\frac{\gamma' \beta' \Omega'}{Le} (1+\beta' \eta')^{-2} \exp[\Phi]\right] \left[\frac{d \eta'}{d\bar{x}}\right]^2 = 0 \qquad [2.3.21]$$

with the boundary conditions of:

$$\eta' = 1/2 \qquad @ \ \bar{x} = 0$$

$$\eta' = -1/2 \qquad @ \ \bar{x} = 1 \qquad [2.3.22]$$

Equation [2.3.21] is a non-linear second order differential equation in η'. It can be solved numerically. However, the numerical solution of the above is of limited usefulness, for the parametric dependence of $\eta'(\bar{x})$ is not easily discernible.

An approximate solution is obtained by linearizing eq. [2.3.21]. In absence of condensation in the medium, the temperature distribution would be linear:

$$\eta' = 0.5 - \bar{x} \qquad [2.3.23]$$

Equation [2.3.23] is linearized about the above. Let

$$\eta' = 0.5 - \bar{x} + \epsilon$$

such that

$$\epsilon^2 << 1 \quad , \qquad [2.3.24]$$

The boundary conditions [2.3.25] are chosen such that the boundary conditions [2.3.22] are satisfied:

$$\epsilon(\bar{x}=0) = \epsilon(\bar{x}=1) = 0 \qquad [2.3.25]$$

Equation [2.3.24] is introduced into eq. [2.3.21]. The terms of order ϵ^2 and higher powers are neglected. The following linear differential equation in ϵ is obtained:

$$\frac{d^2\epsilon}{d\bar{x}^2}\left[1 + \frac{\Omega' \gamma'}{Le}\right] + \frac{d\epsilon}{d\bar{x}}\left[\frac{-2\gamma'^2\beta'\Omega'}{Le}\right] + \frac{\gamma'^2\beta'\Omega'}{Le} = 0 \qquad [2.3.26]$$

The above is solved in conjunction with boundary conditions [2.3.25] to yield:

$$\epsilon = 0.5\left[\bar{x} - 0.5\ \frac{\exp(\lambda'\bar{x}) - 1}{\exp(\lambda') - 1}\right] \qquad [2.3.27]$$

where

$$\lambda' = \frac{2\ \gamma'^2\ \beta'\ \Omega'}{Le + \gamma'\ \Omega'} \qquad [2.3.28]$$

Then,

$$\eta' = 0.5\left[1 - \bar{x} - \frac{\exp(\lambda'\bar{x}) - 1}{\exp(\lambda') - 1}\right] \qquad [2.3.29]$$

The above is an approximate solution of $\eta'(\bar{x})$. It must be noted here that $\eta'(\bar{x})$ is in terms of parameters as of yet unrestircted: $\Delta T'$, T_r', and L_w. The term λ' depends on the values of T_r' and $\Delta T'$; the length scale is reduced by L_w.

$\eta'(\bar{x})$ has a very simple form and is a function of only one paramter. The term λ' has an important physical significance which is discussed in the following. Heat released by the condensation process in the medium is equal to the excess of outflow of heat-flux at $\bar{x}=1$ over the inflow of heat-flux at $\bar{x}=0$:

$$(\dot{q}/A)_{gen} = -k(dT/dx)\Big|_1 + k(dT/dx)\Big|_0 \quad [2.3.30]$$

Using eq. [2.3.29] the above can be written as:

$$(\dot{q}/A)_{gen} = 0.5(\lambda' \; k \; \Delta T') \quad [2.3.31]$$

Heat-flux conducted across the medium in absence of condensation is

$$(\dot{q}/A)_{cond} = k \; \Delta T' \quad [2.3.32]$$

Therefore, the ratio of heat released by condensation to heat conducted across the medium is $\lambda'/2$. This term represents the effect of heat released by condensation on the temperature profile. The heat-flux, for a given set of boundary temperatures, with condensation is $\lambda'/2$ times larger than the heat-flux, for the same values of boundary temperatures, with no vapor condensation present. The term λ' is called the latent heat transport coefficient. The reduced temperature profile for different values of the latent heat transport coefficient is plotted in Fig. 2.3.2. As the plot indicates the reduced temperature varies from 0.5 to -0.5, and is convex downwards. The effect of increased condensation rate, i.e. increasing λ', is translated into increase in the convexity of the profile. The heat-flux generated by the condensation of vapor leaves the medium at $\bar{x}=1$. Hence, as λ' increases the gradient of the η'-profile at $\bar{x}=1$ increases. The linear variation of temperature with position is characterized by a zero value of λ', i.e. conduction in absence of condensation. It can be easily shown that $\eta'(\bar{x})$, eq. [2.3.29], reduces to a linear profile as $\lambda' \longrightarrow 0$.

As mentioned earlier eq. [2.3.24] can be solved exactly by numerical means. The numerical procedure for obtaining the solution is based on an iterative scheme. Equation [2.3.24] can be rearranged into the followiong form:

$$\frac{d\,\eta'^{,n+1}}{d\bar{x}} = f(\,\eta'^{n},\ (d\eta'/d\bar{x})^{n};\ \Omega', \gamma', \mathrm{Le}, \beta') \qquad [2.3.33]$$

where n is the iteration number. The scheme consists of

discretrizing the x-scale into a finite number of points. Then, eq. [2.3.33] can be written as a matrix eqaution:

$$[A].[\eta'^{n+1}] = [B] \qquad [2.3.34]$$

Matrix [A] is the tridiagonal matrix corresponding to the discretization of $d\eta/d\bar{x}$ term. The vector $[\eta'^{n+1}]$ consists of the values of η' at the discret location. Martrix [B] contains the values of function f, of eq. [2.3.33], evaluated at the discrete points. The iteration scheme consists of successive solution of eq. [2.3.34]. At each stage the old values of η' are used to generate matrix [B]. Then, the new value of $[\eta']$ is obtained by solving eq. [2.3.34]. The matrix equation is solved by the standard procedure of LU-decomposition of matrix [A], accompanied with a forward/backward solver. Equation [2.3.34] is solved iteratively until $[\eta']$ converges to its final value. The major probelm with the method of successive iteration resides in the slow convergence and oscillations of $[\eta']$.

The perturbation solution, eq.[2.3.29], is compared with the numerical solution for two different situations. Clearly as λ' increases, the agreement between the numerical solution and the approximate solution decreases. Figures 2.3.3 and 2.3.4 demonstrate the comparison of the numerical solution with the perturbation solution for η' values of 2.04 and 4.12, respectively. Both plots are generated using the same reference temperature of 550°R. In Fig. 2.3.3 the temperature difference is 40°R and in Fig. 2.3.4, 80°R. The agreement between the numerical solution and the perturbation solution for the case of λ' = 2.04 is astonishingly good, Fig. 2.3.3. In Fig. 2.3.4 the

values of λ' is doubled, yet the agreement between the two results remains exceedingly good. Hence, the perturbation solution can be used as a very close and accurate approximation to $\eta'(\bar{x})$.

The condensation rate per unit volume, , can be obtained from eq. [.2.3.7]:

$$k(d^2T/dx^2) + \Gamma h_{fg} = 0.$$

Let

$$\bar{\Gamma} = \frac{\Gamma L_w^2}{D_v C'_r} \qquad [2.3.35]$$

Then, using eq. [2.3.29], the non-dimensional condensation rate is :

$$\bar{\Gamma} = \frac{Le\ \beta'}{\Omega'} \frac{\lambda'^2}{2} \frac{\exp(\lambda' x)}{\exp(\lambda') - 1} \qquad [2.3.36]$$

This explains the strong influence of temperature-drop across the domain on the condensation rate intensity.

Equation [2.3.36] can be integrated over the length of the condesing-zone to yield the condensation rate per unit area, $(\dot{w}/A)_T$:

$$(\dot{w}/A)_T = \int_0^{L_w} \Gamma \, dx \qquad [2.3.37]$$

Then,

$$\frac{(\dot{w}/A)_T \, L_w}{D_v \, C'^*_r} = \frac{Le \; \beta'}{\Omega'} \; \frac{\lambda'}{2} \qquad [2.3.38]$$

Again, as before, the condensation rate per unit area has a very simple formulation and depends linearly on the latent heat transport coefficient, λ'. Using eq. [2.3.28], the term ($Le \; \beta' \; \lambda'/2\Omega'$) may be written as:

$$\frac{Le \; \beta'}{\Omega'} \; \frac{\lambda'}{2} = \frac{\gamma'^2 \; \beta'^2 \; Le}{Le + \Omega' \; \gamma'} \qquad [2.3.39]$$

The reduced condensation rate has a parametric dependence on the latent heat transport coefficient, λ'. The paramteric dependence of ($\overline{\Gamma}\,\Omega'$/Le β') on λ' is explored in Fig. 2.3.5. The figure indicates that the condensation rate increases as the vapor approaches the colder edge. This increase is very dramatic for larger values of λ'. Fig. 2.3.5 is to some extent not very clear. In this figure ($\overline{\Gamma}\,\Omega'$/Le β') is plotted against $\overline{x}$. At low values of $\overline{x}$, the profiles of ($\overline{\Gamma}\,\Omega'$/Le β') crossover eachother. This is unphysical, for one would expect larger condensation rate intensities at all locations for increasing values of λ'. This inconsistency is due to the aggregation of (Ω'/Le β') term with $\overline{\Gamma}$. The (Ω'/Le β') term is a function of λ', and cannot be lumped together with $\overline{\Gamma}$. The profile of η' for the two situations discussed in Fig. 2.3.3 and 2.3.4 are plotted in Fig. 2.3.6. The plots correspond to the temperature profiles characterized by a mean temperature value of 550°R, and a ΔT of 40 and 80°R, resepectively. The values of β' and Ω' corresponding to these two cases are denoted on the figure. The reduced condensation rate per unit volume, $\overline{\Gamma}$, is plotted against reduced length, $\overline{x}$. It may be observed that at low values of $\overline{x}$, the difference in the condensation rates corresponding to the two cases is not discernible. However, at $\overline{x}$=1, the ratio of condensation rate with λ' = 4.12, is about eight times larger than the condensation rate with λ' = 2.014. This large difference corresponds to a mere doubling of the temperature drop across the wet-zone. The reason for this abrupt increase may be explored by studying the dependence of λ' on β' from eq. [2.3.28]. Equation [2.3.28] indicates that λ' is linearly proportional to β'. Hence, the condensation rate per unit volume is proportional to the third power of the temperature difference:

$$\Gamma \sim \lambda \beta^2 \sim \beta^3$$

The above indicates that for the same value of mean temperature, a doubling of the temperature drop, i.e. doubling β', causes a four-fold increase in the total volume of condensate.

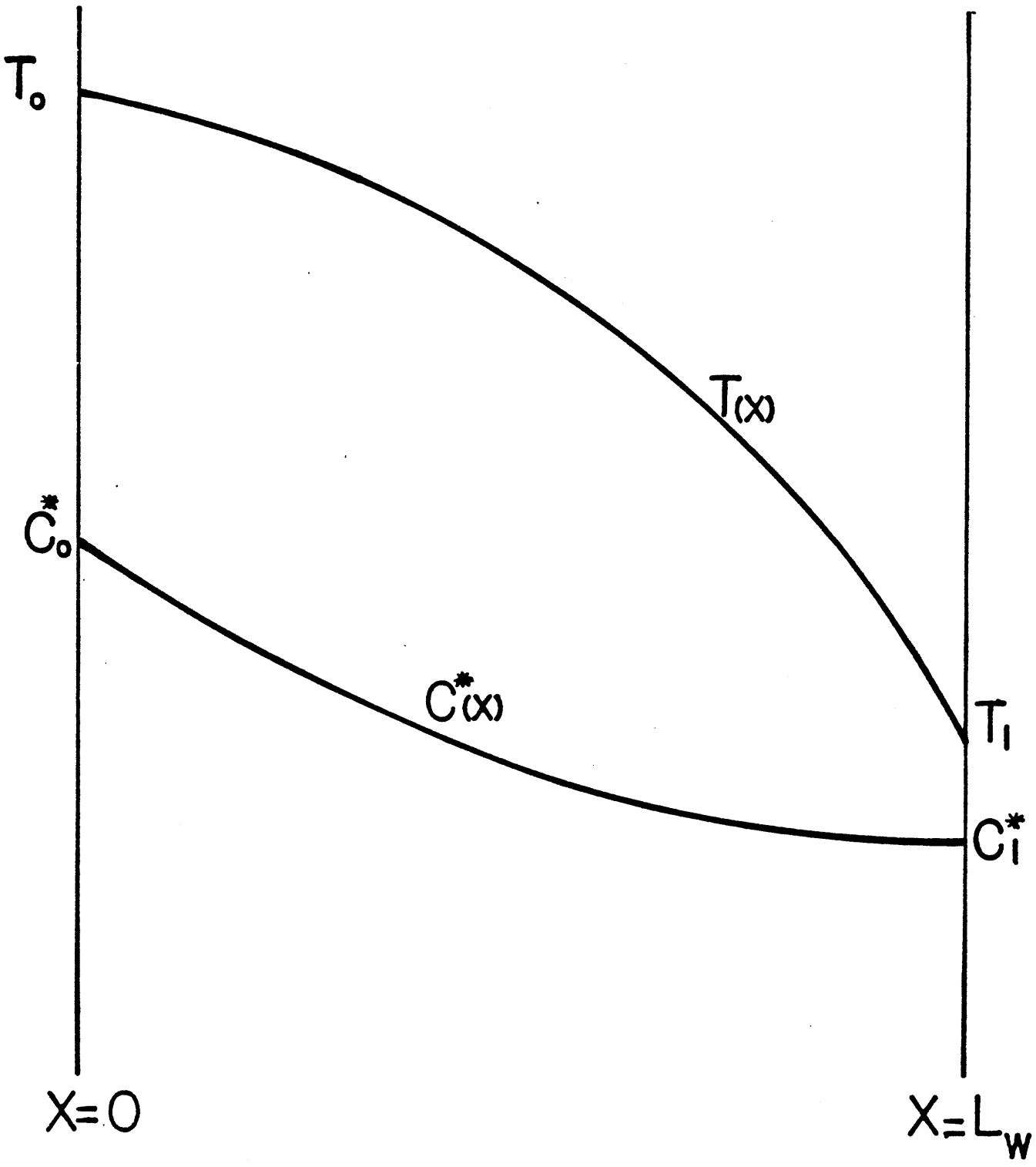

Fig. 2.3.1 Temperature and Vapor-Concentration Profile in the Condensation-Region

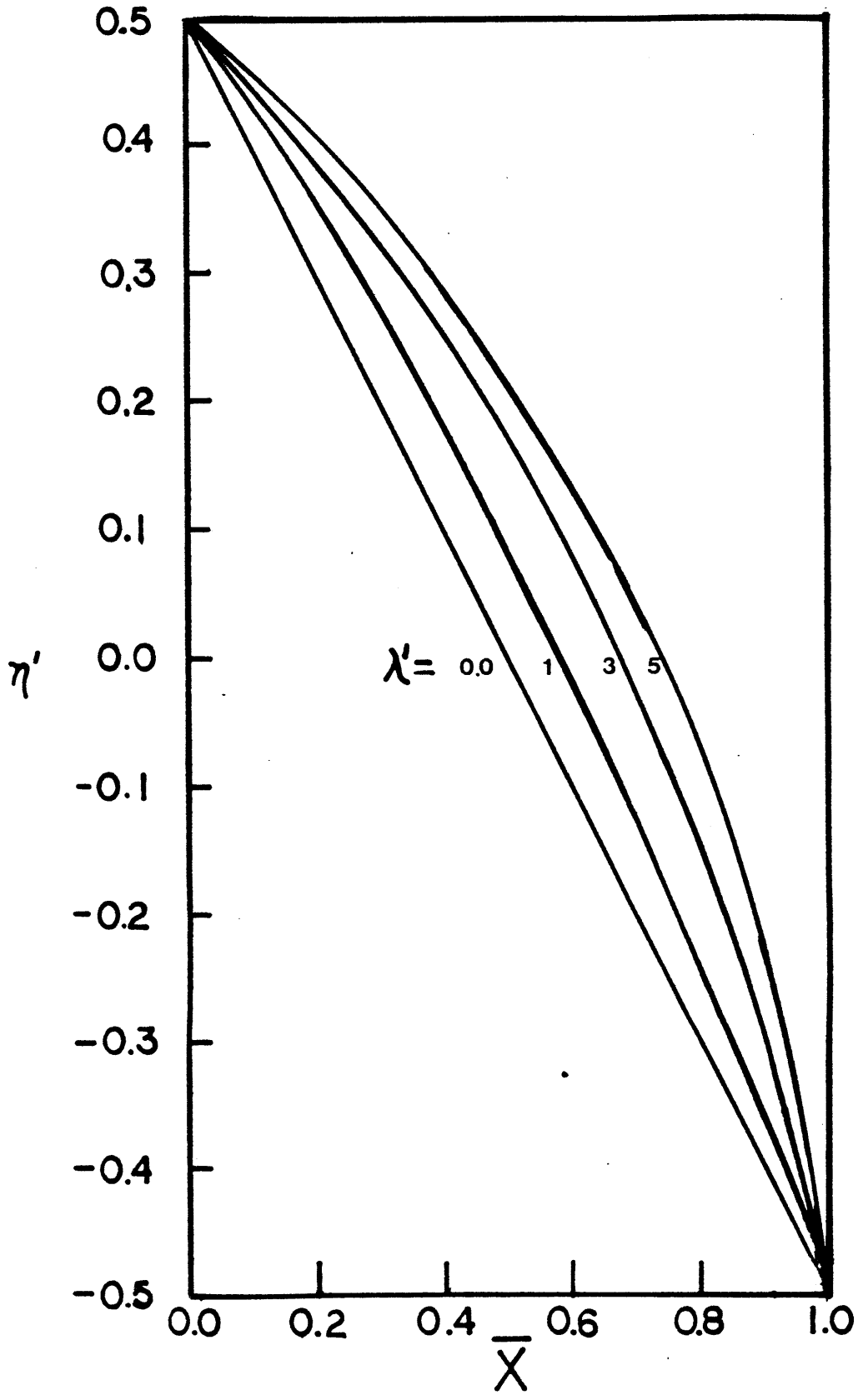

Fig. 2.3.2 Reduced Temperature Profile For different values of λ'

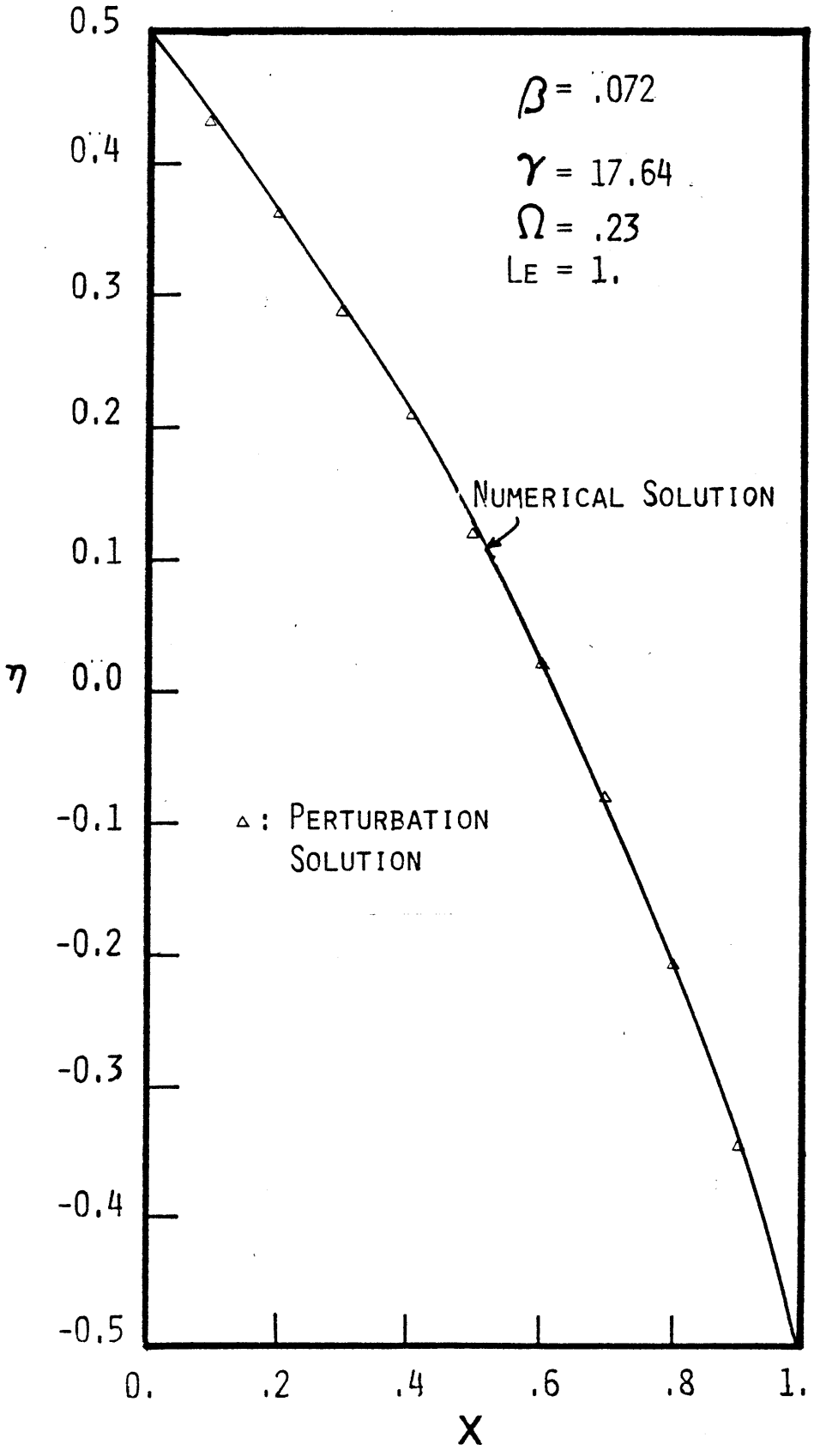

Fig. 2.3.3 Comparison of the Analytical Solution with the Numerical Results of The Reduced Temperature-Profile

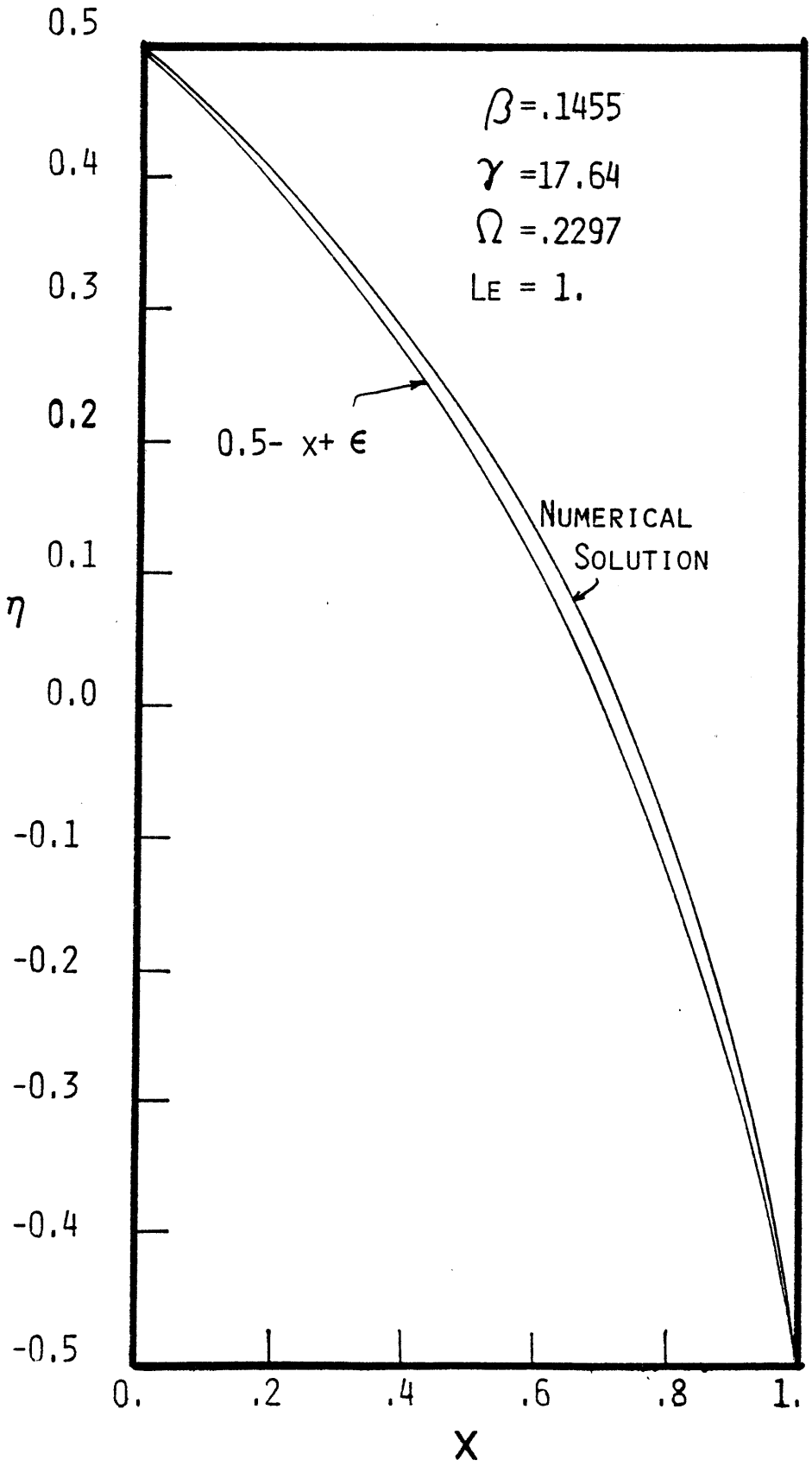

Fig. 2.3.4 Comparison of Analytical Solution with the Numerical Results of Reduced Temperature Profile

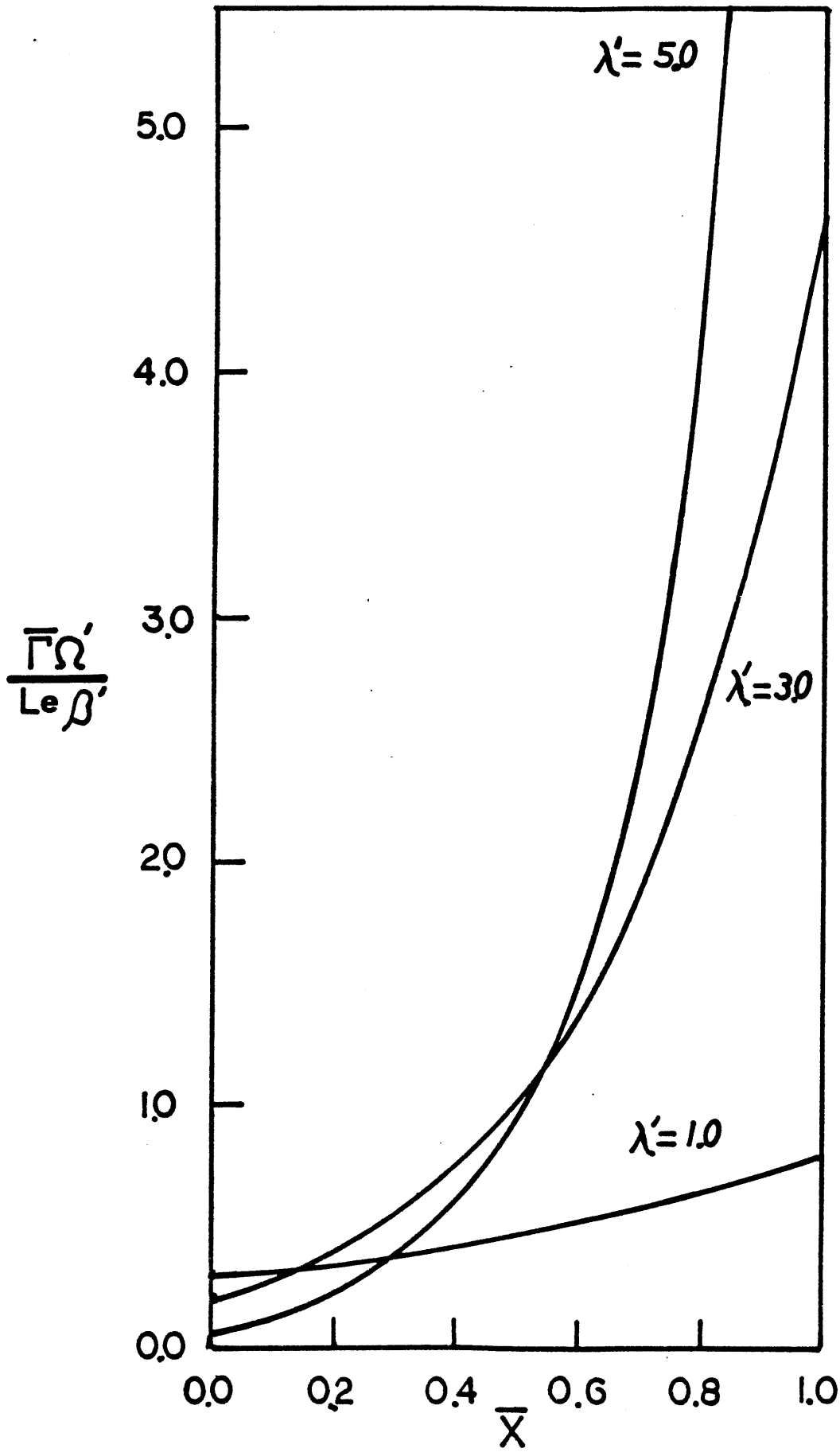

Fig. 2.3.5 A condensation-rate profile for different values of λ'.

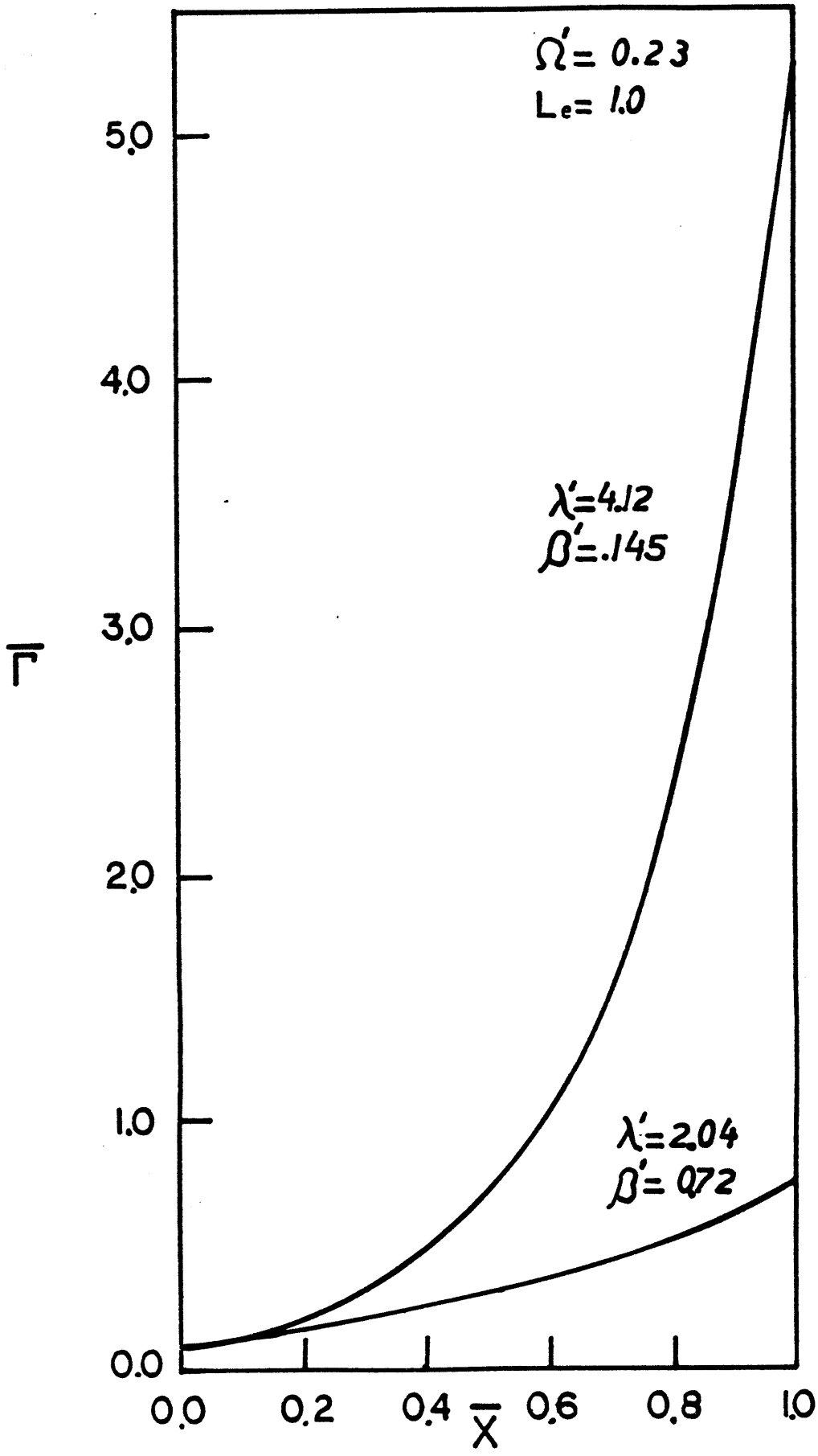

Fig. 2.3.6 The Reduced Condensation-rate Profile for two different boundary conditions.

2.4 LIQUID DIFFUSION IN THE CONDENSATION REGION

In the previous section the flow of heat and vapor in the condensation-region was studied. The non-dimensional rate of vapor condensation intensity, $\bar{\Gamma}$, was shown to be:

$$\bar{\Gamma} = \frac{Le\ \beta'}{\Omega'} \frac{\lambda'^2}{2} \frac{\exp(\lambda'\bar{x})}{\exp(\lambda') - 1}$$

where

$$\bar{\Gamma} = \frac{\Gamma L_w^2}{D_v C'_r}$$

In this section the diffusion of the condensate in the porous medium will be studied.

Consider a porous medium of width L_w, sandwiched by two dry regions. Vapor condenses in the medium at a condensation rate per unit volume of $\Gamma(x)$. Liquid transport in the porous medium is controlled by the gradient of liquid-content, θ :

$$J_1 = -D_1(\theta)(\partial\theta/\partial x) \qquad [2.4.1]$$

where D_1 is a phenomenologically defined liquid diffusivity, and is a function of liquid-content. Continuity of liquid may be written as:

$$\frac{\partial \theta}{\partial t} = \frac{\partial}{\partial x}\left[D_1(\theta)\ \frac{\partial \theta}{\partial x}\right] + \frac{\Gamma(x)}{\rho\ \epsilon} \qquad [2.4.2]$$

where

ρ = the density of the condensate

ϵ = void-fraction of the medium

The above is non-dimensionalized into the following form:

$$\frac{\partial \theta}{\partial Fo''} = \frac{\partial}{\partial \overline{x}}\left[\frac{D_1(\theta)}{D_{1m}}\ \frac{\partial \theta}{\partial \overline{x}}\right] + \frac{\Gamma(x)\ L_w^2}{D_{1m}\ \rho\ \epsilon} \qquad [2.4.3]$$

where

$$Fo'' = D_{lm}t/L_w^2$$

D_{lm} = some mean value of liquid diffusivity.

Solution of eq. [2.4.3] requires a definition of the functional dependence of liquid diffusivity on liquid-content. This dependence is a function of the geometry and structure of the medium. Considerable affort has been devoted to the formulation of a universal form of liquid diffusivity [72]. However, no universally accepted form of $D_l(\theta)$ exists. Nevertheless, certain assumptions regarding liquid diffusivity in a porous medium may be made. In many types of porous media liquid diffusivity remains negligibly small until a critical value of liquid-content is reached. For liquid-contents less than the critical value, liquid is in a pendular state and does not exhibit the tendency to diffuse. Hence, for liquid-contents less than the critical value the non-dimensional boundary equations associated with eq. [2.4.3] are:

$$\begin{aligned}
\partial\theta/\partial\bar{x} &= 0 && @\ x = 0 && \forall Fo'' \\
\partial\theta/\partial\bar{x} &= 0 && @\ x = 1 && \forall Fo'' \\
\theta &= 0 && @\ Fo'' = 0 && \forall \bar{x}
\end{aligned} \qquad [2.4.4]$$

For values of liquid-content in excess of the critical value, liquid diffusion takes place. The flux of the diffusing liquid is proportional to the excess of liquid-content over the critical liquid-content. The solution of the transient problem corresponding to the evolution of liquid-content during condensation can be only solved numerically. However, the case of unsteady diffusion may be solved analytically with a uniform initial liquid-content distribution. It must be recognized that the unsteady solution obtained by the following initial conditions does not relate to the evolution of liquid-content during condensation. Nevertheless, as the steady-state solution is independant of initial conditions, the steady-state results describe the liquid-content profile after a sufficiently long period of condensation. Under this situtation, the non-dimensional boundary equations associated with eq. [2.4.3] are:

$$\begin{aligned} \theta &= \theta_c \quad @ \quad \overline{x} = 0 \quad \forall\, Fo'' \\ \theta &= \theta_c \quad @ \quad \overline{x} = 1 \quad \forall\, Fo'' \\ \theta &= \theta_c \quad @ \quad Fo'' = 0 \quad \forall\, \overline{x} \end{aligned} \qquad 2.4.5$$

In order to analyze the phenomenon of liquid diffusion efficiently and take advantage of the possible simplifications two cases are studied:

Case(1): Condensate with no mobility $D_l \rightarrow 0$
Case(2): Condensate with finite mobility $D_l \neq 0$.

2.4.1 Immobile Condensate

During the early stages of condensation the condensate is in pendular state, and very little, if any liquid motion takes place (for a more detailed description of the phenomenon see chapters 5 and 6). Under these circumstances, the condensate may be considered to be immobile.

Let the liquid diffusivity be independant of liquid content, $D_l = D_{lm}$. Then if :

$$\frac{\Gamma(x)\ L_w^2}{D_l\ \rho\ \epsilon} >> \frac{\partial^2\theta}{\partial\bar{x}^2} \qquad [2.4.6]$$

the diffusion term in eq.[2.4.3] can be ignored. As

$$\frac{\partial^2\theta}{\partial\bar{x}^2} \sim O(1) \qquad [2.4.8]$$

then,

$$D_l << \frac{\Gamma(x)\, L_w^2}{\rho\, \epsilon} \qquad [2.4.9]$$

Using eqs. [2.3.38] and [2.3.39], the above requirement can be written as:

$$\frac{D_l}{D_v} << \frac{Le\, \beta'}{\Omega'} \quad \frac{C'_r}{\rho\, \epsilon} \quad \frac{\lambda'}{2} \quad \frac{1.}{\exp(\lambda') - 1} \qquad [2.4.10]$$

The above inequality establishes the upper value of liquid diffusivity, below which the effects of liquid diffusion can be ignored. With the inequality [2.4.10] satisfied, the liquid continuity equation becomes:

$$\frac{d\theta}{dFo''} = \frac{\Gamma(x)\, L_w^2}{D_l\, \rho\, \epsilon} \qquad [2.4.11]$$

Substituting for $\Gamma(\overline{x})$ from eq. [2.3.39] results in :

$$\frac{d\theta}{dFo''} = M \frac{C'_r}{\rho\ \epsilon} \frac{Le\ \beta'}{\Omega'} \frac{\lambda'^2}{2} \frac{\exp(\lambda'\bar{x})}{\exp(\lambda') - 1} \qquad [2.4.12]$$

where

$$Fo'' = D_{lm}t/L_w^2$$

$$M = D_v/D_l.$$

The rate of increase of liquid content, for small values of liquid diffusivity is independant of the magnitude of liquid diffusivity. This is clear in the above equation as the D_l terms in Fo'' and M cancel out. This ambiguity is removed by the introduction of a new Fourier number based on vapor diffusivity:

$$Fo' = M\ Fo'' = D_v t/L_w^2$$

Upon integration eq. [2.4.12] becomes:

$$\theta(\bar{x},\ Fo') = \left[\frac{C'_r}{\rho\ \epsilon} \frac{Le\ \beta'}{\Omega'} \frac{\lambda'^2}{2} \frac{\exp(\lambda' x)}{\exp(\lambda') - 1}\right] Fo' \qquad [2.4.13]$$

In studying the above equation, the form of the condensation-rate intensity, eq. [2.3.36], may be recalled. It will be then noted that the liquid-content profile is proportional to the condensation rate. Indeed, the above liquid-content profile result could have been easily derived by considering the following simple argument: In absence of liquid diffusion the rate of condensate accumulation is proportional to the condensation rate. The constant of proportionality would have to translate the volume of condensed-vapor to the volume of liquid-condensate. It, then would have to be the ratio of vapor-density to liquid-density. Furthermore, liquid-content increases linearly with time for all locations. Therefore, eq. [2.4.13] could have been easily obtained. The liquid-content distribution normalized by the medium void-fraction is plotted in Fig. 2.4.1 for two values of λ'. It may be recalled that these two cases correspond to a mean temperature value of 550°R and temperature drops of 40 and 80°R. Fig. 2.4.1 is in essence the same as Fig. 2.3.6, except for a change of scale on the ordinate. Clearly, the liquid-content at the colder-edge, $\bar{x}=1$, is higher than at $\bar{x}=0$.

It has been mentioned that liquid-content rises montonically until it reaches a critical-value. Above this value liquid diffusion begins and the liquid-content undergoes a transeint change. The time-scale corresponding to the onset of liquid diffusion may be calculated from eq. [2.4.13]. In Fig. 2.4.2 a plot of the ratio of critical Fourier number to the critical liquid-content as a function of the latent heat transport coefficient, λ', for water is presented. As the value of liquid-content is largest at $\bar{x}=1$, eq. [2.4.13] is evaluated at this location. The results is plotted in Fig. 2.4.2 for different values of mean temperature T_r. The plot indicates that the ratio $(Fo'_c/\epsilon\,\theta_c)$ decreases with increasing values of latent heat transport coefficient, λ'. Hence, for a given value of critical liquid-content and medium void-fraction the time required to reach the onset of liquid diffusion decreases with

increasing values of Λ'. For the range of temperature that are encountered in the application of these results, the variations in the mean temperature, T_r, have negligible effects on the $(Fo'_c/\epsilon\ \theta_c)$ profile. This is shown in Fig. 2.4.2 by plotting the profile for two values of mean temperature, 510°R and 570°R. As the values of temperature are measured on the absolute scale, the variations on the relative scale, e.g. Celsius, must be significant to cause a noticeable effect.

2.4.2 Mobile Condensate

In this case the condensate is considered to have a finite and nonzero value of liquid diffusivity. Furthermore, the value of liquid diffusivity is such that the inequality [2.4.10] is not satisfied. Then, none of the terms in the continuity equation can be ignored:

$$\frac{\partial \theta}{\partial Fo''} = \frac{\partial}{\partial \bar{x}}\left[\frac{D_l(\theta)}{D_{lm}}\ \frac{\partial \theta}{\partial \bar{x}}\right] + \frac{\Gamma(\bar{x})\ L_w^2}{D_{lm}\ \rho\ \epsilon}$$

The above equation is accompanied by the following boundary conditions:

$$\theta = \theta_c \qquad @\ \bar{x} = 0 \qquad \forall Fo''$$

$$\theta = \theta_c \qquad @\ \bar{x} = 1 \qquad \forall Fo''$$

$$\theta = \theta_c \qquad @\ Fo'' = 0 \qquad \forall \bar{x}$$

Equation [2.4.4] is linear in . Therefore θ can be considered to be the sum of two behaviors :

$$\theta(\bar{x},\ Fo'') = \theta_s(\bar{x}) + \theta_t(\bar{x}, Fo'') \qquad [2.4.14]$$

The θ_s term is the steady-state liquid-content distribution and is not a function of time. The θ_t term is the time dependant portion of the solution, and is a function of both time and space. The overall behavior of θ is obtained by the addition of the steady solution with the transient one. Introducing eq. [2.4.14] into eq. [2.4.4] results into two sets of equations. The first set deals with the steady-state solution:

$$\frac{\partial}{\partial x}\left[\frac{D_l(\theta)}{D_{lm}}\frac{\partial\theta}{\partial x}\right] + \frac{\Gamma(x)\ L_w^2}{D_{lm}\ \rho\ \epsilon} = 0 \qquad [2.4.15]$$

The value of liquid diffusivity for liquid-contents less than the θ_c is zero. Hence, the liquid content at all locations is at least equal to θ_c. Any liquid in excess of this value is subject to diffusion. Hence,

$$\theta_s(0) = \theta_c$$

$$\theta_s(1) = \theta_c \qquad [2.4.16]$$

The second set of equations deals with the unsteady behavior of θ :

$$\frac{\partial}{\partial \bar{x}} \left[\frac{D_l(\theta)}{D_{lm}} \frac{\partial \theta_t}{\partial \bar{x}} \right] = \frac{\partial \theta_t}{Fo''}, \qquad [2.4.17]$$

$$\theta_t(\bar{x}=0, Fo'') = 0$$

$$\theta_t(\bar{x}=1, Fo'') = 0$$

$$\theta_t(\bar{x}, 0) = -\theta_s(\bar{x}) \qquad [2.4.18]$$

The system of eqs.[2.4.15] and [2.4.17] is incomplete, for it requires a definition of $D_l(\theta)$. In section 2.4.1 the possible behavior of liquid diffusivity was discussed. It is assumed, in this section, that the initial value of liquid content is larger than the critical value, θ_c,. Then the liquid diffusivity is non-zero. Let it be some constant value, D_l. For the case of constant liquid diffusivity eq. [2.4.15] can be written as:

$$\frac{d^2\theta_s}{d\bar{x}^2} + \frac{\Gamma(x)\ L_w^2}{D_l\ \rho\ \epsilon} = 0 \qquad [2.4.19]$$

Integrating the above twice yields:

$$\theta_s(\bar{x}) = -\int_0^{\bar{x}}\int_0^{\bar{x}} \frac{\Gamma(x)\ L_w^2}{D_l\ \rho\ \epsilon}\, d\bar{x}\, d\bar{x} + c_1\bar{x} + c_2 \qquad [2.4.20]$$

Applying the boundary conditions [2.4.16] yields

$$c_2 = \theta_c$$

$$c_1 = +\int_0^1\int_0^{\bar{x}} \frac{\Gamma(x)\ L_w^2}{D_l\ \rho\ \epsilon}\, d\bar{x}\, d\bar{x} \qquad [2.4.21]$$

$$\eta'(\bar{x}) = 0.5 - \bar{x} + \epsilon$$

and

$$\epsilon = 0.5\left[\bar{x} - \frac{\exp(\lambda'\bar{x}) - 1}{\exp(\lambda') - 1}\right]$$

The term in the curly brackets in eq. [2.4.24] is equal to $\epsilon(\bar{x})$. The term $\epsilon(\bar{x})$, may be recalled, represents the effect of heat released by condensation on the temperature distribution. It is the difference between the linear temperature profile, corresponding to the case of pure conduction, and the temperature distribution with the effect of condensation present. The liquid-content at steady state is proportional to the same difference, $\epsilon(\bar{x})$. The constant of proportionality consists of two types of terms. One type depends on the values of temperature at the condensation-zone region: β', Ω', C'_r. The other type of terms are the properties of condensate and medium : M, ρ, ϵ, and Le.

The steady-state liquid-content distribution is plotted against reduced length for different values of λ' in Fig. 2.4.3. The liquid-content plot is offset by θ_c. The liquid-content distribution is a strong function of the latent heat transport coefficient, λ'. The temperature gradient, and consequentially the saturation vapor-concetration, become steeper with increasing

Hence,

$$\theta_s(\bar{x}) = -\int_0^{\bar{x}}\int_0^{\bar{x}} \frac{\Gamma(\bar{x})\ L_w^2}{D_1 \rho \epsilon}\, d\bar{x}\, d\bar{x} + \bar{x}\int_0^{1}\int_0^{\bar{x}} \frac{\Gamma(\bar{x})\ L_w^2}{D_1 \rho \epsilon}\, d\bar{x}\, d\bar{x} \quad [2.4.22]$$

The condensation rate per unit volume, $\Gamma(\bar{x})$, is given in eq. [2.3.39]; the integrand in eq.[2.4.22] becomes:

$$\frac{\Gamma(\bar{x})\ L_w^2}{D_1 \rho \epsilon} = M \frac{C'_r}{\rho \epsilon} \cdot \frac{Le\ \beta'}{\Omega'} \cdot \frac{\lambda'^2}{2} \cdot \frac{\exp(\lambda'\bar{x})}{\exp\lambda' - 1} \quad [2.4.23]$$

Performing the integration of eq. [2.4.22], a very simple result is obtained:

$$\theta_s(\bar{x}) = \theta_c + M \frac{C'_r}{\rho \epsilon} \frac{Le\ \beta'}{\Omega'} \left\{ \frac{1}{2}\left[\bar{x} - \frac{\exp\lambda'\bar{x} - 1}{\exp\lambda' - 1}\right] \right\} \quad [2.4.24]$$

Recall that

$\bar{x}$. As the condensation rate per unit volume is proportional to the second derivative of saturation-concentration, both the condensation rate intensity and the steady-state liquid-content profiles vary more sharply as the vapor approaches the colder side. Hence, the point of maximum liquid-content lies closer to the colder-boundary.

The time dependent portion of liquid-content is described by eq. [2.4.17]. For a constant value of liquid-diffusivity, it may be written as:

$$\frac{\partial \theta_t}{\partial x} = \frac{\partial \theta_t}{\partial Fo''} \qquad [2.4.25]$$

The above can be solved by the method of seperation of variables. Let:

$$\theta_t = \Theta X \qquad [2.4.26]$$

Then, eq.[2.4.25] becomes:

$$\frac{X''}{X} = \frac{\Theta'}{\Theta} = -a_n^2 \qquad [2.4.27]$$

The above consists of two equations which are solved to yield:

$$X = c_1 \sin(a_n \bar{x}) + c_2 \cos(a_n \bar{x}) \qquad [2.4.28]$$

$$\Theta = c_3 \exp\left[-a_n^2 . Fo''\right] \qquad [2.4.29]$$

Applying the boundary conditions:

$$\theta_t(0, Fo'') = \theta_t(1, Fo'') = 0$$

yields, the eigen-values equation:

$$a_n^2 = n\pi \qquad [2.4.30]$$

Then,

$$\theta_t(\bar{x},\ Fo'') = \sum_n c_n \exp\left[-a_n^2 \cdot Fo''\right] \sin(a_n \bar{x}) \qquad [2.4.31]$$

The coefficients c_n are determined by applying the initial condition:

$$\theta_t(\bar{x},0) = -\theta_s(\bar{x}) \qquad [2.4.32]$$

Using eq. [2.4.23] for $\theta_s(\bar{x})$ results in:

$$c_n = -\frac{M\ C'_r\ Le\ \beta'\ \lambda'}{2\ \rho\ \epsilon\ \Omega'} \left\{ \frac{\int_0^1 \sin(a_n \bar{x}) \left[\bar{x} - \frac{\exp \lambda' \bar{x} - 1}{\exp \lambda' - 1}\right] d\bar{x}}{\int_0^1 \sin\ (a_n \bar{x})\ d\bar{x}} \right\} \qquad [2.4.33]$$

Performing the integration yields:

$$c_n = \frac{M\ C'_r\ Le\ \beta'\ \lambda'}{2\ \rho\ \epsilon\ \Omega'} \left\{ (-1)^n - \frac{1 + (-1)^n}{1 + \frac{\lambda'}{(n\pi)}\ (\exp \lambda' - 1)} \right.$$

$$+ \frac{(-1)^n - 1}{\exp \lambda' - 1} \Bigg\} \qquad [2.4.34]$$

The unsteady term $\theta_t(\bar{x}, Fo'')$ is defined by eq. [2.4.31] and [2.4.34]. It decays exponentially with reduced time, Fo''.

The overall behavior of liquid-content, for a nonzero value of liquid diffusivity, is:

$$\theta(\bar{x}, Fo'') = \theta_s(\bar{x}) + \theta_t(\bar{x}, Fo'') \qquad [2.4.35]$$

For

$$n \pi Fo'' >> 1 \qquad [2.4.36]$$

liquid content reaches its steady-state value. In physical parameters, the time scale above which the steady-state solution can be assumed to hold is related to liquid diffusivity as:

$$t >> L_w/D_l \qquad [2.4.37]$$

The liquid-flux at any location is :

$$J_l = -D_l \ (\partial\theta/\partial x) \qquad [2.4.38]$$

Recall that liquid-content consists of a transient and a steady component, then:

$$J_l = -D_l \ (\partial\theta_t/\partial x) \ - D_l(d\theta_s/dx) \qquad [2.4.39]$$

Using eq.[2.4.23] and [2.4.31] :

$$\frac{d\theta_s}{d\bar{x}} = \frac{M\ C'_r}{\rho\ \epsilon} \cdot \frac{Le\ \beta'}{\Omega'} \left\{ \frac{1}{2} \left[1 - \frac{\lambda'\ \exp \lambda' \bar{x}}{\exp \lambda' - 1} \right] \right\} \qquad [2.4.40]$$

and

$$\frac{\partial \theta t}{\partial \bar{x}} = \frac{M\ C'_r\ Le\ \beta'}{\rho\ \epsilon\ \Omega'} \sum_n c'_n \cdot \exp\left[-a_n\ Fo''\right] a_n \cdot \cos(a_n \bar{x}) \qquad [2.4.41]$$

where c_n' is defined by the above and eq. [2.4.34]. The percentage of condensate that leaves the medium, at steady-state, at $\bar{x}=0$ is:

$$\alpha = \frac{D_l \left.\frac{d\ \theta_s}{dx}\right|_{x=0}}{\int_0^{L\omega} \Gamma(x)\ dx} \qquad [2.4.42]$$

From eq. [2.4.42] and [2.3.41] :

$$\alpha = \frac{\exp \lambda' - 1 - \lambda'}{\lambda' (\exp \lambda' - 1)} \qquad [2.4.43]$$

A plot of this parameter as a function of λ' is presented in Fig. 2.4.4. Clearly, were $\Gamma(x)$ a constant the liquid-fluxes J_0 and J_1 would be equal. In general, the condensation rate increases with distance. However, the increase is more dramatic for large values of latent heat transport coefficient. The portion of the condensate that leaves at the cold-edge increases with increasing λ'. This is equivalent to the decrease in α with increasing λ'.

Using eqs. [2.4.42] and [2.3.38] the liquid-flux leaving the boundary of the condesation-region at $\bar{x}=0$ may be written in the following non-dimensional form:

$$\frac{J_0 L_w}{D_v C'_r} = \frac{Le\ \beta'}{\Omega'} \cdot \frac{\exp \lambda' - 1 - \lambda'}{2(\exp\lambda' - 1)} \qquad [2.4.44]$$

Similarly, the liquid-flux leaving the condensation-region at $\bar{x}=1$ is:

$$\frac{J_1 L_w}{D_v C'_r} = \frac{Le\ \beta'}{\Omega'} \frac{(\lambda'-1)\exp\lambda' + 1}{2(\exp\lambda' - 1)} \qquad [2.4.45]$$

Equations [2.4.44] and [2.4.45] are plotted in Fig. 2.4.5. Aggregating the $(\Omega'/Le\ \beta')$ term with the $(J\ L_w/D_v\ C'_r)$ while investigating the dependence of the latter on λ' is not rigorously correct, for $(\Omega'/Le\ \beta')$ is a function of λ'. However, for indicative purposes the terms $(J_0\ L_w\ \Omega'/D_v\ C'_r\ Le\ \beta')$ and $(J_1\ L_w\ \Omega'/D_v\ C'_r\ Le\ \beta')$ are plotted versus λ' in Fig. 2.4.5. The results indicate that as the latent heat transport coefficient increases, the two liquid-fluxes increase at unequal rates. The liquid-flux J_0 increases at a decreasing pace, whereas the J_1 term increases at an increasing pace. The difference in the behavior of the two indicates that as the condensation rate increases a larger portion of the condensate leaves the condensation-region at the $\bar{x}=1$ boundary. This is

consistent with the previous findings as discussed in reference to Fig. 2.4.4.

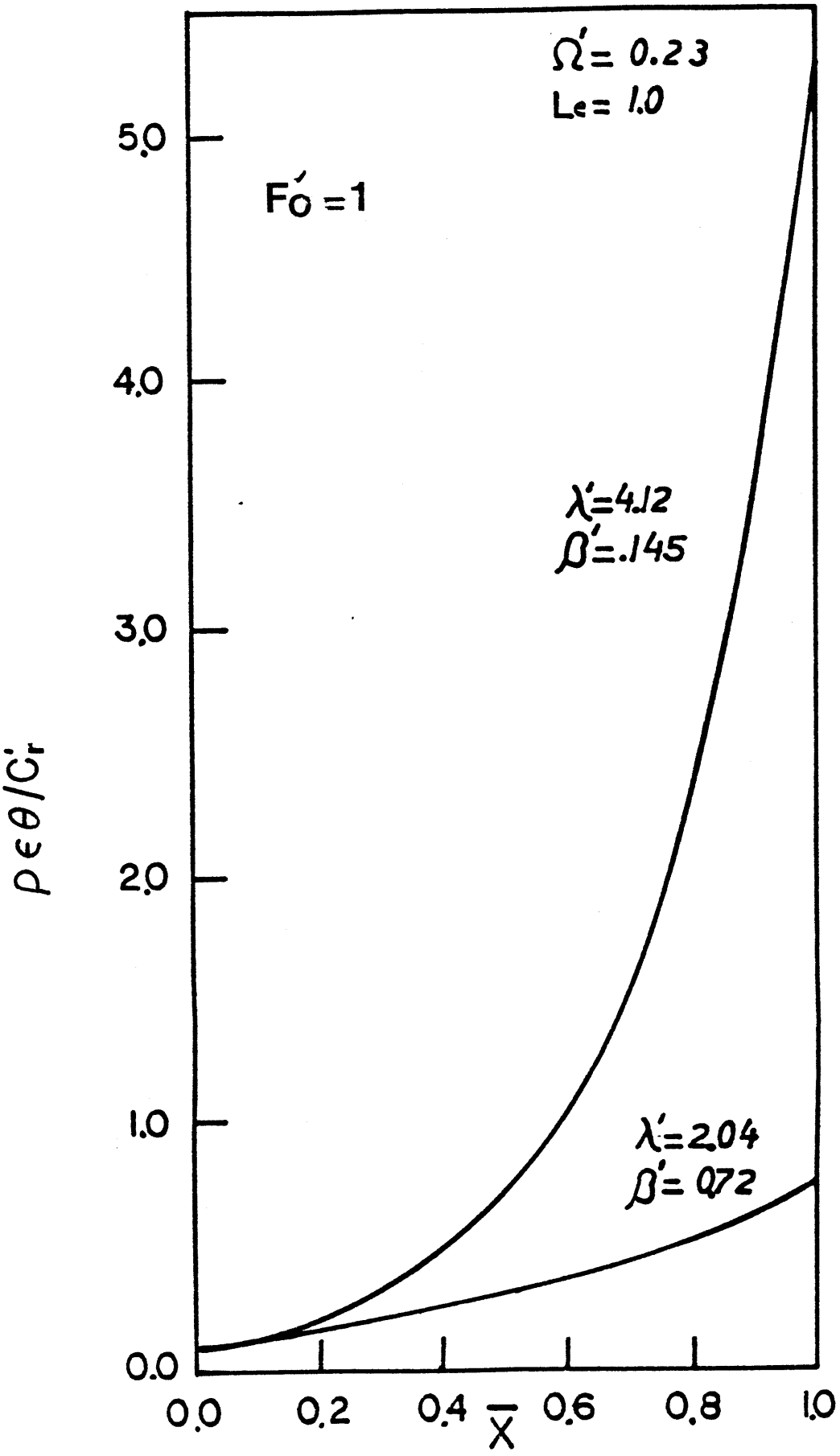

Fig. 2.4.1 Normalized Liquid-Content Profile at Fó=1

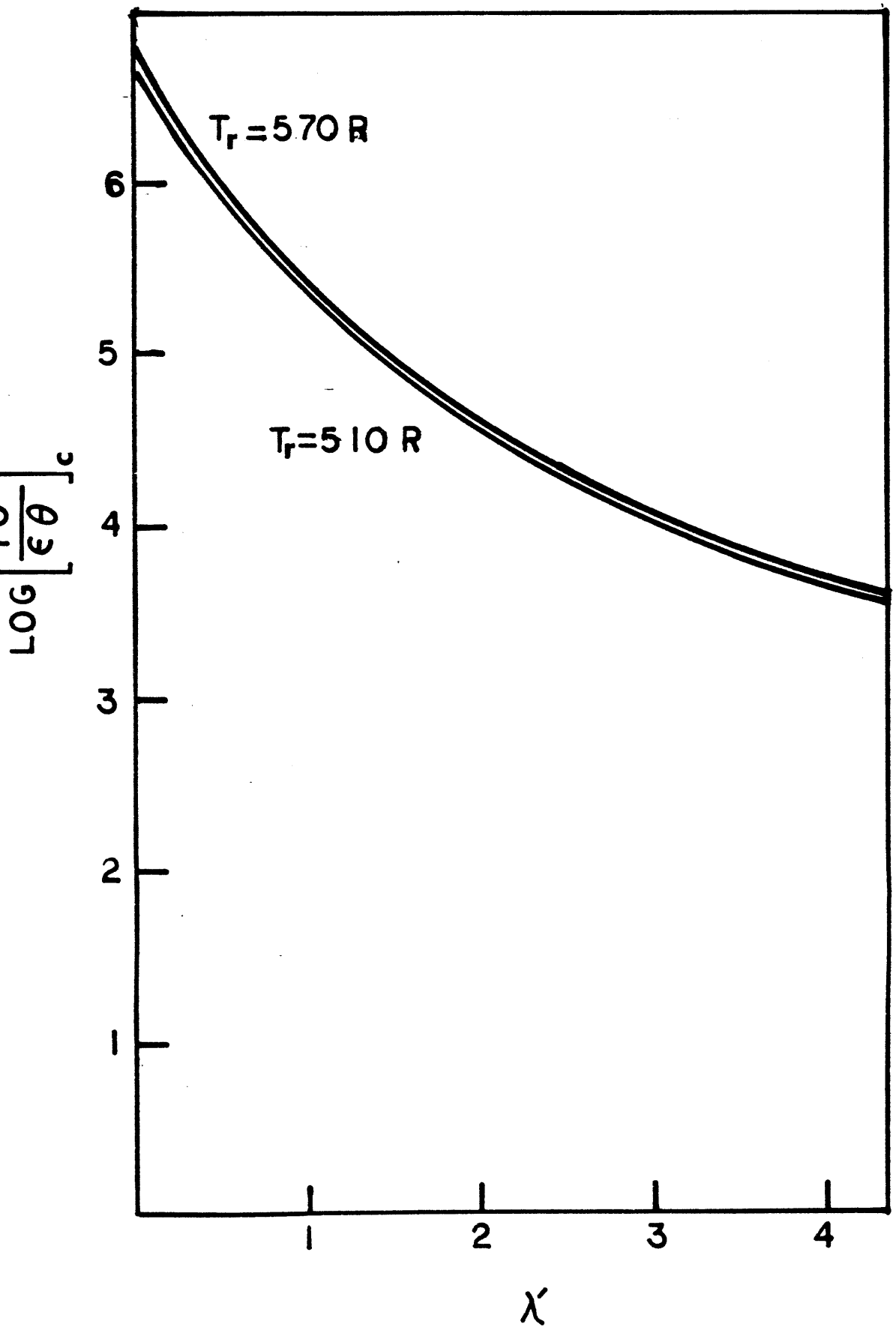

Fig. 2.4.2 The plot of critical $Fo'/\epsilon\theta_c$ versus λ' for different values of the mean temperature

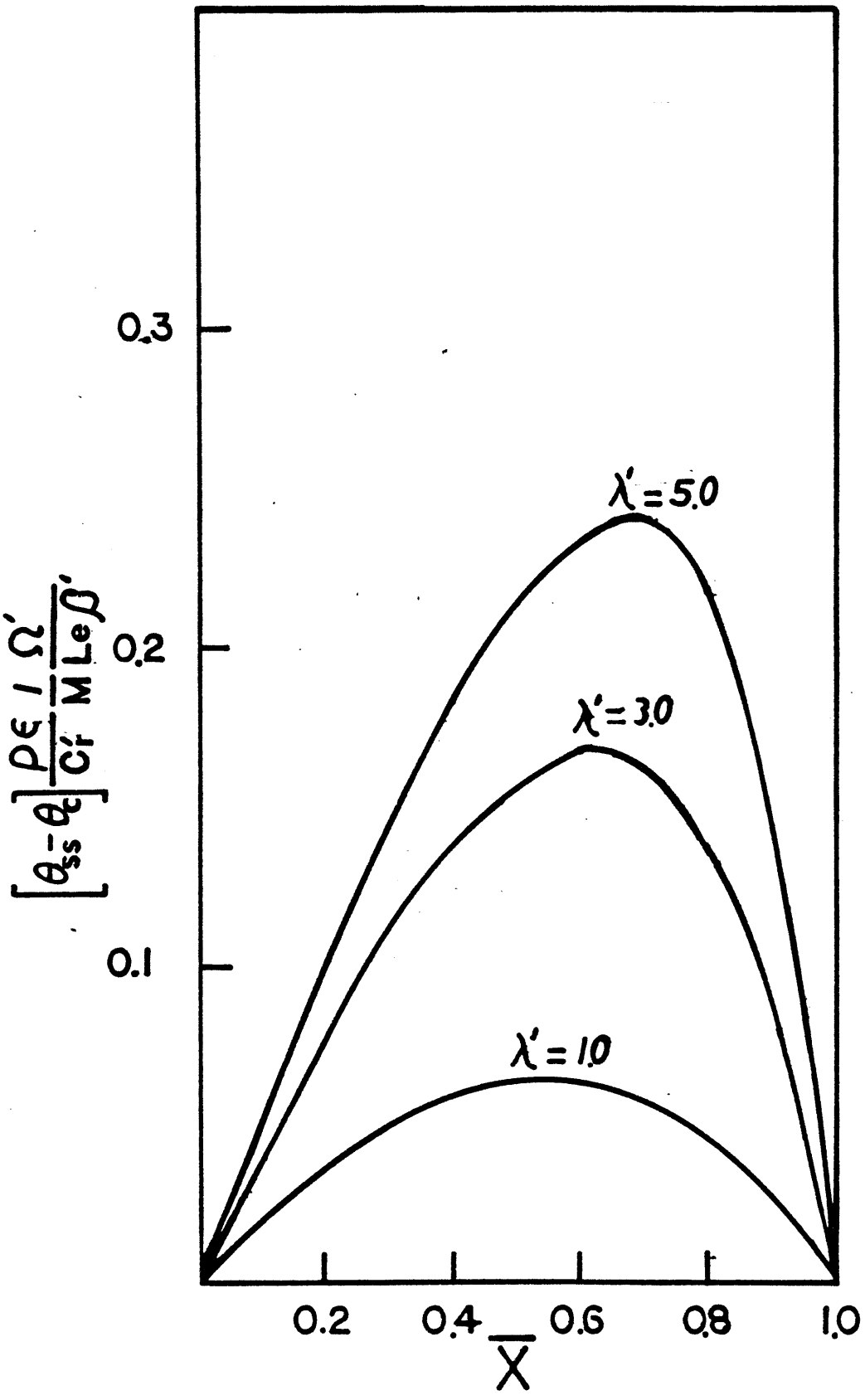

Fig. 2.4.3 The normalized steady-state liquid-content-Profile for nonzero values of liquid-diffusivity.

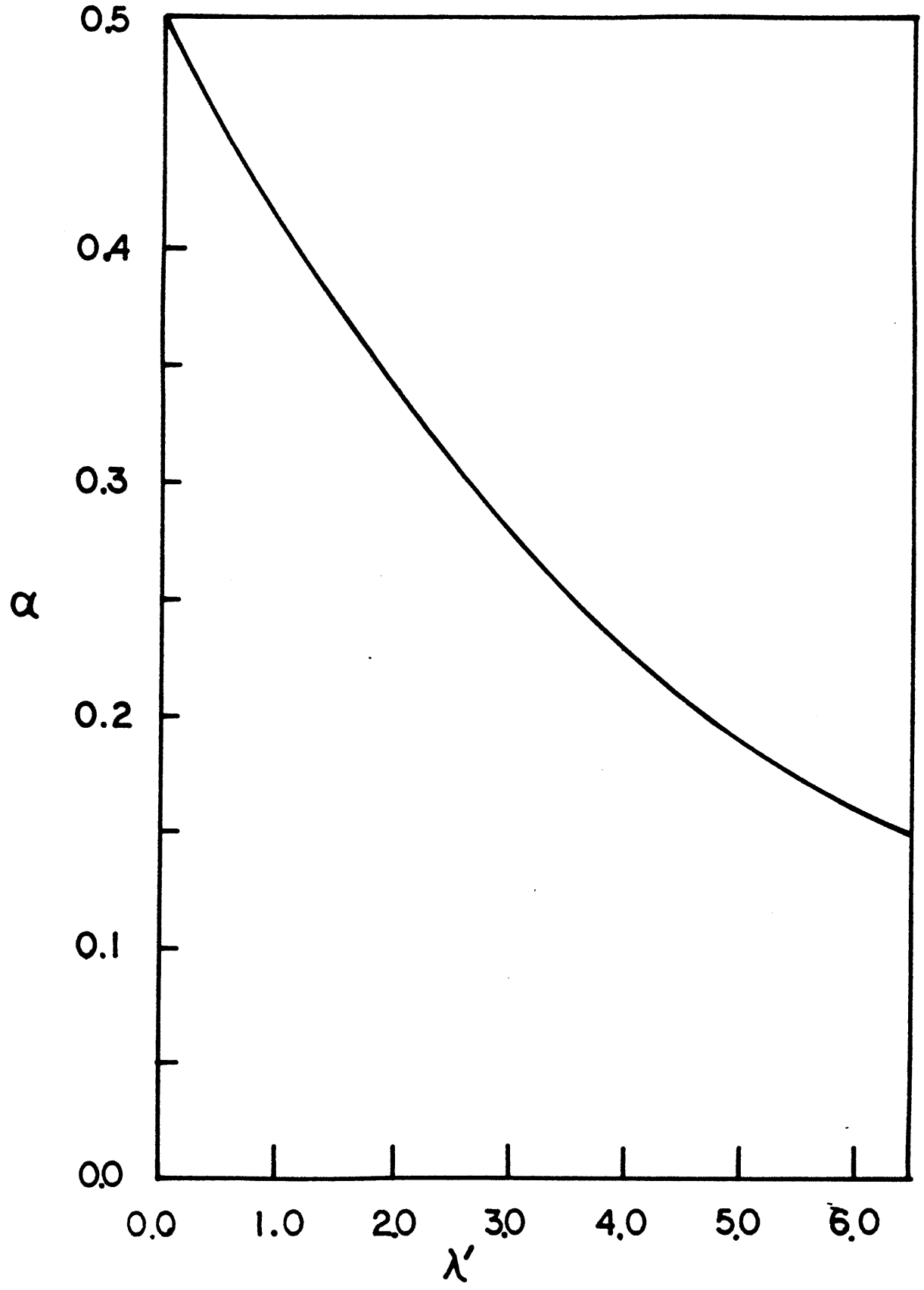

Fig. 2.4.4 The plot of the percentage of condensate leaving the condensation region at x=0, versus the latent heat transport coefficient.

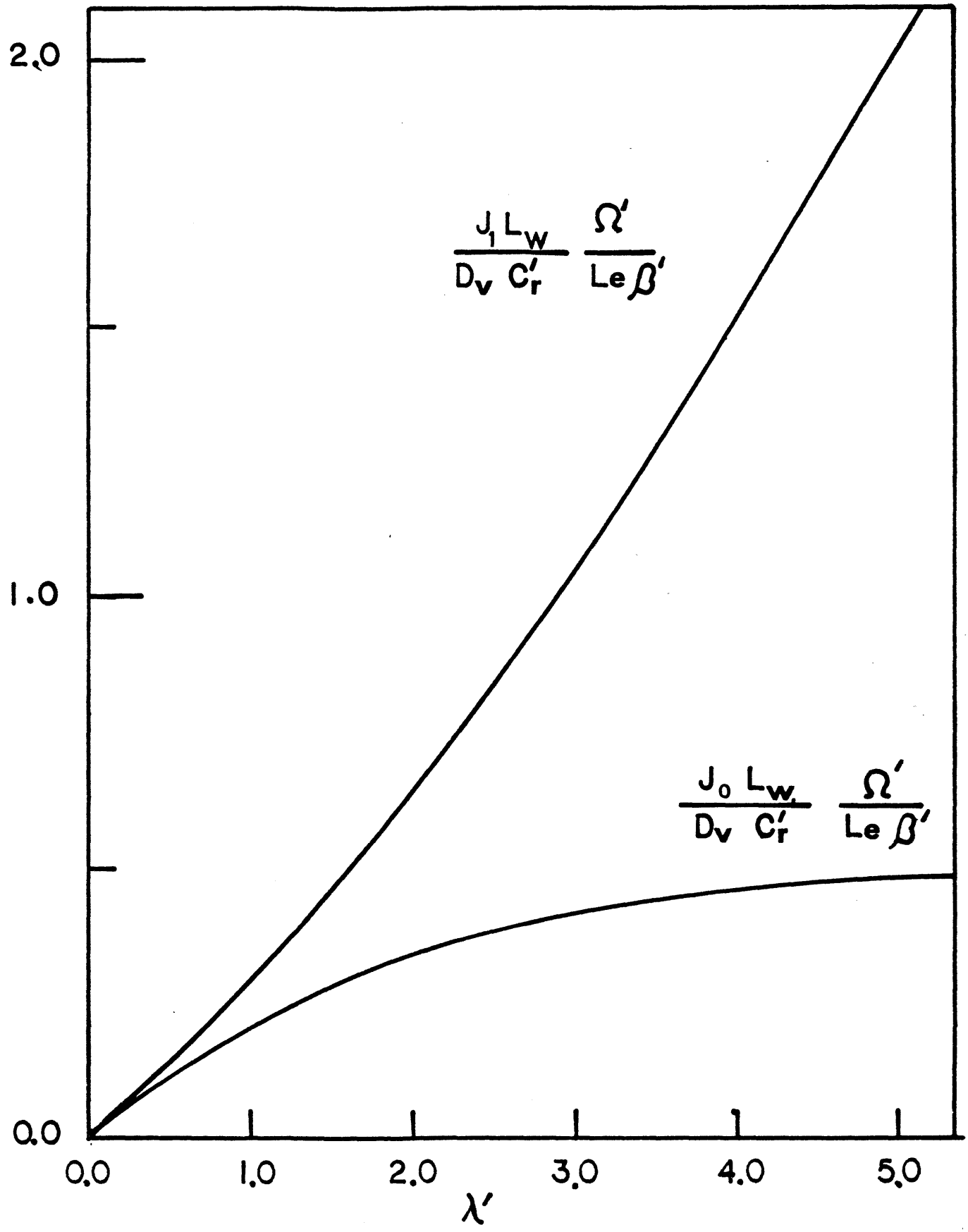

Fig. 2.4.5 Variations of liquid-fluxes leaving the two sides of the condensation-region with the latent heat transport coefficient.

2.5 HEAT AND MASS TRANSFER WITH CONDENSATION IN A POROUS SLAB

CASE I: IMMOBILE CONDENSATE

In section 2.3 the temperature profile in the condensation-zone was obtained. In section 2.4 the phenomenon of liquid diffusion in porous media was studied. It was there shown that for immobile condensates the rate of increase of liquid-content, in non-dimensional form, is of the following form:

$$\frac{d\theta}{dFo'} = \frac{C'r}{\rho\epsilon} \cdot \frac{Le\ \beta'}{\Omega'} \cdot \frac{\lambda'^2}{2} \cdot \frac{\exp \lambda' \bar{x}}{\exp \lambda' - 1} \qquad [2.4.12]$$

At this stage a new Fourier number based on the total length of the slab is defined:

$$Fo^* = Fo' \ (L_T/L_w)^2$$

Then eq. [2.4.12] may be written as:

$$\frac{d\theta}{dFo^*} = \left(\frac{L_T}{L_w}\right)^2 \frac{C'_r \, Le \, \beta'}{\rho \epsilon \Omega'} \frac{\lambda'^2}{2} \frac{\exp \lambda' \bar{x}}{\exp \lambda' - 1} \qquad [2.4.12(b)]$$

The right hand side of the above equation contains two types of constants. One type depends on the properties of the medium and the condensate: M, ρ, ϵ. The other type depends on the values of temperature at the two boundaries of the condensation-zone: λ', Ω', β, C'_r. These latter numbers are functions of the mean temperature in the condensation-zone, T'_r, and the temperature drop across the condensation-zone: $\Delta T'$. The length scale is non-dimensionalized by the width of the condensation-region, L_w. The reduced temperature distribution of section 2.3, and the results of sectin 2.4 were obtained by treating T'_r, $\Delta T'$, and L_w as floating parameters. In this section the length-scale L_w, the location of the condensation-region in the slab, and the boundary temperatures are obtained by matching the temperature and vapor-concentration profiles in the condensation-region with those of the adjacent dry regions.

Recall the original problem, Fig. 2.5.1. A porous slab seperates two reservoirs with different temperatures and vapor-concentrations. The relative humidity of both reservoirs is less than 100%. Vapor migrates from the reservoir of high vapor-concentration to the reservoir with lower vapor-concentration. The diffusing vapor condenses into liquid in some region of the porous slab, sandwiched between two dry regions. The temperature and vapor-concentration profiles in the dry regions can be easily shown to be linear. Let the total length of the slab be L_T, and the length scale in the slab be

denoted by z. The x-scale is used for the condensation-zone. Hence,

$z = L_0$ Corresponds to $\overline{x} = 0$

$z = L_1$ Corresponds to $\overline{x} = 1$

$L_0 - L_1$ Corresponds to L_w.

The process of matching the temperature and concentration profiles at the boundaries of the condensation-region and the adjacent dry regions consists of imposing conditions of equality of temperature, vapor-concentration, vapor-flux and heat-flux. At $\overline{x}=0$,corresponding to $\overline{z}=L_0$, continuity of heat-flux and vapor-flux can be written as:

$$\frac{T_h - T_0}{L_0} = - \left. \frac{dT^*}{dz} \right|_{L_0} \qquad [2.5.1]$$

and,

$$\frac{C_h - C^*_0}{L_0} = - \frac{dC^*}{dz}\bigg|_{L_0} \qquad [2.5.2]$$

The continuity of the fluxes at $\bar{x}=1$, corresponding to $z=L_1$, is:

$$\frac{T_1 - T_c}{L_T - L_1} = - \frac{dT^*}{dz}\bigg|_{L_1} \qquad [2.5.3]$$

and,

$$\frac{C^*_1 - C_c}{L_T - L_1} = - \frac{dC^*}{dz}\bigg|_{L_1} \qquad [2.5.4]$$

In the condensation-region the vapor and liquid co-exist in equilibirium. Clearly, then, vapor is at saturation concentration throughout the condensation-region. This is indicated by the asterisk in the C* term. Also the temperature in the condensation-region is identified by the asterisk.

Four unknowns are associated with equations [2.5.1] through [2.5.4]. The unknows are: T_0, T_1, L_0, and L_1. Hence, there are sufficient number of equations to solve for the four unknowns.

Let the temperature be non-dimensionalized with reference to a new mean temperature and temperature-drop:

$$T_r = \frac{T_h + T_c}{2}$$

$$\Delta T = T_h - T_c$$

$$\eta = \frac{T - T_r}{\Delta T} \qquad [2.5.5(a)]$$

The reference temperature T_r is the mean temperature of the slab, and ΔT is the temperature drop across the slab. With the above definitions the reduced temperature varies from 0.5 to -0.5 across the slab:

$$\eta = 0.5 \qquad @\ \overline{z} = 0$$

$$\eta = -0.5 \qquad @\ \overline{z} = 1.$$

Associated with the definitions of T_r and ΔT, a new set of non-dimensional parameters are defined:

$$\beta = \Delta T / T_r$$

$$\Omega = h_{fg}\, C_r / \rho\, c_p\, T_r$$

$$\nu = h_{fg} / R\, T_r \qquad [2.5.5(b)]$$

The terms defined in eq. [2.5.5] have conjugates defined with respect to the mean temperature and temperature drop across the condensation-zone. The ones defined for the condensation-zone are differentiated from the above by carrying a prime superscrpit. The primed-quantites (e.g. η'. λ',etc.) can be transformed into unprimed quantities easily, once $\Delta T'$ and T'_r are given in terms of ΔT and T_r.

Equations [2.5.1] through [2.5.4] are non-linear and coupled. In order to solve for the unknowns the equations must be solved simultaneously. As the schemes for solution of systems of coupled nonlinear equations are not necessarily convergent, the four equations are manipulated in order to reduce the coupling between them. Consider eq. [2.5.2]:

$$\frac{C_h - C^*_0}{L_0} = - \left. \frac{dC^*}{dz} \right|_{L_0} \qquad [2.5.2]$$

As C* is a unique function of temperature, the above can be written as:

$$\frac{h_h C^*_h - C^*_0}{L_0} = - \left. \frac{dC^*}{dT} \cdot \frac{dT}{dz} \right|_{L_0} \qquad [2.5.6]$$

Eliminating the L_0 term between the above and eq.[2.5.1] yields:

$$\frac{h_h C^*_h - C^*_0}{T_h - T_0} = \left. \frac{dC^*}{dT} \right|_{T_0} \qquad [2.5.7]$$

Equation [2.5.7] is an implicit equation in terms of T_0. Similarly, an implicit equation for T_1 can be obtained by eliminating the length-scale between eqs. [2.5.3] and [2.5.4]:

$$\frac{C^*_1 - h_c C^*_c}{T_1 - T_c} = \left. \frac{dC^*}{dT} \right|_{T_1} \qquad [2.5.8]$$

The saturation vapor-concentration is a unique function of

temperature. Using the Clausius-Clapeyron relation and the perfect gas approximations for vapor, the following relations were obtained in section 2.3:

$$C^* = C_r \exp \frac{\gamma \beta \eta}{1+\beta \eta} \qquad [2.5.9]$$

and,

$$\frac{dC^*}{dT} = \frac{C^* h_{fg}}{R T^2} \qquad [2.5.10]$$

Using the above approximations, eqs. [2.5.7] and [2.5.8] become, respectively:

$$\frac{h_h \exp[\Phi_h] - \exp[\Phi_0]}{\eta_h - \eta_0} = \gamma \beta (1+\beta \eta_0)^{-2} \exp[\Phi_0] \qquad [2.5.11]$$

and,

$$\frac{\exp[\Phi_1] - h_c \exp[\Phi_c]}{\eta_1 - \eta_c} = \gamma\beta(1+\beta\eta_1)^{-2} \exp[\Phi_1] \qquad [2.5.12]$$

The two equations are implicit functions of the two unknowns, η_0 and η_1. There is no length-scale coupling between them. The equations can be further simplified by the following approximation:

$$(1 + \eta\beta) \sim 1$$

Then eq. [2.5.11] becomes:

$$1 - h_h \exp\left[\gamma\beta\tau_h[\eta_h - \eta_0]\right] + \gamma\beta[\eta_h - \eta_0] = 0 \qquad [2.5.13]$$

and eq.[2.5.12] becomes:

$$1 - h_c \exp\left[\gamma\beta\tau_c[\eta_c - \eta_1]\right] + \gamma\beta[\eta_c - \eta_1] = 0 \qquad [2.5.14]$$

where τ_h and τ_c are correction factors, and are approximately equal to one. Equations [2.5.13] and [2.5.14] are both of the form:

$$1 - h_i \exp(u_i) + u_i = 0 \qquad i=c,h \qquad [2.5.15]$$

where

$$u_c = \eta_c - \eta_1 \qquad < 0$$

$$u_h = \eta_h - \eta_0 \qquad > 0 \qquad [2.5.16]$$

A plot of eq. [2.5.15] , for τ_i=1, is given in Fig. 2.5.2. For a given value of humidity the equation has two u-roots: one positive and one negative. The positive values of u correspond to η_0 and the negative values correspond to η_1. When the cold side humidity, h_c, is put into eq. [2.5.15] the negative root must be used, and when h_h is used the correct root to use is the positive one. Hence, given the humidity levels at the hot-side and cold-side, the roots of eq. [2.5.15] can be obtained (either graphically or numerically), to generate the values of η_0 and η_1 from eq. [2.15.16].

Once the values of η_0 and η_1 are known, the values of T', and T'_r can be generated:

$$\Delta T' = (\eta_0 - \eta_1)\,\Delta T$$

$$T'_r = (\eta_0 + \eta_1)\,\Delta T + T_r \qquad [2.5.17]$$

With values of $\Delta T'$ and T'_r known, the paramters that define the solution of section 2.3, e.g. λ', Ω', etc., can be readily calculated.

The four original boundary conditions, eq. [2.5.1]-[2.5.4] were combined to generate two equations, eqs. [2.5.7] and [2.5.8]. The two equations were then solved to generate η_0 and η_1. As the four original equations were independant, and that only two of the unknowns are solved for, any two of the original four may be used to solve for the length-scales. Consider the following equations which imply continuity of heat-flux at the boundaries:

$$\frac{\eta_h - \eta_0}{\overline{L}_0} = - \left.\frac{d\eta}{dz}\right|_{\overline{L}_0} \qquad [2.5.18]$$

and,

$$\frac{\eta_1 - \eta_c}{1 - \bar{L}_1} = - \left. \frac{d\eta}{dz} \right|_{1-\bar{L}_1} \qquad [2.5.19]$$

By applying the chain rule to the right-hand side of the two equations, the following is obtained:

$$\frac{\eta_h - \eta_0}{\bar{L}_0} = - \left. \frac{d\eta}{d\eta'} \cdot \frac{d\bar{x}}{d\bar{z}} \cdot \frac{d\eta'}{d\bar{x}} \right|_{\bar{x}=0} \qquad [2.5.20]$$

$$\frac{\eta_1 - \eta_c}{1 - \bar{L}_1} = - \left. \frac{d\eta}{d\eta'} \cdot \frac{d\bar{x}}{d\bar{z}} \cdot \frac{d\eta'}{d\bar{x}} \right|_{\bar{x}=1} \qquad [2.5.21]$$

The temperature distribution in the condensation-zone has already been obtained in section 2.3. The gradient of reduced temperature in the condensation-zone is:

$$\frac{d\eta'}{d\bar{x}} = - \frac{1}{2} \left[1 + \frac{\lambda' \exp \lambda' \bar{x}}{\exp \lambda' - 1} \right] \qquad [2.5.22]$$

The $d\bar{z}/d\bar{x}$ term is the correction factor that must be applied to the length-scale in the condensation-zone, i.e. x-scale, to transform it to the z-scale. It is:

$$(d\bar{z}/d\bar{x}) = \bar{L}_1 - \bar{L}_0 \qquad [2.5.23]$$

The term $(d\eta'/d\eta)$ transforms the differential variations of η' to variations in η :

$$(d\eta/d\eta') = (\Delta T'/\Delta T) \qquad [2.5.24]$$

Equations [2.5.20] and [2.5.21] are solved simultaneously to generate the length-scales. The length scales are:

$$\bar{L}_1 = \frac{2\left[\frac{\Delta T}{\Delta T'}\right] + \left[1 + \frac{\lambda'}{\exp\lambda' - 1}\right]}{2\cdot\frac{\Delta T}{\Delta T'} + 2 + \frac{\lambda' \exp\lambda'}{\exp\lambda' - 1}} \qquad [2.5.25]$$

and,

$$\overline{L_0} = \frac{1 + \dfrac{\lambda'}{\exp\lambda' - 1}}{2\,\dfrac{\Delta T}{\Delta T'} + 2 + \dfrac{\lambda' + \lambda'\exp\lambda' - 1}{\exp\lambda' - 1}} \qquad [2.5.26]$$

The length-scale in the condensation-region is reduced by the $(d\bar{z}/d\bar{x})$ factor:

$$\frac{d\bar{z}}{d\bar{x}} = \frac{1}{1 + \dfrac{1}{2}\left[\dfrac{\Delta T'}{\Delta T}\;2 + \dfrac{\lambda' + \lambda'\exp\lambda'}{\exp\lambda' - 1}\right]} \qquad [2.5.27]$$

With the results obtained in this section, the case of heat and mass transfer with condensation in a porous slab with immobile condensate is completely solved. The case of immobile condensate corresponds to the early stages of condensation. Hence, the obtained solution applies only to the early stages of condensation. The period for which this solution is valid depends on the value of critical liquid-content, which is a property of the medium. Once the value of critical liquid-content is established, eq. [2.4.13(b)] or Fig. 2.4.2 may be used to calculate the length of the period over which the condensate is immobile and the results of this section apply. The temperature and the vapor-concentration distributions in the condensation-region have been obtained in section 2.3. The rate

of condensate accumulation $\Gamma(\bar{x})$ was derived in section 2.5. Those results were obtained in terms of three undefined parameters : T_0, T_1, and L_w. The length-scales and the temperature values at the boundaries of the condensation-region were obtained in this section. Hence, the solution is completed.

The analytical results obtained in this and other sections was in part due to use of Clausius-Clapeyron relation, and the perfect gas law in approximating the behavior of the vapor. The closed form solution of $\epsilon(\bar{x})$ was obtained by linearizing the energy equation. Furthermore, in the process of manipulating the boundary conditions, certain approximations were made. In order to assess the total effect of the approximations an illustrative example is solved.

ILLUSTRATIVE EXAMPLE:

In this example the analytical results are compared with the numerical solution for a specific slab with defined boundary conditions. In the numerical solution of the energy equation and the boundary equations the values of saturation vapor-concentration were obtained directly from the steam-tables. The energy equation was solved by an iterative scheme. The bounday equations were solved by the method of flase-locii.

Consider a porous slab of 1-ft thickness. The properties of the slab are similar to those of fiberglass insulation board:

$$\rho = .0763 \quad \text{lbm/Ft}^3$$

$$c_p = .24 \quad \text{BTU/lbm-°F}$$

$k = .016$ BTU/hr-ft-°F

$D_v = 0.8$ ft^2/hr

$D_l = 0.$

The values of temperature and humidity on the hot and cold sides are:

$T_h = 90.°F$

$Tc = 25.°F$

$h_h = 90\%$

$h_c = 90\%$

The boundary values are chosen such that a large portion of the slab consists of the condensation-region. Hence, the shape of the temperature profile would be more clear.

The location of the condensation-region, and the temperature distribution in the slab are calculated both numerically and analytically, and are shown in Fig. 2.5.3. The analytical soltuion is shown by circles, and the numerical results are indicated by squares. The analytical solution is very close to the numerical solution. There is some error in defining the location and width of the condensation-zone, but he agreement on the temperature distribution in the condensation-zone is extremely good. Overall the errors are negligibly small.

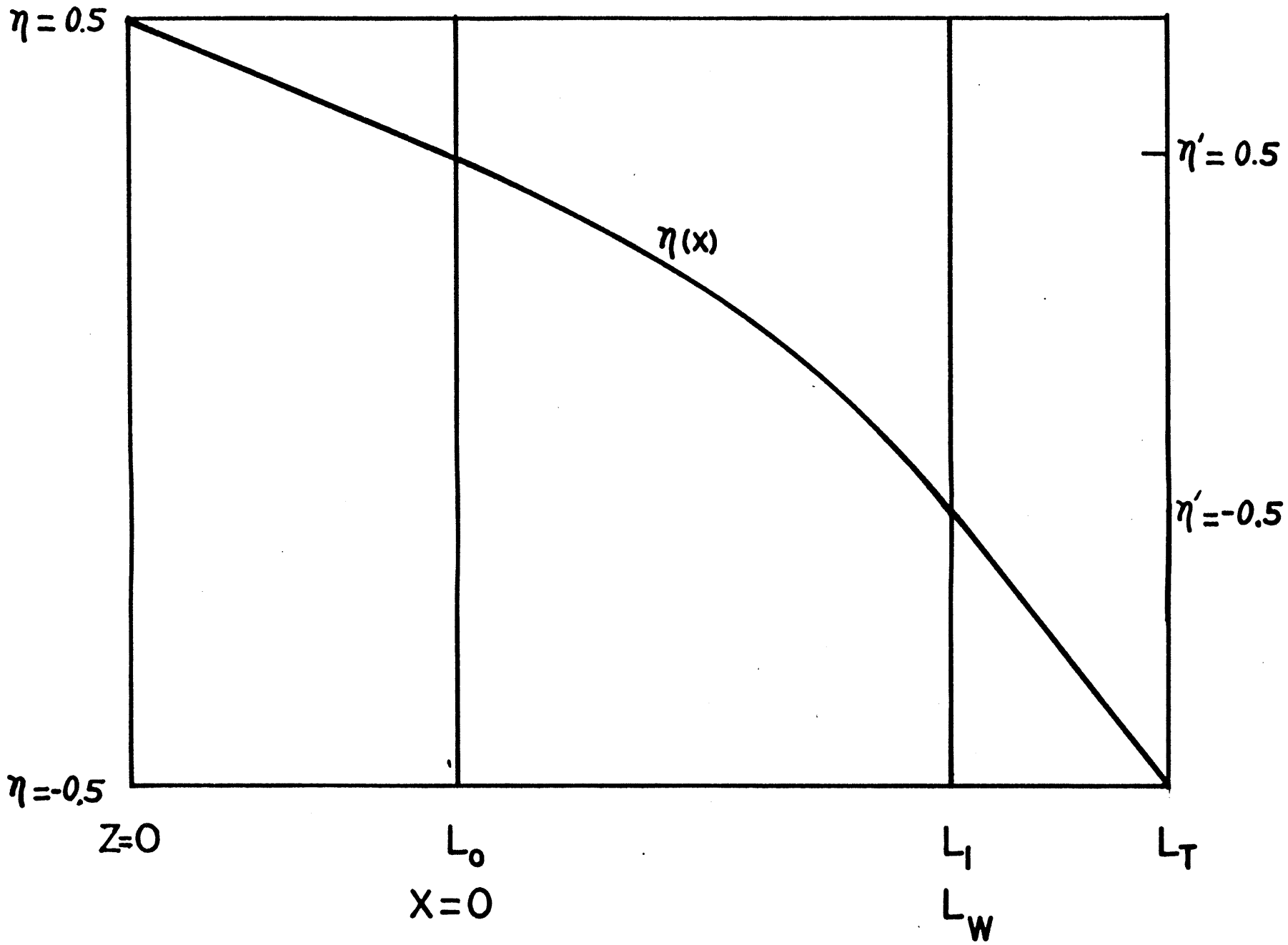

Fig. 2.5.1 Schemtaic Profile of the Matched Reduced Temperature for the case of Pendular Condensate

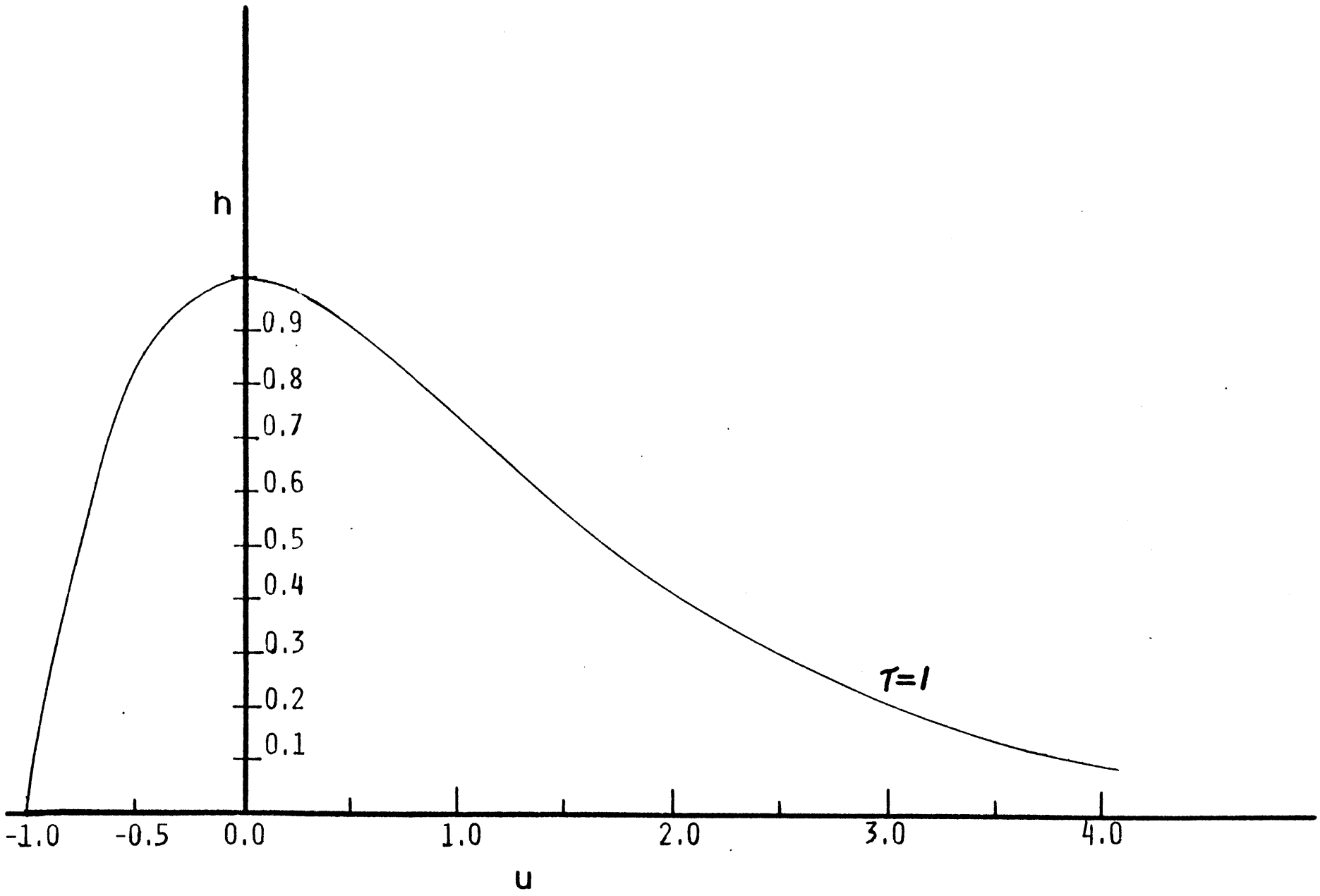

Fig. 2.5.2 Plot of the boundary equation variable u versus humidity

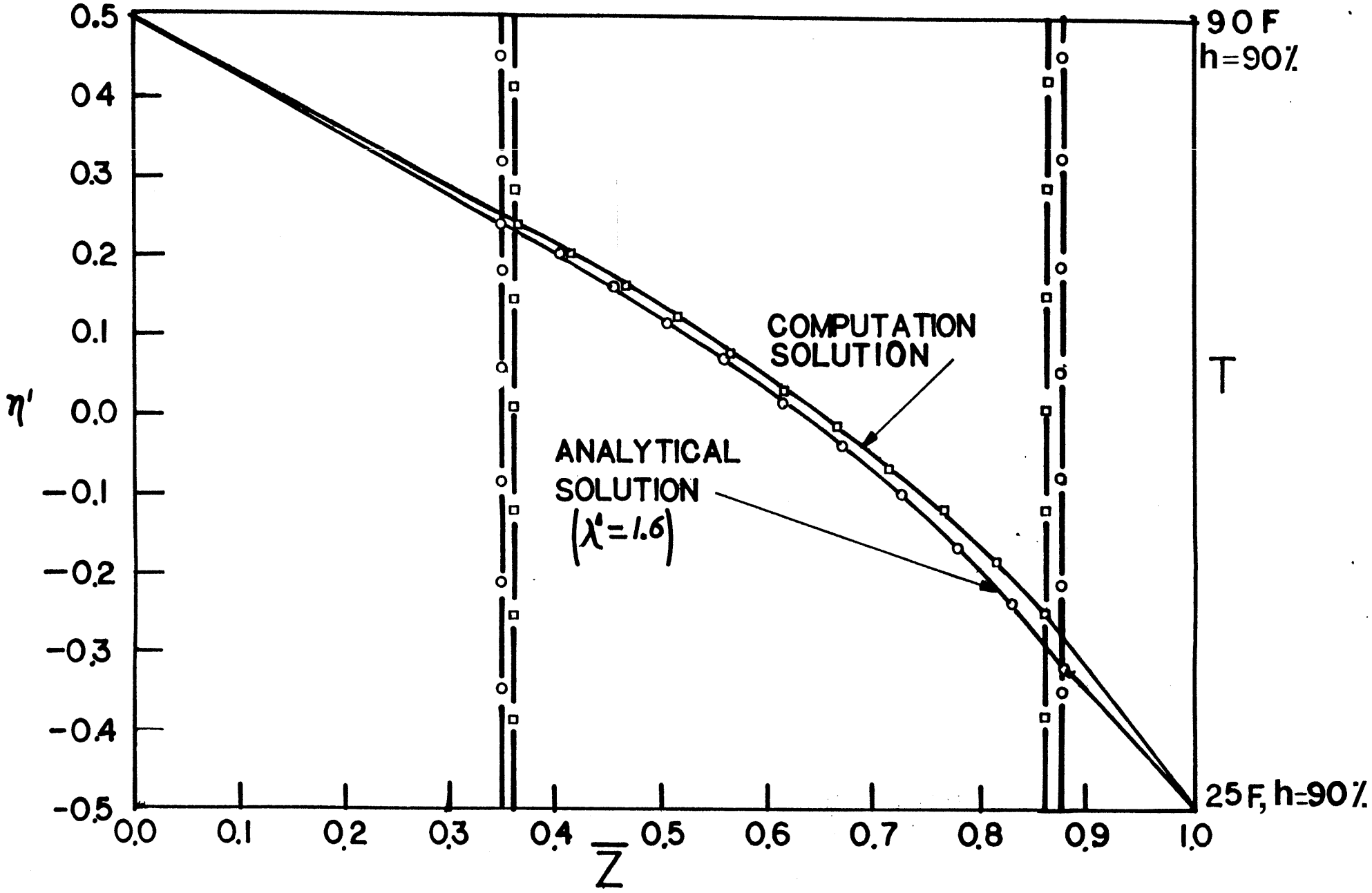

Fig. 2.5.3 Comparison of the Analytical Solution with the Numerical Results of the Reduced-Temperature Profile in a Porous Slab

2.6 HEAT AND MASS TRANSFER WITH CONDENSATION IN A POROUS SLAB

CASE II : MOBILE CONDENSATE

The phenomenon of liquid diffusion in the presence of a liquid source in a porous slab was studied in section 2.4. These results along with those of section 2.3 were used in section 2.5 to study heat and mass transfer during condensation in a porous slab for immobile condensate. In this section the phenomenon of heat and mass transfer with mobile condensate will be studied. The synthesis of the results in this and the previous section will bracket the phenomenon of condensation in a porous slab completely.

Consider Fig. 2.6.1. As before, the temperatures T_h and T_c, and relative humidity values h_h, h_c are imposed on the boundaries of the slab. Condensation occurs in some region of the porous slab. The temperature field inside the condensation-region was obtained, in section 2.3, to be :

$$\eta'(\bar{x}) = \frac{1}{2}\left[1 - \bar{x} - \frac{\exp \lambda' \bar{x} - 1}{\exp \lambda' - 1}\right]$$

According to the arguements of section 2.4, during condensation the following chain of events takes place. At the early stages of condensation the liquid is in a pendular state and does not exhibit any tendency to diffuse. During this period the liquid-content in the condensation-region increases linearly with time. The results of section 2.5 apply for this period of condensation. As the level of liquid-content increases beyond the critical value, the liquid begins to diffuse in response to the existing liquid-content gradients. Then, the liquid-content distribution undergoes a transient change until it reaches a steady-state profile. The transient and steady-state liquid content distributions are given in section 2.4 in terms of the condensation rate. The condensation rate is obtained from solution of the temperature and concentration profiles inside the slab. In this section the temperature and concentration profiles of the condensation-region are matched with those of the adjacent dry regions. Four otherwise unknown parameters emerge from this matching: the width and location of the condensation-region, and the values of temperature on the boundaries of the condensation-region, T_0, and T_1.

As the liquid-content in the medium increases beyond the critical value, the liquid-content distribution and the location of the condensing front undergoes a transient change. The solution of this transient behavior is not readily available in terms of simple and closed form functions. The transient behavior may be obtained by treating the phenomenon quasi-steadily, and obtaining the solution over a finite discrete time-steps. This is not reported in this work. The extension of the steady-state solution to obtain the transient behavior is not trivial.

The focus of this section is on the formulation of the phenomenon after the liquid-content distribution and the location of the condensation-region have reached their steady-state values. The steady-state liquid-content distribution is given by

eq. [2.4.23]:

$$\theta_s(\bar{x}) = M \frac{C'_r}{\rho \epsilon} \frac{Le\ \beta'}{\Omega'} \left\{ \frac{1}{2} \left[\bar{x} - \frac{\exp \lambda' \bar{x} - 1}{\exp \lambda' - 1} \right] \right\}$$

At steady-state the mass of condensed-vapor is equal to the amount of liquid evaporated at the boundaries, and there is no net accumulation of condensate in the medium. A fraction of the condensate leaves the condensation-region at the boundary x=0, and the remainder leaves at $\bar{x}$=1. The fraction of condensate that leaves at $\bar{x}$=0 is given by eq. [2.4.43]:

$$\alpha = \frac{\exp \lambda' - 1 - \lambda'}{\lambda' (\exp \lambda' - 1)}$$

The condensate that leaves the boundaries of the condensation-region evaporates into the adjacent dry-regions. The process of evaporation absorbs a certain amount of heat that must be supplied by conduction. The width, location and boundary temperatures of the condensation-region are determined by the conditions of continuity of heat and vapor-flux across the boundaries of the condensation-region and the adjacent dry regions. The constraint of steady-state liquid-content profile appears in the form of liquid-flux leaving the boundaries at $\bar{x}$=0, and $\bar{x}$=1.

Consider Fig. 2.6.1. As before, the z-scale and x-scale are

used to denote the length scale in the slab and in the condensation-region, respectively. At $z=L_0$ the following heat and mass balances may be written:

$$-k \frac{T_h - T_0}{L_0} = -k \left.\frac{dT^*}{dz}\right|_{L_0} + J_0 h_{fg} \quad [2.6.1]$$

and,

$$-D_v \frac{C_h - C^*_0}{L_0} = - \left.\frac{dC^*}{dz}\right|_{L_0} - J_0 \quad [2.6.2]$$

where J_0 is the liquid-flux which leaves the condensation-region. Equation [2.6.1] states that the heat-flux entering the slab at z=0 equals to the sum of heat-flux absorbed by the evaporation of the diffusing liquid, J_0, and the heat-flux conducted into the condensation-region. Equation [2.6.2] states that the amount of vapor that diffuses into the condensation-region equals the sum of vapor-flux entering the slab at $z=L_0$ and the vapor-flux created by the evaporation of the diffusing liquid-flux, J_0.

Heat and mass balance at $z=L_1$ yields:

$$-k \frac{T_1 - T_c}{L_T - L_1} + J_1 h_{fg} = - k \left. \frac{dT^*}{dz} \right|_{L_1} \qquad [2.6.3]$$

and

$$D_v \frac{C^*_1 - C_c}{L_T - L_1} = -D_v \left. \frac{dC^*}{dz} \right|_{L_1} + J_1 \qquad [2.6.4]$$

Equation[2.6.3] states that the heat-flux conducted out of the condensation-zone, i.e. at $\bar{x}$=1, provides for the evaporation of the liquid-flux, J_1, with the remainder fo the heat-flux leaving the boundary at $\bar{z}$=1. Vapor-flux leaving the slab at $\bar{z}$=1, equals the sum of the vapor-flux diffusing out of the condensation-region, and the vapor-flux created by the evaporation of the liquid-flux, J_1, eq. [2.6.4].

Equations [2.6.1]-[2.6.4] are the boundary conditions necessary to solve for T_0, T_1, L_0, L_1. However, these equations are highly nonlinear, especially due to the existence of the J_0 and J_1 terms. Brute force solution of coupled nonlinear equations often results in failure and frustration as the iteration schemes may not converge. Hence, similar to the study of section 2.5, these equations are manipulated such that the number of coupled terms is decreased. Furthermore, introduction of physical insights simplifies the equations and reveals simple relations which may be otherwise cloaked under cumbersome terms.

Under steady-state conditions, the condensate migrates towards the boundaries of the condensation-region and evaporates. Hence, as there is no net accumulation of condensate, the vapor-flux entering the slab must equal the vapor-flux leaving it:

$$D_v \frac{C^*_1 - C_c}{L_T - L_1} = D_v \frac{C_h - C^*_0}{L_0} \qquad [2.6.5]$$

By the same token, since there is no net mass change in the porous slab, there is no assocaited energy change. Therefore, the heat-flux entering the prous slab must equal to the heat-flux leaving the slab:

$$k \frac{T_h - T_0}{L_0} = k \frac{T_1 - T_c}{L_T - L_1} \qquad [2.6.6]$$

In order to reduce the coupling between the boundary equation, the length-scales in eq. [2.6.5] and [2.6.6] may be eliminated to yield:

$$\frac{T_h - T_0}{C_h - C^*_0} = \frac{T_1 - T_c}{C^*_1 - C_c} \qquad [2.6.7]$$

Non-dimensionalizing the above results in :

$$\frac{\eta_h - \eta_0}{\eta_c - \eta_1} = \frac{h_h \exp[\Phi_h] - \exp[\Phi_0]}{h_c \exp[\Phi_c] - \exp[\Phi_1]} \qquad [2.6.8]$$

The above equation defines the relation:

$$f(\eta_0, \eta_1; h_h, h_c, T_h, T_c) = 0 \qquad [2.6.9]$$

where a vlaue of η_0 corresponds to each value of η_1. The relative humidities h_h and h_c appear as the explicit parameters in the solution, whereas the temperatures T_h and T_c appear implicitly in γ and β.

Equations [2.6.1] and [2.6.3] may be combined to yield the total rate of condensation per unit area:

$$J_0 \, h_{fg} = k \frac{T_h - T_0}{L_0} + k \left. \frac{dT^*}{dz} \right|_{L_0} \qquad [2.6.10]$$

and

$$J_1 \, h_{fg} = k \frac{T_1 - T_c}{L_T - L_1} + k \left. \frac{dT^*}{dz} \right|_{L_1} \qquad [2.6.11]$$

As

$$(\dot{W}/A)_T = J_0 + J_1$$

then, using eq. [2.6.6], and the addition of eq. [2.6.10] with eq. [2.6.11] gives:

$$h_{fg} \, (\dot{W}/A)_T = -k(dT^*/dz)\Big|_{L_0} + k(dT^*/dz)\Big|_{L_1} \qquad [2.6.12]$$

Using the results of section 2.3 on $\eta'(x)$, and applying the chain-rule to eq. [2.6.12] yields:

$$(\dot{W}/A)_T = \frac{\lambda'}{2} \frac{k\,\Delta T}{h_{fg}} \frac{d\eta}{d\eta'} \frac{d\bar{x}}{d\bar{z}} \qquad [2.6.13]$$

which is identical to the results previously obtained, eq. [2.3.41]:

$$(\dot{W}/A)_T = \frac{D_v\, C'_r}{L_w} \frac{Le\ \beta'}{\Omega'} \frac{\lambda'}{2}$$

Liquid-flux J_0 which evaporates at $z=L_0$ is:

$$J_0 = \alpha\,(\dot{W}/A)_T$$

Using eq. [2.4.43]:

$$\alpha = \frac{\exp\lambda' - 1 - \lambda'}{\lambda'(\exp\lambda' - 1)}$$

results in

$$\frac{J_0\, h_{fg}}{k\,\Delta T} = \frac{d\eta}{d\eta'}\,\frac{d\bar{x}}{d\bar{z}}\,\frac{\exp\lambda' - 1 - \lambda'}{2(\exp\lambda' - 1)} \qquad [2.6.14]$$

Similarly,

$$\frac{J_1\, hfg}{k\,\Delta T} = \frac{d\eta}{d\eta'}\,\frac{d\bar{x}}{d\bar{z}}\,\frac{\lambda'\exp\lambda' - \exp\lambda' + 1}{2(\exp\lambda' - 1)} \qquad [2.6.15]$$

where as before:

$$\frac{d\eta}{d\eta'} = \frac{\Delta T'}{\Delta T}$$

and

$$\frac{d\bar{x}}{d\bar{z}} = \frac{1}{\bar{L}_1 - \bar{L}_0}$$

Equation [2.6.9] is one implicit equation which relates η_0

and η_1. Once one other equation of the form:

$$f_2(\eta_0, \eta_1; h_h, h_c, T_h, T_c) = 0 \qquad [2.6.16]$$

is identified, the two can be solved, in theory, to generate η_0 and η_1. As we would like f_2 to be independant of the length scales, the choice of startegies in manipulating the boundary equations is limited. The equations with the same length-scale must be paired together: [2.6.1] with [2.6.2], and [2.6.3] with [2.6.4]. Then the length scale is eliminated between each pair. This will generate two new equations.

Consider eqs. [2.6.1] and [2.6.2]. The length-scale is eliminated by dividing the two equations onto eachother:

$$\frac{C_h - C^*_0}{T_h - T_0} = - \frac{J_0 + D_v \left.\frac{dC^*}{dz}\right|_{L_0}}{J_0 h_{fg} - k \left.\frac{dT^*}{dz}\right|_{L_0}} \qquad [2.6.17]$$

Using the Clausius-Clapeyron relation, and the ideal gas law, eq.[2.6.17] becomes:

$$\frac{h_h \exp[\Phi_h] - \exp[\Phi_0]}{\eta_h - \eta_0} =$$

$$0.5\gamma\beta\left[1 + \frac{\lambda'}{\exp\lambda' - 1}\right](1+\eta_0\beta)^{-2}\exp[\Phi_0] +$$

$$- \frac{Le}{\Omega\gamma}\left(1 - \frac{\lambda'}{\exp\lambda' - 1}\right) \qquad [2.6.18]$$

where,

$$\Phi_i = \frac{\gamma\beta\eta_i}{1+\beta\eta_i} \qquad i=, h, c, 0, 1$$

By the same argument eqs.[2.6.2] and [2.6.3] may be combined to yield:

$$\frac{h_c \exp[\Phi_c] - \exp[\Phi_1]}{\eta_c - \eta_1}$$

$$0.5\gamma\beta\left[1 + \frac{\lambda' \exp\lambda'}{\exp\lambda' - 1}\right](1+\eta_1\beta)^{-2}\exp[\Phi_1] +$$

$$- \frac{Le}{\Omega \gamma} \left[1 - \frac{\lambda' \exp \lambda'}{\exp \lambda' - 1} \right] \qquad [2.6.19]$$

In eq. [2.6.18] η_1 , and in eq. [2.6.19] η_0 appear implicitly in λ'. Hence these two equations are implicit in terms of and η_0, and η_1. There are now three implicit equations involving η_0 and η_1: eqs. [2.6.8], [2.6.18], and [2.6.19]. Of these any two are independant and can be used in a successive iteration scheme to solve for η_0 and η_1. The last part of this section is devoted to a brief discussion on the proper choice of the equations as it relates to the convergence of the iterative schemes.

Once the values of η_0 and η_1 are known, the length scales can be obtained from the boundary equations. Consider eq. [2.6.1]:

$$k \frac{T_h - T_0}{L_0} = -k \left. \frac{dT^*}{dz} \right|_{L_0} + J_0 h_{fg}$$

and eq. [2.6.14]

$$\frac{J_0 h_{fg}}{k \Delta T} = \frac{d\eta}{d\eta'} \frac{d\bar{x}}{d\bar{z}} \frac{\exp \lambda' - 1 - \lambda'}{2(\exp \lambda' - 1)}$$

Equations [2.6.1] is non-dimensionalized into the following form:

$$\frac{\eta_h - \eta_0}{\overline{L_0}} = \frac{1}{2} \frac{d\eta}{d\eta'} \frac{d\overline{x}}{d\overline{z}} \left(1 + \frac{\lambda'}{\exp\lambda' - 1}\right) + \frac{J_0 \, h_{fg}}{k \, \Delta T} \quad [2.6.20]$$

Combining the above with eq. [2.6.14] yields the following simple result:

$$\frac{\eta_h - \eta_0}{\overline{L_0}} = \frac{d\eta}{d\eta'} \frac{d\overline{x}}{d\overline{z}} \quad [2.6.21]$$

Similarly, eq.[26.13] and eq.[2.6.15] are combined to yield:

$$\frac{\eta_1 - \eta_c}{1 - \overline{L_1}} = \frac{d\eta}{d\eta'} \frac{d\overline{x}}{d\overline{z}} \quad [2.6.22]$$

The above result was expected beacause it indicates that the heat-flux entering the slab is equal to the heat-flux leaving it:

$$\frac{\eta_h - \eta_0}{\overline{L_0}} = \frac{\eta_1 - \eta_c}{1 - \overline{L_1}}$$

Recognizing

$$(dz/dx) = \overline{L_1} - \overline{L_0}$$

and

$$(d\eta/d\eta') = (\Delta T'/\Delta T)$$

$$\eta_h = 0.5$$

$$\eta_c = -0.5$$

Then,

$$\overline{L_0} = \frac{\eta_h - \eta_0}{\frac{\Delta T}{\Delta T'} + 1 - (\eta_0 - \eta_1)} \qquad [2.6.23]$$

and,

$$\overline{L_1} = \frac{\frac{\Delta T}{\Delta T'} + (\eta_h - \eta_0)}{\frac{\Delta T}{\Delta T'} + 1 - (\eta_0 - \eta_1)} \qquad [2.6.24]$$

With η_0 and η_1 known, the above two equations yield the values of L_0 and L_1.

The solution of systems of nonlinear equations is a topic of current research. There are no general prescriptions, and each case must be studied individually. In the solution of systems of nonlinear equations extra care must be taken to ensure the convergence of the iteration scheme. When the two equations to be solved iteratively are chosen, each is identified to accept one of the unknowns as an input and supply the other unknown as the output. The equations must be arra ed such that the output would correspond to the zero of the function. The method of false-locii [73] offers an efficient method for obtaining the zero of an implicit function. The output of one equation is then supplied to the other equation as the input. Following this approach successively the two unknowns could converge to the roots of the two equations. One necessary condition for convergence is the form of the equations. Each equation may be

written in a variety of forms, however, it is necessary that the derivative of the function with respect to the unknown variable be less than one [73]. The other necessary condition for convergence is to start the iteration sufficiently close to the final values. This condition offers an insurmountable obstacle in many cases, and many initial values must be tried before the final solution is obtained. However, in the problem under study the inital values of η_0, and η_1 may be supplied by the solution of the immobile condensate problem, section 2.5. The values of η_0 and η_1 are obtained by the simultaneous solution of two of the three equations: [2.6.8], [2.6.18], and [2.6.19]. The three equations are non-linear and implicit in η_0 and η_1. Equation [2.6.8] was used to calculate η_0 for a given value of η_1. Equation [2.6.19] accepted η_0 as the input and would calculate η_1. The successive iteration of these two equations converges to the final soltuion within ten to fifteen iterations.

In summary, the problem of heat and mass tranfer with phase change for mobile condensates was studied in this section. The equations describing the temperature profile, location and width of the condensation-region are obtained. In order to demonstrate the solution technic developed in this chapter, an illustrative example is presented.

ILLUSTRATIVE EXAMPLE

In this example the steady-state position, and the temperature and concentration profiles of the condensation-region in a porous slab are obtained. The boundary conditions are:

$T_h = 90.°F$

$T_c = 25.°F$

$h_h = 90\%$

$h_c = 90\%$

The properties of the slab are given in the illustrative example of section 2.5. The two eqs. [2.6.8] and [2.6.9] are solved simultaneously to generate the values of η_0 and η_1. The solution of the two equations consists of a successive iteration scheme, where the output of one equation is used as the input to the other. It may be recalled that one condition for the convergence of the iterative scheme is to start the iteration with values which are sufficiently close to the final answers. The values of η_0 and η_1 obtained from the solution of the problem for the case of non-diffusive condensate, section 2.5, are used as the initial guesses. The iteration scheme converges to the following values of η_0 and η_1:

$\eta_0 = .3997$

$\eta_1 = -.4856$

Equations [2.6.23] and [2.3.24] are used to generate the length-scales:

$$\overline{L_0} = .1$$

$$\overline{L_1} = .986$$

The latent heat transport coefficient, λ', has a numerical value of 2.52. The temperature profile inside the condensing-region is generated using this value of λ'. The above information is presented in Fig. 2.6.2.

The discontinuities in the temperature profile at the boundaries is indicative of the amount of energy absorbed by the evaporation of the liquid-fluxes, J_0 and J_1. The location of the condensation-region obtained for the above boundary conditions for the case of immobile condensates is also shown and compared with these results in Fig. 2.6.3. The comparison of the two results indicates that liquid-diffusion leads to the enlargement of the condensation-region. For the case of diffusive condensate, the heat-flux into the slab at $\overline{z}=0$ is larger than the heat-flux associated with the non-diffusive condensate. The same relation holds for the heat-flux leaving the slab at $\overline{z}=1$.

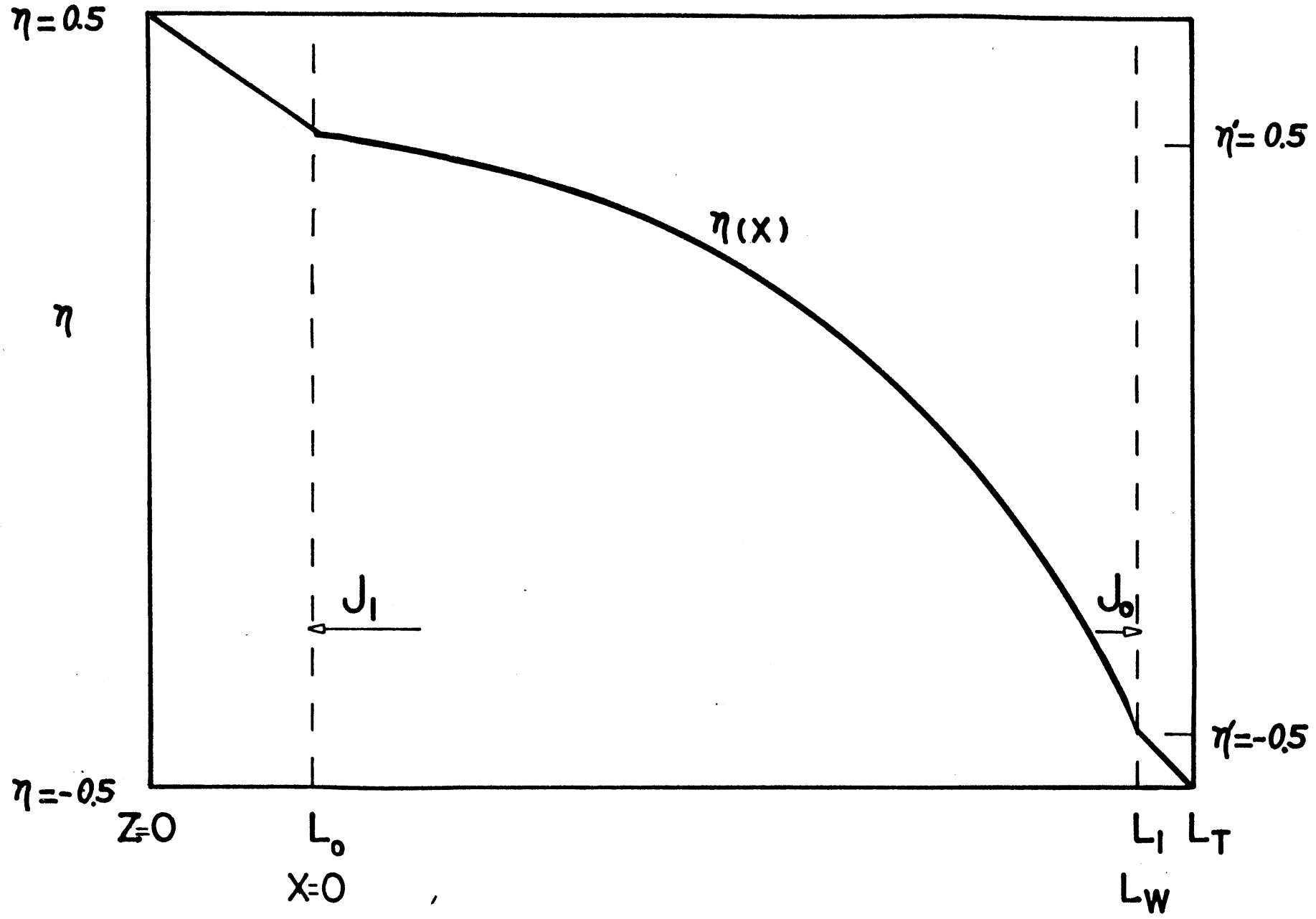

Fig. 2.6.1 Schematic Profile of the Matched Reduced-Temperature Profile for the Case of Diffusive Condensate

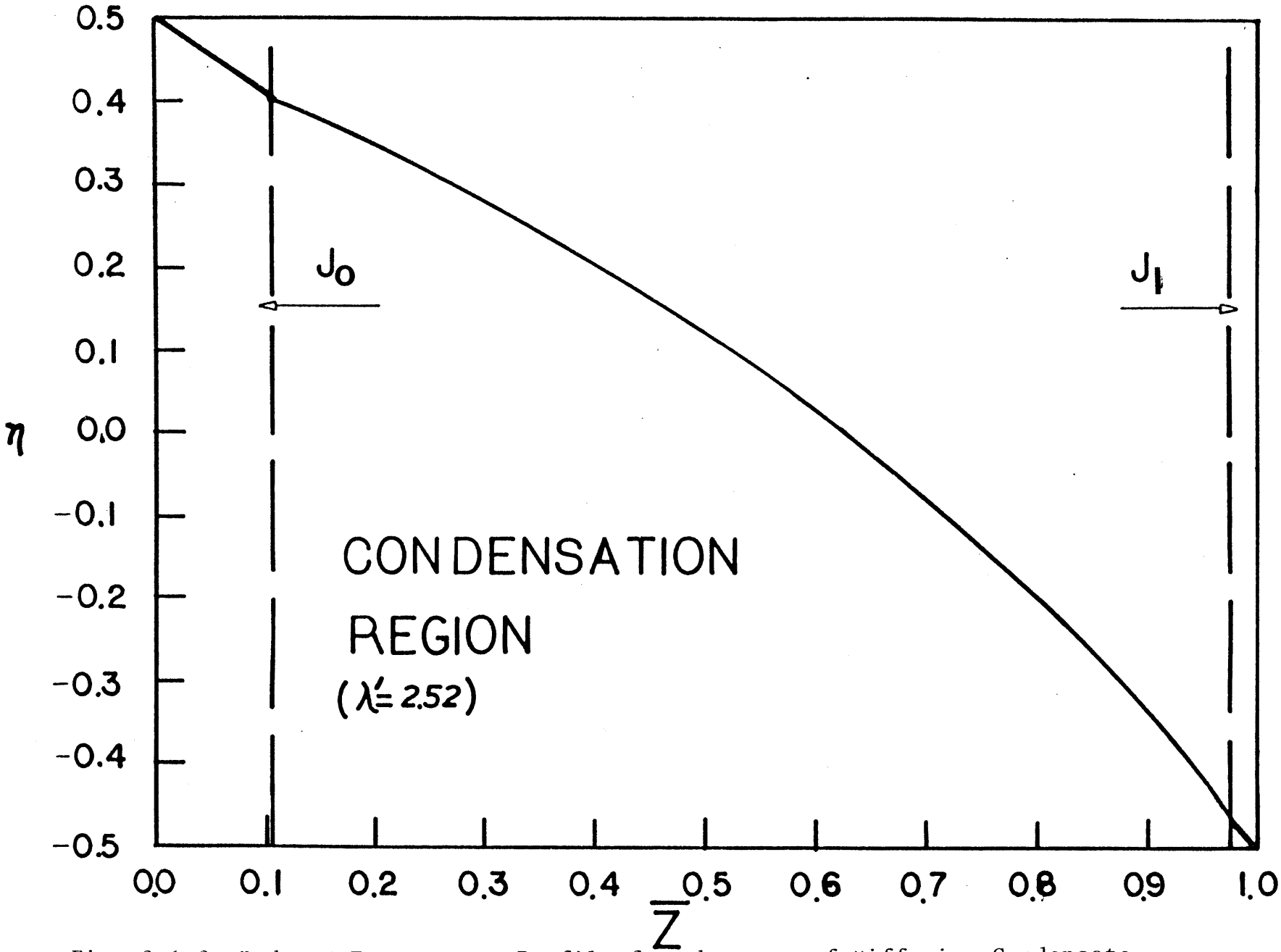

Fig. 2.6.2 Reduced-Temperature Profile for the case of Diffusive-Condensate

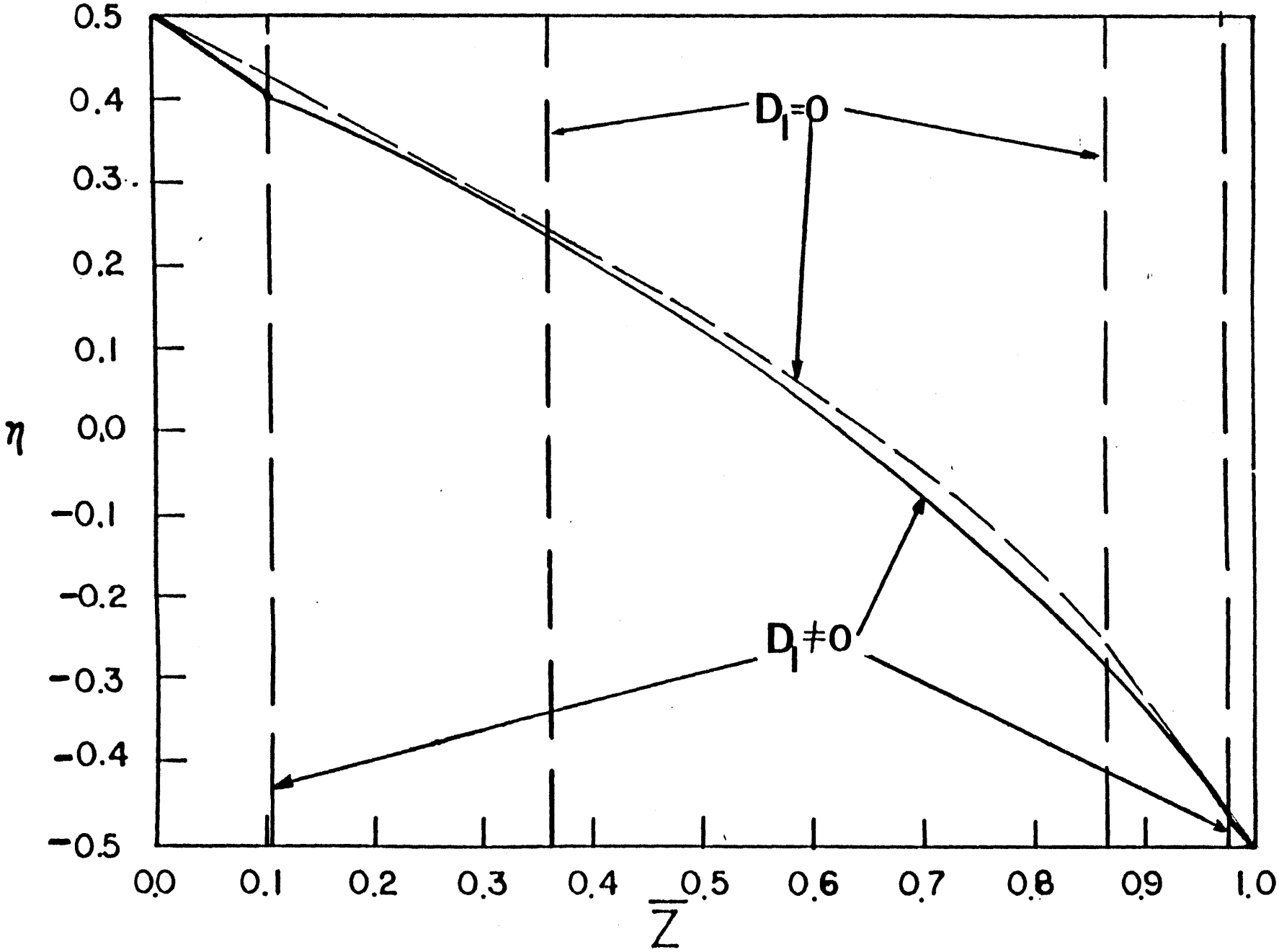

Fig. 2.6.3 Comparison of the Reduced Temperature Profile for Non-Diffusive and Diffusive Condensate

2.7 EFFECTS OF HEAT AND VAPOR CONVECTION ON CONDENSATION IN A POROUS SLAB

The study of heat and mass transfer of the previous sections was performed by considering only the diffusional mode of heat and vapor transport. In this section the effects of convective transport will be discussed.

Mass and heat convection are associated with the bulk flow of a species that has the capacity to store and transmit heat and mass. The carrier species obeys the phenomenological transport realtions, in the sense that the flux of the species is proportional to the gradient of its conjugate potential. In the case of heat and mass tranport in a porous medium, the carrier is a gas, most probably air. The air-flux is associated with the pressure gradient across the slab:

$$U = -D \vec{\nabla} P \qquad [2.7.1]$$

D'Arcy's Law has historically been used to define the laminar flow of fluids in porous media. For a one-dimensional flow:

$$u = - \frac{k^*}{\mu} \frac{dP}{dx} \qquad [2.7.2]$$

where

k^* = permeability of the porous medium

μ = fluid viscosity.

The medium permeability, k^*, depends on the internal geometry and structure of the medium. For a porous slab of known width L_T, and pressure boundary values P_0 at $\bar{x}=0$, and P_1 at $\bar{x}=1$, eq. [2.7.2] may be written as:

$$u = \frac{k^*}{\mu} \frac{P_0 - P_1}{L_T} \qquad [2.7.3]$$

The above indicates that once the pressure values of the two reservoirs, Fig. 2.2.1, and the medium permeability are known, the infiltration velocity, u, can be directly calculated. In the following the effects of convection on heat and vapor-flux continuity in the condensation-region is discussed first. Then, the energy and continuity equations for the dry-zones are

developped. Third, the boundary equations necessary to match the solutions of the condensation-region with those of the dry regions are given. In the last section, the effect of convection on the condensation rate and liquid diffusion is discussed.

The heat-flux per unit area convected out of a differential element of the medium with thickness Δx is:

$$(\dot{q}/A)_{conv} = \rho c_p u (dT/dx) \Delta x \qquad [2.7.4]$$

where

ρ = density of the infiltrating species

c_p = specific heat capacity of the infiltrating species

The product ρc_p indicates the capacity of the carrier species, in this case air, to store heat. The above convection term is introduced into the energy equation of the condensiong-region, eq. [2.3.7], to yield

$$k(d^2T/dx^2) - \rho c_p u (dT/dx) + \Gamma h_{fg} = 0 \qquad [2.7.5]$$

Vapor-flux per unit area convected out of the differential element is:

$$(\dot{W}/A)_{in} = -u(dC/dx)\,\Delta x \qquad [2.7.6]$$

Combining the above with the vapor-continuity equation in the condensation-region, eq. [2.3.5] yields:

$$D_v (d^2C^*/dx^2) - u(dC^*/dx) = \Gamma \qquad [2.7.7]$$

Note that in the above the vapor-concentration is at saturation levels, and is denoted by C^*. Equations [2.7.5] and [2.7.7] can be combined by eliminating the condensation rate $\Gamma(x)$. The resulting equation is non-dimensionalized into the following form:

$$\frac{d^2\eta'}{dx^2} - Pe\,\frac{d\eta'}{dx} + \frac{\Omega'}{Le\ \beta'}\,\frac{d^2\bar{C}^*}{d\bar{x}^2} - PeLe\,\frac{d\bar{C}^*}{d\bar{x}} = 0 \quad [2.7.8]$$

where

$$Pe\ (\text{Peclet Number}) = (\rho\, c_p\ u\ L_w/k)$$

Peclet number indicates the ratio of heat transported by convection to heat transferred by conduction. The other non-dimensional groups and variables which appear in eq. [2.7.8] are all defined in eqs. [2.3.10] and [2.3.12]. The saturation vapor-concentration is a unique function of temperature. The Clausius-Clapeyron relation, eq.[2.3.14], and the perfet gas law, eq. [2.3.15] are used to define the functional dependence of saturation vapor-concetration on temperature. Introducing the above into eq. [2.7.8] results in a non-linear differential equation in reduced-temperature, :

$$\left[1 + \frac{\Omega'\gamma'}{Le}\,(1+\eta'\beta')^{-2}\exp[\Phi]\right]\frac{d^2\eta'}{dx^2} +$$

$$-Pe\left[1 + \Omega'\gamma'\,(1+\eta'\beta')^{-2}\exp[\Phi]\right]\frac{d\eta'}{dx} +$$

$$\left[\frac{\gamma'^2\beta'\Omega'}{Le}\,(1+\eta'\beta')^{-2}\exp[\Phi]\right]\frac{d^2\eta'}{dx^2} = 0 \quad [2.7.9]$$

where as before:

$$\Phi = \frac{\gamma' \beta' \eta'}{1 + \beta' \eta'}$$

The above is associated with the following boundary conditions:

$$\eta' = 0.5 \qquad @ \ \bar{x} = 0$$

$$\eta' = -0.5 \qquad @ \ \bar{x} = 1 \qquad [2.7.10]$$

The solution to eq. [2.7.9] may be derived by linearisation technics. Eq. [2.7.9] must be linearized around the solution to the energy equation without the condensation term :

$$(d\eta'/d\bar{x}) - Pe(d\eta'/d\bar{x}) = 0 \qquad [2.7.11]$$

The effect of convection on the temperature-distribution would be to cause an increase in the concavity of the temperature profile

obtained in section 2.3. This translates into an increase in the condensation rate.

The energy equation in the dry regions is identical to eq. [2.7.5] without the heat source term:

$$k(d^2T/dz^2) - \rho c_p u (dT/dz) = 0 \qquad [2.7.12]$$

The vapor-concentration in the dry region is less than the saturation concentration; otherwise condensation would occur. The vapor- continuity equation in the dry region resembles eq. [2.7.7] with the condensation rate equal to zero:

$$Dv(d^2C/dx^2) - u(dC/dx) = 0 \qquad [2.7.13]$$

Equations [2.7.12] and [2.7.13] are associated with the following boundary conditons:

-For the region adjacent to the "hot" reservoir

$$C = h_h C^*_h \quad \& \quad T = T_h \qquad @\ z = 0$$

$$C = C^*_0 \quad \& \quad T = T_0 \qquad @\ z = L_0$$

-For the region adjacent to the "cold" reservoir:

$$C = h_c C^*_c \quad \& \quad T = T_c \qquad @\ z = L_T$$

$$C = C^*_1 \quad \& \quad T = T_1 \qquad @\ z = L_1 \qquad [2.7.14]$$

The solution to the energy equation in the condensation-region as obtained from eq. [2.7.9] would be in terms of the values of temperature at x=0, and x=1, and the width of the condensation-region. To solve for the three unknowns, the temperature and concentration profiles of the condensation-region must be matched with the temperature and concentration profiles of the two dry regions. For the condition of zero liquid-diffusivity, the continuity of heat and vapor may be written as:

$$\left.\frac{dT}{dz}\right|_{L_0} = \left.\frac{dT^*}{dz}\right|_{L_0}$$

$$\left.\frac{dC}{dz}\right|_{L_0} = \left.\frac{dC^*}{dz}\right|_{L_0}$$

and

$$\left.\frac{dT}{dz}\right|_{L_1} = \left.\frac{dT^*}{dz}\right|_{L_1}$$

$$\left.\frac{dC}{dz}\right|_{L_1} = \left.\frac{dC^*}{dz}\right|_{L_1} \qquad [2.7.15]$$

For the case of non-zero liquid diffusivity, the boundary equations are modified to reflect the presence of evaporating liquid-fluxes at the boundaries of the condensation-region:

$$-\left.\frac{dT}{dz}\right|_{L_0} + \left.\frac{dT^*}{dz}\right|_{L_0} = \frac{J_0\ h_{fg}}{k\ T}$$

$$-\left.\frac{dC}{dz}\right|_{L_0} + \left.\frac{dC^*}{dz}\right|_{L_0} = \frac{J_0}{D_v}$$

and

$$-\left.\frac{dT^*}{dz}\right|_{L_1} + \left.\frac{dT}{dz}\right|_{L_1} = \frac{J_1 h_{fg}}{k \Delta T}$$

$$-\left.\frac{dC}{dz}\right|_{L_1} + \left.\frac{dC^*}{dz}\right|_{L_1} = \frac{J_1}{D_v} \qquad [2.7.16]$$

With either of the two sets of equations, eq. [2.7.15] or [2.7.16], the temperature profile as well as the width of the condensation-region may be determined. Once, the temperature distribution is obtained, eq. [2.3.5] may be used to calculate the condensation-rate. Although the solution to the above systems of equation is not obtained here, an order of magnitude study casts light on the relative importance of convection on the condensation rate. In eq. [2.7.9] the coefficient multiplying the $Pe(d\eta'/dx)$ is very similar to the coefficient multiplying the $(d^2\eta'/dx^2)$ term. The only difference between the two lies in the absence of Lewis number in the first coefficient. For values of Lewis number of order 1, the two coefficients are identical. The water vapor has a Lewis number of about 1 in air. With Peclet number equal to zero:

$$(d^2\eta'/dx^2) \quad \sim o\left(\lambda'^2\right)$$

and

$$(d\eta'/dx)^2 \sim o\left(\lambda'^2\right)$$

Hence, it can be argued that the convection effects are negligible if:

$$Pe << \lambda'$$

Typically the latent heat transport coefficient is of order 1 (it varies from 0.5 to 5). Therefore, for the convection effects to be negligible:

$$Pe << O(1)$$

For

$$Pe \sim \lambda'$$

the condensation rate is caused by equal contributions from vapor diffusion and vapor convection. It may be recalled ,from Fig. 2.3.5, that the condensation rate, in absence of convection is a a strong function of the latent heat transport coefficient. Therefore, the condensation rate would increase significantly with increasing values of Peclet number. An increase in the condensation rate, perhaps as much as twice if Pe $\sim \lambda'$, would lead to shorter time-periods for the liquid-content to build up to the critical value, above which the condenate begins to diffuse. The steady-state liquid-content distribution will also be a strong function of the Peclet number. The peak value and the mean of the liquid-content distribution increase with Peclet number.

2.8 HEAT AND MASS TRANSFER IN A POROUS SLAB ASSOCIATED WITH THE FORMATION OF SOLID-CONDENSATE

In the previous sections the phenomenon of heat and mass transfer associated with the formation of liquid-condensate has been considered. In this section the results of the previous sections are used to modify the analytical model to incorporate the formation of solid-condensate.

Under suitable conditions, vapor in a porous slab can condense into two forms of condensate: liquid and/or solid phase. Fig. 2.8.1 depicts a situation where both solid and liquid-condensate are present. As indicated the region of liquid-condensate lies closer to the warmer side of the slab, and the region of solid-condensate lies closer to the colder side. It is, of course, possible for the condensation-region to comprise only of solid, or liquid condensate.

The heat released as a consequence of phase change is proportional to the latent heat of phase change. The latent heat of solidification associated with vapor to solid phase change is numerically different from the latent heat of vaporization, associated with vapor to liquid transition. It was shown in section 2.3 that the parameter that scales the effect of heat released by condensation is the latent heat transport coefficient, λ'. Therefore, the two subregions associated with the liquid and solid-condensate are characterized by different values of the latent heat transport coefficient.

Solid-condensate may be generally assumed to be immobile, whereas the liquid-condensate is capable of diffusion under certain conditions. The diffusion of liquid takes place towards the dry region and the solid-condensate zone, Fig. 2.8.1. The diffusing liquid evaporates at the boundary between the dry region and the condensation-region, $z=L_0$. On the other hand, the liquid which migrates towards the solid-condensate zone solidifies at the boundary $z=L_m$. Therefore, at the frost/liquid boundary heat is released, whereas at the dry/liquid boundary heat is absorbed.

The condensation of vapor into solid and liquid form cannot be treated by a single formulation, for the diffusive behavior of the condensates, as well as their thermodynamic properties are different. Hence, the condensation-region is broken into two, corresponding to each type of condensate. The analysis of the previous sections applies to each condensation-subregion and its adjacent dry-region. The solid-condensate may be assumed to be immobile; once the values of liquid-content in the medium exceed the critical value, the liquid-condensate diffuses in response to gradients in the liquid-content distribution. The temperature and concentration profiles of the two sections are matched at the the boundary $z=L_m$ to generate the temperature and concentration profile of the whole region. In this section the boundary equations necessary to perform the matching of profiles is developed, and the solution methodology is discussed.

During the early stages of condensation in a porous medium, liquid diffusivity is approximately zero. During this period no liquid diffusion out of the liquid-condensate zone takes place. Hence, the condensation-region consists of two zones where only vapor and heat-fluxes cross the regions' boundaries. The solution to this problem can be easily affected by considering the following partitioning of the condensation-region. Consider Fig. 2.8.2. In this figure the slab with the condensation zones is indicated. The liquid-condensate zone and its adjacent dry

region are seperated by an imaginary boundary from the solid-condensate zone and its adjacent boundary. The temperature at this imaginary boundary is equal to the freezing temperature of the condensate. Let the liquid-condensate zone and its adjacent dry-region be named as domain-I ,and the solid-condensate zone and its neighboring dry region as domain-II. Let the total length of the domains be $L_{T,I}$, and $L_{T,II}$. The values of the length scales is not known and are part of the solution.

The temperature and concentration profiles in both domains may be obtained by the tools of the previous sections, with the length scales and the values of temperature at the boundaries of the condensation-region remaining undefined.

The heat-flux continuity across the boundary $z=L_m$, may be written as:

$$\left.\frac{dT}{dz}\right|_I = \left.\frac{dT}{dz}\right|_{II} \qquad [2.8.1]$$

Taking advantage of the non-dimensionalization of the previous sections, the above may be written as:

$$\Delta T'_I \left.\frac{d\bar{x}}{d\bar{z}}\right|_I \left.\frac{d\eta'}{d\bar{x}}\right|_I = \Delta T'_{II} \left.\frac{d\bar{x}}{d\bar{z}}\right|_{II} \left.\frac{d\eta'}{d\bar{x}}\right|_{II} \quad [2.8.2]$$

where

$$\left.\frac{d\eta'}{d\bar{x}}\right|_I = -\frac{1}{2}\left[1 + \frac{\lambda'_I \exp\lambda'_I}{\exp\lambda'_I - 1}\right] \quad [2.8.3]$$

and

$$\left.\frac{d\eta'}{d\bar{x}}\right|_{II} = -\frac{1}{2}\left[1 + \frac{\lambda'_{II}}{\exp\lambda'_{II} - 1}\right] \quad [2.8.4]$$

Then, the following relation between the length scales of the two domains may be obtained:

$$\left.\frac{d\bar{x}}{d\bar{z}}\right|_I = \frac{\Delta T'_{II}}{\Delta T'_I} \frac{1 + \dfrac{\lambda'_{II}}{\exp\lambda'_{II} - 1}}{1 + \dfrac{\lambda'_I \exp\lambda'_I}{\exp\lambda'_I - 1}} \quad [2.8.5]$$

The above with the constraint:

$$\left.\frac{d\bar{z}}{d\bar{x}}\right|_{I} + \left.\frac{d\bar{z}}{d\bar{x}}\right|_{II} = 1 \qquad [2.8.6]$$

is sufficient to define the length-scales.

For the case where liquid diffusion is present, the solution is slightly more complex. In domain-I a portion of the condensate diffuses out of the condensation-region in form of liquid and evaporates at its boundary with the adjacent dry region. The continuity of mass and heat at this boundary is analogous to the case discussed in section 2.6. With J_0 denoting liquid-flux at $z=L_0$, eq. [2.4.4.5], the boundary equations are:

$$D_v \frac{C_h - C^*_0}{L_0} = -D_v \left.\frac{dC^*}{dz}\right|_{L_0} - J_0 \qquad [2.8.7]$$

and,

$$k \frac{T_h - T_0}{L_0} = -k \left.\frac{dT^*}{dz}\right|_{L_0} + J_0 h_{fg} \qquad [2.8.8]$$

At the boundary of the solid-condensate with the dry region, the vapor and heat-flux continuity are:

$$\frac{C^*_1 - C_c}{L_T - L_1} = \left.\frac{dC^*}{dz}\right|_{L_1} \qquad [2.8.9]$$

and,

$$\frac{T_1 - T_c}{L_T - L_1} = \left.\frac{dT^*}{dz}\right|_{L_1} \qquad [2.8.10]$$

The liquid-flux leaving the liquid-condensate subregion and entering the solid-codensate subregion freezes at the boundary of the two subregions. The solidification process is accompanied by release of energy which must be conducted out through the solid-condensate region. With J_1 denoting the liquid-flux leaving the wet zone and entering the solid zone, at $z=L_m$, the boundary equations are:

$$-k \left.\frac{dT^*}{dz}\right|_{L_m^-}^{+} J_1 h_{fs} = -k \left.\frac{dT^*}{dz}\right|_{L_m^+} \qquad [2.8.11]$$

and,

$$-D_v \left.\frac{dC^*}{dz}\right|_{L_m^-} = -D_v \left.\frac{dC^*}{dz}\right|_{L_m^+} \qquad 2.8.12$$

where

h_{fs} = Latent heat of solidification

Equations [2.8.7]-[2.8.12] constitute a set of nonlinear coupled equations. They are sufficient to define all the unknown parameters. However, the solution of such a large number of coupled equations is not a trivial task. The solution of the above is not carried out in this work, and hence, is not reported.

For liquid-contents less than the critical values, where no liquid diffusion takes place, the condensation-region may be treated as a uniform domain. By treating the region as uniform, the solutions of section 2.5 may be used directly at the cost of losing some accuracy in the final results. The source of error lies in the difference between the latent heat of vaporization and the latent heat of solidification. This difference is insignificant in many instances. For example, the values of latent heat of vaporization and solidification for water is 1070 BTU/lbm, and 1220 BTU/lbm, respectively. The error incurred in treating the condensation-region as a uniform domain is discussed in the illustrative example of this section.

Under certain conditions the condensation-region may consist solely of solid-condensate. This situation is identical to the case of liquid-condensate with zero mobility, section 2.5. The only difference between the two lies in the proper choice of the

thermodynamic properties. Clearly, there are no upper bounds on the ice-content in the slab, except for, perhaps, the ones assocaited with the mechanical strength of the medium.

In this section, the phenomenon of heat and mass transport associated with the formation of solid-condensate was studied. The form and solid-condensate. The different regimes of liquid-diffusivity and their effects on the process of condensation was also investigated. In the remainder of this section an illustrative example involving the results of this section is presented.

ILLUSTRATIVE EXAMPLE

Consider a porous slab with the same properties as discussed in the illustrative example of section 2.5. The slab boundary conditions are chosen such that both solid and liquid condensate are formed in the medium. The boundary values are:

$$T_H = 90.°F$$

$$T_C = -20.°F$$

$$h_H = 90\%$$

$$h_C = 90\%$$

The temperature profile and the location of the condensation-region are obtained for the case of none diffusive liquid-condensate. The solution is obtained by partitioning the condensation-region into two zones at the point where the temperature equals 32.°F, the freezing temperature for water. The temperature profile and location of the condensation-region in each domain is obtained using the results of section 2.5. The following boundary values are associated with domain-I:

$$T_{H,I} = 90.°F$$

$$T_{C,I} = 32.°F$$

$$h_{H,I} = 90\%$$

$$h_{C,I} = 100\%$$

Using the solution methodology of section 2.5, the following results are found:

$$\eta_{0,I} = .212$$

$$L_{0,I} = .3741$$

$$\lambda'_{I} = 1.67$$

$$\Delta T'_I = 38.3\ ^\circ F$$

With the following boundary values, the solution for the solid-condensate region, domain-II, is obtained:

$$T_{H,II} = 32.^\circ F$$

$$T_{C,II} = -20.^\circ F$$

$$h_{H,II} = 100\%$$

$$h_{C,II} = 90\%$$

The results are:

$$\eta_{1,II} = -.341$$

$$L_{1,II} = .8766$$

$$\lambda'_{II} = 1.099$$

$$\Delta T'_{II} = 41.57^\circ F$$

The temperature and concentration profiles of the two domains are matched using eqs. [2.8.1]-[2.8.6]. The values of the length-scale multipliers are calculated to be:

$$\left.\frac{d\bar{z}}{d\bar{x}}\right|_{II} = 0.355$$

$$\left.\frac{d\bar{z}}{d\bar{x}}\right|_{II} = 0.645$$

The above results indicate that the reduced length scale in domain-I is decreased by a factor of 0.645, and that of domain-II is reduced by a factor of 0.355. The matched reduced temperature profile is presented in Fig. 2.8.3. It consists of two different profiles matched at $z=L_m$.

It has been suggested in this section that for the case of immobile liquid-condensate, the entire condensation-region may be approximated as one homogeneous condensation-region. This treatment would assume that the differences in the thermodynamic properties of the two condensates may be ignored. The results of section 2.5 were applied directly to the boundary conditions of this example. The thermodynamic properties of the solid-condensate were assumed to be identical to that of the liquid-condensate. The results of this approach is shown of Fig. 2.8.3. The solutions obtained by the two different technics are not very different, indicating that the difference between the latent heats of vaporization and solidification is negligible. Hence, the condensation-region may be treated as a homogeneous

domain, and the results of section 2.5 may be applied directly to cases where both solid and liquid condensate are present.

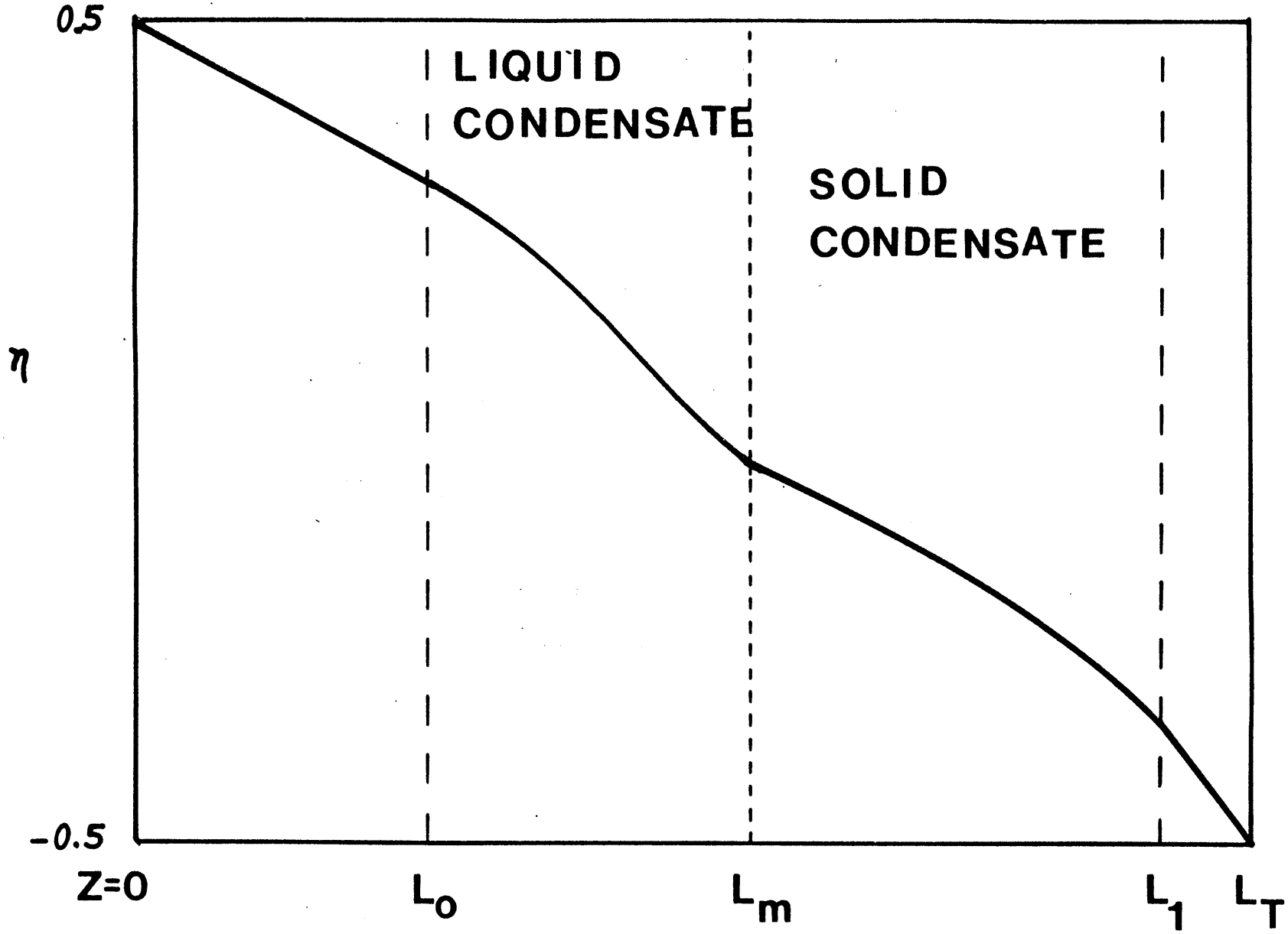

Fig. 2.8.1 Schematic Profile of the Reduced-Temperature For the case where both Solid and Liquid Condensate are Present.

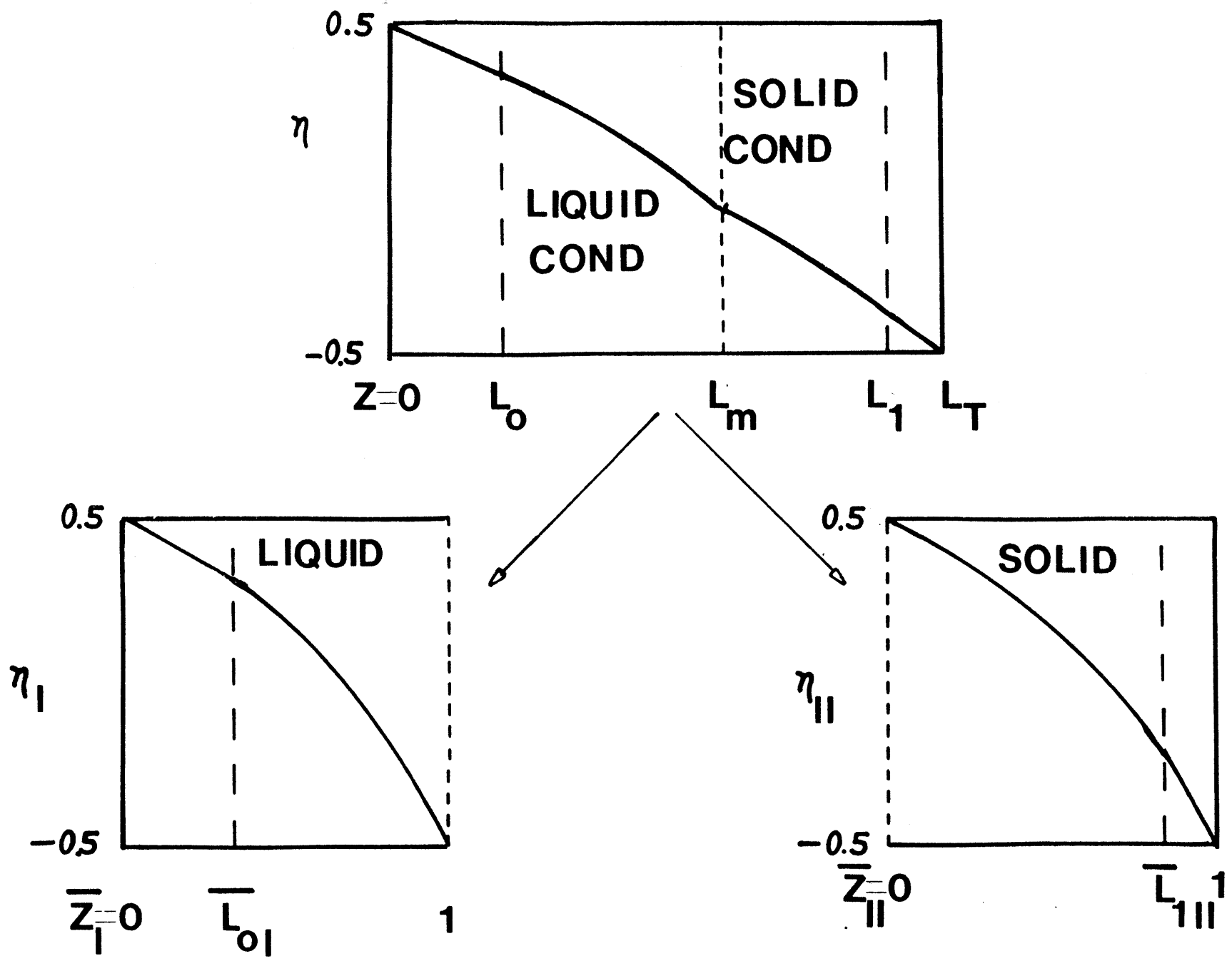

Fig. 2.8.2 Schematic of Procedure to Calculate the Reduced-Temperature Profile for the Case where Liquid and Solid Condensate are Present.

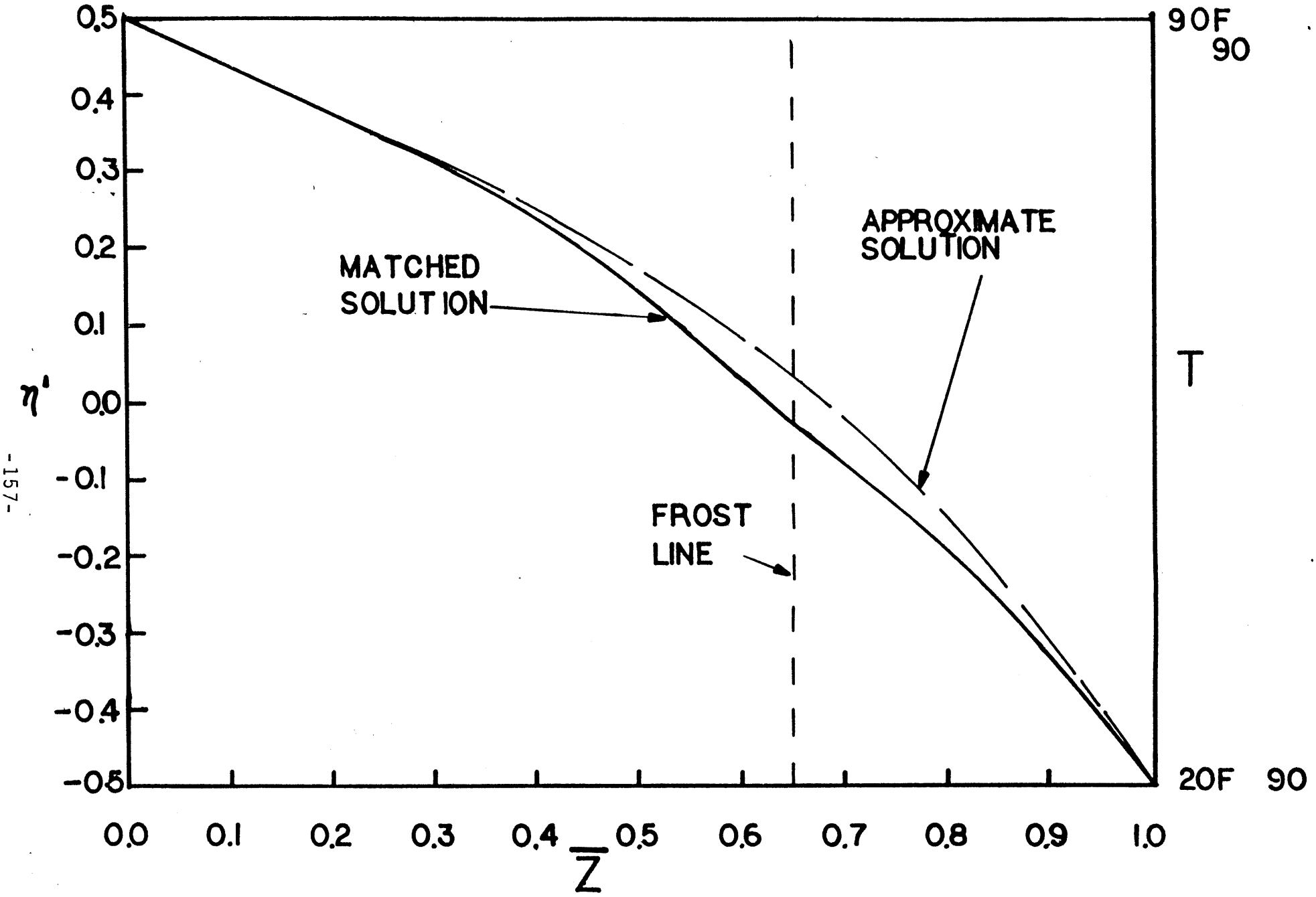

Fig. 2.8.3 Comparison of the Approximate Solution with the Matched Solution of Reduced-Temperature Profile in the Condensation-Region where both solid and Liquid Condensate are Present

CHAPTER 3

HEAT AND MASS TRANSPORT WITH PHASE CHANGE IN A POROUS SLAB: SPATIALLY - UNSTEADY SOLUTIONS

3.1 INTRODUCTION

In the previous chapter the phenomenon of heat and mass transfer during condensation was studied. In that analysis the study was focused on condensation in the porous media for two regimes of liquid-content: low values of liquid-content which implied zero liquid diffusivity, and moderate liquid-contents where liquid diffusion was present. In this chapter the phenomenon of drying in a porous slab for the two regimes of liquid-content will be studied. The study assumes the existence of a nonzero liquid-content distribution in the medium. The

initial liquid-content distribution may be assumed to be related to the liquid-content distribution at the end of a condensing period. The wet region is assumed to be bounded by two dry regions. This assumption is not critical to the results of this study. At the beginning of the drying process, time equals zero, the values of temperature and humidity at the boundaries of the slab are changed to new values. The new values are inconsistent with the existence of the condensation-zone. These new boundaries might require a larger, smaller, or no condensation-region. Hence, the width and location of the condensation-region will have to change in order to accomodate the new boundary values. The purpose of the study in this chapter is to analyze the transient behavior of the condensation-region's boundaries and liquid-content. The final location of the condensation-region can be obtained by performing the analysis of chapter 2 with the new boundary values.

Consider Fig. 3.1. The wet region is indicated to be located from $z=L_0$ to $z=L_1$. The intial liquid-content distribution is considered to be an input. Let us assume that the origin of liquid in the medium is related to a period of condensation in the slab. Let the tranisent be initialized by a step increase in the value of temperature at the boundary $z=L_T$ of the slab. Naturally, any combination of the four boundary values: T_h, T_c, h_h, h_c may be changed. The behavior of the system would be different depending on the magnitude and direction of change in any of the four boundary conditions. In order to preserve continuity of notation and present aconcise discussion, the increase in only one boundary value is considered in this chapter. This is not a restrictive assumption and may be withdrawn once the new notation of temperature and concentration is completed. With the above assumption, the hot and cold reservoir exchange their significance. The temperature at $z=L_T$ is now denoted as T_H, and the temperature at $z=0$, is T_C. The relative humidity values are now h_H and h_C, correspondiong to T_H and T_C. In short the 'hot' reservoir now lies to the right of

the slab, and the 'cold' reservoir lies to the left of the slab.

With the new boundary values, heat and vapor diffuse into the slab in a manner analogous to diffusion in a semi-infinite plane. There are three transient time-scales associated with the change in the boundary conditions. One time-scale corresponds to the storage of heat, another to storage of vapor, and the third to the storage(depletion) of liquid. It will be later shown that the transients corresponding to storage of heat and vapor take place at a rate significantly faster than the one assocaited with depletion of liquid. For this reason, the temperature and vapor-concentration transients are considered to constitute the first transient, and the liquid-content transient to be the second transient.

During the first transient the temperature and the vapor-concetration of the medium increase. During the second transient the condensate at the boundaries of the wet zone evaporates in response to the addition of heat and removal of vapor. The behavior of temperature and vapor-concentration profiles during the first transient are depicted in Fig. 3.2 and 3.3. During this transient some liquid evaporation occurs. As it will be shown later that the first transient is much smaller than the second transient any changes in the location of the wet zone are ignored. Fig. 3.2 and 3.3 indicate that the temeperature and vapor concentration in the condensation-region increase until such a state is reached where evaporation at the wet zone's boundaries becomes the dominant mode of heat and mass transfer. The increase in the vapor-concentration in condensation-region is supplied by two sources. These sources are diffusion from the the slab boundaries and internal evaporation. The density ratio of vapor to liquid for most fluids is very small. Hence, the amount of liquid required to satisfy the changes in the vapor-concentration is very small. It is assumed that the amount of liquid required to provide for the changes in vapor-concentration in the wet-zone is an insignificant amount in

comparison with the amount of liquid present in the medium. As it is argued that that the time constant assocaited with liquid depletion is dominant, the movement of the boundaries of the condensation-region may be approximated by a series of quasi-steady steps. At each step a certain amount of liquid evaporates at the fronts and the fronts change their positions. During this time-step the values of temperature, vapor-concentration, and liquid-content of the wet-zone undergo change. The changes in the temperature and vapor-concentration and liquid-cotent are, according to the assumption to be proved later, may be considered to be instantaneous in comparison to the duration of the time-step.

It is necessary to point out that evaporation takes place primarily at the boundaries of the wet-zone and a fraction of that vapor condenses into liquid phase inside the wet zone, simultaneously. At the end of the first transient a certain temperature profile is established in the medium. Corresponding to this temperature profile, a vapor saturation-concentration is established. The condensation rate has been shown to be proportional to the second spatial derivative of the vapor saturation-concetration, C^*. As indicated in Fig. 3.2, the C^*-profile has a positive second derivative, indicating the vapor-flux into an element, in the direction of positive x, is larger than the vapor-flux leaving the element. The difference condenses into liquid phase.

The above discussions on condensation imply that for quasi-steady changes the temperature profile, and consequentially the vapor-concetration-profile, corresponds to the solution of the energy equation with a nonlinear heat source distribution. The soltuion to this equation has been obtained in section 2.3. It was there shown that in the condensation-region the reduced temperature, λ', is of the following form:

$$\eta' = \frac{1}{2}\left[1 - x - \frac{\exp \lambda' x - 1}{\exp \lambda' - 1}\right]$$

where λ' is the latent heat transport coefficient and equals:

$$\lambda' = \frac{2\ \gamma'^2 \beta'\ \Omega'}{Le + \Omega'\ \gamma'}$$

The value of λ' depends on the values of temperature at the boundaries of the condensation-region, T_0 and T_1. These two values change at each time-step. The location and width of the condensation-region are also time-dependant.

As mentioned earlier, the analysis assumes a liquid-content distribution in the wet zone. As condensation occurs in the wet zone, simultaneously with frontal evaporation, the values of liquid-content in the medium, and consequentially liquid-fluxes, become a critical parameter in the study. It may be recalled that liquid diffusion for liquid-content values less than the critical value is zero. With the values of liquid-content in the medium less than the critical value, condensation in the wet-zone translates into a linear increase of liquid-content with time. If the values of liquid-content are at or near the critical value, condensation in the wet-zone leads to the establishment of liquid-fluxes which migrate towards the dry regions and evaporate at the boundaries of the wet-zone. This causes a decrease in the rate of movement of the boundaries.

Hence, the drying phenomenon needs to be studied for two cases of initial liquid-content:

Case I- Liquid-content values consistently less than the critical value throughout the drying process.

Case II- Liquid-content values at and above the critical level and liquid diffusion present.

In the next sections heat and mass continuity equations for the two cases will be obtained.

3.2 SPATIALLY-UNSTEADY HEAT AND MASS TRANSFER WITH PHASE CHANGE

CASE I: IMMOBILE CONDENSATE

In this section the phenomenon of drying in a porous slab is considered. The inital liquid-content is assumed to be limited to a section of the slab which is referred to as the wet-zone. As the relative humidity of both sides of the slab is less than 100% the wet-zone is bounded by two dry regions. The liquid in the wet-zone is assumed to be in pendular state and does not exhibit any tendency to diffuse. However, as condensation occurs in the wet-zone during frontal evaporation, the values of liquid-content increases with time. For non-diffusive condensates, liquid-content is found to increase linearly with time, eq. [2.4.13]:

$$\theta(\bar{x},Fo^*) = \left[\frac{C'_r}{\rho\epsilon}\left(\frac{L_T}{L_w}\right)^2\left[\frac{Le\ \beta'}{\Omega'}\right]\frac{\lambda'^2}{2}\ \frac{\exp\lambda' x}{\exp\lambda' - 1}\right] Fo^* + \theta(x,0)$$

where all the terms in the above equation are defined in section

2.4. In order to insure that liquid diffusion can be ignored throughout the transient period, it is required that the values of liquid-content in the medium never exceed the critical value of liquid-content during the transient. This imposes a constraint on the duration of transient:

$$Fo^*_{max} = \left[\theta_c - \left| \theta(x,0) \right|_{max} \right] \frac{C'_r}{\rho \epsilon} \cdot \frac{Le\ \beta'}{\Omega'} \cdot \frac{\lambda'^2}{2} \cdot \frac{\exp \lambda' x}{\exp \lambda' - 1} \qquad [3.2.1]$$

where $\left| \theta(x,0) \right|_{max}$ indicates the maximum value of initial liquid-content value. For Fourier numbers less than Fo^*_{max}, liquid diffusion is ignored during the transient movement of the the wet-zones' boundaries. However, if the duration of the transient exceeds Fo^*_{max}, then liquid begins to diffuse and the liquid-content undergoes a transient behavior. This transient behavior is discussed in section 2.4. The solution developped in this section does not allow for any liquid diffusion and the transient in the liquid-content profile. The analysis for the case of diffusive condensate is discussed in section 3.3.

Consider the drying of a wet slab as depicted in Fig. 3.1. The z-scale denotes the length-scale in the slab, whereas the x-scale corresponds to the length-scale in the wet-zone. It may be noted that the positive x-direction corresponds to the negative z-direction. The choice of the x-scale is made so that the results of section 2.3 on the temperature-profile in the wet-zone be readily used. The boundary at $z=L_1$ is assumed to have a temperature T_1 lower than T_H. Mass balance at this boundary involves the diffusion of vapor into the wet-zone,

generation of vapor by the evaporation of liquid at the boundary and the diffusion of vapor from the slab boundary. The mass balance may be written as:

$$D_v \frac{C_H - C^*_1}{L_T - L_1} - D_v \left.\frac{dC^*}{dz}\right|_{L_1} = \rho \epsilon \theta (z=L_1, t) \frac{dL_1}{dt} \quad [3.2.2]$$

The above indicates that the vapor supplied by evaporation at the front equals to the difference between vapor diffusing into the wet-zone and the vapor arriving into the slab. It must be noted that the term dL_1/dt is negative, i.e. the front is receding, and hence, the terms in eq. [3.2.2] have the correct signs.

Heat-flux entering at the slab boundary minus the heat conducted into the wet-zone is absorbed by the evaporation of liquid at the front. The evaporation of liquid at the front causes the motion of the front:

$$k \frac{T_H - T_1}{L_T - L_1} - k \left.\frac{dT^*}{dz}\right|_{L_1} = h_{fg} \rho \epsilon \theta (z=L_1, t) \frac{dL_1}{dt} \quad [3.2.3]$$

The term T^* indicates the value of temperature inside the wet-zone. In equations [2.3.2] and [2.3.3] the term $\theta(z=L_1)$ corresponds to the instantaneous value of liquid-content at the

boundary. It is determined from eq. [2.4.13].

Similar to eqs. [2.3.2] and [2.3.3], heat and mass balance at the $z=L_0$ boundary may be written as:

$$D_v \frac{C^*_0 - C_C}{L_0} - D_v \left.\frac{dC^*}{dz}\right|_{L_0} = \rho\epsilon\theta\ (z=L_0,t)\ \frac{dL_0}{dt} \quad [3.2.4]$$

and,

$$k \left.\frac{dT^*}{dz}\right|_{L_0} - k \frac{T_0 - T_C}{L_0} = h_{fg}\rho\epsilon\theta\ (z=L_0,t)\ \frac{dL_0}{dt} \quad [3.2.5]$$

In the above the terms $\theta(z=L_0)$ is determined by eq. [2.4.13].

The four boundary equations [3.2.2]-[3.2.5] and the time dependant liquid-content equation [3.2.1] constitute a system of five nonlinear coupled equations. Solution of this set as presented is quite difficult. In order to facilitate the solution process the five equations are manipulated to reduce their coupling.

The rate of change of the length-scales in the boundary equations are eliminated to yield a pair of implicit equations in T_0 and T_1. Eliminating the dL_1/dt term in eqs. [3.2.2] and

[3.2.3] yields:

$$\frac{D_v\, h_{fg}}{k} \cdot \frac{C_H - C^*_1}{L_T - L_1} + \frac{T_H - T_1}{L_T - L_1} = \left[\frac{D_v\, h_{fg}}{k} \cdot \frac{dC^*}{dT} + 1\right] \frac{dT^*}{dz}\bigg|_{L_1}$$

[3.2.5]

The above equation in the non-dimensional form is:

$$\frac{\eta_H - \eta_1}{1 - \bar{L}_1} + \frac{\Omega}{Le\,\beta} \frac{h_H \exp[\Phi_H] - \exp[\Phi_1]}{1 - \bar{L}_1} =$$

$$\left[1 + \frac{\Omega}{Le\,\beta}(1+\eta\beta_1)\exp[\Phi_1]\right] \frac{d\bar{x}}{d\bar{z}} \frac{d\eta}{d\eta'} \frac{d\eta'}{d\bar{x}}\bigg|_{\bar{x}=0}$$

[3.2.6]

It may be recalled that:

$$\frac{d\eta'}{d\bar{x}} = -\frac{1}{2}\left[1 + \frac{\lambda' \exp \lambda' \bar{x}}{\exp \lambda' - 1}\right]$$

$$d\bar{z}/d\bar{x} = \bar{L}_1 - \bar{L}_0$$

and

$$\frac{d\eta}{d\eta'} = \frac{\Delta T'}{\Delta T}$$

Then eq. [3.2.6] may be written as:

$$\left|\eta_H - \eta_1\right| + \frac{\Omega}{Le\,\beta}\, h_H \exp[\Phi_H] - \exp[\Phi_1] =$$

$$-\frac{1}{2}\left[1+\frac{\Omega\gamma}{Le}(1+\beta\eta_1)^{-2}\exp[\Phi_1]\right]\frac{1-\bar{L}_1}{\bar{L}_1-\bar{L}_0}\,\frac{\Delta T'}{\Delta T}\quad 1+\frac{\lambda'}{\exp\lambda' - 1}$$

[3.2.7]

Equation [3.2.7] is an implicit equation involving η_0 and η_1. η_1 appears explicitly, whereas η_0 appears implicitly in the $\Delta T'/\Delta T$ and λ' terms.

Similarly eqs. [3.24] and [3.2.5] may be manipulated to yield:

$$\eta_0 - \eta_C + \frac{\Omega}{Le\,\beta}\left[\exp\left[\Phi_0\right] - h_C\exp\left[\Phi_C\right]\right] =$$

$$\frac{1}{2}\left[1+\frac{\Omega\gamma}{Le}(1+\beta\eta_0)^{-2}\exp\left[\Phi_0\right]\right]\frac{\overline{L_0}}{\overline{L_1}-\overline{L_0}}\frac{\Delta T'}{\Delta T}\left[1+\frac{\lambda'\exp\lambda'}{\exp\lambda'-1}\right]$$

[3.2.8]

Equations [3.2.7] and [3.2.8] are two implicit equations in η_0 and η_1. Both equations are dependant on the values of L_0 and L_1. The effect of the presence of these terms on the solution scheme will be discussed later.

The four independant boundary equations have been manipulated to yield the two equations [3.2.7] and [3.2.8]. There is enough information in the original four equations to generate the necessary equations to predict the rate of movement of the two boundaries. The dC^*/dz term in eq. [2.3.2] may be written as:

$$\frac{dC^*}{dz} = \frac{dC^*}{dT}\cdot\frac{dT}{dz}$$

Substituting this value into eq. [3.2.2] and introducing the equivalent of dT*/dz term from eq. [3.2.3] yields

$$\frac{\rho\epsilon\theta(z=L_1,t)}{D_v}\left[1+\frac{D_v\,h_{fg}}{k}\,\frac{dC^*}{dT}\right](L_T-L_1)\,\frac{dL_1}{dt}=$$

$$(C_H-C^*_1)-\left.\frac{dC^*}{dT}\right|_{T_1}\cdot(T_H-T_1) \qquad [3.2.9]$$

The above may be written in the following non-dimensional form:

$$\theta(\bar{z}=\bar{L}_1,\bar{t})\,\frac{d(1-\bar{L}_1)^2}{d\bar{t}}=$$

$$2\,\frac{\exp[\Phi_1]-h\mathrm{Hexp}[\Phi_H]+(1+\beta\eta_1)\exp[\Phi_1][\eta_H-\eta_1]}{1+\frac{\Omega\gamma}{\mathrm{Le}}(1+\beta\eta_1)^{-2}\exp[\Phi_1]}$$

[3.2.10]

where

$$\bar{t}=\mathrm{Fo}^*.\,\frac{C_r}{\rho\epsilon}$$

As mentioned in section 2.1, the movement of the fronts may be considered as a quasi-steady process. The crux of the arguement on the quasi-steady treatment of the issue was to establish that the time-scale for the movement of the boundary, i.e. change in liquid-content, is much larger than the ones associated with change in values of temperature and vapor-concetration. The time-scale corresponding to changes in temperature and vapor-concentration are of the order of and D_v, respectively. The time scale associated with the boundary movement is obtained from eq. [3.2.11] and is

$$\tau_{B.M.} \sim \frac{\rho \epsilon L_T^2}{D_v C_r} \qquad [3.2.12]$$

The above indicates that the time scale is of the order of the ratio of the density of condensate to the vapor. For reasonable values of properties, the time-scale for boundary-movement is much larger than the time-scale associated with variations in temperature and vapor-concentration.

The scheme for the solution of equations obtained in this section is as follows. The situation is initiated by the inital location of the wet-zone and the liquid-content profile. Equations [3.27] and [3.2.8] are then solved simultaneously to generate the values of η_0 and η_1. Then equation [2.4.13] is used to calculate the new values of liquid-content at the boundaries. The rate of movement of the boundaries is given by eq. [3.2.10] and [3.2.12]. With the values of η_0 and η_1, and $\theta(L_0,t)$,and $\theta(L_1,t)$ known, a step in reduced-time is taken and the new locations of the fronts are obtained. The new location values are then fed into eq. [3.2.7] and [3.2.8] to generate the

Equations [3.2.10] indicates the movement of the $\bar{z}=\bar{L}_1$ front. As the boundary approaches its final position the rate of change of the length-scale goes to zero. The final positiona of the boundary corresponds to the solution of eq. [3.2.10] with the right hand side of equation equal to zero. This is identical to the condition obtained in section 2.5, for obtaining the value of $_0$. Hence, eq. [3.2.10] converges to the steady solution.

Equations [3.2.4] and [3.2.5] are manipulated similary to to yield:

$$\theta(\bar{z}=\bar{L}_0,t)\ \frac{d\bar{L}_0^2}{d\bar{t}} =$$

$$2\ \frac{\exp[\Phi_0] - h_C\exp[\Phi_H] - (1+\beta\eta_0)^{-2}\exp[\Phi_0][\eta_0 - \eta_C]}{1 + \frac{\Omega\,\nu}{Le}\ (1+\beta\eta_0)^{-2}\exp[\Phi_0]}$$

[3.2.11]

Equations [3.2.10] and [3.2.12] relate the movement of the wet-zone boundaries to the values of temperature and liquid-content at the boundaries. Each of the two equations depends explicitly on only the value of reduced temperature corresponding to that boundary. Hence, the four equations which were extremely coupled are now reduced to forms were the coupling terms are not as ubiquituous as before.

new values of θ_0, and θ_1. Time-stepping continues until the boundaries reach their final location. This solution scheme is used in the illustrative example, section 3.4.

3.3 SPATIALLY-UNSTEADY HEAT AND MASS TRANSFER WITH PHASE CHANGE

CASE II : MOBILE CONDENSATE

In section 3.2 the simultaneous transfer of heat and mass during frontal evaporation for non-diffusive condensates was discussed. In this section heat and mass trasfer during frontal evaporation for the case of diffusing-condensate is considered. In general, liquid diffusivity in porous media is negligibly small for small values of liquid-content. As the values of liquid-content in the region exceed a critical value, the liquid diffusion in response to the spatial gradients of liquid-content begins. The analysis of this section corresponds to the case where the liquid-content in the medium is at such levels that liquid diffusion may not be ignored.

Consider Figure 3.3. The liquid-content distribution in the wet-zone is assumed to be at a steady-state value. The steady-state liquid-content distribution corresponding to situations where liquid-diffusion is present is discussed in section 2.4. According to the results of that section the steady-state liquid-content distribution is given by eq. [2.4.23]:

$$\theta_{ss}(\bar{x}) = M \frac{C'_r}{\rho\epsilon} \frac{Le\ \beta'}{\Omega'} \left\{ \frac{1}{2} \left[\bar{x} - \frac{\exp \lambda' \bar{x} - 1}{\exp \lambda' - 1} \right] \right\}$$

It may be recalled that liquid diffusion takes place once liquid-content exceeds a critical value, θ_c. Below this critical value liquid diffusion is absent. Hence, the steady-state liquid-content distribution for diffusing condensate consists of two parts: a base value of θ_c at all locations, and an additional liquid-content distribution superimposed on top of the base value. At steady-state the liquid-flux leaving the condensation-region equals the total amount of condensed vapor. The diffusing liquid flows to the boundaries of the condensation-region and evaporates. The liquid-flux leaving the condensation-region at $\bar{x}=0$ is denoted by J_0. J_0 is a fraction of the total amount of vapor condensed in the condensation-region:

$$J_0 = \alpha \, (\dot{W}/A)_T$$

where

$$\alpha = \frac{\exp \lambda' - 1 - \lambda'}{\lambda' \, (\exp \lambda' - 1)} \qquad [2.4.43]$$

The total amount of condensate per unit time is:

$$(\dot{W}/A)_T = \frac{\lambda'}{2} \, \frac{k \, \Delta T}{h_{fg}} \, \frac{d\eta}{d\eta'} \, \frac{1.}{\bar{L}_1 - \bar{L}_0} \qquad [2.6.13]$$

Combining the above two equations yields:

$$\frac{J_0\, h_{fg}}{k\, \Delta T} = \frac{\Delta T'}{\Delta T}\ \frac{1.}{\overline{L}_1 - \overline{L}_0}\ \frac{\exp \lambda' - 1 - \lambda'}{2\ (\exp \lambda' - 1)} \qquad [3.3.1]$$

The liquid-flux leaving the boundary of the condensation-region at $\bar{x}=1$ is:

$$J_1 = (1 - \alpha)\ (\dot{W}/A)_T,$$

which may be written as:

$$\frac{J_1 h_{fg}}{k\, \Delta T} = \frac{\Delta T'}{\Delta T}\ \frac{1.}{\overline{L}_1 - \overline{L}_0}\ \frac{(\lambda' - 1) \exp \lambda' + 1}{2(\exp \lambda' - 1)} \qquad [3.3.2]$$

It has already been established that during frontal evaporation, condensation occurs in the condensation-region. The condensation rate is shown to be proportional to the second spatial gradient of vapor saturation-concentration. At steady-state there is no condensate accumulation in the wet-zone, and the liquid-content distribution is always at the steady-state

value given by eq.[2.4.23]. At the boundary of the wet-zone and its adjacent dry regions no liquid-content gradient should exist, for an infinite liquid-flux would have to set up in response to a discontinuity in the liquid-content distribution. However, as liquid diffusivity for liquid-contents less than θ_c is zero, all liquid-contents less than θ_c do not qualify as diffusible species and may remain stationary. The liquid-content at the boundaries never exceed θ_c. On the other hand, as liquid diffusion takes place across the boundary, the value of liquid-content at the boundary is always at θ_c.

Consider the boundary $z=L_1$. The mass balance at the boundary is:

$$D_v \frac{C_H - C^*_1}{L_T - L_1} = -D_v \frac{dC^*}{dz} + J_0 = \rho \epsilon \theta_c \frac{dL_1}{dt} \quad [3.3.3]$$

Equation [3.3.3] indicates that the vapor-flux entering the slab plus the vapor-flux generated by the recession of the wet-zone front and the diffusing liquid-flux, J_0, is diffused into the wet-zone. It may be recalled that our notation corresponds to an arbitrary assignment of a positive value to the difference $C^*_C - C^*_1$. This, of course, may turn out to be negative. The effect of the J_0 term may be taken to represent an increase in the amount of vapor that must be diffused away from the front. This leads to a decrease in the rate of recession of the front.

Energy balance at the $z=L_1$ boundary yields:

$$k \frac{T_H - T_1}{L_T - L_1} - k \frac{dT^*}{dz}\bigg|_{L_1} - J_0 h_{fg} = -h_{fg} \rho \epsilon \theta_c \frac{dL_1}{dt} \quad [3.3.4]$$

The above equation states that the heat-flux necessary to evaporate the liquid-flux J_0 and cause the movement of the boundary equals the heat-flux supplied at the boundary z=1, minus the heat-flux conducted into the wet-zone. The presence of the J_0 term in eq. [3.3.4] translates into a heat sink which decreases the heat supplied to the front for evaporation, and causes a decline in the rate of boundary movement.

Similar arguements may be made in the devlopment of heat and mass transfer continuity equations at the $z=L_0$ boundary. Vapor continuity at the $z=L_0$ boundary yields:

$$D_v \frac{C^*_0 - C_C}{L_0} - D_v \frac{dC^*}{dz}\bigg|_{L_0} - J_1 = \rho \epsilon \theta_c \frac{dL_0}{dt} \quad [3.3.5]$$

Heat-flux balance at the same boundary yields:

$$k \frac{dT^*}{dz} - k \frac{T_0 - T_C}{L_0} - J_1 h_{fg} = h_{fg} \rho \epsilon \theta_c \frac{dL_0}{dt} \quad [3.3.6]$$

Equations [3.3.3]-[3.3.6] comprise a set of coupled equations. In order to obtain less coupled forms of these equations, they are manipulated in a manner analogous to section 3.2.

Equations §3.3.3] and [3.3.4] are combined to eliminate the dL_1/dt term. The liquid-flux terms cancel out indicating that the effect of liquid diffusion and evaporation at the boundaries is intimately coupled to the movement of the boundaries. The resulting equation in non-dimensional form is:

$$\left(\eta_H - \eta_1\right) + \frac{\Omega}{Le\,\beta}\left[h_H \exp[\Phi_H] - \exp[\Phi_1]\right] =$$

$$\frac{1}{2}\left[1 + \frac{\Omega}{Le\,\beta}(1+\beta\eta_1)^{-2}\exp[\Phi_1]\right]\frac{1-\bar{L}_1}{\bar{L}_1-\bar{L}_0}\frac{\Delta T'}{\Delta T}\left[1+\frac{\lambda'}{\exp\lambda' - 1}\right]$$

[3.3.7]

Similarly, eqs.[3.3.5] and [3.3.6] may be combined to yield:

$$\eta_0 - \eta_C + \frac{\Omega}{Le\,\beta}\left[h_H \exp[\Phi_H] - \exp[\Phi_1]\right] =$$

$$\frac{1}{2}\left[1+\frac{\Omega\nu}{Le}(1+\beta\eta_0)\bar{e}^{2}\exp[\Phi_0]\right]\frac{\bar{L}_0}{\bar{L}_1-\bar{L}_0}\frac{\Delta T'}{\Delta T}\left(1+\frac{\lambda'\exp\lambda'}{\exp\lambda'-1}\right)$$

[3.3.8]

Equations [3.3.7] and [3.3.8] may be considered as two implicit equations in η_0 and η_1, with parametric dependence on L_0 and L_1. For a given set of length-scales there exists at least one pair of η_0 and η_1 which satisfy the above equations. The solution may contain more than one pair of roots, yet only one would be physically meaningful, i.e. lies between -.5 and .5.

In order to calculate the rate of movement of the $z=L_1$ boundary , eqs. [3.3.3] and [3.3.4] may be combined to yield the following non-dimensional equation:

$$\theta_c \frac{d\bar{L}_0^{2}}{d\bar{t}} =$$

$$2\,\frac{\exp[\Phi_0]-h_c\exp[\Phi_c]-(1+\eta\beta_0)\exp[\Phi_c][\eta_0-\eta_c]}{1+\frac{\Omega\nu}{Le}(1+\beta\eta_0)\exp[\Phi_0]}$$

$$-\,2\,\frac{J_1\,L_0}{D_v\,C_r} \qquad [3.3.9]$$

where

$$\bar{t} = Fo^*. \frac{C_r}{\rho \epsilon}$$

The liquid-flux term, J_0, is given in eq.[3.3.1].

Similarly, eqs.[3.35] and [3.36] may be combined to yield:

$$\theta_c \frac{d(1-\bar{L}_1)^2}{dt} =$$

$$2 \frac{\exp[\Phi_1] - h_H \exp[\Phi_H] + (1+\beta\eta_1)^{-2\gamma\beta} \exp[\Phi_1][\eta_H - \eta_1]}{1 + \frac{\Omega\gamma}{Le}(1+\beta\eta_1)^{-2}\exp[\Phi_1]}$$

$$- 2 \frac{J_0 (1 - L_1)}{D_v C_r} \qquad [3.3.10]$$

The liquid-flux term, J_1, is given in eq. [3.32]

Equations [3.3.9] and [3.3.10] are two coupled nonlinear differential equations. Comments on the procedure for their solution will be given at the end of this section.

The effect of liquid diffusion on the rate of movement of the boundaries may be analyzed by comparing he results of this section with those of section 3.2. The implicit equations relating η_0 to η_1 with parametric dependence on L_0 and L_1 are identical to both cases. This implies that for a given set of length-scales the temperature values at the boundaries are the same, irregardless of the presence and magnitude of liquid diffusion. The rate of movement of the boundaries without liquid diffusion are given in eqs. [3.2.10] and [3.2.12]. Equations [3.3.9] and [3.3.10] apply for the situations where liquid diffusion is present. The comparison of the two pairs of equations reveals that the two pairs are identical except that eqs.[3.3.9] and [3.3.10] each have an extra term representing the existence of the liquid-fluxes. The presence of liquid diffusion causes primarily a decrease in the rate of movement of the boundaries. The system of equations consisting of eqs. [3.3.7]-[3.3.10] describe the transient behavior of frontal drying. They must be solved at each time-step. Eqs. [3.3.7] and [3.3.8] may be treated as two simultaneous equations in η_0 and η_1 with parametric dependence on the length-scales. The two equations [3.3.9] and [3.3.10] define the rate of movement of the condesing-region boundaries. They are two nonlinear coupled differential equations. The scheme in solving these equations is to use the values of L_0 and L_1, along with the values of η_0 and η_1 to calculate the dL/dt terms at every time-step. The errors introduced in this scheme are of the order of Δt. This solution scheme is used in solving the illustrative example of section 3.4.

3.4 ILLUSTRATIVE EXAMPLE

In this section an illustrative example reagrding the solution techniques developed for frontal evaporation in a porous slab is presented.

Consider a porous slab whose properties are given in the illustrative example of section 2.5. The initial liquid-content distribution for both diffusive and non-diffusive condensate is shown in Fig. 3.4. The liquid-content distribution is associated with a 4000-hour long period of condensation in the slab with the following boundary values:

$$T_h = 90.°F$$

$$T_c = 25.°F$$

$$h_h = 90\%$$

$$h_c = 90\%$$

The location of the condensation-region assocaited with the above boundaries is:

$$\overline{L_0} = .3507$$

$$\overline{L_1} = .8857$$

At time equals to zero the boundary values are changed to the following values:

$$T_h \longrightarrow 60°F$$

$$T_c \longrightarrow 80°F$$

$$h_h = 80\%$$

$$h_c = 85\%$$

As mentioned in section 3.1 the notation is changed such that now:

$T_H = 90.°F$ Corresponds to $z=1$

$T_C = 60.°F$ Corresponds to $z=0$

After the initial transients where values of temperature and vapor-concentration have undergone changes, the boundaries of the condensation-region begin to move. The rate of movement of the boundaries depends on the presence or absence of liquid diffusion. The results of section 3.2 apply to the situation

where liquid diffusion is absent, whereas the results of section 3.3 apply to the situation with liquid diffusion present. The behavior of the fronts is studied for both cases.

For the case of non-diffusing condensate, value of liquid-content at the fronts is determined by eq. [2.4.13(b)], which states that the liquid-content in the wet-zone increases linearly with time. The reduced temperature-distribution at Fo*=1000 is shown in Fig. 3.5. The discontinuities of the temperature-gradients at the boundaires of the wet-zone with the dry regions are indicative of the heat-flux absorbed by the frontal evaporation.

For the case of diffusive condensate, the liquid-content in the profile is assumed to be given by eq. [2.4.23]. Fig. 3.4 shows this profile for an assumed initial condition where the mass of liquid is identical to the case of Dl=0. The reduced temperature distribution at a subsequent period of Fo*=1000 is shown in Fig. 3.6. As in 3.5 the discontinuities in the temperature-gradients correspond to the heat-flux absorbed by the evaporation of the diffusing liquid and the amount corresponding to critical liquid-content at the front. The differences between Fig. 3.5, and Fig. 3.6 are very small implying that at the onset of drying the effects of liquid-diffusion is negligible. However, these small effects add up in time to cause a noticeable effect on the duration of drying.

The movement of the boundaries of the wet-zone for both cases of liquid-diffusivity is obtained by time-stepping. The results appear in Fig. 3.7. The boundary movements for both diffusive and non-diffusive condensates begin at approximately the same rates. Vapor condenses in the wet-zone in both cases. For non-diffusive condensate, the condensate remains iommobile at the site of condensation. On the other hand, the diffusive condensate migrates towards the boundary. Hence, the rate of

movement of the boundary for diffusive-condensate is less than the one for non-diffusive condensate. This behavior is clearly exhibited in Fig. 3.7.

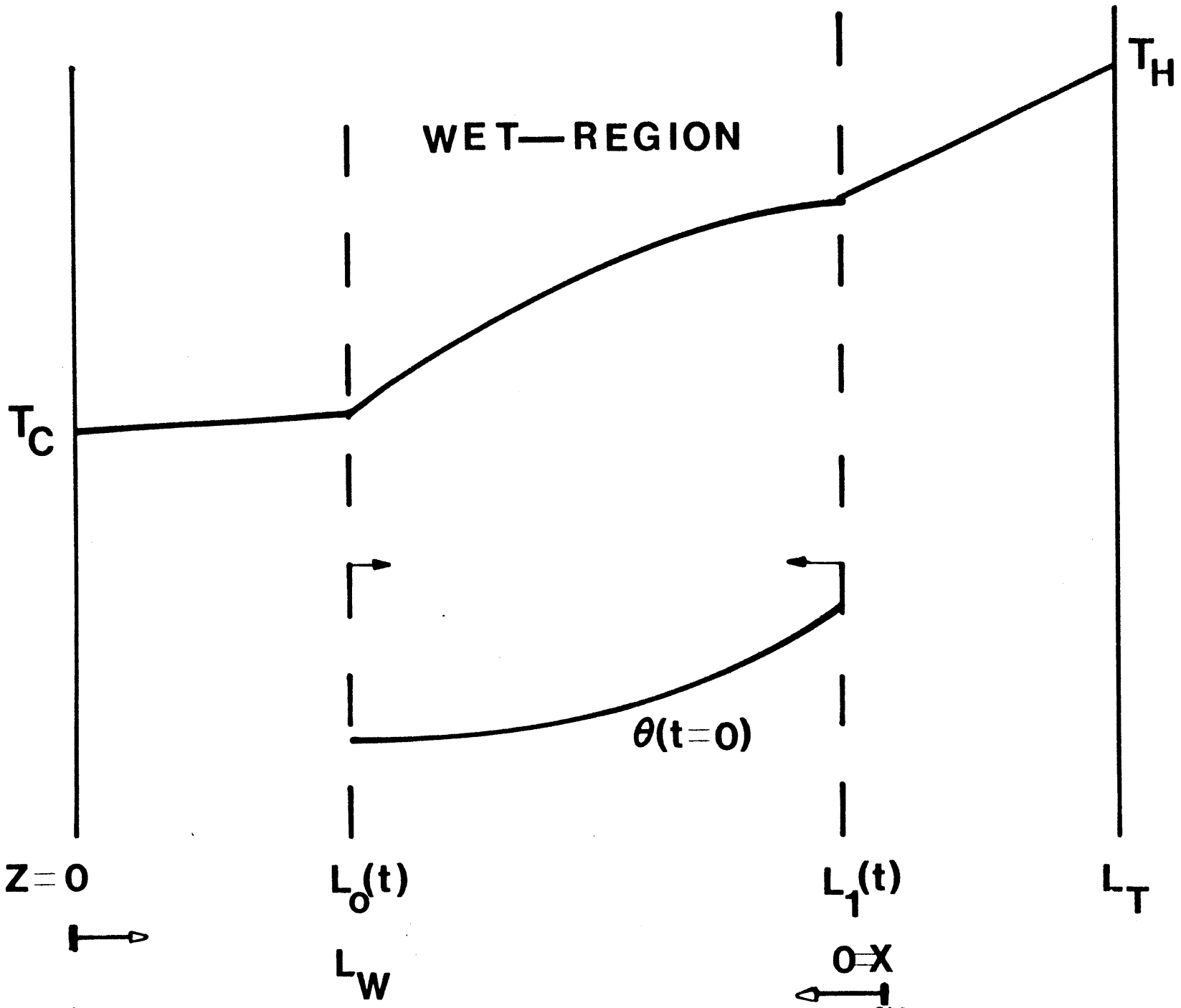

Fig. 3.1 A schematic of Temperature and Liquid-Content Profile During The Drying of A Moist Slab

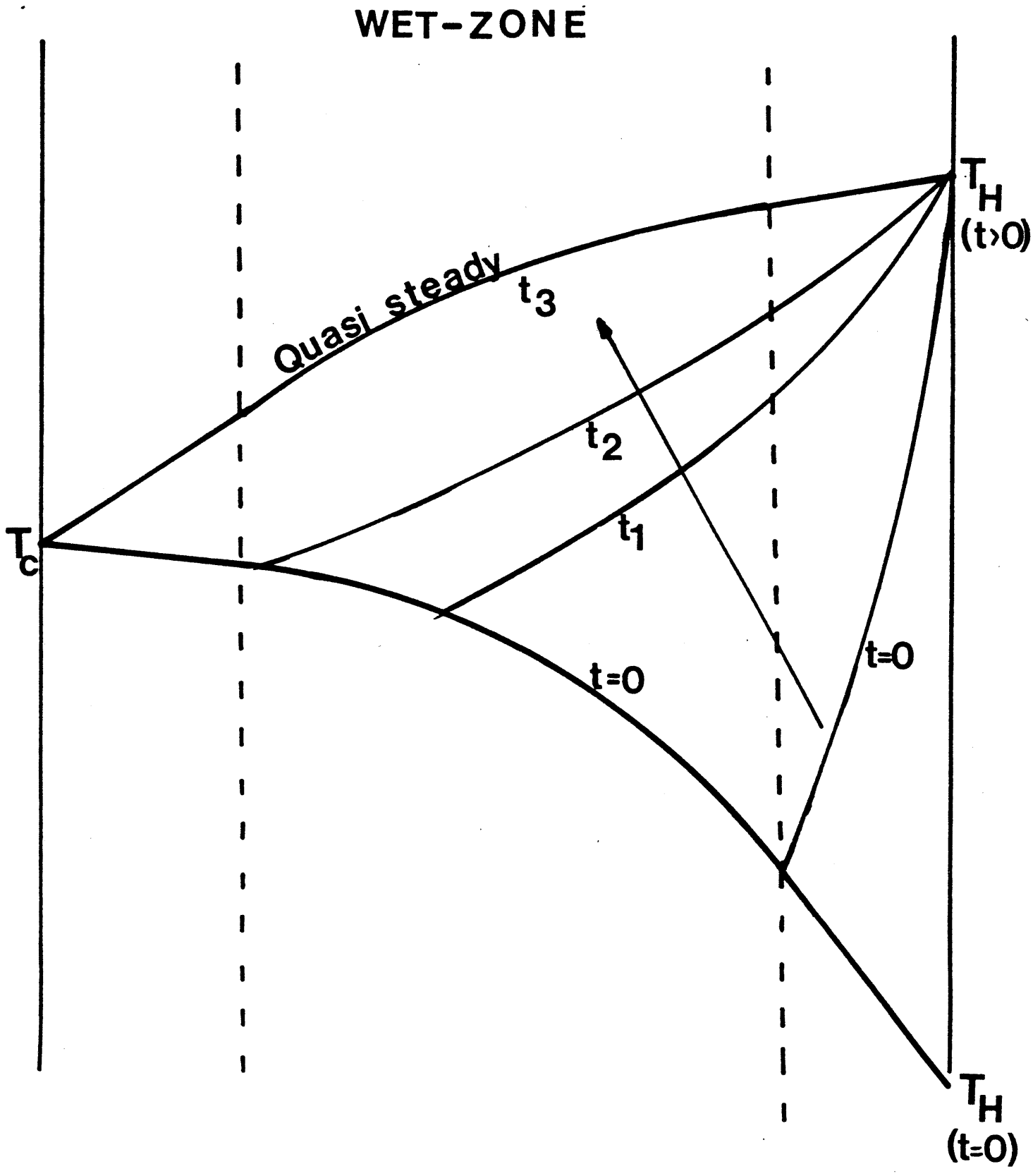

Fig. 3.2 Schematic of the Transient Behavior of the Temperature Profile after a step change in T_H

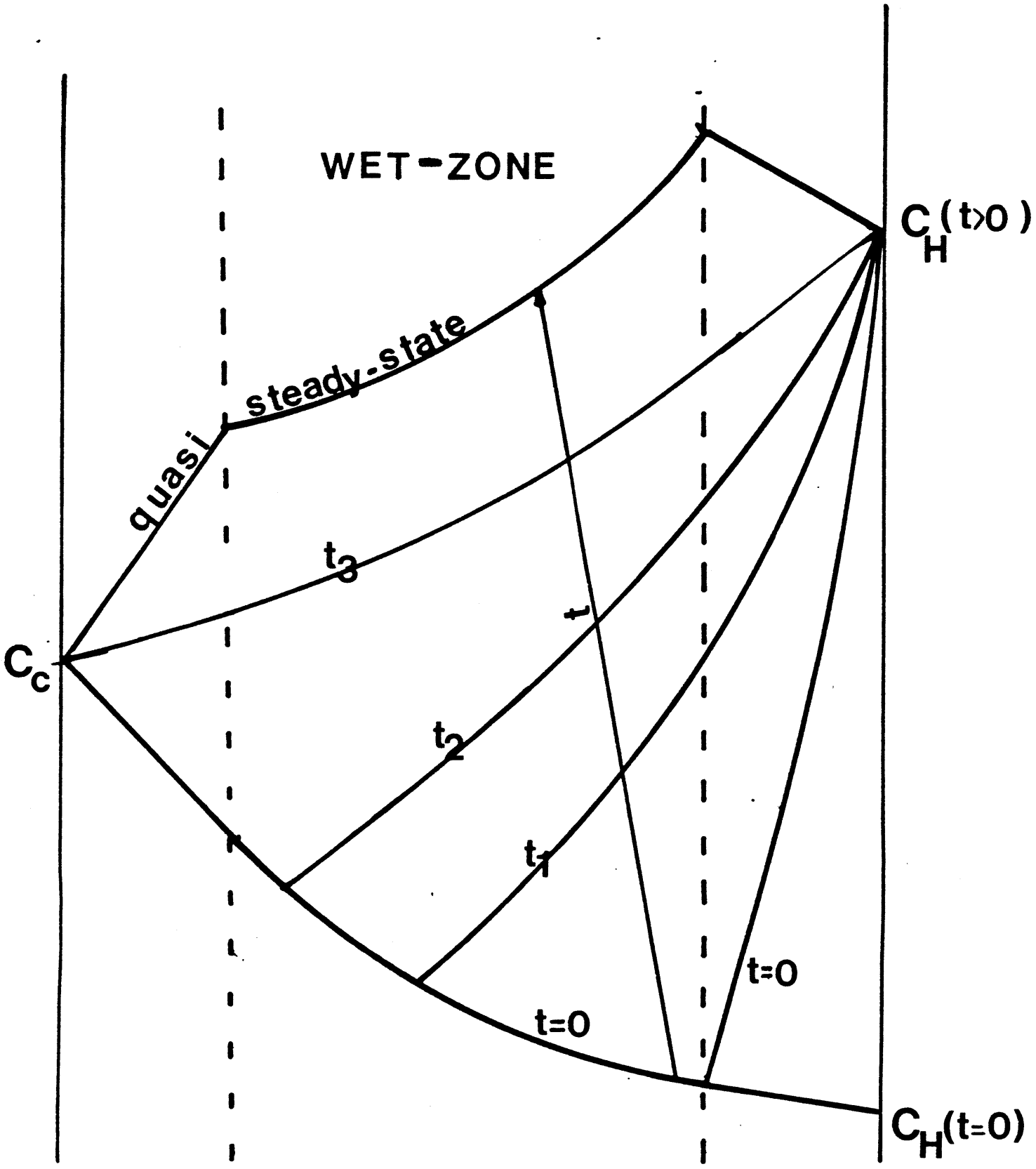

Fig. 3.3 Schematic of the Transient behavior of the Concentration Profile after a step change in C_H

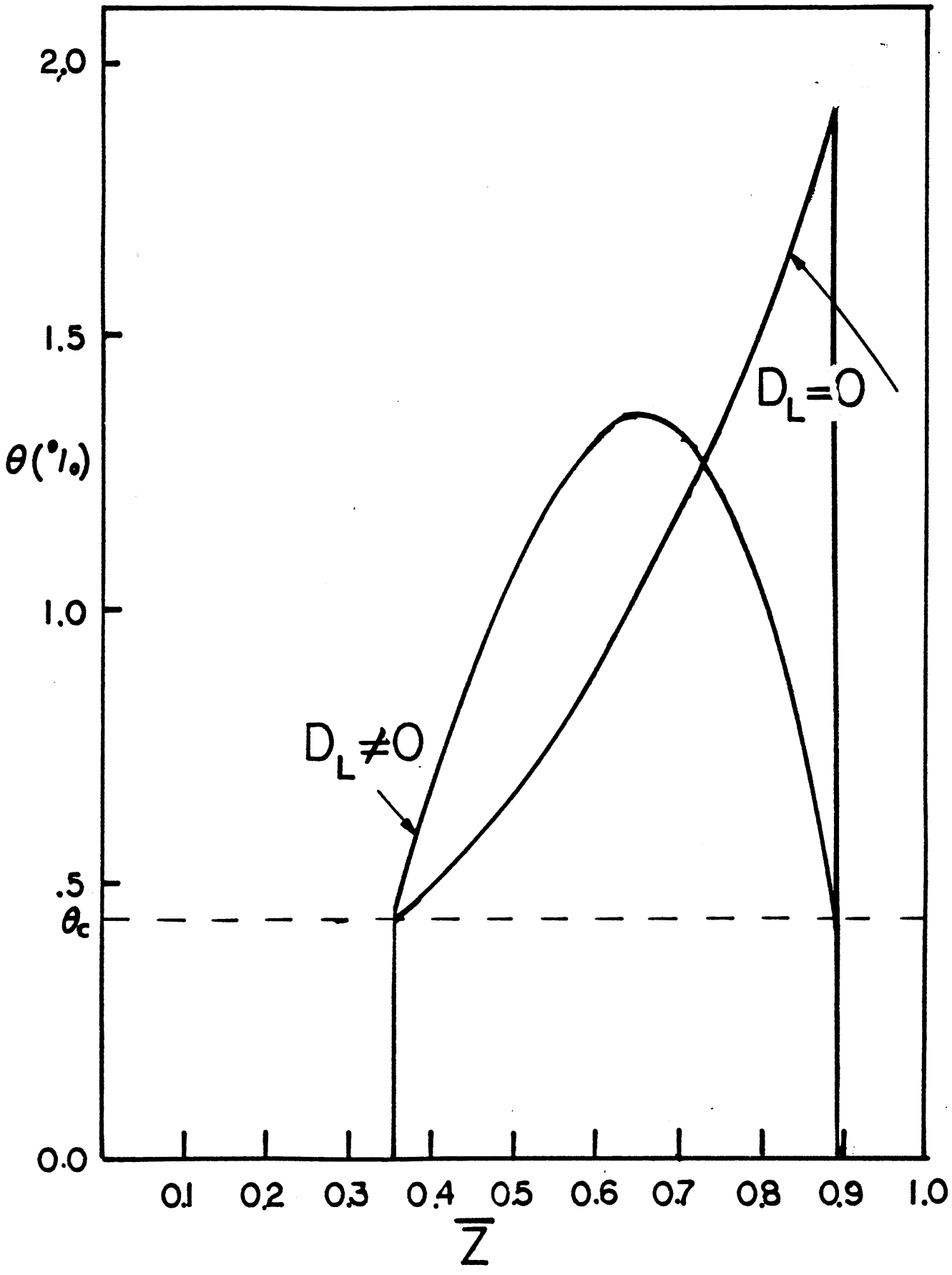

Fig. 3.4 Initial Liquid-Content Profiles for the cases of Diffusive and Non-Diffusive Condensate

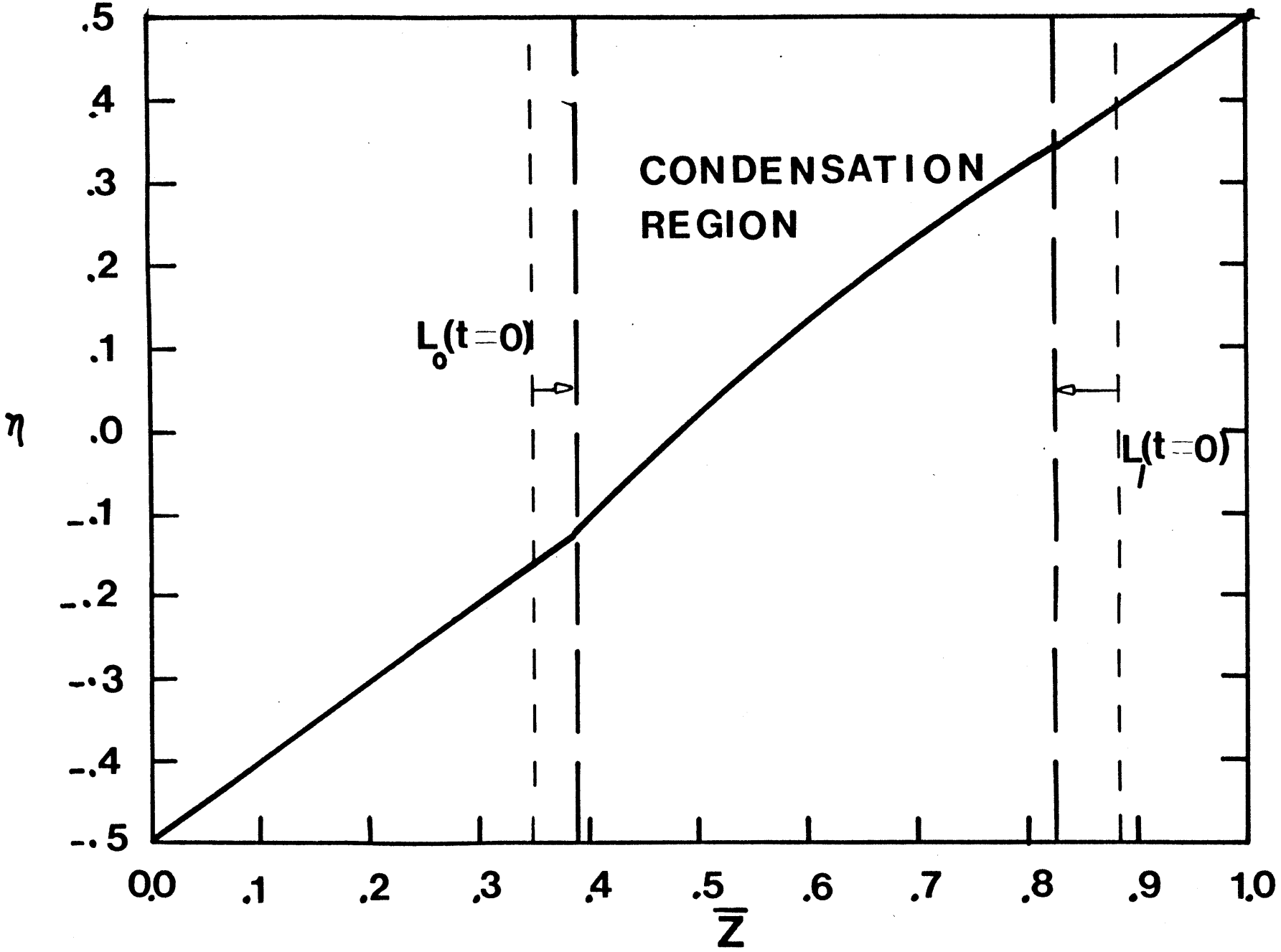

Fig. 3.5 The Reduced Temperature Profile during Frontal-Evaporation at Fo*=1000, for the case of Non-diffusive Condensate

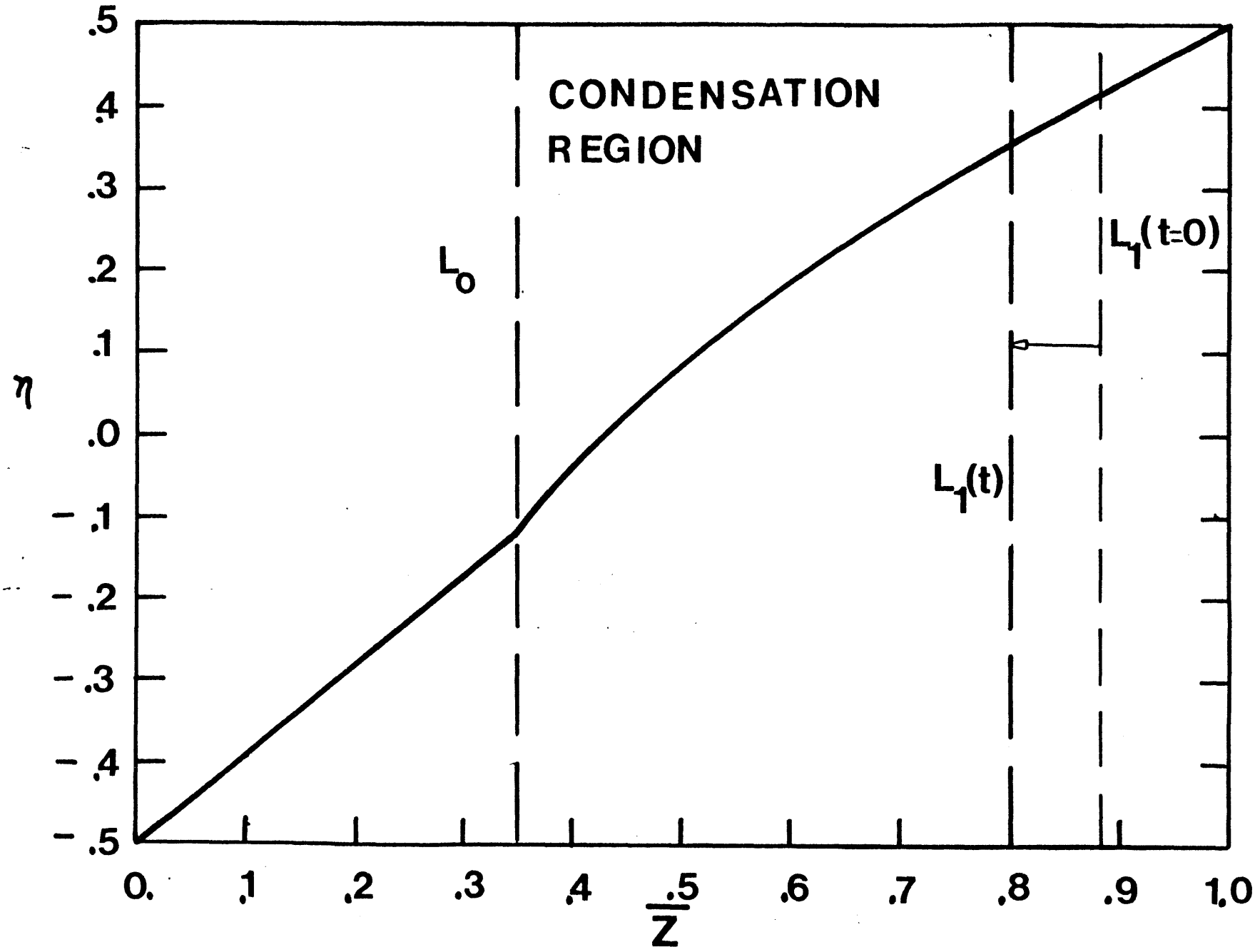

Fig. 3.6 Reduced-Temperature Profile During Frontal-Evaporation at Fo*=1000 For the case of Diffusive Condensate

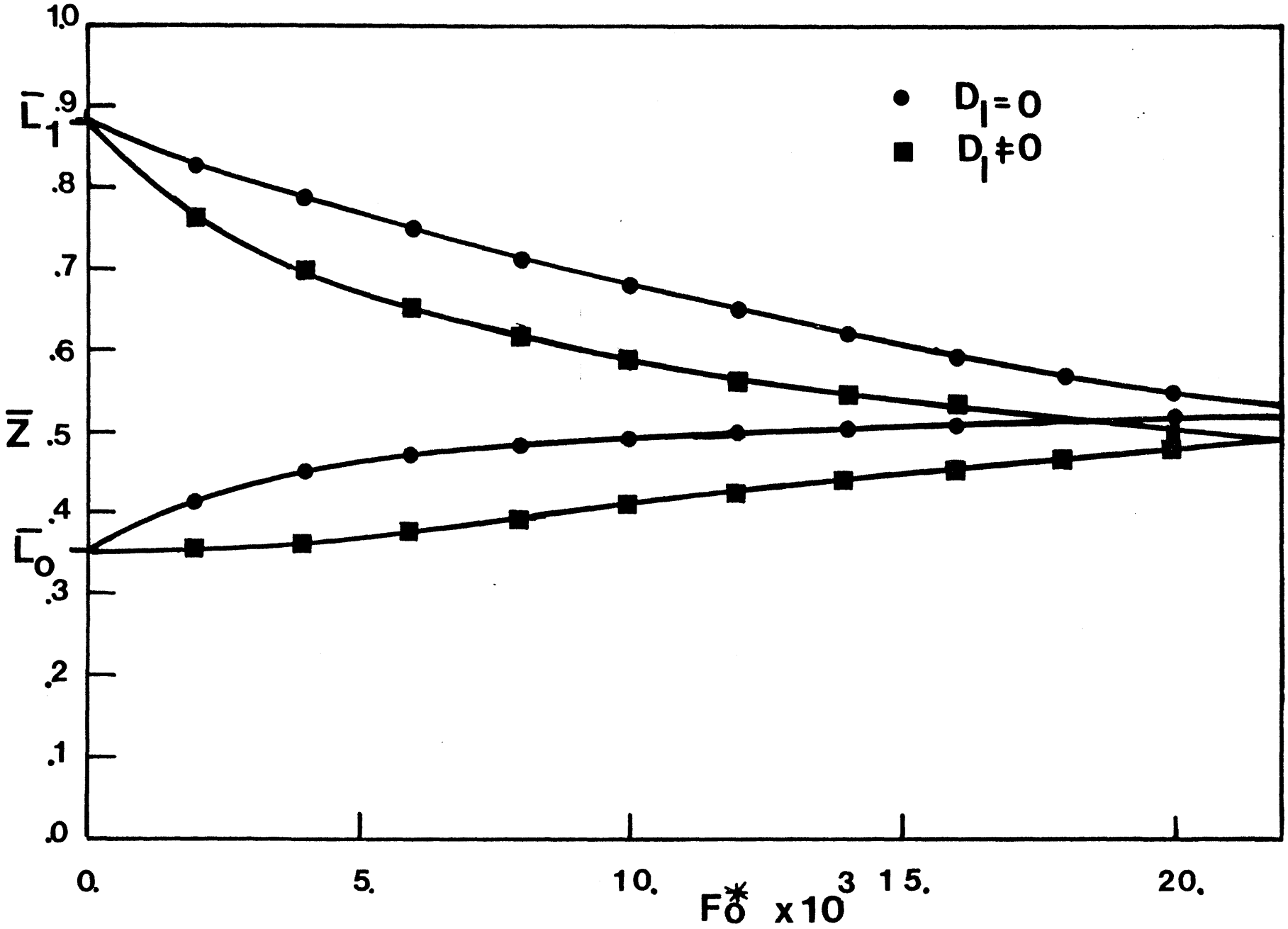

Fig. 3.7 Movement of the Boundaries of the Condensation-Region For the two cases of Diffusive and Non-Diffusive Condensate

CHAPTER 4

HEAT AND MASS TRANSFER WITH PHASE CHANGE IN A COMPOSITE WALL

4.1 INTRODUCTION

In general, insulated building structures consist of various layers, with each layer serving a purpose, be it resistance to heat and/or vapor-flux, load support, or mere cosmetics. The structure usually consists of an insulating slab, surrounded on both sides by layers of boards and sidings. The layers have various values of thermal-conductivity and vapor-permeability. Furthermore, heat and mass transfer from the surrounding ambient is controlled by natural or forced convection heat and mass transfer coefficients. Heat and mass transfer with phase change in a composite wall is effected by the characteristics of each and every layer. In this chapter the analysis of the previous chapters is extended to the study of composite walls.

In a composite wall, each layer is characterized by a value

of thermal-conductivity and vapor-diffusivity. As the values of the thermal and diffusive resistances of the layers and the outside boundary layers are unequal, the temperature and concentration drop across the layers are unequal. The layers with the largest resistance cause the largest drop, and vice versa. The temperature and vapor-concentration profiles across the wall may be calculated by neglecting the possibility of existence of a condensation-region. This assumptions leads to linear temperature and concentration profiles in each layer. Also, the vapor saturation-concentration profile associated with the temperature profile may be obtained. Condensation occurs in the layer(s) where the vapor-concentration exceeds the vapor saturation-concentration. The extent of condensation-region is determined by the balance of heat and vapor fluxes, as discussed in chapters 2 and 3.

Clearly, condensation may occur in any layer of the composite wall. However, there are certain characteristics that render the insulating layer a preferred layer for the occurence of condensation. These conditions are discussed in section 4.2. In the same section the analysis of the previous chapters is modified to incorporate the presence of the wall and ambient boundary layers on condensation in the insulation slab.

Vapor-barriers have been traditionally used to inhibit the flow of vapor into the wall structure. The vapor-barriers are made out of sheets of materials which are impermeable to vapor and liquid flow, and are usually situated next to the insulation. The presence of vapor-barriers effects the temperature and concentration profiles, as well as the condensation rate in the wall. Heat and mass transfer in a porous slab with an impermeable boundary is studied in sections 4.3, 4.4, and 4.5. A quantitative discussion on the implications of different locations of the vapor-barrier in the composite wall is given in section 4.6.

4.2 GENERALIZED BOUNDARY EQUATIONS ASSOCAITED WITH HEAT AND MASS TRANFER IN A COMPOSITE WALL

A wall structure typically consists of an insulating layer and various other sidings. The sidings are characterized by different values of thermal-resistance and vapor-diffusivity. The two sides of the structure are exposed to ambient conditions (In this chapter the term ambient replaces the term reservoir used in chapters 2 and 3). Wind current or natural convection in the ambient effect the flow of heat nad vapor through the structure. In this section these effects are modelled and incorporated into the previous results.

In a composite wall, condensation may occur in any layer. Nevertheless, the probability of occurence of condensation in the insulation is larger than in any other layer. The insulation has the smallest thermal-conductivity in the structure. This implies that the largest temperature-drop takes place across the insulation. The vapor saturation-concentration profile associated with the temperature profile drops steeply across the insulation, too. On the other hand, the open pore insulations have high values of vapor-diffusivity. This translates to a small vapor-concentration gradient in the insulation. Vapor condenses whenever its concentration reaches the saturation value. Hence, a rapidly declining saturation-concentration profile is likely to crossover a slowly declining vapor-concentration profile, and lead to condensation.

In chapters 2 and 3 the simultaneous transport of heat and

mass with phase change for a single porous slab was studied. In that study the values of temperature and relative-humidity on the two boundaries of the slab were specified. However, in a composite structure the porous slab is surrounded by various layers, each with a different value of thermal-conductivity and vapor-diffusivity. Therefore, the temperature and vapor-concentration values at the insulation boundaries become functions of the overall heat and mass transfer through the strucuture. On the warm side, the values of temperature and vapor-concentration on the insulation's boundary are lower than the ones in the warm ambient. On the cold-side, they are larger than the ones in the cold ambient. As the vapor-concentration cannot exceed the saturation levels, it is possible to envisage situations where the diffusive and thermal properties of the layers on the colder edge are such that the condensation-region in the insulation extends into the adjacent layers. In order to define the insulation's boundary values, the resistances to flow of heat and vapor on the two side of the insulation must be identified.

Heat-flux per unit area of a layer with thickness x_i, and thermal conductivity k_i is:

$$(\dot{q}/A)_i = k_i \ (\Delta T_i/\Delta x_i) \qquad [4.2.1]$$

where ΔT_i = Temperature drop across the ith-layer

The above may be written as:

$$(\dot{q}/A)_i = \Delta T_i / R_i \qquad [4.2.2]$$

The term R_i denotes the resistance to heat flow and is a property of the medium:

$$R_i = \Delta x_i / k_i \qquad [4.2.3]$$

Vapor-flux per unit area of a layer with thickness x_i and vapor-diffusivity D_i is:

$$(\dot{W}/A)_i = D_i \ (\Delta C_i / \Delta x_i) \qquad [4.2.4]$$

where ΔC_i = Vapor-concentration drop across the ith-layer

Equation [4.2.4] may be written in a form analogous to eq. [4.2.2]:

$$(\dot{W}/A)_i = \Delta C_i / R^*_i \qquad [4.2.5]$$

where R^*_i denotes the resistance to the flow of vapor. Each layer in the wall is characterized by a value of R and R^*.

Heat and vapor tranfer at the outer boundaries of the wall area affected by the air-flow patterns. The outer boundaries may be subject to natural-convection patterns or forced air-convection. Convective heat-flux is characterized by the heat transfer coefficient:

$$h = \frac{(\dot{q}/A)}{\Delta T} \qquad [4.2.6]$$

where ΔT is the temperature difference between the outer layer and the ambient temperature. Similarly, convective mass transfer is characterized by a mass transfer coefficient:

$$h_D = \frac{(\dot{W}/A)}{\Delta C} \qquad [4.2.7]$$

The heat and mass tranfer coefficients are functions of air-flow field and air properties. As the convection of heat and mass are similar in nature, the heat and mass transfer coefficients are related to eachother. The equivalence of the two coefficients is represented by the Colburn analogy:

$$Sh = Nu\ (Sc/Pr)^{1/3}$$

where

$$Sh\ [\text{Sherwood Number}] = h_D L/D$$

$$Nu\ [\text{Nusselt Number}] = hL/k$$

$$Sc\ [\text{Schmidt Number}] = \nu/D$$

$$Pr\ [\text{Prandtl Number}] = \nu/\alpha \qquad [4.2.8(a)]$$

Equation [4.2.8] may be simplified into the following form:

$$h_D = \frac{h}{\rho c_p}\left(\frac{Pr}{Sc}\right)^{2/3} \qquad [4.2.8(b)]$$

The above indicates the relation between mass transfer and heat transfer coefficients. Hence, the thermal and diffusive resistances associated with the convective transport mechanisms are:

$$R = 1/h$$

and

$$R^* = 1/h_D \qquad [4.2.9]$$

Consider Fig. 4.2.1. This is a schematic of a typical wall structure. The insulation is bounded on both sides by layers of sidings. The outside ambient conditions are given as T_{ho}, h_{ho}, T_{co}, and h_{co}. Heat and vapor flow through the structure from left to right. Assume that vapor condenses in some region of the insulation. In accordance with the notation of the previous chapters, the condensation-region is shown to be bounded by two dry region of length L_0 and L_T-L_1. The temperature and relative humidity of the two insulation boundaries are denoted by subscripts h and c. The thermal and diffusive resistances associated with each layer are shown in Fig. 4.2.1. The thermal and diffusive resistances as defined by eqs. [4.2.3],[4.2.5], [4.2.6], and [4.2.7] apply to the situations where no condensation takes place. Hence, such definitions of resistance are associated only with the dry regions of the insulation. These resistances are:

$$R_{c0} = L_0/k_{ins}$$

$$R^*_{c0} = L_0/D_{ins}$$

$$R_{c1} = (L_T-L_1)/k_{ins}$$

$$R^*_{c1} = (L_T-L_1)/D_{ins} \qquad [4.2.10]$$

The total thermal and diffusive resistances from the ambient to the boundary of the condensation-region are obtained by the addition of resistance of all layers. Hence, heat-flux per unit area into the wall is:

$$(\dot{q}/A)_{in} = \frac{T_{ho} - T_0}{\sum_1^3 R_i + R_{c0}} \qquad [4.2.10]$$

and heat-flux per unit area out of the wall is:

$$(\dot{q}/A)_{out} = \frac{T_1 - T_{co}}{\sum_4^6 R_i + R_{c1}} \qquad [4.2.11]$$

Similarly, the vapor-fluxes per unit area into and out of the wall are:

$$(\dot{W}/A)_{in} = \frac{C_{ho} - C^*_0}{\sum_1^3 R^*_i + R^*_{c0}} \qquad [4.2.12]$$

and

$$(\dot{W}/A)_{out} = \frac{C^*_1 - C_{co}}{\sum_4^6 R^*_i + R^*_{c1}} \qquad [4.2.13]$$

It may be recalled that the results of chapters 2 and 3 were obtained by matching the gradients of temperature and vapor-concentration in the condensation-region with those of the dry regions, eqs. [2.6.1]-[2.6.4], [3.2.3]-[3.2.5], and [3.3.3]-[3.3.6]. In these set of boundary equations the heat and vapor fluxes in and out of the the condensation-region were defined by the values of temperature and vapor-concentration at the boundaries of the slab. However, these values are not readily available anymore, for their values depend on the thermal and diffusive properties of the ensemble of the layers. Therefore, eqs. [4.2.10]-[4.2.13] must be used as the equations defining heat and vapor fluxes into the condensation-region. The matching of the temperature and concentration profiles between the wet-zone and the adjacent dry ones must be carried out using eqs. [4.2.10]-[4.2.13]. These modifed boundary equations are referred to as generalized boundary equations. Unfortunately, due to the nature of the generalized boundary equation, the algebraic manipulations conducted in sections 2.5, 2.6, 3.2 amd 3.3 cannot be affected. Hence, the elegant and simple results of the previous chapters cannot be derived.

Nevertheless, in order to use the results of chapters 2 and 3, the values of T_h, T_c, h_h, and h_c may be obtained in another manner. The presence of the sidings must be handled in a manner different from the one which leads to the generalized boundary equations. Considering the case of spatially-steady condensation, for both diffusive and non-diffusive types of condensate, the insulation's temperature and concentration boundary values may be estimated by assuming a linear temperature and concentration drop across every layer, i.e. ignoring the

presence of condensation in the domain. These estimates may be used to obtain the location, and the boundary temperature values of the condensation-region. This new information may be then used to obtain better estimates of T_h, T_c, h_h, and h_c by using the concept of "voltage dividers'. The concept of "voltage divider" is a term used in the study of electrical circuits, and relates the potential drop across a resistance, which is located in series with a group of resistances, to the total potential drop across the network. Hence, the temperature drop across the dry regions of the insulation are:

$$\frac{T_h - T_0}{T_{ho} - T_0} = \frac{\sum_1^3 R_i + R_{c0}}{R_{c0}} \qquad [4.2.14]$$

and

$$\frac{T_1 - T_c}{T_1 - T_{co}} = \frac{\sum_4^6 R_i + R_{c1}}{R_{c1}} \qquad [4.2.15]$$

The vapor-concentration drops may be obtained similarly.

By successive iteration the values of T_h, T_c, h_h, and h_c converge to their final values, and the case of spatially-steady condensation in a composite wall is solved.

A similar iteration scheme may be introduced for the spatially-unsteady cases. In this situation, the insulation's

boundary values are obtained at each time-step by successive iteration. This results in the increase of the computational load. However, as the actual boundary-values do not vary much at each time-step, the number of iterations required turn out to be relatively small.

4.3 HEAT AND MASS TRANSFER WITH PHASE CHANGE IN A POROUS SLAB WITH AN IMPEREMEABLE BOUNDARY

In many wall structures vapor-barriers are used to decrease the possibility of condensation in the insulation. It will be later shown in chapter 7 that the optimum positioning of the vapor-barrier vis-a-vis the vapor-concentration gradient depends on the climatic conditions. The vapor-barrier may be positioned in oder to stop vapor-flux in cold-season, yet it may have detrimental effects during the warm-season when the vapor-flux changes direction due to the excess of ambient vapor-concentration over the vapor saturation-concentration corresponding to the temperature of the vapor-barrier. In this section, the effect of an impermeable barrier on the cold side of a porous slab will be studied.

Consider Fig. 4.2. This is a schematic of a porous slab subject to temperature and vapor-concentration gradient.The boundary $z=L_T$ is considered to be impermeable to both vapor and liquid-fluxes. Let us consider the case where the effects of condensation on temperature profile is negligible, such that there is a linear temperature-drop across the slab. The vapor saturation-concentration, C^*, corresponding to the temperature profile is indicated in Fig. 4.2. With the $z=L_T$ boundary impermeable to vapor-flux, vapor migrates into the porous slab until one of the following three happens: first, if the vapor-concentration on the hot-side is less than the saturation-concentration corresponding to the temperature at the cold-edge, the porous slab will have a uniform vapor-concentration equal to that of the hot-side. In this case

condensation does not occur in the medium. With $C_h > C^*_c$, two possible modes of condensation is possible: regional or planar. Regional condensation refers to the situation where the following equality hold for some length-scale L_0:

$$\frac{C_h - C^*_0}{L_0} = \left.\frac{dC^*}{dz}\right|_{L_0} \qquad [4.3.1]$$

If a value of L_0 exists such that the above equation is satisfied, the condensation-region extends from $z=L_0$ to the vapor-barrier. This case resembles the situation discussed in chapter 2. For given values of L_T, T_h, and T_c, eq. [4.3.1] imposes a lower limit on the level of humidity at the hot-side. The threshold value of C_h is obtained by evaluating eq. [4.3.1] at the largest possible value of L_0, i.e. L_T:

$$C_{h\,min} = C^*_c - L_T \left.\frac{dC^*}{dz}\right|_{L_T} \qquad [4.3.2]$$

The threshold value is shown in Fig. 2.3.1. For values of C_h such that :

$$C^*_c < C_h < C_{h,min}$$

condensation occurs only at the plane of $z=L_T$. This mode of condensation is referred to as planar-condensation.

The different modes of condensation in a porous slab with an impermeable boundary may be compared with the case of permeable boundary. In the case where both sides of the slab are permeable, condensation occurs only for $C_h > C_{h\ min}$. No planar-condensation occurs in this case because the vapor diffuses out of the slab at $z=L_T$. However, with an impermeable boundary the vapor diffuses into the slab, and since there is no outflow, the level of concentration in the medium increases with time. Eventually, the value of concentration at the cold-edge reaches the saturation value. As the vapor-concentration cannot exceed its saturation values, the diffusing vapor condenses into liquid.

The presence of an impermeable boundary has two siginificant effects. First, condensation occurs at hot-side humidity values lower than if there were no vapor-barriers. Second, the impermeable boundary causes an increase in the condensation-rate intensity. In order to evaluate the effects of the impermeable boundary on heat and mass transfer in a porous slab, the two possible modes of condensation are studied seperately in the next two sections

4.4 CONDENSATION IN A POROUS SLAB WITH AN IMPERMEABLE BOUNDARY

CASE I: REGIONAL CONDENSATION

The effects of placing an impermeable boundary on the cold-edge of a porous slab, subjected to temperature and concentration gradients were studied in the previous section. It was shown there that for $C_h > C_{h\ min}$, a condensation-region is established. The condensation-region is bounded by the impermeable boundary and extends into the porous slab. The location of the condensation-region in the slab is determined by the continuity of vapor and heat fluxes at the boundary of the wet-zone.

The case under study in this section is a special case of the general problems studied in chapters 2 and 3. The presence of the impermeable boundary imposes two new conditions. First, the relative humidity at the cold-edge, h_c, equals one. Second, liquid-flux at the cold-edge is zero. The first conditions translates into the condition that the condensation-region extends to the cold-edge of the slab. The second condition implies that for mobile condensates, the liquid-content profile has a zero-gradient at $z=L_T$, and that at steady-state all the condensate leaves the condensation-region from the $z=L_0$ boundary. These new conditions modify the results of chapter 2. The objective of this section is not to rederive the previous results with different boundary-conditions, for the modification of those

results is straight-forward.

The significant effect of the impermeable boundary is the increase in the condensation rate per unit area. In order to assess the increase of the condensation rate, consider a condensation region of width L_w. With no vapor-barriers, the condensation-rate per unit area in the domain is equal to the difference between the vapor-flux into the domain and the vapor-flux out of the domain:

$$\int_0^{Lw} \Gamma(x)dx = - D_v \left.\frac{dC^*}{dx}\right|_0 + D_v \left.\frac{dC^*}{dx}\right|_{L_T} \qquad [4.4.1]$$

With the boundary at $x=L_w$ impermeable to vapor, the vapor-flux into the domain condenses into liquid form. Therfore, the ratio of condensation-rate per unit area with an impermeable boundary to the one with a permeable boundary is:

$$\Lambda = \frac{1}{1 - \dfrac{(dC^*/dx)_{L_0}}{(dC^*/dx)_0}} \qquad [4.4.2]$$

Using the non-dimensional notation of the previous chapters, and the temperature profile results of section 2.3, the above may be written as:

$$\Lambda = \frac{1}{1 - s},$$

where

$$s = \left(\frac{1+0.5\beta'}{1-0.5\beta'}\right)^2 \frac{\exp\lambda' - 1 + \lambda'\exp\lambda'}{\exp\lambda' - 1 + \lambda'} \exp\left[\frac{-.5\gamma'\beta'}{1-.5\beta'} + \frac{-.5\gamma'\beta'}{1+.5\beta'}\right]$$

[4.4.3]

A plot of Λ versus the latent heat transport coefficient, λ', is given in Fig. 4.3. The plot is generated for a mean temperature value of 510. °R. The results indicate that the increase in condensation-rate per unit area is significant at small values of λ', which corresponds to small values of β'. As the value of λ' increases, at fixed T'_r, the vapor-flux at the cold-edge becomes negligible and Λ approaches 1. In most practical cases the latent heat transport coefficent has a value in the range of 0.5 to 5. Hence, the effect of an impermeable boundary is to increase the condensation rate by a factor of 2 to 4. It must be noted that the effect of the impermeable boundary as demonstrated by the ratio Λ is a lower bound. In absence of the impermeable boundary, the condensation-region is bounded by two dry regions. With the placement of the barrier, the width of the condensation-region is extended to the cold-edge. The vapor-flux leaving the condensation-region ,in the case of no barrier, is larger than the flux that would have left if there were no vapor-barriers and the cold-side humidity were equal to one. Hence, the ratio of condensation rates defined by eq. [4.4.3] is a lower bound.

The presence of layers in the wall other than the insulation may be incorporated into the results of this section by the iteration scheme discussed in section 4.2.

The significant increase in the condensation-rate per unit area which is attributeable to the placement of a vapor-barrier implies that incorrectly positioned vapor-barriers may cause severe condensation problems.

4.5 CONDENSATION IN A POROUS SLAB WITH AN IMPERMEABLE BOUNDARY

CASE II: PLANAR CONDENSATION

Planar-condensation in a porous slab refers to the situation where vapor condensation takes place only at the impermeable boundary. In section 4.3, it was shown that for planar-condensation the condition on the hot-side vapor-concentration is:

$$C^*_c < C_h < C^*_c - L_T \left.\frac{dC^*}{dz}\right|_{L_T}$$

The condensation-rate per unit volume is define as a pulse function at the $z=L_T$ edge. The condensation rate per unit area equals to the vapor-flux at the cold-edge:

$$(\dot{W}/A)_T = \int_0^{Lw} \Gamma(x)\, dx = -D_v \frac{C_h - C^*_c}{L_T} \qquad [4.5.2]$$

Theoretically, condensation takes place over an infinitesimal thickness. However, in reality condensation takes place over a finite, nevertheless very small, width at the cold-edge boundary. During the early period of condensation, when the condensate is immobile, liquid-content increases linearly with time. As the liquid-content exceeds the critical value, θ_c, liquid begins to diffuse into the porous slab. At the boundary of the infinitesimally small condensation-region, the diffusing liquid evaporates. The difference between the condensation rate, and the evaporated liquid-flux goes into the advance of the wet-zone boundary into the porous slab. Inside the wet-zone liquid and vapor co-exist in equilibirium . Therefore, the temperature profile in the wet-zone is described by the results of section 2.3.

The condensation rate per unit area is related to the liquid-flux which evaporates at the wet-zone boundary, J_0, and the movement of the boundary:

$$\int_0^{Lw} \frac{\Gamma(x)\, L_w^2}{\rho\epsilon}\, dx = J_0 - \rho\epsilon\theta_c \frac{dL_0}{dt} \qquad [4.5.2]$$

All the terms in the above have been previously defined. The dL_0/dt term is negative indicating that the boundary is moving into the slab, i.e. length L_0 is decreasing.

Continuity of mass at the moving boundary may be written as the balance between the vapor-flux entering the slab, the vapor-flux entering the wet-zone, the vapor-flux generated by the evaporation of the diffusing liquid, and the increase in the

width of the wet-zone:

$$D_v \frac{C_h - C^*_0}{L_0} + J_0 + D_v \frac{dC^*}{dz} = -\rho \epsilon \theta_c \frac{dL_0}{dt} \quad [4.5.3]$$

Similarly, the heat balance may be written as:

$$k \frac{T_h - T_0}{L_0} + k \frac{dT^*}{dz} - J_0 h_{fg} = \rho \epsilon \theta_c h_{fg} \frac{dL_0}{dt} \quad [4.5.4]$$

The steady-state location of the wet-front is reached when the dL_0/dt term vanishes. Equations [4.5.3] and [4.5.4] without the dL_0/dt terms are identical to the boundary equation obtained for mobile condensates in section 2.6. The only difference is that in this case all of the condensed vapor leaves the $z=L_0$ boundary, i.e. $\alpha=1$. Therefore, the steady-state location of the front may be obtained by the results of section 2.6.

The presence of an impermeable boundary on a porous slab, causes condensation to occur for a wider range of hot-side humidity values, than if the barrier were not there. The steady-state condensation rate and the location of the condensation-region are determined by the results of section 2.6. The presence of other layers in the wall may be incorporated into these results by the iteration scheme discussed in section 4.2.

4.6 VAPOR-BARRIERS IN A COMPOSITE WALL

In the previos sections the effects of an impermeable barrier on one side of a porous slab were identified. The inclusion of a vapor-barrier on one side of a porous slab was found to have two important consequences. First, condensation occurs for a wider range of boundary-conditions. Second, as the vapor-barrier arrests the flow of vapor out of the insulation, the condensation rate is increased. In this section a more qualitative study of the effects of vapor-barriers in composite walls is undertaken.

The optimum location of the vapor-barrier in a building wall depends on the climatic conditions as well as the materials used in the wall construction. In this section the importance of climatic conditions is studied. The role played by the other wall layers is the subject of study of chapter 7.

The vapor-barriers are used to inhibit the flow of vapor into the insulation. Yet, the direction of vapor-flux is not the same throughout the four seasons. Therefore, the location of the barrier with respect to the insulation is not a unique choice. Consider the following possibilities: A building may or may not be heated during the cold-season, and it may or may not be air-conditioned during the warm-season. In each case the wall might or might not have a vapor-barrier. Furthermore, the vapor-barrier could be on the side closer to the inside, or on the side closer to the outside. In total there are twelve

possibilities. It is not the intention of this work to investigate all possibilities completely. Yet a few are chosen to investigate the effects of climatic conditions, and the location of the vapor barrier on such issues as the intensity of condensation, and the possibility of dry-out during the next season. In the following examples, it is assumed that the vapor-barrier is completely impermeable to vapor and liquid flow.

Consider the case of a building with winter heating and no summer air-conditioning, Figs. 4.4-4.6. With the vapor-barrier on the inner-side, Fig. 4.4, the vapor-flux across the insulation is zero during the cold-season. Hence, no vapor-condensation occurs during the cold-season. Furthermore, as the building is not air-conditioned during the summer, it may be assumed that the building is approximately at the same temperature as outside. The relative humidity throughout the wall is uniform and most likely to be less than 100%. Therefore, the possibility of condensation during the warm-season does not exist. With vapor-barriers on the outer-side of the building, Fig. 4.5, the insulation is not protected against condensation during the cold-season. As the vapor-concentration on the warm side is larger than the saturation-concentration corresponding to the temperature on the cold-side, the vapor condenses in the insulation. As already discussed in the previous sections, the condensation-region may extend to the vapor-barriers, or be restricited to the plane of the vapor-barrier. The condensation rate is largest next to the vapor-barrier. As the building is not air-conditioned during the summer, the wall temperature is uniform and equal to the ambient's temperature. The driving potential for the evaporation of the condensate is the difference between the saturation concentration at the wet-zone boundary and the inside vapor-concentration. The process of evaporation requires a heat input which must be supplied from both the inside and outside. This requires a decrease in the temperature at the condensation-region's boundary, as shown in Fig. 4.5. The dip in

the temperature leads to a lower value of saturation-concetration at the wet-zone front, reducing the driving mass transfer potential. Hence, with no summer air-conditioning, the amount of condensate evaporating towards the inner-side of the building is modest. Let this case be compared with the situation where no vapor-barrier is present, Fig.4.6. In this case the building is capable of experiencing vapor-exchange with both the inside and outside. During the cold season the condensation region does not necessarily extend to the outer-edge. This is becasue the relative humidity on the cold-edge is not any more restricited by the vapor-barrier to equal one. The condensation-rate per unit area, is, also, less than the case where the vapor-barrier was present. During the warm-season, the absence of vapor-barriers allows evaporation to the outer-side of the building to proceed. The discussion on the effect of evaporation on the temperature-profile, as presented for the case with vapor-barrier on the outer-side, applies to this situation as well. However, in this case the evaporation rate will be more than the previous case because the condensate can evaporate to both inside and outside . In sum, the presence of a vapor-barrier on the outer-side results in a decrease in the rate of evaporation of the condensed vapor.

The situations where the building is air-conditioned during the warm-season is shown in Figs. 4.7-4.8. Fig. 4.7 is a schematic of the case where the vapor-barrier is located on the inner-side. As before, the location of the vapor-barrier on the inner-side inhibits the flow of vapor and its subsequent condensation in the insulation during the cold-season. However, the vapor-barrier does not inhibit the flow of vapor into the insulation during the warm season. The inside of the building is air-conditioned which implies that the temperature of the vapor-barrier is less than that of the outside. As the saturation-concentration increases rapidly with increasing temperature, a concentration-gradient is set up across the insulation which leads to condensation. The condensate would

have to evaporate during the cold-season, when the outside vapor-concentration is less than that of the inside.

Figure. 4.8 corresponds to the situation where the vapor-barrier is located on the outer-side of the insulation. In this setup vapor migrates into the insulation and condenses during the cold-season. As the building is air-conditioned, the condensate evaporates into the building during the warm-season and the insulation dries up.

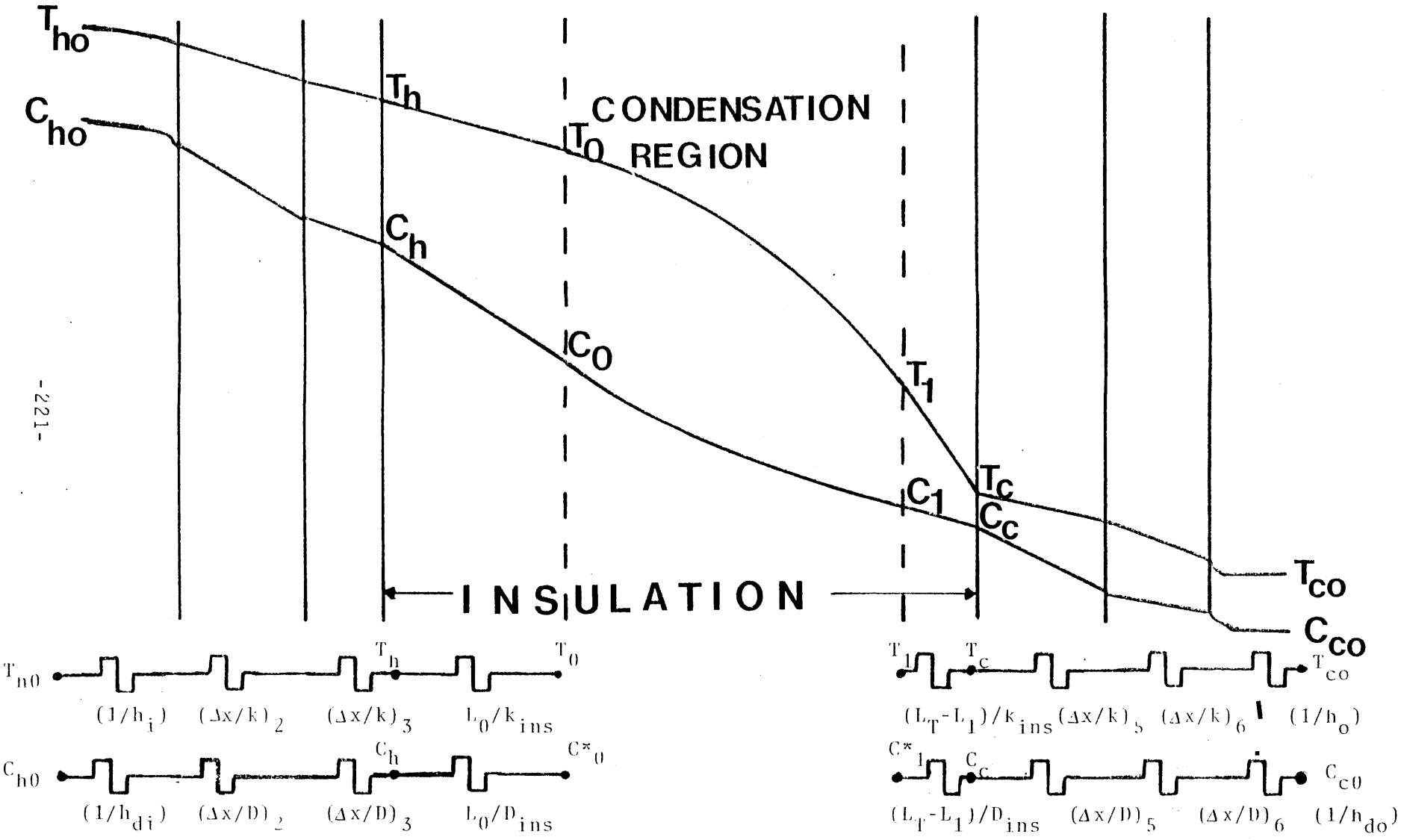

Fig. 4.1 A Schemtaic of a Typical Wall Structure with the Associated Thermal and Diffusive Resistances

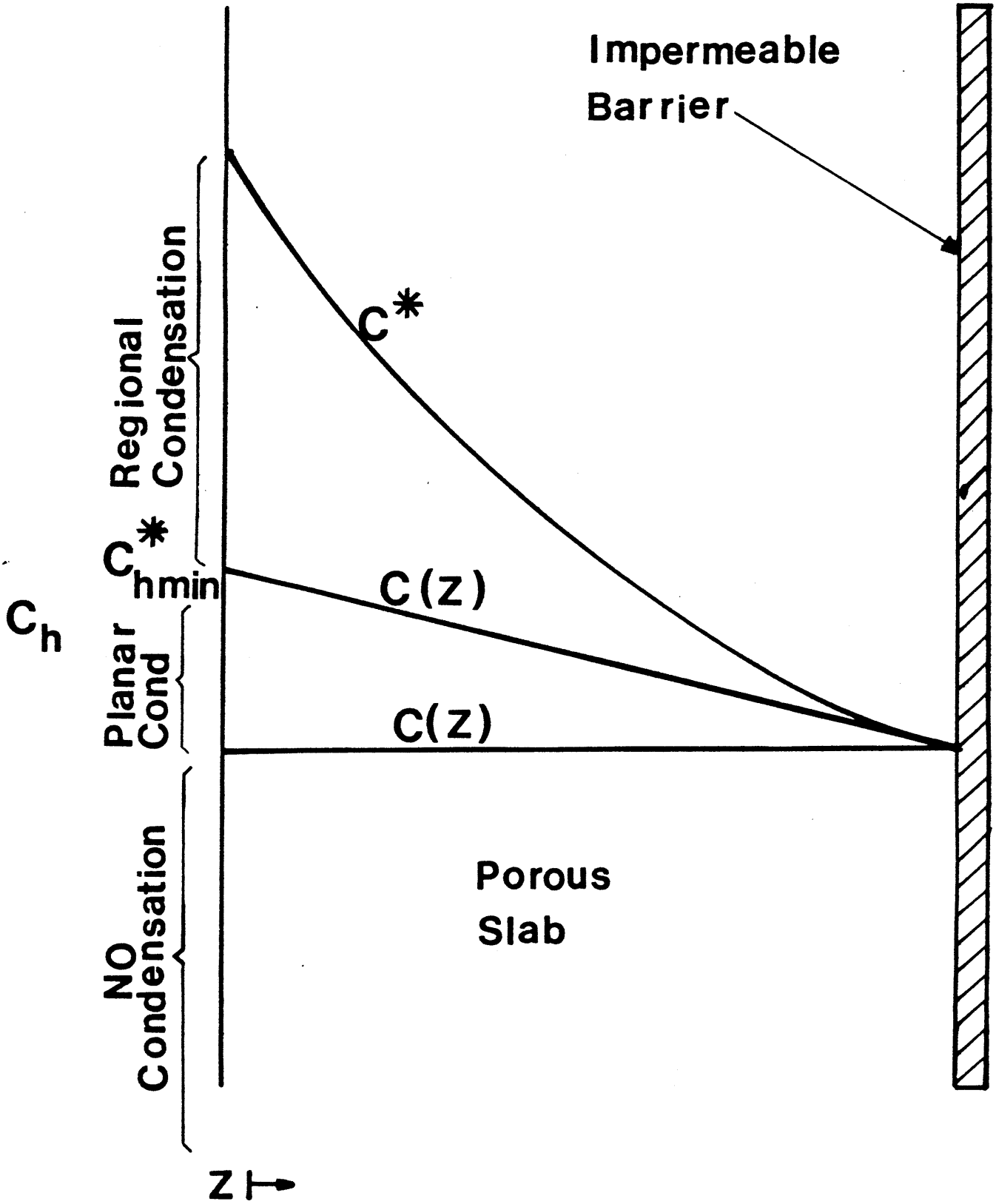

Fig. 4.2 Schematic of Various modes of Condensation as a Function of C_h for a Porous Slab with an Impermeable Boundary

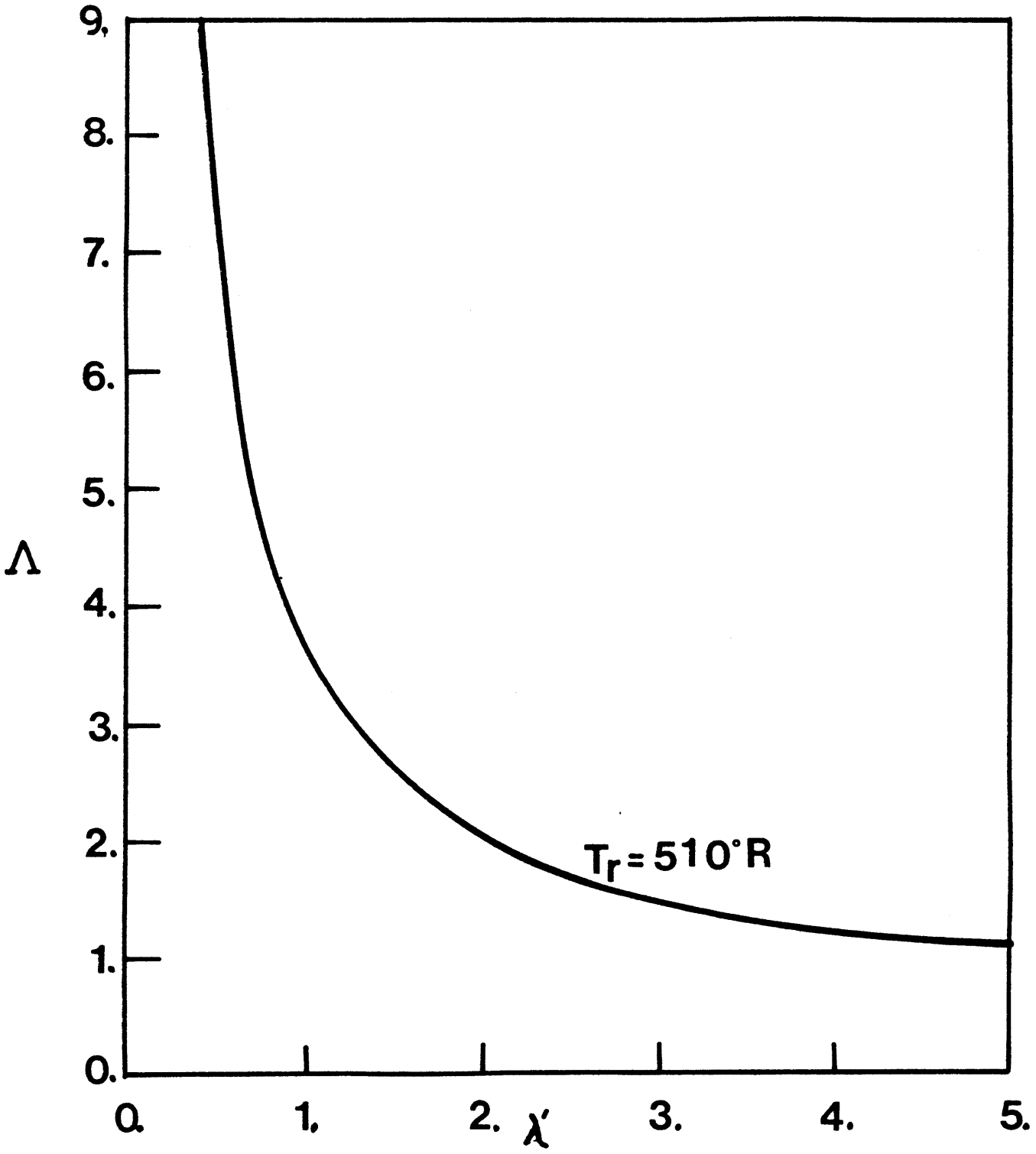

Fig. 4.3 The ratio of Condensation rate per unit area of the Porous Slab with an Impermeable Boundary to the case where the Impermeable Boundary is Absent versus λ'.

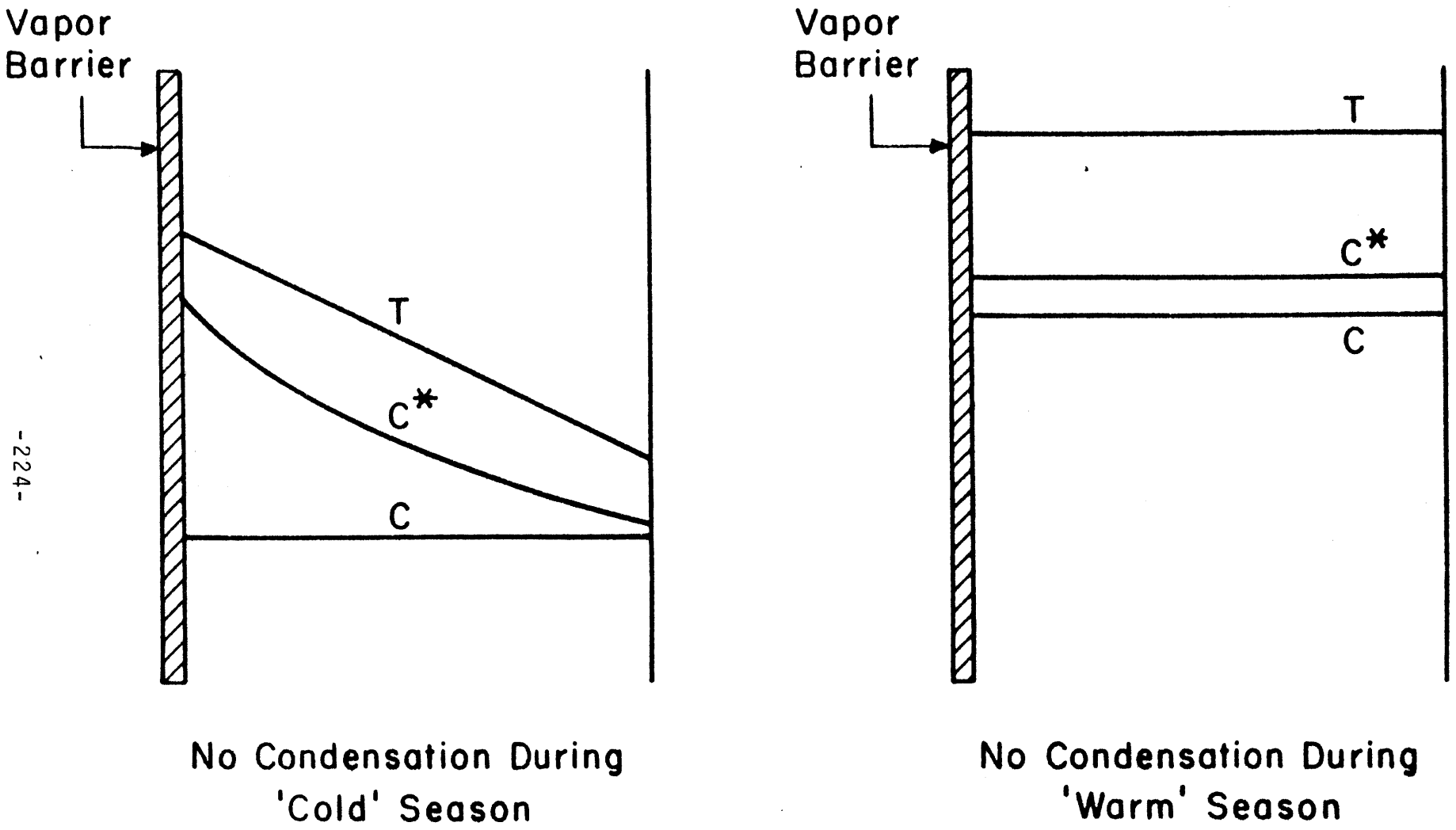

Fig. 4.4 Building with Winter Heating and no Summer Air-Conditioning Vapor-Barrier on The Inner-side

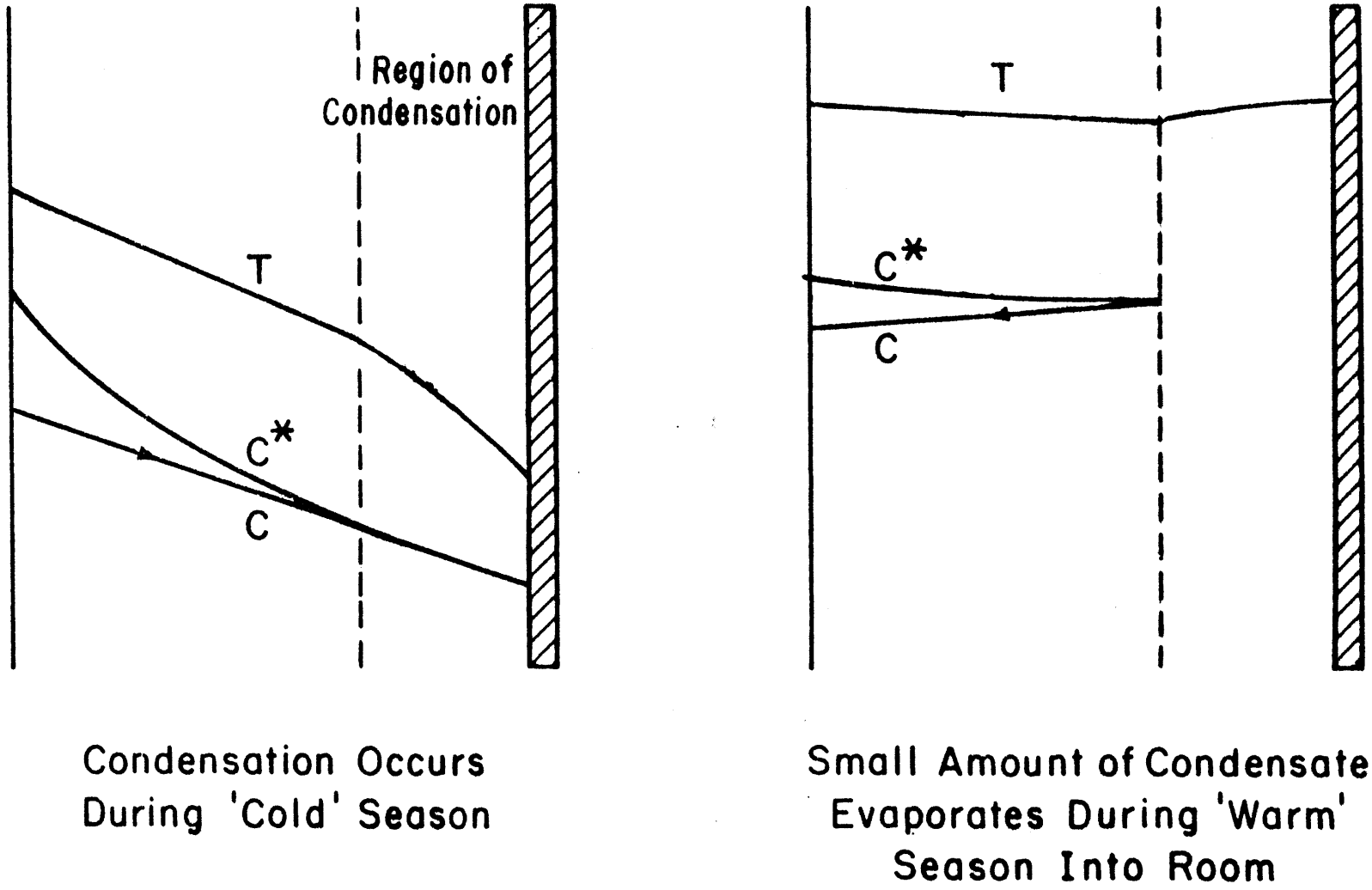

Fig. 4.5 Building With Winter Heating and no Summer Air-Conditioning

Vapor Barrier on the Outer-Side

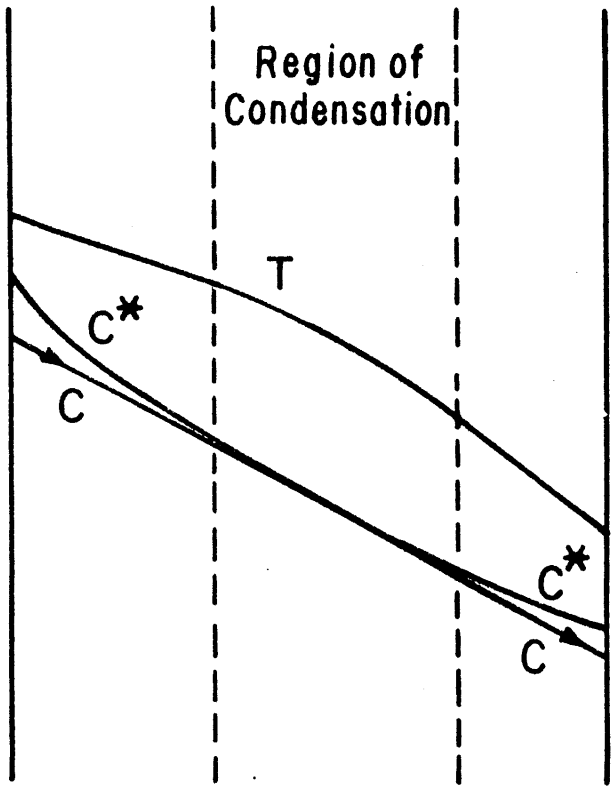

Condensation During
'Cold' Season

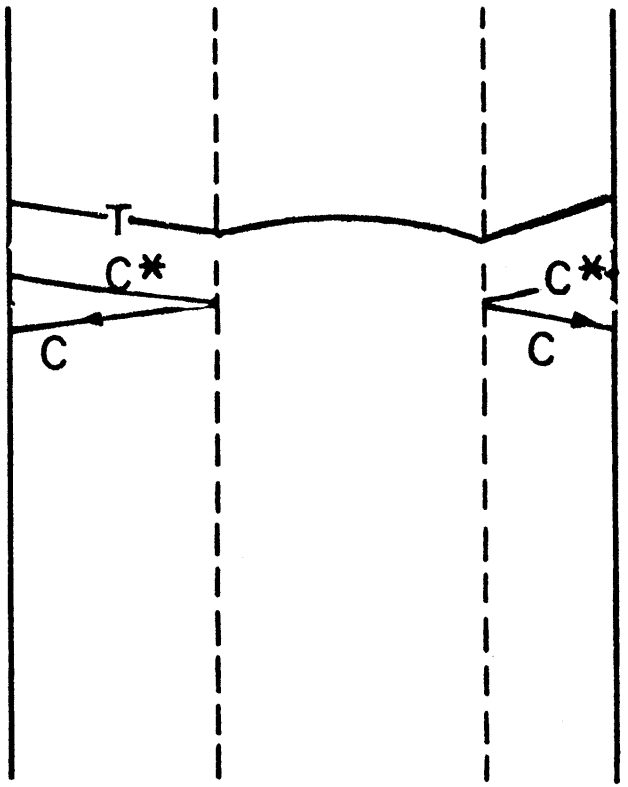

Evaporation to Inside and
Outside During 'Warm' Season

Fig. 4.6 Building with Winter Heating and no Summer Air-Conditioning

No Vapor-Barriers

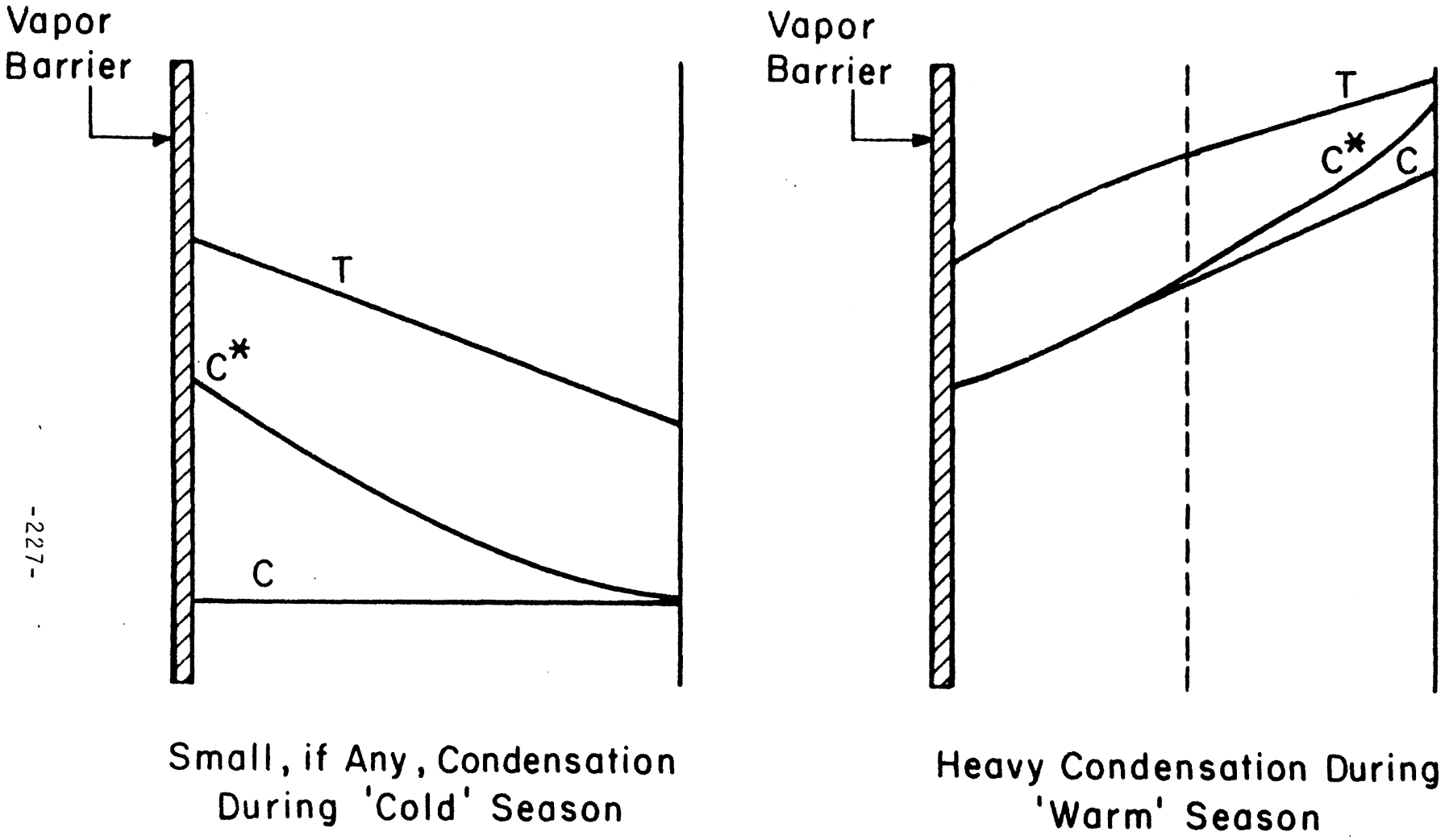

Fig. 4.7 Building with Winter Heating and Summer Air-Conditioning Vapor-Barrier on the Inner-Side

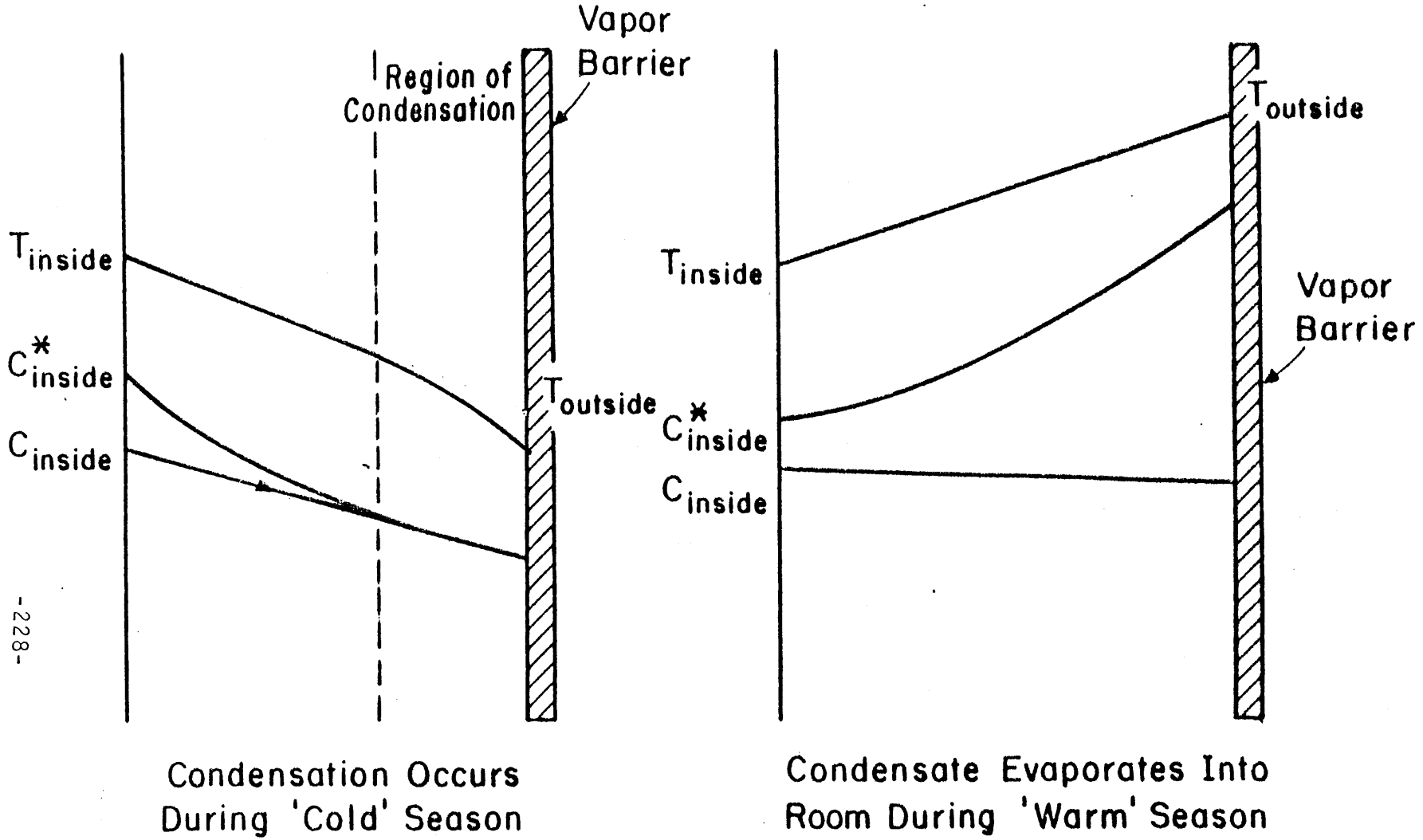

Fig. 4.8 Building with Winter Heating and Summer Air-Conditioning Vapor-Barrier on the Outer-Side

CHAPTER 5

LIQUID DIFFUSION IN FIBROUS INSULATION: MODEL

5.1 INTRODUCTION

In the study of simultaneous heat and mas transport with phase change in a porous slab, liquid-diffusion plays a prominent role. In the previous chapters liquid-diffusivity was defined phenomenologically. In this and the next chapter liquid-diffusion in unsaturated fibrous media is investigated. Liquid-diffusion in porous media has been the subject of study for many decades. The emphasis of the research in this area has been on geological flows with applications to hydrology and resource extraction. Liquid-diffusion in fibrous media constitutes a special case of flow in porous media. In contrast to most geological media, fibrous insulation has large values of void-fraction and pore sizes. The study of liquid-diffusion in fibrous media has not received much attention in the scientific

community. The properties of the medium are discussed in the next section. It will be shown that the medium is anisotropic and highly inhomogeneous. The model starts with a simple homogeneous geometric model. Parameters that control suction-potential, viscous-drag, and liquid-diffusion in a homogeneous fibrous-medium are identified. The effects of the inhomogeneities in the medium are then incorporated into the model. The model predictions are compared with the experimental results in chapter 6. Although the model is defined for an ordered arrangement of fibers, the agreement between the model and the experimental results are found to be satisfactory. The study reveals the attributes of the fiberglass insulation which play an important role in liquid-diffusion through the fibrous medium.

5.2 GEOMETRIC MODEL OF THE MEDIUM

Liquid diffusion in porous media is a strong function of the structure of the medium. The medium under study consists of fiberglass filaments held together by a phenolic binder. The filaments do not have a uniform diameter and their lengths vary from millimeters to centimeters. The filaments crossover eachother at irregular intervals. The bats of fiberglass are manufactured from many layers piled on top of eachother. The three orthogonal axes in the cartesian coordinates are identified as across, along, and through the layers, Fig. 5.1(a). A microscopic study of the insulation reveals that the majority of the filaments run across and along the layers and a very small percentage go from one layer to the other. The spatial distribution of the filaments and the binder in the medium is not uniform, causing the insulation to be highly inhomogeneous. Two types of insulation are under study. They have void-fraction values of 95-99%, with an average fiber radius of 3.56×10^{-6} meters.

In sum, the fiberglass insulation is an inhomogeneous assemblage of fiberglass filaments and phenolic binder. It is characterized by an anisotropic fiber-density and a non-uniform void-fraction distribution.

The medium under study is not amenable to simple and straightforward modelling. The parameters that describe the

geometry and structure of the medium must be identified. However, the sole identification of the parameters is not sufficient, for methods to estimate their values must be developed too. In study of the compelx medium, statistical estimators are used to estimate the parameters. The choice of the estimators is not unique. However, all estimators must be chosen such that they be consistent with eachother and the physical reality of the medium.

The main constituent of the insulation is the fiber filament. The fiber filaments have a well-spread radius distribution. The average value of this distribution is approximately known to be $3.56X10^{-6}$ meters [74]. This value is used as the estimator for the fiber-radius.

In order to account for the anisotropic fiber-density, a directional fiber-density parameter is introduced and denoted by n_i/N. The directional fiber-density is the ratio of the number of fibers of unit length along direction i to the total number of fibers of unit length in a unit volume. The subscript i corresponds to the direction index, i=1,2,3. It is readily recognised that for a given set of three orthogonal directions, a set of three directional fiber densities exist. However, the fibers in the medium are neither lined up along the three orthogonal directions, nor are of uniform length. The study of the medium under a microscope reveals that there are definitely more fibers along the batt than across it; the number of fibers through the layers is less than the other two directions. Hence, the directional fiber-density is a good estimator of the anisotropic distribution of fibers in the medium.

The medium is also highly inhomogeneous. The inhomogeneity is parameterized by a non-uniform void-fraction frequency distribution. Experimentation and observation indicate that void fraction changes occur mostly from one layer to the other. It is proposed that the layer be considered as the basic element, and

There is no text material missing here.
Pages have been incorrectly numbered.

P. 233

assumed to have a uniform void-fraction. The medium consists of many layers, each with a different void-fraction. The average of the layers' void-fraction equals the bulk void-fraction. The overall behavior of the medium is determiend by the proper aggregation of all layers.

The phenolic binder in the medium appears as the surface coating of the fibers and, at times, in realtively large masses. In as so far as the binder appears as the filaments' coating, its effect can be modelled as a slight increase in the fiber-radius. The fiber-radius is not known exactly, and is estimated by its mean value. Therefore, the coating will at most cause a slight variation in the fiber-radius estimator. This variation is ignored in this study. Large volumes of the binder are observed to appear at infrequent intervals and random locations. The size of these volumes is at least two or three orders of magnitude larger than the volume of a typical filament. The large binder volumes cause local blockage of the medium at random locations. The inclusion of this phenomenon would impose a severe constraint on modelling, for the model would have to incorporate variations both at the microscopic and macroscopic levels. As the microscopic geometry and structure of the medium is of interest, the presence of large volumes of the phenolic binder is ignored.

The fibers, in a layer, are modelled to be arranged in an ordered rectangular array. If N denotes the total number of fibers of unit length in a unit volume, then

$$\epsilon = 1 - N\pi r_f^2 \qquad [5.2.1]$$

The filaments are distributed unequally along the three othrogonal axes. The three axes are numbered 1, 2, and 3 for along, across, and through the layers, respectively. The number of filaments in the direction i is denoted by n_i; hence:

$$\sum_{1}^{3} \frac{n_i}{N} = 1 \qquad [5.2.2]$$

where

n_i/N = The directional fiber-density.

Directional void fraction, ϵ_i, is defined as the void-fraction based on the number of filaments parallel to direction i:

$$\epsilon_i = 1 - \frac{n_i}{N} (1 - \epsilon) \qquad [5.2.3]$$

With the filaments arranged in a square array, the half-distance between two adjacent filaments, in direction i, is:

$$r_{oi} = r_f \sqrt{\frac{\pi}{4(1 - \epsilon_i)}} \qquad [5.2.4]$$

5.3 LIQUID DIFFUSION IN HOMOGENEOUS FIBROUS MEDIA

In the study of liquid diffusion in unsaturated fibrous media we are interested in identifying the mechanics of fluid flow, and the medium properties that affect the flow. To this end the study is broken into three sections. These are the study of capillay forces which propel the flow, viscous forces that retard the flow, and the synthesis of the viscous and capillay forces to develop a model on liquid diffusion. The nature of capillary and viscous forces depend on the geometry and structural arrangements of the medium. In section 5.2 the medium was modelled as an ordered matrix of fibers arranged in a sqaure array. In this section the fluid mechanics of flow through a homogeneous fibrous medium will be studied. The effect of the inhomogeneity of the medium on the model will be discussed in the next section.

5.3.1 Suction Potential

Surface tension forces in a fibrous medium act at the menisci formed by the placement of fibers relative to eachother. When a fixed amount of liquid is introduced into the medium, minesci are formed at certain locations. These locations are referred to as suction sites in this manuscript. The surface tension forces at these suction-sites are not necessarily equal and the imbalance causes the liquid to move in a certain

direction. As the fluid moves some new suction-sites become activated, and some of the already-wet ones dry up. Movement of the liquid ceases only when the configuration of active suction-sites is such that the net force on the liquid mass is zero. In the case where the medium is exposed to an infintely large liquid reservoir, liquid is drawn into the medium until the medium is fully saturated, provided that the medium is hydrophylic, i.e. the contact angle of a meniscus is less than 90°.

As has been mentioned earlier, the shape and size of the menisici is determined by the relative positioning of the fibers. Some illustrative possibilites are demonstrated in Fig. 5.2. The stable configuration of a fixed volume of liquid corresponds to the one whose surface energy is less than all other possible configurations. This is the reason for the spherical shape of liquid drops, for a sphere has the smallest ratio of surface area to volume. The liquid in case (i) has a smaller surface than the one is case (ii). The liquid mass in case (ii) moves towards the fiber-crossing until its configuration resembles that of case(i). Hence, in Fig. 5.2 case(i) is a stable configuration, whereas case (ii) is not.

The configurations shown in Fig. 5.2 are but a handful of possibilites. It is clear that no simple and unique formulation relating the shape of the meniscus to the geometric properties of the medium can be presented. Therefore, a phenomenological approach to the modelling is followed.

The strength of the suction sites is inversely proportional to a characteristic length scale which is called the suction-radius, r_s. The geometric parameter that relates the medium to the suction-radius is the separation distance between the fibers. Consider an array of fibers as shown in Fig. 5.1(b). The liquid is in contact with four fibers wetting one-fourth of the perimeter of each filament. The surface forces acting at the interface of fibers and liquid create a pressure

drop across the interface. The force on each fiber is:

$$F = \frac{1}{4} \left[2 \pi r_f \sigma \cos\gamma \right] \qquad [5.3.1.1]$$

where γ is the contact angle between the liquid and the fibers, and is a chemcial property of the fiber/liquid ensemble. The total force in direction i is:

$$F_i = 2 \pi r_f \sigma \cos\gamma \qquad [5.3.1.2]$$

The pressure drop across the liquid interface acts on the area designated in Fig. 5.1(b). This area is

$$A_i = \frac{\pi r_f^2}{1 - \epsilon_i} \qquad [5.3.1.3]$$

Hence,

$$\Delta P_i = \frac{2\,\sigma \cos\gamma\ (1 - \epsilon_i)}{r_f} \qquad [5.3.1.4]$$

The strength of the suction sites is inversely proportional to the suction-radius. Defining a suction radius r_s as:

$$r_s = \frac{2\,\sigma \cos\gamma}{\Delta P} \qquad [5.3.1.5]$$

Such that, the suction-radius in a round tube is equal to the tube radius; Equation [5.3.1.4] can be combined with eq.[5.3.1.5] to yield:

$$r_{si} = \frac{r_f}{1 - \epsilon_i} \qquad [5.3.1.6]$$

The above equation relates the suction-radius in the i-th direction to the fiber-radius and the directional void-fraction.

5.3.2 Viscous Drag

The flow of liquid in porous media is retarded by the viscous forces. In this section the phenomenon of viscous drag in fibrous media is studied and modelled.

Visous drag is caused by the no-slip condition at the surface of fibers. In developing a model that would predict the viscous drag in fibrous media the flow may be modelled as flow through a pipe, i.e. the Hagen Pouiseuille flow,:

$$Q = -\frac{\pi r_d^4}{8\mu} \cdot \frac{dP}{dx} \qquad [5.3.2.1]$$

In the above, r_d is the equivalent hydraulic radius of the medium. The model should be able to relate the hydraulic radius to the properties of the medium. A definition for the hydraulic radius of an anisotropic fibrous medium is obtained by analyzing the flow as flow over an ensemble of cylinders. In the remainder of this section flow past a matrix of cylinders is studied and the flow-rate/pressure-drop relationship is obtained.

The fibrous medium has been modelled as a three dimensional matrix of fibers arranged in an ordered square array. The number

of fibers in the three orthogonal directions are unequal and characterized by the directional fiber-density parameter, n_i/N. In the solution of the flow-field in any specific direction i the following is proposed: Assume that the flow is equivalent to the linear super-position of two flows: flow along a bank of cylinders and flow across a bank of cylinders. With the above assumption the flow field in the medium is obtained by once solving the Navier-Stokes equations with only the fibers that are parallel to the the flow, and once with all the fibers that are perpendicular to the flow. The two solutions are then linearly super-imposed and the flow-rate/pressure-drop relationship is generated.

There is one major reservation about the superposition assumption. In the flow of liquid over an array where both along and across fibers are present the flow field is effected by the simultaneous presence of the fibers in the three directions. The superposition solution does not account for the pressure drop across the fiber crossings and the distortions that the fiber-crossings and fiber "knots" introduce into the flow field. In order to account for the presence of fiber crossings solid spheres may be introduced at the points where the fibers intersect. The radius of the spheres would be a multiple of the fiber radius, with the multiple larger than one and less than ten. However, it is reasonable to assume that due to the large values of the void-fraction, which translates into large fiber-separation distances, the effect of the spheres is negligible on the pressure-drop.

The pressure drop across an ordered three-dimensional array of fibers is the weighted sum of the pressure drop due to flow along, and across the fibers. Consider the viscous flow of a

fluid along a one-dimensional array of cylinders all with radius r_f. This corresponds to the 3-D array, where all the fibers that do not lie parallel to the flow are removed. For viscous flow the Navier-Stokes equation reduces to:

$$\frac{d^2u}{dr^2} = -\frac{1}{\mu}\frac{dP}{dz} \qquad [5.3.2.2]$$

with the no-slip boundary condition at the solid surfaces. In order to solve the above a symmetric cell is chosen such that the whole flow field is generated by reflecting the cell over its sides. The symmetric property of the cell implies that the condition of zero velocity gradient must be satisified at the cell's boundaries. In Fig. 5.1(c) a triangular cell which can generate the flow-field is shown. Sparrow [75] used the triangular cell and solved equation [5.3.2.2] with the boundary-condition of zero velocity at the filament surface and zero velocity gradient at the remainder of cell's boundaries. For void-fraction values larger than 90%, he has obtained:

$$\frac{\bar{u}}{-\frac{1}{\mu}\frac{dP}{dz}r_f^2} = \frac{2\left[\xi_i^4\left(\frac{1}{2\pi}\left\{\ln\xi_i^2+\ln 2-3\right\}+\frac{1}{6}\right)+\frac{1}{4}\xi_i^2-\frac{\pi}{64}\right]}{\xi_i^4-\frac{\pi}{4}}$$

[5.3.2.3]

where ξ_i is the non-dimensionalized fiber-seperation distance:

$$\xi_i = \sqrt{\frac{\pi}{4 \frac{n_i}{N} (1 - \epsilon)}}, \qquad [5.3.2.4]$$

Now consider the viscous flow of a liquid perpendicular to a bank of tubes. The Navier-Stokes equations for viscous flow and continuity expressed in cylindrical coordinates are:

$$\frac{\partial p}{\partial r} = \mu \left[\nabla^2 v_r - \frac{v_r}{r^2} - \frac{2}{r^2} \frac{\partial v_\theta}{\partial \theta} \right] \qquad [5.3.2.5]$$

$$\frac{1}{r} \frac{\partial P}{\partial \theta} = \mu \left[\nabla^2 v - \frac{v_\theta}{r^2} + \frac{2}{r^2} \frac{\partial v_r}{\partial \theta} \right] \qquad [5.3.2.6]$$

$$\frac{\partial v_r}{\partial r} + \frac{v_r}{r} + \frac{1}{r}\frac{\partial v_\theta}{\partial \theta} = 0 \qquad [5.3.2.7]$$

The stream function, Ψ, is defined as:

$$v_r = \frac{1}{r}\frac{\partial \Psi}{\partial \theta} \qquad [5.3.2.8]$$

and,

$$v_\theta = -\frac{\partial \Psi}{\partial r} \qquad [5.3.2.9]$$

Then equations [5.3.2.5]-[5.3.2.7] become:

$$\nabla^4 \Psi = 0 \qquad [5.3.2.10]$$

To obtain the boundary conditions necessary to solve the above, consider a cylinder to be moving with velocity U, perpendicular to its axis in a fluid cell of radius r_o. Then at $r=r_f$:

$$u = \bar{u}$$

$$v_r = -\bar{u}\cos\theta$$

$$v = -\bar{u}\sin\theta \qquad [5.3.2.11]$$

and at $r = r_o$

$$v_r = 0$$

$$\frac{\partial v_\theta}{\partial r} + \frac{1}{r}\frac{\partial v_r}{\partial \theta} - \frac{v_\theta}{r} = 0 \qquad [5.3.2.12]$$

The above can be solved to yield:

$$\frac{\bar{u}}{-\frac{1}{\mu}\frac{dP}{dz}r_f^2} = \frac{\zeta_i^2\left[\ln\zeta_i - \frac{1}{2}\left(\frac{\zeta_i^4-1}{\zeta_i^4+1}\right)\right]}{4\pi} \qquad [5.3.2.13]$$

where

$$\zeta_i = \sqrt{\frac{\pi}{4\left[1 - \frac{n_i}{N}\epsilon\right]}} \qquad [5.3.2.14]$$

(For a more detailed discussion of the above see [76])

Equations [5.3.2.3] and [5.3.2.14] are the flow-rate/pressure-drop relationships for flow in 1-D arrays of fibers, arranged along and perpendicular to the flow, respectively. The pressure drop across a three dimensional array is the weighed sume of the pressure drop along the fibers and across the fibers. Force per unit length of the fibers which are parallel to the flow, which is in direction i, is:

$$\left(\frac{F}{L}\right)_{i,||} = \left(\frac{dP}{dz}\right)_{i,||} \pi r_{oi}^2 \qquad [5.3.2.15]$$

where $(dP/dz)_{i,||}$ is defined in eq. [5.3.2.3]. Force per unit length of fibers perpendicular to the flow is:

$$\left(\frac{F}{L}\right)_{i,\perp} = \left(\frac{dP}{dz}\right)_{i,\perp} \pi r_{oi}^2 \qquad [5.3.2.16]$$

where $(dp/dz)_{i,\perp}$ is defined in eq. [5.3.2.14]. There are n_i fibers of unit length per unit area parallel to the flow and $N-n_i$ fibers perpendicular to the flow. Then:

$$\left(\frac{\Delta P}{L}\right)_i = n_i\left(\frac{F}{L}\right)_{i,||} + (N-n_i)\left(\frac{F}{L}\right)_{i,\perp} \qquad [5.3.2.17]$$

which can be written as:

$$\left(\frac{\Delta P}{L}\right)_i = N\left[\frac{n_i}{N}\left(\frac{F}{L}\right)_{i,||} + 1-\frac{n_i}{N}\left(\frac{F}{L}\right)_{i,\perp}\right] \qquad [5.3.2.18]$$

Using eqs. [5.1.3], [5.3.2.3], and [5.3.2.14] with [5.3.2.18] yields:

$$\left(\frac{dP}{dx}\right)_i = -\frac{4\mu\overline{u}_i}{r_f^2} S_i(n_i/N, \epsilon) \qquad [5.3.2.19]$$

where S_i is the parameter that denotes all the terms that represent the effect of void-fraction and anisotropic fiber-density on the pressure drop:

$$\frac{S(n_i/N, \epsilon)}{1-\epsilon} = \frac{\left(1 - \frac{n_i}{N}\right)\pi}{\ln\zeta_i - \frac{1}{2}\left[\frac{\zeta_i^4-1}{\zeta_i^4+1}\right]} + \frac{\frac{n_i}{N}\xi_i^2\left(\xi_i^2 - \frac{\pi}{4}\right)}{8\left[\xi_i^4\left(\frac{1}{2\pi}\left\{\ln\xi_i^2+\ln 2-3\right\} + \frac{1}{6}\right) + \frac{1}{4}\xi_i^2 - \frac{\pi}{64}\right]} \quad [5.3.2.20]$$

Equation [5.3.2.19] is the flow-rate/pressure-drop relationship for laminar flow in direction-i through a three dimensional array of fibers with unequal directional fiber-densities. Figure 5.3 is a plot of S_i versus n_i/N with ϵ as the parameter. S_i demonstrates a strong dependance to mass-fraction, $1-\epsilon$. At a given ϵ, the value of S_i decreases as the ratio of fibers along the flow to the fibers across the flow increases up to a certain value of n_i/N. Beyond this value of n_i/N, S_i increases.

Equation [5.3.2.19] can be written in the form of Darcy's law. In the next equation the matrix [k*] is the diagonal matrix of permeabilities:

$$[\bar{u}] = - \frac{1}{\mu} [k^*][dP/dx] \qquad [5.3.2.21]$$

where

$$k^*_i = \frac{r_f^2}{4 S_i} \qquad [5.3.2.22]$$

At the beginning of the discussion on viscous drag, the possibility of a formulation based on a hydraulic radius analogy between the medium and a round capillary was presented. It was then suggested that developping a phenomenological relationship for the hydraulic radius is not immediately possible. The analogous Hagen-Pouiseuille flow is characterized by:

$$\left(\frac{dP}{dx}\right)_i = - \frac{8 \mu}{r_{di}^2} \bar{u}_i \qquad [5.3.2.1]$$

where r_d is the hydraulic radius. Comparing the above with eq. [5.3.2.19] yields:

$$r_{di} = r_f \sqrt{\frac{2}{S_i}} \qquad [5.3.2.23]$$

Clearly, as S_i is a very complicated function of n_i/N and ϵ, r_{di} could have not been formulated properly if the flow was not studied in detail as flow over a 3-D array of fibers.

5.3.3 Liquid Diffusion

Liquid diffusion in unsaturated porous media is controlled by the balance of surface tension forces with the viscous drag forces. Consider a unit volume of the material with unit surface area and unit width exposed to a reservoir of diffusing liquid. Liquid diffuses into the medium with a velocity U. The pressure-drop asscoiated with a flow velocity U is given by eq. [5.3.2.19]. This pressure drop is balanced by the surface tension forces acting at the meniscie, eq. [5.3.1.4]:

$$\frac{4\,\mu_i\, S_i}{r_f^2}\, u_i = \frac{2\,\sigma \cos\gamma}{r_s\, L_i} \qquad [5.3.3.1]$$

where L_i is the length of the diffused front in the i-th direction. Recognizing that

$$U_i = dL_i/dt \qquad [5.3.3.2]$$

yields:

$$L_i \frac{dL_i}{dt} = \frac{\sigma \cos \gamma}{2 \mu} \frac{r_f^2}{S_i r_s} \qquad [5.3.3.3]$$

Integrating the above with the initial condition of :

$$L_i(t=0) = 0. \qquad [5.3.3.4]$$

results in:

$$L_i = \sqrt{\frac{\sigma \cos \gamma}{\mu} \frac{r_f^2}{S_i r_s} t} \qquad [5.3.3.5]$$

For liquid diffusion in a round capillary Washburn[77] has shown that :

$$L_i = \sqrt{\frac{\sigma \cos \gamma}{2 \mu} r t} \qquad [5.3.3.6]$$

Equation [5.3.3.5] can be written as

$$L_i = \sqrt{\alpha r^*_i t} \qquad [5.3.3.7]$$

where α is the liquid diffusivity and is a function of the properties of the medium and the diffusing liquid:

$$\alpha = \sigma \cos \gamma / 2 \mu \qquad [5.3.3.8]$$

With the above formulation r^*_i is defined to be the equivalent suction-radius in direction i:

$$r^*_i = \frac{2(1 - \epsilon)n_i/N}{S_i} r_f \qquad [5.3.3.9]$$

The equivalent suction-radius is based on the analogy that if the fibrous medium were to be modelled as an assemblage of round capillaries, the capillaries would have a radius of r^*. This parameter is a function of the medium void-fraction, fiber-radius, and the directional fiber-density.

5.4 EFFECTS OF THE INHOMOGENEITIES OF THE MEDIUM ON LIQUID DIFFUSION

In the previous section the phenomena of surface tension forces, viscous drag and liquid difusion in a homogeneous medium were studied. The parameters that describe each of the pheneomena were identified and related to the properties of a homogeneous 3-D ordered array of fibers. As noted in section 5.2, the medium under study is not homogeneous. Variations of the void-fraction take place in the three orthogonal directions. However, it has been observed that for a given layer, the variations of void-fraction from one layer to the neighboring ones are more pronounced than the variation along the layers. The variations of the void-fraction in the i=3 direction can be assumed to take place from one layer to the other, with the void-fraction being constant in each layer. This is due to the small thickness of the layers which does not allow for significant variations of void-fraction. The length scale for variations across and along the layers has been observed to be larger than the one associated with variations from one layer to the next. Hence, it is proposed that the inhomogeneity of the medium be parameterized by a step-wise void-fraction distribution in the through-direction,i=3, with the void-fraction being constant in each layer, Fig. 5.4.

In this section the effects of inhomogeneity of the medium on liquid diffusion, viscous drag and suction potential is

studied. By introducing a void-fraction distribution, the macroscopic behavior of the medium with regards to the three above mentioned phenomena is obtained by proper statistical aggregation. The statistical analysis requires a proper definition of aggregation. The analysis is straight forward for suction-potential and viscous drag. However, simultaneous liquid diffusion along many interconnected layers is by nature different from liquid diffusion along an ensemble of isolated layers. This phenomenon will be described later and its implications demonstrated.

The inhomogeneity of the medium is represented by a void-fraction frequency distribution subject to the constraint:

$$\int_0^1 \epsilon\, f(\epsilon)\, d\epsilon = \epsilon_T \qquad [5.4.1]$$

where

ϵ_T = The macroscopic void-fraction of the medium.

5.4.1 Effect of Inhomogeneity on Suction Potential

Every layer is assumed to be characterized by a uniform value of void-fraction, and, hence, by one value of suction

radius, r_s. It follows that for a given void-fraction distribution in the medium, $f(\epsilon)$, a corresponding suction-radius distribution, $f(r_s)$ exists

5.4.2 Effect of Inhomogeneity on Viscous Drag

According to eqs. [5.3.2.19] and [5.3.2.20], the pressure drop across the medium is a function of the void-fraction, and the directional fiber-density. Hence, each layer, with a uniform void-fraction, is characterized by a value of S , and the medium by a frequency-distribution f(S). Liquid can flow in two possible directions: along the layers and perpendicular to them. In flow along the layers the flow can be either along the i=1 or i=2 direction.

Consider flow along the layers. In this situation flow passes through a set of parallel conduits. This is analogous to the flow of electric current through a set of parallel resistances. The equivalent resistance to flow is

$$S_{eq}(n_i/N, \epsilon_T) = \left[\int_0^1 \frac{f(\epsilon)\, d\epsilon}{S(n_i/N, \epsilon)} \right]^{-1} \qquad i=1,2 \qquad [5.4.2]$$

When a number of resistances are placed in parallel to eachother, the equivalent resistance is always smaller than the smallest

resistance. In other words, the value of S obtained for an ordered homogeneous medium, eq. [5.3.2.20], is the maximum value that any medium, with the same ϵ and n_i/N can have. Any distortions in the equality of fiber-spacing leads to a decrease in the value of S, which translates to a decrease in the pressure drop for the same flow rate.

In the case of flow through the layers, flow passes through the layers arranged serially. Hence, the equivalent S is:

$$S_{eq}(n_i/N, \epsilon_T) = \int_0^1 f(\epsilon)\, S(n_i/N, \epsilon)\, d\epsilon \qquad i=3 \qquad [5.4.3]$$

5.4.3 Effect of Inhomogeneity on Liquid Diffusion

The phenomenon of liquid diffusion in a homogeneous fibrous medium has been identified to be controlled by the diffusion-radius, r^*. This parameter emerges from the balance of surface tension forces with the viscous forces and is a function of the directional fiber-density void fraction. The medium under study is layered, with the layers having a non-uniform void-fraction distribution. Hence, as each layer is characterized by a certain value of void-fraction, it is also characterized by a unique value of r^*. The study of liquid diffusion in the fibrous insulation is seperated into diffusion in the plane of the layers, and diffusion through the layers.

The directional fiber-desnity in the direction perpendicular to the layers is very small. This implies that the seperation distance between the fibers is very large. Therefore, the number and/or the strength of the suction sites in the direction perpendicular to the layers is not sufficient to cause a well-defined diffusion pattern as discussed in section 5.3.1. Hence, liquid diffusion from one layer to the other cannot be properly represented by the equivalent suction-radius model; and the model needs to be amended.

5.4.3.I Diffusion Through The Layers

Diffusion in the fibrous media is caused by the action of surface tension forces acting at the menisci. In section 5.3.1 the nature of these forces and the geometry of the menisci was studied. It was shown that a measure of the strength of the the suction sites is the equivalent suction-radius, r_s. The smaller the value of r_s, the stronger the suction potential would be. The suction-radius is related to the properties of the medium as:

$$r_{si} = \frac{r_f}{\frac{n_i}{N}(1 - \epsilon)} \qquad [5.4.4]$$

The relative strength of the suction-sites in different directions depends on the ratio of directional fiber-density values:

$$\frac{r_{si}}{r_{sj}} = \frac{n_j/N}{n_i/N} \qquad [5.4.5]$$

Hence, if the directional fiber-densities in any two directions are not significantly different, the suction potentials in the two directions are effectively equivalent. This is the case for the two orthogonal directions in the plane of the layers, (i=1,2). Conversely, when the directional fiber-density in a given direction is much smaller than the fiber-density in the other direction, the suction potential in that direction will be much weaker than the potential in the other direction. The directional fiber-density in the the direction perpendicular to the layers is found to be about one-tenth of the values of the direction fiber-density values in the other two directions. This implies that the suction sites connecting one layer to the next are very weak. For liquid to move from one layer to the other, all suction sites with suction-radii smaller than r_{s3} should be fully wet and deactivated. This requirement translates to a critical value of liquid content, below which liquid will not travel from one layer to the next. The value of critical liquid-content corresponds to the percentage of the suction-radii, in the plane of the layer, which are smaller than r_{s3}.

However, the above discussion assumes a uniform distribution of fiber-density in the i=3 direction. If one were to assume

that the fiber-spacing in this direction varies, then it is possible to envisage a situtation where there are suction sites much stronger, but less numerous than before. This is to say that the values of r_{s3} are not constant, and some may be close to r_{s2} and r_{s1}. Then, liquid would diffuse from one layer to the other as shown in Fig. 5.5. Liquid diffuses in the plane of the layer until it reaches a suction-site which connects the two adjacent layers. Then, it diffuses from the layer to the next, and travels in the plane of the new layer until it reaches another suction site in the i=3 direction. This model does not rule out the previous model based on a critical value of liquid-content in the layer. The non-uniformity of the fiber density in the i=3 direction reduces the numerical value of the critical liquid-content from the one based on a uniform directional fiber-density.

Consider the following: Assume that the liquid travels a distance L_o, along the layer before it reaches a suction-site connecting the layer to the next. Furthermore, assume that the layer has a uniform thickness h. Then, the diffusing liquid would have to travel $(L_o^2+h^2)^{0.5}$ from one layer-connection to the other. Diffusion takes place primarily in the plane of the layer, and is characterized by r^* (Recalling that r^*_1 and r^*_2 are not significantly different an average of the two is used). Then the time that it takes for the liquid to travel from one layer to the next is:

$$t = \frac{L_o^2 + h^2}{\alpha\, r^*} \qquad [5.4.6]$$

The above may be rewritten as:

$$h = \sqrt{\alpha\, r^{*} \left[\frac{1}{\left[\frac{L_o}{h} \right]^2 + 1} \right] t} \qquad [5.4.7]$$

The above represents liquid diffusion in the i=3 direction. Comparing the above with eq. [5.3.3.7]:

$$L_i = \sqrt{\alpha\, r^{*}_{i}\, t} \qquad [5.3.3.7]$$

indicates that the two equations are very similar. Equation [5.4.7] states that liquid diffusion in the directin perpendicular to the layers is caused by a tortuous diffusion in the plane of the layers. The effect of the tortuous path is represented by the tortuosity factor,

$$\tau = \frac{1}{\left[\frac{Lo}{h} \right]^2 + 1} \qquad [5.4.9]$$

The L_o/h factor indicates the extent of interconnection between adjacent layers. It is solely a property of the medium.

The above formulation yields the value of tortuosity based on one value of r^*, and L_o/h. Clearly, both of these paramters have a non-uniform distribution in the medium; consequentially there must exist a distribution of the tortuosity factor. It will be later shown that seperating the distribution of r^* from that of τ is not possible.

5.4.3.II Diffusion In The Plane Of The Layers

Liquid diffusion in the plane of the layers is given by eq. [5.3.3.7]:

$$L_i = \sqrt{\alpha\ r^*_i\ t} \qquad i=1,2 \qquad [5.3.3.7]$$

where r^*_i is defined in eq. [5.3.3.9]. The diffusion-radius is a function of void-fraction and the directional fiber-density. Each layer is characterized by a value of r^*_1 and r^*_2, corresponding to the value of the void-fraction in the layer. Therefore, corresponding to $f(\epsilon_{1,2})$ a non-uniform $f(r^*_{1,2})$ exists.

The above formulation implicitly assumes that liquid diffusion takes place along an assemblage of isolated layers, and does not take into account the possibility of liquid movement from one layer to the other. In order to elucidate this point consider the case of two round capillaries with radii r_1, and r_2, with r_2 larger than r_1. With the two capillaries isolated, liquid diffusion takes place according to the Washburn solution:

$$L_1 = \sqrt{\alpha\, r_1\, t} \qquad [5.4.10]$$

and,

$$L_2 = \sqrt{\alpha\, r_2\, t} \qquad [5.4.11]$$

Now consider the situation where the two capillaries are inter-connected. The term "inter-connected" implies that at any location along the two capillaries pressure is the same. This is to say that liquid can freely move from one capillary to the other. It can be easily shown [78] that with the coupled capillaries:

$$L_1 = \sqrt{\alpha r'_1 t} \qquad [5.4.12]$$

and,

$$L_2 = \sqrt{\alpha r'_2 t} \qquad [5.4.13]$$

where

$$r'_1 = g_1(r_2/r_1)\, r_1 \qquad [5.4.14]$$

and,

$$r'_2 = g_2(r_2/r_1)\, r_2 \qquad [5.4.15]$$

In the above g_1 and g_2 are non-linear functions of r_2/r_1, and are plotted in Fig. 5.6. When the two radii are of the same

order of magnitude $g_1(r_2/r_1)$ is larger than r_2/r_1, and $g_2(r_2/r_1)$ is smaller than one, but not smaller than r_1/r_2. Hence, the smaller capillary, which if uncoupled would trail the larger one, leads the larger capillary. However, as the ratio of r_2/r_1 increases g_2 approaches one and g_1 approaches r_2/r_1. The net result being that at large values of r_2/r_1 the two capillaries travel at the rate very close to that of the isolated large one. These results indicate that liquid diffusion in coupled capillaries is distinctly different from diffusion in isolated ones. The reason for this lies in the ability of the liquid to move from one capillary to the other. This flow takes place at such a rate as to cause the pressure at any location, behind the meniscus of the trailing capillary, to be the same in both capillaries.

The effect of coupling between many capillaries of different radii is very complicated. The equations cannot be easily decoupled. The system of n-capillaries is described by a set of n coupled nonlinear differential equations, with a singularity at time equals to zero. There is no guarantee that a closed form solution to such as system exists [79]. However, by studying the behaviour of two coupled capillaries, cetain observations may be made and generalized to the case of n-capillaires. Let us assume that the variations of radius in the n-capillaries is not lager than an order of magnitude. The coupling of the capillaries has two effects. First, the capillary with the largest radius, which if uncoupled would move furtherest the fastest, will slow down substantially. Second, the distribution of the effective radius which characterizes the coupled liquid diffusion, $f(r_c)$, is less peaked and more flat than $f(r)$, for the coupling brings the values of effective radii, r_c, closer to eachother.

The observations made above can be extended to liquid diffusion in n-interconnected layers. According to the above, $f(r^*)$ based on $f(\epsilon)$ is an approximation to $f(r^*_c)$, where $f(r^*_c)$ includes the effect of the coupling between the n-layers.

Incorporating the effect of coupling into the model is not quantitatively possible. However, it is possible to predict that $f(r^*_c)$ will be more flat and less peaked than $f(r^*)$. Also $r^*_{c\text{-}max}$ will be smaller than r^*_{max}. The decrease in the peakendness of $f(r^*)$ and the relative decrease of $r^*_{c\text{-}max}$ from r^*_{max} is a strong function of the relative values of r^*. With variations of r^* not in excess of an order of magnitude, the variations in $f(r^*_c)$ and $r^*_{c\text{-}max}$ should be noticeable, but not so large as to render $f(r^*)$ an inaccurate estimator of $f(r^*_c)$.

5.5 MODEL SUMMARY AND RATIONALE FOR CHOICE OF EXPERIMENTS

In the previous sections the phenomenon of liquid diffusion in fibrous insulation has been studied. In this section a summary of the model is presented, and a series of experiments are proposed. The experiments are designed to serve two purposes. One is to generate the unknown paramters of the model. The other is to test the model for consistency and accuracy.

The model for liquid diffusion in the fibrous insulation is based on a simple geometric representation of the medium. The medium is modelled as a three dimensional ordered array of fibers arranged in a square lattice. The anisotropicity of the medium is modelled by the introduction of the directional fiber-densities. The inhomogeneity of the medium is modelled by a non-uniform void-fraction distribution. Other characteristic properties of the medium are the mean fiber-raius and the tortuosity factor. Suction-potential, viscous drag, and liquid diffusion in the medium are studied. In each of these studies the physical parameters that control the phenomenon in a layer are related to the properties of the homogeneous medium. The overall behaviour is obtained by statistical aggregation over the range of void-fraction values of the layers. Suction potential is identified by an equivalent suction-radius distribution, $f(r_s)$. The viscous drag is identified by the S_{eq} term . The equivalent suction-radius distribution, $f(r^*)$, represents the phenomenon of liquid diffusion.

In order to evaluate $f(r_s)$, S_{eq}, and $f(r^*)$, three inputs are required. The model inputs and output paramters are:

INPUT: $f(\epsilon)$, n_i/N, r_f
OUTPUT: $f(r_s)$, S_{eq}, $f(r^*)$

Of the above inputs, the fiber mean-radius is known within some accuracy; and n_i/N is postulated by observing the medium under microscope. Only $f(\epsilon)$ is unknown and needs to be measured experimentally. Each of the following three can be used to back-calculate $f(\epsilon)$: $f(r_s)$, $f(r^*)$, S_{eq}. Once one of the three is used to generate $f(\epsilon)$, $f(\epsilon)$ can be input to the model to predict the other two.

In order to check the consistency and accuracy of the model, as well as solving for the unknown $f(\epsilon)$, it is proposed that experiments be conducted to measure the three outputs of the model. Each experimental result is then used to back-calculate $f(\epsilon)$, and predict the other two experimental results. To elucidate this scheme consider Figure 5.7. In this figure, $f(r_s)$, $f(r^*)$, S_{eq} are circled. From each circle two arrows emanate, indicating that the experimental values of the encircled quantity are used, through the model, to predict the other two experimental results. As indicated, each experimetnal result is compared with the model prediction two times. This is the ultimate test of consistency of the model and accuracy of the experiments.

In short, three sets of experiments need to be conducted to measure $f(r_s)$, S_{eq}, and $f(r^*)$. The model does not predict the value of tortuosity; this must be measured experimentally.

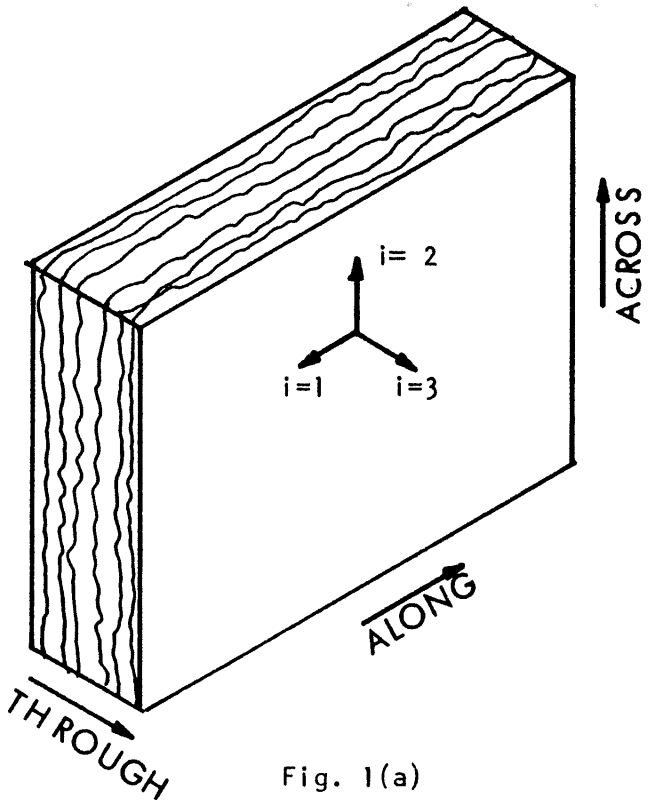

Fig. 1(a)

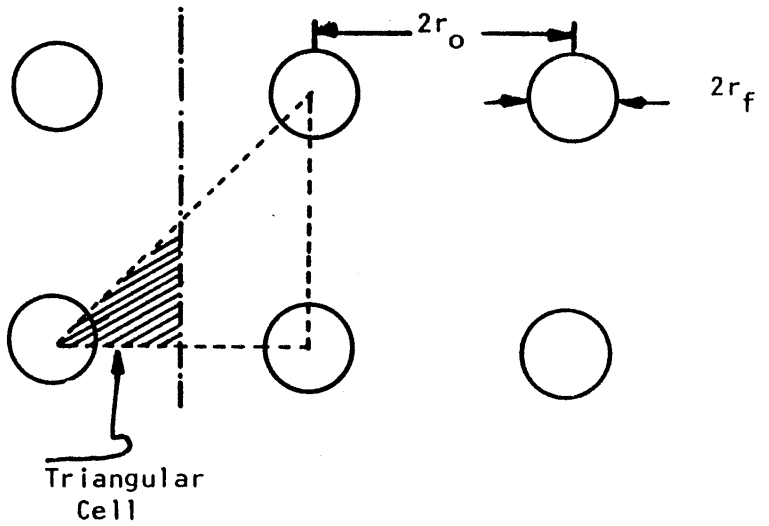

Fig. 1(c)

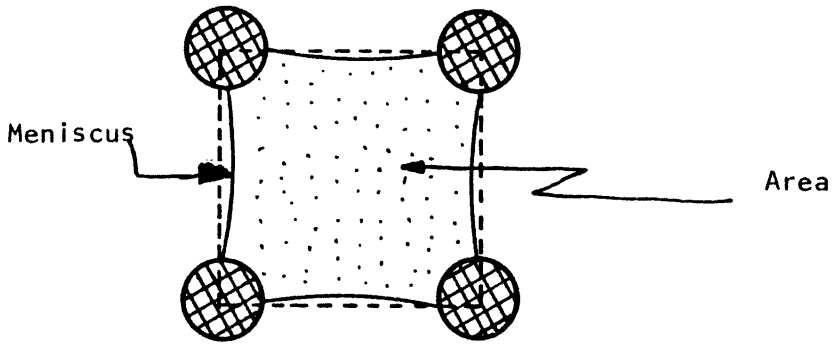

Fig. 1(b)

Fig. 51. Schematics of the Proposed geometric Model of The Fiberglass Insulation

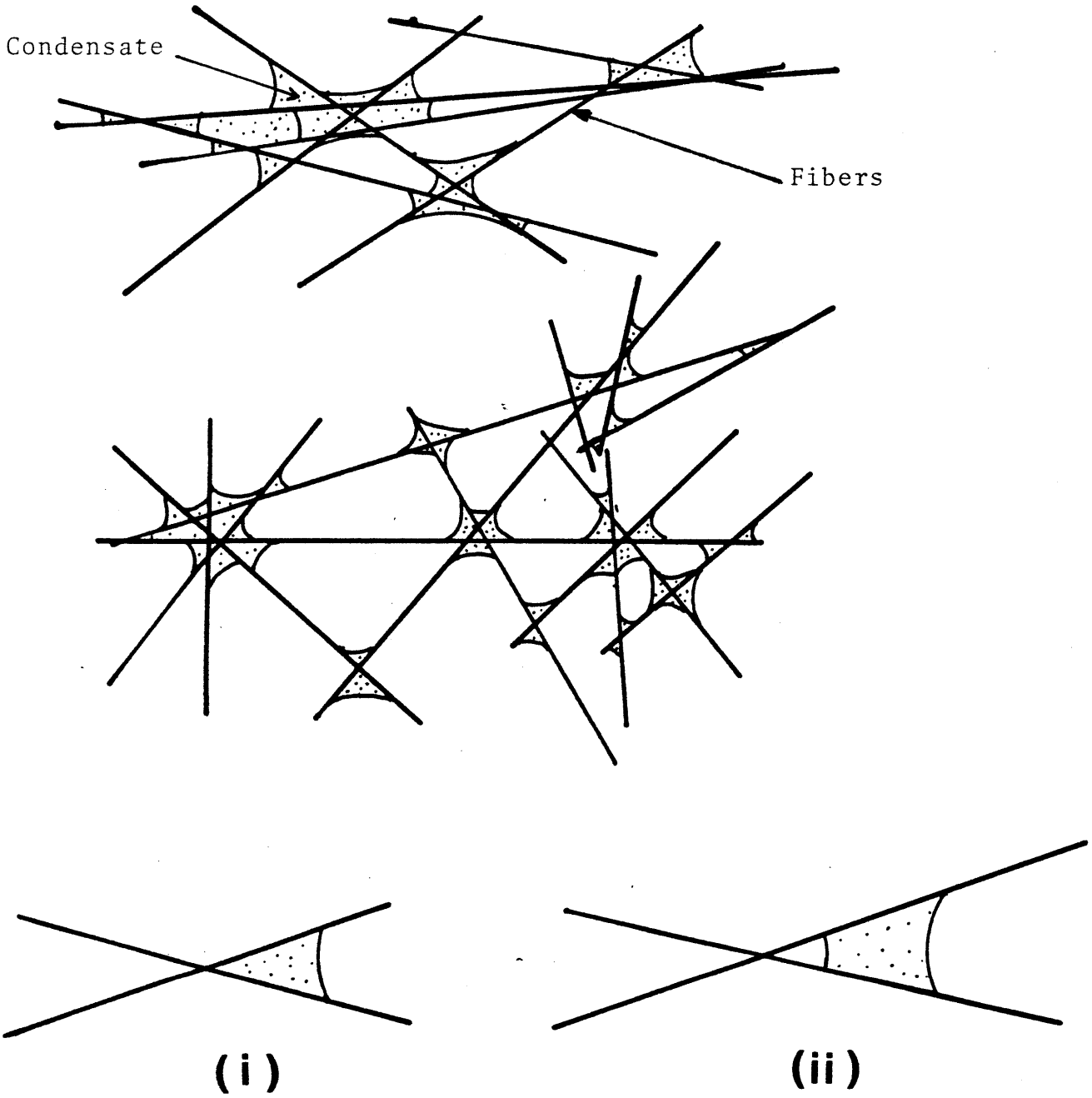

Fig. 5.2 Schematic Representation of the Fiber-Arrangements and the Suction-Sites in a Fibrous Insulation

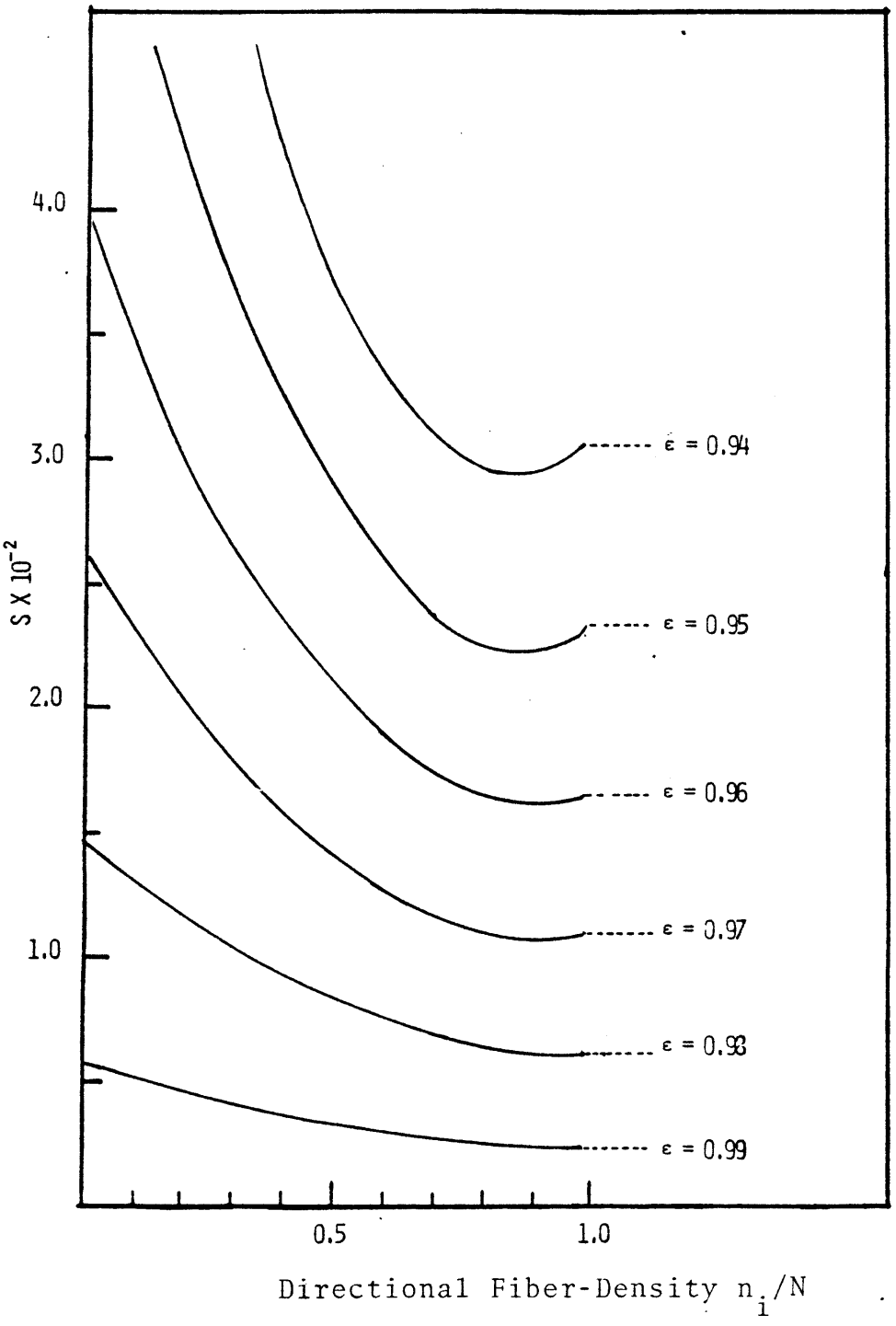

Fig. 5.3 The Plot of S versus the Directional fiber-density for Different values of Void-Fraction

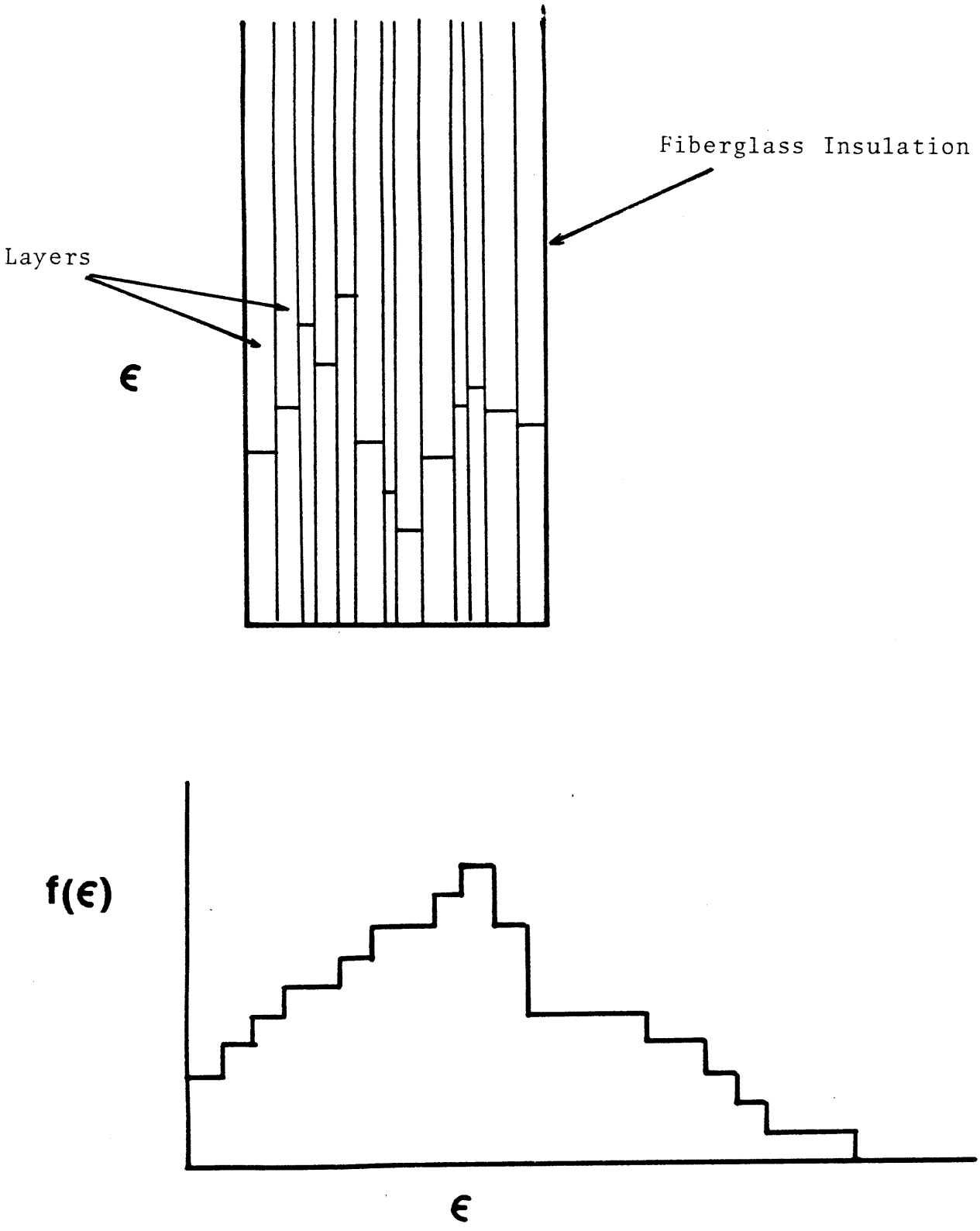

Fig. 5.4 Schematic of the Proposed Model for Void-Fraction Distribution

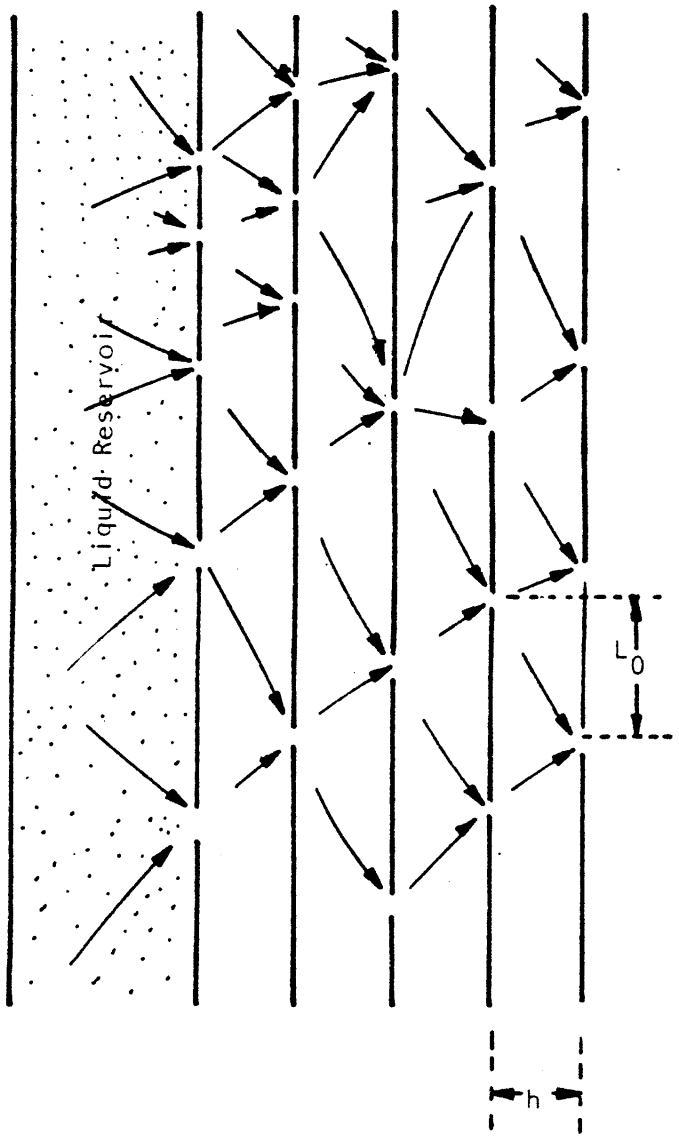

Fig. 5.5 Schematic of the Proposed Liquid-Diffusion From One Layer to the Next

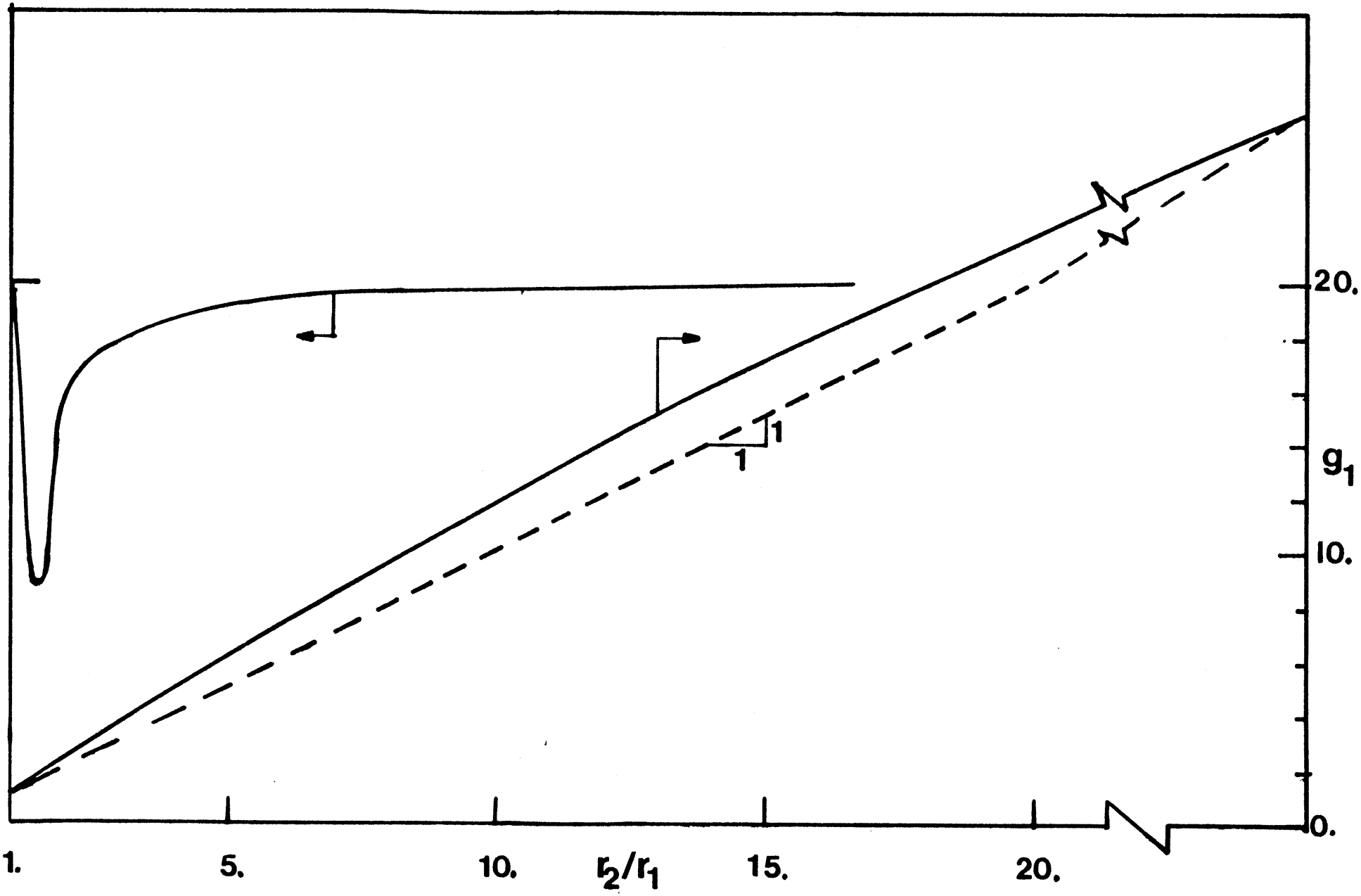

Fig. 5.6 Plot of g_1 and g_2 as a function of the radius ratio

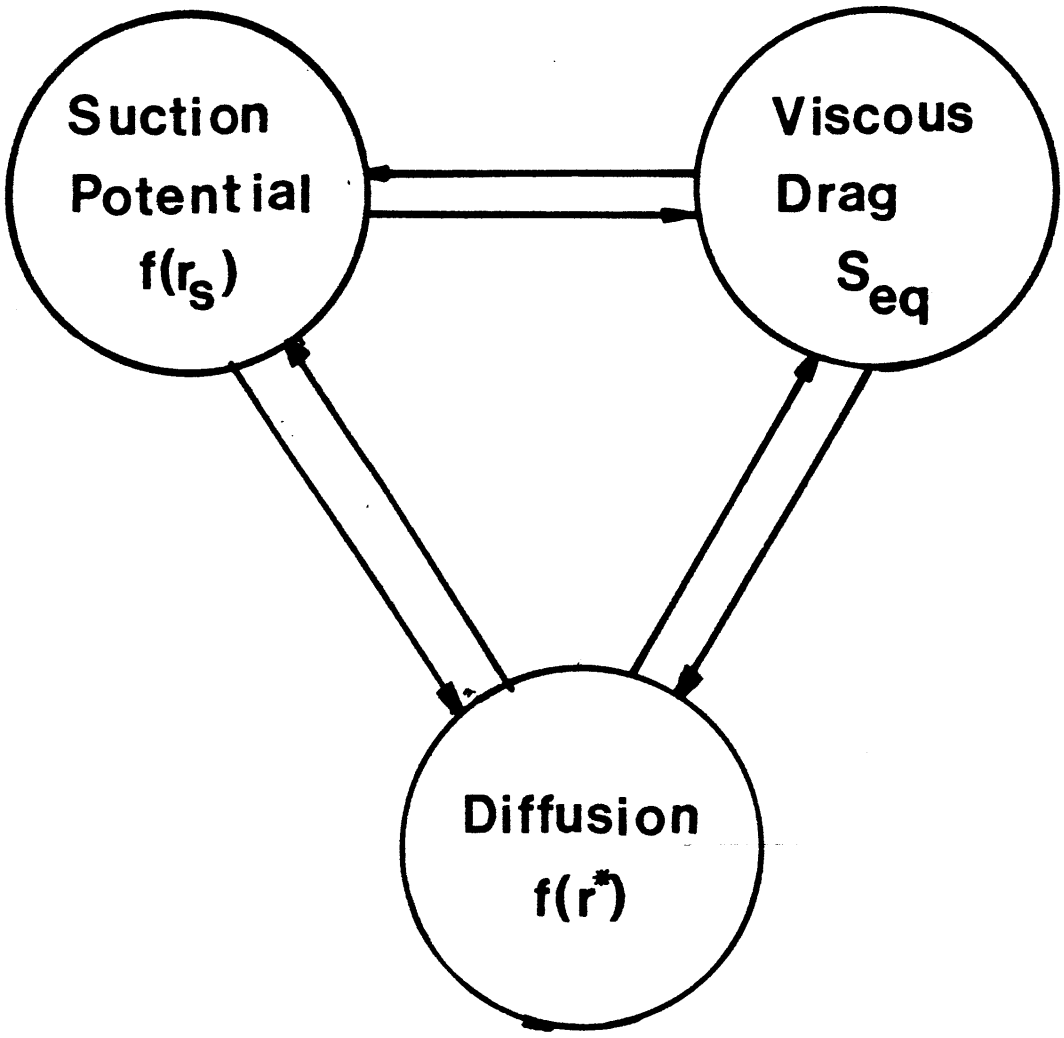

Fig. 5.7 A Schematic of the Manner that the Different Parts of the Model on Liquid-Diffusion are Related. The arrows indicate that the Experimental Observations of the Encircled Entity Predict the Values of the Other Encircled Entities.

CHAPTER 6

LIQUID DIFFUSION IN FIBROUS INSULATION:

EXPERIMENTS AND OBSERVATIONS

6.1 GENERAL CHARACTERISITICS OF THE TEST SAMPLES

Two types of fiberglass insualtion were used for the experiments. They are manufactured by Owens-Corning Inc. The

macroscopic void-fractions of the insulations were 94.5 and 98.2%. The medium with 94.5% is ordinarily used as a roof insulation, whereas the other one could be used for walls. The widely used pink insualtin was not used, because it did not withstand the stresses caused by the surface tension forces and would undergo permenant structural deformation. The directional fiber density of both types of insulation were investigated using a microscope. They were found to be approximately 52., 43., and 5.%, corresponding to i=1,2,3 directions.

6.2 LIQUID CONTENT MEASURMENT PROBES

Measurement of liquid-content in porous media requires special instrumentation. Several measurement technics have been developed by various researchers[80-85]. However, they were found not to be suitable for measurment of liquid-content in fibrous insulation. Liquid-content probes have been developed to measure the volumetric liquid-content in the fibrous insulation. In the process of preliminary experimentation with the insulation, it was discovered that de-ionized water dissolved some of the phenolic-binder of the insulation and became ionized. Therefore, it was decided to take advantage of this phenomenon, and build the liquid-content probes around it. Hence, resistance-probes were developed. The probe takes advantage of the electric resistivity of the liquid and measures the volume of liquid in the medium. The probe consists of two long stainless steel needles of .46 mm diameter, seperated by 6.26 mm., Fig. 6.1. The probe is inserted into the medium and the electric resistance between the two needles is measured.

The electric resistance of the probe is measured using an alternating-current resistance measurement circuit. The choice of a.c. measurement as opposed to the d.c. resistance-measurement was dictated by the working liquid. The resistvity of the liquid was caused by the ions which were dissolved in it. Were one to impose a d.c. voltage across the probes, the ions in the liquid would be seggregated and migrate towards the two needles depending on the sign of their electric charge. This would, in turn, result in a time-varying resistivity in the medium.

However, with an a.c. voltage across the probes, the ions in the liquid would not migrate in a specific direction, but would rather oscillate back and forth respondiong to the alternating electric-field. The unwelcome feature of a.c. resistance-measurment technic is the electric capacitance which is set up in-between the two legs of the probe. The electric impedance of a resistance oscillated at a frequency ω is

$$Z_R = R$$

and the impedance of an electric capacitance oscillated at the same frequency is:

$$Z_C = 1/(C\omega)$$

The equivalent circuit to the probe would be a capacitor and resistor in parallel. Hence, the equivalnet impedance would be:

$$Z_T = \left(C\omega + \frac{1}{R} \right)^{-1}$$

It is clear from the above, that as the frequency of oscillation increases the impedance of the capacitor dominates that of the resistor. Hence, the frequency of the oscillator had to be chosen such that the capacitance effects be negilgible compared to that of the resistance. Experimentation indicated that at 10 kilo-cycles the effect of capacitance with the probe inserted into a bath of liquid was negligible compared to that of the resistance. The resistance measurement circuit is shown in Fig. 6.2. It works on the basis of a voltage-divider , with the probe being one of the resistances. The voltage across the probe is processed at several stages. It is first amplified, the carrier-wave is then removed by passing the signal through a rectifier and a filter. The output voltage of the circuit would corresponds to the probe resistance by the following relation:

$$\frac{V_{probe}}{V_{input}} = \frac{R_{probe}}{R_{calib} + R_{probe}}$$

where R_{calib} is the caliberation resistance.

In any experiment numerous probes are used. The probes are connected to a switching circuit. The switching-circuit connects the probe to the resistance-measurement circuit sequentially. The switching circuit consists of 5 linear integrated circuit dual-timers 556. The timers were connected in tandem, such that whenever one would turn off, the next would be activated. When activated, the resistance of the timer-chip was about 100 ohms; otherwise it was of the order of Mega-ohms. Each probe was connected to the resistance-measurement circuit for a specific

duration of time. The switching frequency was set by adjusting the appropriate resistances and capacitances in the switching-box, and could vary from milli-seconds to hours. A total of ten probes could be connected through the switching-box to the resistance-measurement circuit. The voltage output of the measurement circuit was plotted on a chart-recorder. The profiles of voltages plotted on the recorder could, then, be interpereted to yield liquid-content profiles. A schematic of the measurement set-up is given in Fig. 6.3.

The output-voltage of the measurement circuit is a function of the volume of liquid bridging the two legs of the probe. By proper installation and caliberation the resistance across the probe could be related to the liquid-content in the medium. Figure 6.4 represents a schematic of the installed probe. The resistance across the probes at 100% wetness is:

$$R(\theta = 100\%) = \rho_e S/A$$

where

ρ_e = elctric resistivity of the medium

S = Distance between the legs of the probe

A = Area through which the electric current flows

= f(D/S)

In the above D and L are the diameter and length of each

probe needle, respectively. With only part of the probe wet its resistance is a function of the liquid content. Therefore:

$$\theta = \text{Function}\left(\frac{R(\theta)}{R(\theta=100\%)} \right)$$

The caliberation curve was developed by making voltage measurements in partially wet medium. The medium was then weighed, dried and weighed again. The difference in the weight of the medium was then translated to liquid-content values. The caliberation curve is shown in Fig. 6.5. The probe's output-voltage is plotted against the value measured by the dry/wet method. The caliberation curve demonstartes that for liquid-contents in excess of 15% the probe predicts the actual values of the liquid-content with a reasonable accuracy. Below liquid-content values of 15%, the liquid becomes pendular and does not bridge the probe needles. Therefore, the probe readings at liquid-contents below 10% are not very reliable.

The a.c.-measurement technic assumes a constant value of medium-resistivity. For this reason a specific procedure was developed to ensure that the liquid had a constant ion-density. This procedure will be described later in this section. The resistivity of the liquid is a function of the mobility of the ions which is, in turn, a function of temperature. The change in resistivity of the liquid as a function of temperature was observed no to be negligible. In order to isolate this effect, a reference cell was built. A pair of probes were installed in the cell which was full of liquid at room temperature. The resistance associated with the output-voltage of this probe is

used as the reference value $R(\theta=100\%)$.

The liquid-content probes work on the basis of measuring the electrical resistance of the liquid in the medium. It has been found experimentally that the phenolic binder dissolves in water and ionizes the water. De-ionized water was brought into contact with pieces of the insulation. The water was then evaporated and a yellow-colored residue was observed. The color of the insulation being yellow, it was inferred that the residue must be the phenolic-binder. The use of the liquid-content probes requires a constant value of resistivity. In order to ensure that the liquid used in the experiments has a constant resistivity a special preparation recipe was developed. Insulation pieces were cut to very small sizes. They were then mixed with de-ionized and distilled water. The mixture was constantly stirred as it boiled for about 30 minutes. In this stage the water became saturated with binder. Then the mixture was cooled to room temperature and filtered. The resulting liquid is saturated with the binder and no more binder dissolves in it. The density and viscosity of the liquid were found, within experiemntal error, to equal those of pure water. The value of surface-tension of the liquid was measured to be 73 dynes/cm at room temerpature; an increase of 10% over that of pure water. The contact angle was observed to be zero.

6.3 MEASUREMENT OF SUCTION-RADIUS DISTRIBUTION

The strength of the suction-potential in the fibrous medium is characterized by the ability of the medium to retain a liquid against an adverse potential. The standard procedure for the measurement of the suction-potential is to enclose the porous medium in a cell and by slowly varying the pressure, displace one fluid by another. By this method, the relationship between pressure and liquid-content can be established. However, in the case of fibrous medium a more simple experiment can be performed, mainly because the variations of the suction-potential from one layer to the other is of interest. In this experiment, the insulation is allowed to absorb liquid from a pool against gravity, Fig. 5.6. The liquid rises in the insulation under the action of surface tension forces until it reaches a steady-state height. The steady-state height distribution in the layers was recorded by visual observation and the probes. The probes were installed at different heights and the value of liquid-content at each height was recorded. The experiment was conducted along the three principal directions of the medium. The experiments on along and across the layers were carried out on 17 different samples. Six samples were used in experiments on absorption through the layers. The observed frequency distribution of the liquid columns in the medium were aggregated to yield a total frequency-distribution. The height frequency-distributions corresponding to experiemnts on along and across the layers were found to be identical.

The liquid columns in the medium are supported by surface

tension forces. Hence on can write:

$$\rho gh = 2\sigma \cos\gamma / r_s$$

where r_s is the suction-radius as defined in section 5.3.1. The observed distibution of the liquid columns is transformed to a suction-radius distribution. The density distribution of the suction-radius for the two types of insulation, in the plane of the layers, is presented in Fig. 6.7 and 6.8. In the experiments on liquid absorption through the layers, the liquid rose to the same level in all samples. The lqiuid rose through the layers to the height of 1.587 cm. and 1.275 cm. in the heavier and lighter insulation, respectively.

6.4 MEASUREMENT OF PRESSURE-DROP/FLOW-RATE RELATION

In flow through saturated porous media a Reynolds number based on a simple definition of the hydraulic radius of the medium can be defined. Hydraulic radius is defined as the ratio of the volume to surface of a capillary. For the ordered-array model:

$$V = 1 - N\pi r_f^2$$

$$S = N\pi r_f$$

where V is the volume of the capillaries, and S is their surface area . Therefore, the hydraulic radius is:

$$r_h = \frac{\epsilon}{1 - \epsilon} r_f$$

Using typical values indicate that the rate of liquid diffusion in the insulation is such that the flow may be considered laminar. Therefore, in the measurement of pressure-drop/flow-rate relationship, only the laminar flow regime is considered. A schematic of the experimental apparatus is shown in Fig. 6.9. The apparatus consists of two chambers that are seperated by a piece of the insulation. Liquid enters one of the chambers and passes through the insulation into the next chamber. The sides of the insulation which are not in contact with the chambers are coated with epoxy glue and rendered impermeable to liquid-flow. The liquid is pumped through the insulation and the flow rate is measured. A number of probes, usually two or three, are inserted into the medium. These help verify that all parts of the insulation are wetted, and that the liquid is not short-circuiting around a more dense section of the insulation. Close to the test-piece two vertical tubes are connected to the two chambers. The pressure-drop across the test piece is measured by the differential rise of liquid in the vertical tubes. Experiments were conducted along the three directions for both types of insulation. For each type of insulation, and along each direction a number of experiments were conducted. Equation [3.3.2.19] was used to transform the observed values of pressure-drop and flow-rate to values of S. Plots of S versus the Reynolds number, based on the hydraulic radius, are given in Figs. 6.10 and 6.11. As indicated the value of S remains constant over a range of Reynolds numbers. The maximum experimental error is 5.4% for the heavier medium and 3.2% for the lighter one.

6.5 EXPERIMENTS ON THE DIFFUSION PHENOMENON

Liquid diffusion in the insulation is controlled by the action of capillary forces. In the medium under study, the capillary forces are not very large. Hence, in studying liquid-diffusion care must be taken so that the effect of the hydrostatic head be negligible compared to the capillary forces. This requires that the height of the test-pieces satisfy the following inequality:

$$\rho gh < (2\sigma\cos\gamma/r_s)$$

The range of observed values of the suction-radii indicate that the thickness of the medium should be made very small. Unfortunately this is only possible for only one type of insulation. When the lighter insulation is cut into pieces of 1-cm. thickness, the pieces lose their structural integrity and the layers seperate. Although diffusion experiments were conducted on both types of insulation, the results for the lighter insulation are considered to be unreliable. The technics used in the experiments on liquid-diffusion in the plane of the layers are different from the ones on liquid-diffusion from one

layer to the other. Hence, each experiment is discussed seperately.

6.5.1 Liquid diffusion in the plane of layers

In this set of experiments, the sample is cut to a height of about 1-cm. It is then epoxyed onto a plexi-glass plate connected to a liquid-reservoir, Fig. 6.12. The liquid is introduced to the reservoir through a syringe, at a rate such that the level of liquid in the reservoir does not fall below or exceed the height of the sample. The liquid introduced at one end of the test-piece diffuses along the layers. Once the insulation gets wet, its color changes drastically. Hence, the motion of the diffusing front is recorded by taking pictures of the sample at regular time-intervals. Fig. 6.13 is a schematic representation of the motion of the diffusion-front. For every experimental run a number of pictures were taken. Each photograph yields the frequency-distribution of the length travelled by the liquid. This frequency-distribution and the time that corresponds to it are reduced through eq. [5.3.3.7] to generate a r^*-distribution. Similar to the experiments on r_s-distribution, the difference in the r*-distributions associated with diffusion across and along the layers were within the range of experimental errors. This is to say that no difference between the diffusion rates along and across the layers was observed. The cumulative r*-distribution for the heavier insulation is given in Fig. 6.14. The Cumulative r*-distribution for the lighter insulation is given in Fig. 6.15. As indicated before, the results for the lighter insulation are not considered reliable.

6.5.2 Liquid Diffusion Through The Layers

A schematic set up of the experiment on liquid-diffusion through the layers is shown in Fig. 6.16. Liquid diffuses through the layers in the manner described in section 5.4.3.I.

Several probes are put in series and inserted into the sample such that the series is in one layer of the insulation. The probes are wired electrically in two different arrangements. In once case each probe series is wired such that all probes are electrically parallel with eachother. In this arrangement, the circuit output corresponds to the average value of liquid-content in the layer. In the other arrangement, each probe is monitered seperately. In this way, liquid diffusion both along and through the layers is observed. Hence, the values of critical liquid-content, as defined in section 5.4 and chapters 2 and 3, are obtained. This is acheived by monitoring the matrix of probes. Consider a probe in a certain position along a certain layer. The value of liquid-content at this location is monitored until the diffusing liquid reaches the same location in the next layer. The value of liquid-content at the first layer at the time of the appearance of liquid at the second layer is taken to be the estimator of the critical liquid-content.

The period of time that it took for the liquid to travel from one set of probes to the next were recorded using the first of the above arrangements. The data for a travel distance of 6.35 mm. is presented in Fig. 6.17. The experimental results indicate that the travel-time between succeeding layers is not only monotonic, but exhibits strong irregularity. Were the tortuosity factor, as defined in eq. [5.4.9], uniform through the

medium the travel-time would increase monotonically as the liquid front travelled a larger distance away from the reservoir. However, the irregular patterns suggest that not only the tortuosity is not uniform, but its variations are such that they overshadow the effects of increased length associated with the front movement. Were the length of the test-samples, which is equal to the thickness of the insulation-boards, an order of magnitude larger, then perhaps, the effect of increased length would show up. Not much information can be derived from the data as presented in Fig. 6.17.

Nevertheless, if one were to hypothesize that the total length through which the liquid has to diffuse is of no significance, and part with the notion of ever-increasing travel-time, one can study the data in another manner. With this assumption, the travel-time between any two sets of probes itself becomes a statistic. Fig. 6.18 exhibits the frequency-distribution of travel-times between <u>any</u> two sets of probes, compiled from eight experiments. A well defined distribution is clearly demonstrated. The next task is to translate the above distribution into a form which would generate some information about the totuosity factor. It was suggested in the above that the length affect is not present in the experimental results. Then eq.[5.4.7] may be rewritten as:

$$2L(dL/dt) = \alpha r^{*} \tau \qquad [6.5.2.1]$$

Assuming that the first L term is relatively constant, one can write:

$$2\ L\ (\Delta L/\Delta t) = \alpha\, r^{*}\tau \qquad [6.5.2.2]$$

which can be re-arranged into the following form:

$$r^{*}\tau = (2/\alpha)(\Delta L/\Delta t)\ \overline{L} \qquad [6.5.2.3]$$

In the above L is the probe seperation distance, L is some representative length scale, and t is the travel-time. A reasonable value of L is one half of the test-piece length. Using the above values and approximation a r^{*} -distribution may be generated. However, it can be easily recognized that given a distribution of one of the variables, r^{*}, and that of the product, the τ—distribution cannot be uniquely defined. Yet, if it is assumed that the two parameters τ and r^{*} are statistically independant, then the average of their proucts equals the product of their averages:

$$\overline{r^{*}\tau} = \overline{r^{*}}\ \overline{\tau} \qquad [6.5.2.4]$$

Using an verage value of $7\text{x}10^{-4}$ cm. for r^{*}, the average value of τ is found to be $1.8\text{x}10^{-2}$. This value of τ corresponds to a value of 7.4 for L_o/h. L_o/h is a measure of the inter-connectedness of the layers. Using an estimate of 2 mm. for an average value of h, there is, on average, one inter-connection between layers

every 1.5 cm.

The results of the experimental measurments of the critical liquid-content is presented in Fig. 6.19. The average critical liquid-content is about 70%. This implies that in a given layer, the liquid-content should rise up to about 70% before the liquid diffuses into the adjacent layer.

6.6 EXPERIMENTAL RESULTS AND DISCUSSIONS

The manner in which all parts of the model are inter-connected has been discussed in section 5.5. It was shown that the parameters and estimators chosen to model the phenomena of suction-potential, viscous drag, and liquid-diffusion are related to eachother. The three phenomena are described by: r_s-distribution, S_{eq}, and r^*-distribution, respectively. However, the three set of parameters are all function of void-fraction distribution, fiber-radius, and directional fiber-density. The fiber radius, and the directional-fiber density are known within a degree of certainty. In theory, the experimental results on any of the three parameters may be used to back calculate the void-fraction distribution. This void-fraction distribution can then be used to calculate the other two parameters. In this manner two objectives ar acheived. First, the model is tested for consistency and accuracy. Second, the limits and accuracy of the estimators are evaluated and ,perhaps, the experiments and estimators can be ranked in terms of accuracy and conceptual correctness.

In the following a brief description of the methodology in reducing the experimental results to the void-fraction distribution is given. Then, the results of each experiment is compared to the model based on the other two experiments. For example, the experimental values of S_{eq} and r^*-distribution are used to calculate two r_s-distributions. These distributions are then compared to the ones obtained experimentally.

At first let some notation be defined. The parameters under study are : rs-distribution, S_{eq}, and r_*-distribution. They are respectively indexed as 1, 2, and 3. A result obtained by reducing the data from a certain experiment will be subscripted by that experiment's index. For example, when the experimental values of S_{eq} is used to predict the r^*-distribution, $f(r^*)$ will be written as $f(r^*)_2$. Hopefully, with this nomenclature room for confusion will be reduced.

The experiment on suction-potential yielded the liquid-column height distribution. The height distribution is reduced to $f(r_s)$ by the following equality:

$$\rho g h = 2\sigma \cos\gamma / r_s \qquad [6.6.1]$$

It has been shown that the suction-potential is related to the fiber-spacings and consequentially to the void-fraction, fiber-radius, and the directional fiber-density:

$$r_s = \frac{r_f}{\frac{n_i}{N}(1-\epsilon)}$$

Hence, the r_s-distribution can be transformed to yield a $f(\epsilon)$. With this value of $f(\epsilon)$, the model, eqs. [4.3.20], [4.4.2], [4.4.3], and [4.3.30], predicts $f(r^*)$ and S_{eq}:

$$f(h) \xrightarrow[exp]{} f(r_s) \longrightarrow f(\epsilon) \longrightarrow \left[f(r^*)_1 \;\; \& \;\; S_{eq,1} \right]$$

The experimental results obtained from the experiment on pressure-drop/flow-rate consist of 3 S_{eq} values. Equations [4.3.30], [4.4.2], and [4.4.3] indicate how these values are related to $f(\epsilon)$. However, it is conceivable that more than one $f(\epsilon)$ can yield the same values of S. Therefore, an additional constraint is required to be satisfied. This constraint is conservation of mass:

$$\int_0^1 \epsilon \, f(\epsilon) \, d\epsilon = \epsilon_T$$

Nevertheless, it is not clear that even with the above constraint, the three values of S define $f(\epsilon)$ uniquely. The void-fraction distribution was back-calculated by assuming it can be described by a Poisson-distribution. By trial and error the distribution which fittted the data best was discovered. The ϵ-distribution was then used to calculate the $f(r_s)_2$ and $f(r^*)_2$:

$$\left[S_{eq} \, , \, \epsilon_{T\,exp} \right] \longrightarrow f(\epsilon) \longrightarrow f(r_s)_2 \;\; \text{and} \;\; f(r^*)_2$$

The experiments on liquid-diffusion in the plane of the layers resulted in the r^*-distributions. Equation [5.3.3.9] indicates the relationship between r^* and ϵ. Hence, the

experimental values of $f(r^*)$ can be reduced to yield a $f(\epsilon)$, which can be used to generate $f(r_s)_3$ and $S_{eq,3}$:

$$f(r^*)_{exp} \longrightarrow f(\epsilon) \longrightarrow \left[f(r_s)_3 \ \& \ S_{eq,3} \right]$$

The cumulative distribution of a function f is denoted by F. In comparing the results, the cumulative-distribution of each parameter is used in order to avoid errors associated with differentiating experimental distributions. The comparison of $F(r_s)_{exp}$ with $F(r_s)_2$ and $F(r_s)_3$, for the heavier medium in given in Fig. 6.20. The comparison indicates that the experimentally observed distribution has the largest spread and incorporates higher values of r_s. The experimental results are obtained by transforming the observed distribution of the height of liquid columns. Equation [6.6.1] indicates that a low value of column-height translates into a large value of r_s. Large volumes of the binder, which were often observed in the medium, arrest the rise of liquid in a layer and, hence, create a bias in the data. This is beleived to explain the observed discrepancy between the experimental distribution and the ones predicted by the model, for the agreement between the two model predictions, $F(r_s)_2$ and $F(r_s)_3$, is good. $F(r_s)_3$ indicates a lower frequency of capillaries at higher values of r_s. This can be explained by the coupling between the layers which causes an effective reduction in the suction-potential. The experimental results and the model predictions for the lighter medium are presented in Fig. 6.21. The trends are identical to the observations made for the heavier medium. The only difference is the extent of deviation between $F(r_s)_2$ and $F(r_s)_3$. However, as mentioned earlier the results of the experiment on liquid-diffusion in the lighter medium are not reliable.

The values of S_{eq} predicted by the model using $f(r_s)$ and $f(r^*)$ are compared with the experimental observations in Fig.6.22, and 6.23 for the heavier and lighter medium, respectively. The results are also compared with the theoretical prediction based on a homogeneous model which was shown to predict the upper limit. The comparison shows that the values of $S_{eq,1}$ are farther from S_{exp} than $S_{eq,3}$. This is similar to the observations on $F(r_s)_2$ and $F(r_s)_3$. Nevertheless, the agreement between the experimental observations and the model predictions are astonishingly good for both types of medium.

Figures 6.24 and 6.25 present the comparison of $F(r^*)_{exp}$ with $F(r^*)_1$ and $F(r^*)_2$ for the heavier and lighter medium, respectively. As before $F(r^*)_{exp}$ for the lighter medium is not very reliable. The observed diffusion results for the two orthogonal directions in the plane of layers were statistically identical. However, the model predicted different r^*-distributions for different values of directional fiber-densities. The results indicate that $f(r^*)_{exp}$ is flatter than the calculated ones for both types of insulation. This confirms the discussion on the effect of coupling between the layers on liquid-diffusion, given in the previous chapter. It may be observed that the effect of directional fiber-density is not pronounced. The agreement between the experimental values and model predictions are very good for the heavier medium. The discrepancy in the lighter medium is still within an understandable range and indicates that the experimental results are not completely random.

In summary, the model, the experiments, and the estimators have been put to a rigorous test. By checking the model in three different manners with data obtained on two types of insulation, the consistency of model, relative accuracy of estimators, and accuracy of experiments are verified. As it stands, the ensemble of model, estimators and the experimental technics have proven to be a successful combination.

6.7 EXPERIMENTS AND DISCUSSIONS ON EFFECT OF GRAVITY ON LIQUID-DIFFUSION

In the detailed analysis and experimentation of the previous sections the effects of gravity on liquid-diffusion was not incorporated. In the development of the model attention was focused on the paramters that characterize the medium. The experiments on liquid-diffusion were also designed such that the effect of gravity be negligible. Nevertheless, the significance of gravitational effect on liquid-diffusion cannot be overlooked. In structures where condensation might take place, the presence of gravity is a determining factor in the behavior of the condensate. In this section the effect of gravity on liquid-diffusion in fibrous insulation is investigated.

By this stage of study, it is well established that the mechanism of liquid-diffusion in the plane of layers is significantly different from diffusion between the layers. Hence, it is reasonable to assume that the effect of gravity depends on the orientation of the layers in the gravitational field. Specifically, two orientations are of interest: layers arranged parallel to gravity, and layers perpendicular to gravity. The former corresponds to such assemblies as walls and the latter to roofs.

In the phenomenon of liquid-diffusion, the gravitational effects interact with the driving forces. When liquid is diffusing in a plane oriented perpendicularly to gravity, the

hydrostatic head in the wet-region adds to the driving potential at the edge of the liquid-front. In the case where the direction of liquid-diffusion is parallel to gravity, the weight of the liquid behind the front adds to the driving forces. With the liquid diffusing in the anti-parallel direction to gravity, the effect of gravity is to reduce the suction forces by the weight of the liquid.

Incorporation of the gravity effects in the formulations of the previous sections is straight-forward. However, there are certain aspects which do not fall within the above category and are, incidentally, very important. Specifically, two issues need to be investigated. First, is the value of liquid-content above which the liquid drops coalesce to form a continuous column. Second, the maximum height of liquid columns that the capillaries can hold against gravity. These questions will be addressed and analyzed in this section.

As vapor condenses in the medium, liquid accumulates in the insulation. As described in sectin 5.4, liquid drops are formed in a fashion such that their surface energy is minimized. This requirement implies that liquid accumulates around fiber-crossings. In this period of accumulation, liquid is in a pendular state and does ot exhibit the tendency to migrate. This is due to the fact that as the volume of liquid is small, not enough menisci are activated to propel the liquid. Then, the criterion for the commencement of condensate motion is that the liquid-content should exceed a critical value. As the volume of condensate increases the liquid drops grow and coalesce to form larger drops and eventually, depending on the extent of the condensation-region, create a column of liquid which has to be supported by the capillay forces against gravity. The maximum column height that can be supported by the surface tension forces is a property of the medium and depends onthe arrangement of the fibers. The critical issue is to determine whether the condensate will begin to diffuse before the forces of gravity

drain it to the bottom of the structure. In the next section a set of experiments which explore this and other questions are discussed.

6.7.1 Experiments

Several experiments have been conducted to investigate liquid-diffusion in the presence of gravity. Some of the experiments were qualitative. They helped in developing an understanding of the physical phenomena at work. Both types of experiments are discussed in this section.

6.7.1.1 Drainage Experiment

An experiment was conducted to measure the ability of the medium to retain columns of liquid. Pieces of insulation were cut along the layers to a height of 50 cm. The pieces were immersed in the binder-saturated liquid for a period of no less than 4 hours. They were then held vertically against gravity and allowed to drain into a liquid pool. Liquid-content probes were inserted into the medium at different locations. The time dependant behavior of liquid drainage was recorded on the chart-recorder. This experiment was conducted for both types of insulation.

The liquid was observed to drain out of the insulation at a fast pace. Figures 6.26 and 6.27 present the steady-state distribution of liquid-content as a function of height, for both

types of insulation. The plotted results are averages of several experiments. The values of liquid-content less than 15% were obtained by weighing the wet samples, drying them, and then weighind the dry samples. The difference in weight was translated to liquid-content values.

One common feature of both types of insulation is that above a certain height the insulation holds a fixed volume of liquid irregardless of the height. This liquid volume is approximately the same for both insulation and is referred to as retained liquid-content. During the drainage process, liquid travels from the top to bottom and essentially washes down all the liquid in its way. Hence, the value of retained liquid-content corresponds to a minimum and stable liquid-content which is strongly held by the fibers. In the regions closer to the bottom of the insulation, the value of liquid-content goes through an abrupt change with height. The change is more abrupt for the lighter insulation, Fig. 6.27. Clearly, the medium cannot sustain liquid columns with heights in excess of 15 cm. for the lighter insulation and 22 cm. for the heavier insulation. Furthermore, the volume of liquid that the capillaries can hold against gravity decreases very rapidly with a small increase in height. The total volume of liquid in the sample supported by the capillaries is the maximum value that the medium can sustain. Hence, any liquid in excess of this volume drains out from the insulation.

The same experiment was conducted to study drainage through the layers. The thickness of the insulation slabs available commercially are about 7 cm. With the gravity acting perpendicular to the plane of layers no significant drainage from compeletely wet samples was observed. Hence, it is concluded that in this orientation the hydrostatic head is not large enough to cause drainage. A height of 7 cm. corresponds to regions of very high saturation in Figs. 6.26 and 6.27. Hence, the observation of no drainage through the layers is reasonable

signifying that liquid is held up in both orientations by capillaries of similar strength.

6.7.1.2 Other Observations

Many quantative observations were made during the course of experimentations. These are described below. The implications of these observations are used to develop a model for the effect of gravity on liquid diffusion.

- After the drainage experiments of the previous section were completed, each sample was turned upside-down. In this arangement the top of the sample had a high liquid-content and the bottom had liquid-content value equal to the retained liquid-content. The liquid was observed to move rapidly to the bottom, and establish a steady-state profile. The profiles were similar to the ones obtained by the drainage experiments.

- The above experiment was continued in the following manner: some liquid was removed from the bottom of the piece. The sample was then turned upside-down once more. As before, liquid diffused to the bottom of the layers. However, it was observed that drainage took place mostly along a few layers. The liquid in the majority of layers drained into a few and then moved to the bottom of the sample.

- A dry piece of insulation, cut along the plane of layers was held vertically. Slowly, small amounts of liquid were introduced onto the top of the layers. After a while, the liquid seeped into the medium. More liquid was then added. It turned out that one of the layers would get wet and liquid would drain through that layer only. This phenomenon can be easily explained

by the notion of retained liquid-content.

- The liquid moving to the bottom of the piece in the previous experiment would collect at the botom of the layer through which it had drained. The liquid-content at the bottom of the sample would build up and slowly diffuse to theadjacent layers. This verifies the concept of critical liquid-content.

6.7.2 Modelling and Discussions

In this section the results of the experimental observations and the models developed for gravity-free diffusion are used to develop a model for the effect of gravity on liquid-diffusion. Attention is focused on the dependance of the gravitational effects on liquid-content.

Consider the situation where condensation takes place inside the insulation. The insulation is oriented such that its layers are parallel to gravity, and its height is in excess of 0.5 m. Condensation takes place uniformly in each layer; yet, condensation rate per unit volume differs from one layer to the other. As condensation begins, liquid drops are formed at various fiber-crossings and remain in the pendular state. As condensation continues the liquid-content in the medium increases. In the model for diffusion of liquid from one layer to the other, the notion of a critical liquid-content has been introduced. The model is based on the reasoning that for liquid to migrate from one layer to another sufficient number of suction-sites must be activated. This is assocaited with the fact that the value of liquid-content in the layer should exceed the critical-value before any diffusion can take place. The value of critical liquid-content was found to be about 70%. In the case under consideration, condensation rate per unit volume

and consequentially the rate of liquid accumulation varies from one layer to the other. Were gravity absent, liquid-content in certain layers would exceed the critical value and liquid would migrate to the other layers. However, with gravity present the situation is completely different. Liquid-content can never reach the critical value. An inspection of Figs. 6.26 and 6.27 indicates that the medium cannot sustain such liquid-content except in the range of 10-20 cm from the bottom. Hence, the liquid will drip downwards before it gets the chance to migrate from one layer to the other.

As the volume of liquid in the medium increases from zero, past the pendular state, liquid drops meet to coalesce. The volume and vertical location of these drops varies. As the volume and height of these coalesced drops increases a few of then become so large that capillary forces cannot sustain them. Hence, they start descending under gravitational forces. During their journey to the bottom of the slab, the liquid volumes come in contact with other ones and coalesce to make even larger volumes. This avalanche effect causes the liquid drops, which were otherwise supported by the capillary forces, to join the draining liquid, for their volume is suddenly increased by many folds. Hence, a large volume of condensate may be washed downwards by the dripping of a small volume. As the liquid-avalanche travels downwards it leaves some liquid behind it. This corresponds to the retained liquid-content values, observed during the drainage experiment, of 5-7%. Therefore, liquid-contents in excess of the value of retained liquid-content are unstable. The probability of an avalanche increases as the values of liquid-content exceed the values of retained liquid-content.

The ability of the medium to hold up liquid is a function of its suction-potential. The frequency-distribution of suction-potential may be estimated by making an analogy between suction-potential and the height of liquid columns, and

liquid-content with frequency-distribution of the potential. This analogy is based on the fact that the percentage of volume which is wet, at a given height, represents the percentage of the suction-sites which can hold liquid up to that height. Clearly, the experiments on drainage indicate that for the medium to hold liquid-contents in excess of 5-7% the height of the liquid columns can vary in a very narrow band. It can, therefore, be inferred that suction-potential is at its low and varies very little for liquid-contents in excess of 20%, Figs. 6.26 and 6.27.

With the above arguments, the following model is presented:

For liquid-contents less than the retained liquid-content, the liquid is in the pendular state and does not exhibit a tendency to move. In this state, the liquid is held by strong suction forces. As the volumetric liquid-content increases the small drops coalesce to form larger ones. However, the suction-potential for liquid-contents in excess of the 5-7% decreases to a relatively uniform value with increasing liquid content. The decrease is dramatic for liquid-contents in excess of 20% for the lighter insulation and 30% for the heavier insulation. Hence, with liquid-contents in excess of these values, it is most likely that some liquid volume becomes so large that the suction forces cannot hold it any more and it falls under its own weight. This fall triggers an avalanche which washes down all of the liquid in the medium except for the amount equal to the retained liquid-content.

For the situations were gravity is perpendicular to the layers, the liquid-content can increase to very large values without any dripping setting it. This is due to the fact that the thickness of commercially available insulation is not large enough for the weight of the columns to exceed the surface tension forces. The maximum value of liquid-content prior to the onset of diffusion is experimentally found to be 70%.

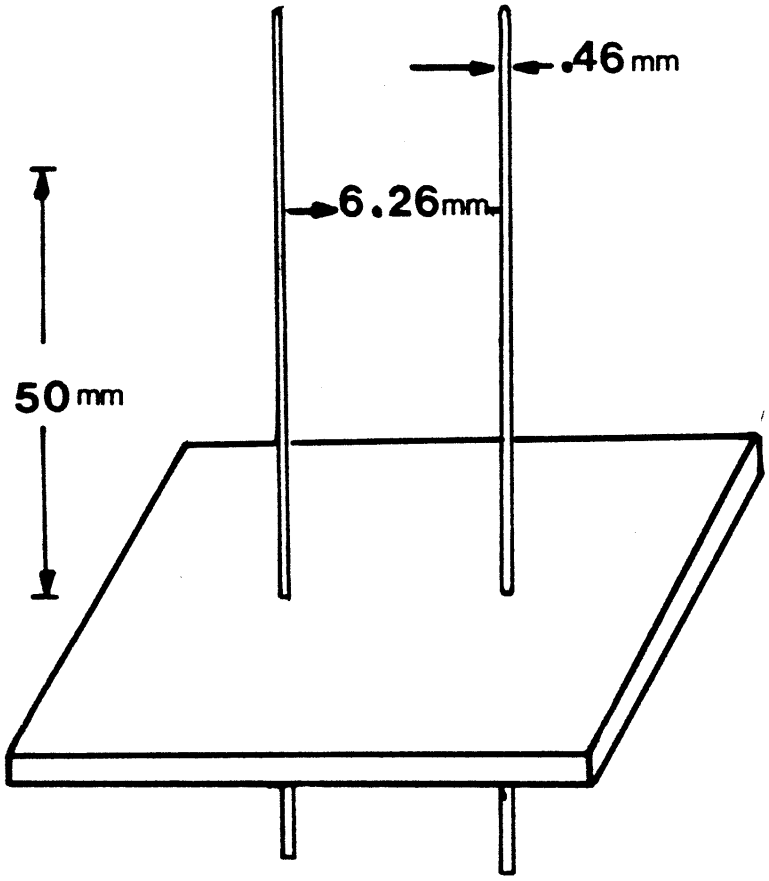

Fig. 6.1 Schematic of Liquid-Content Measurement Probe

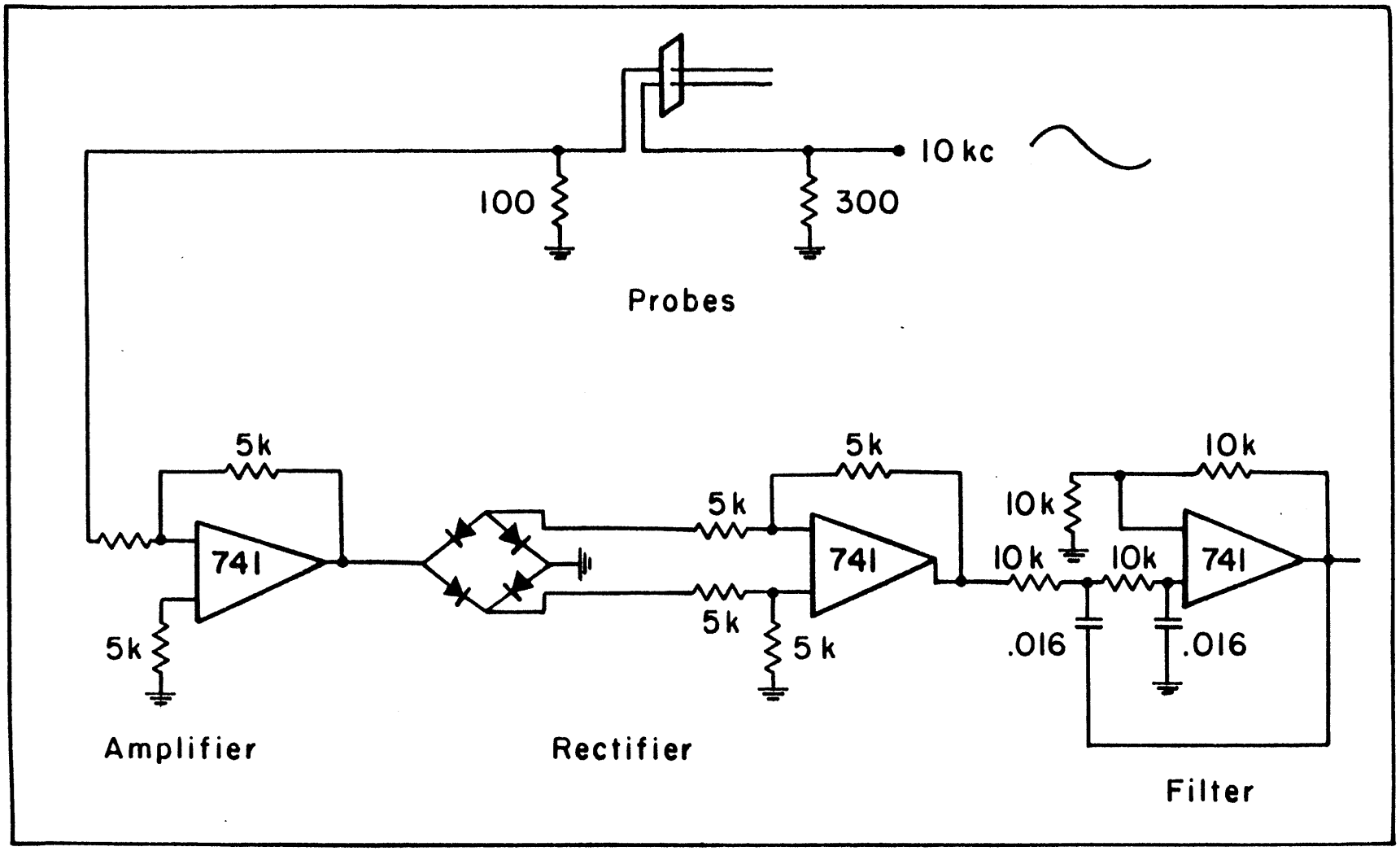

Fig. 6.2 Electronic Schematic of A.C. Resistance Measurement Device

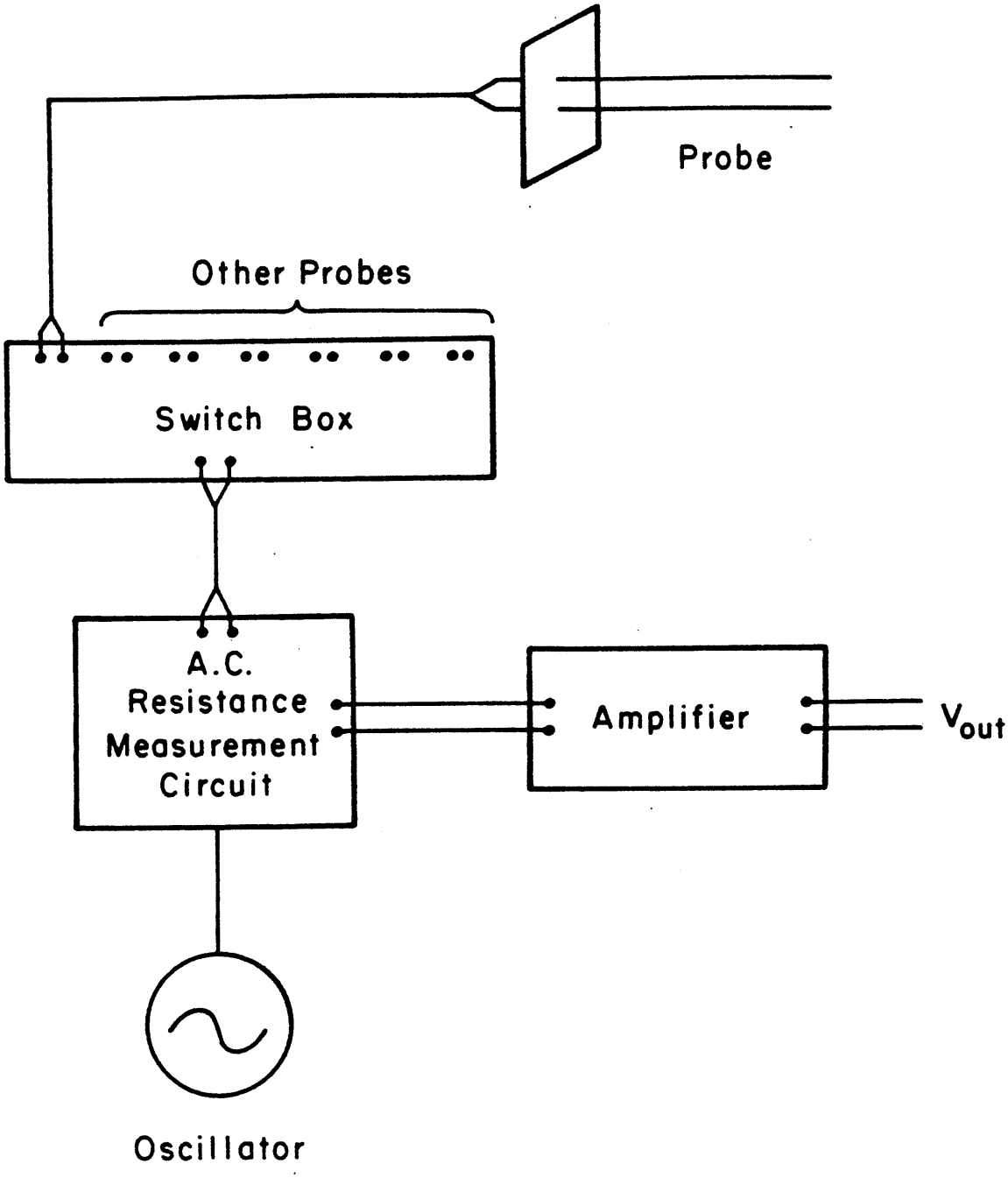

Fig. 6.3 A schematic of The Probe and the Associated Electronic Circuit

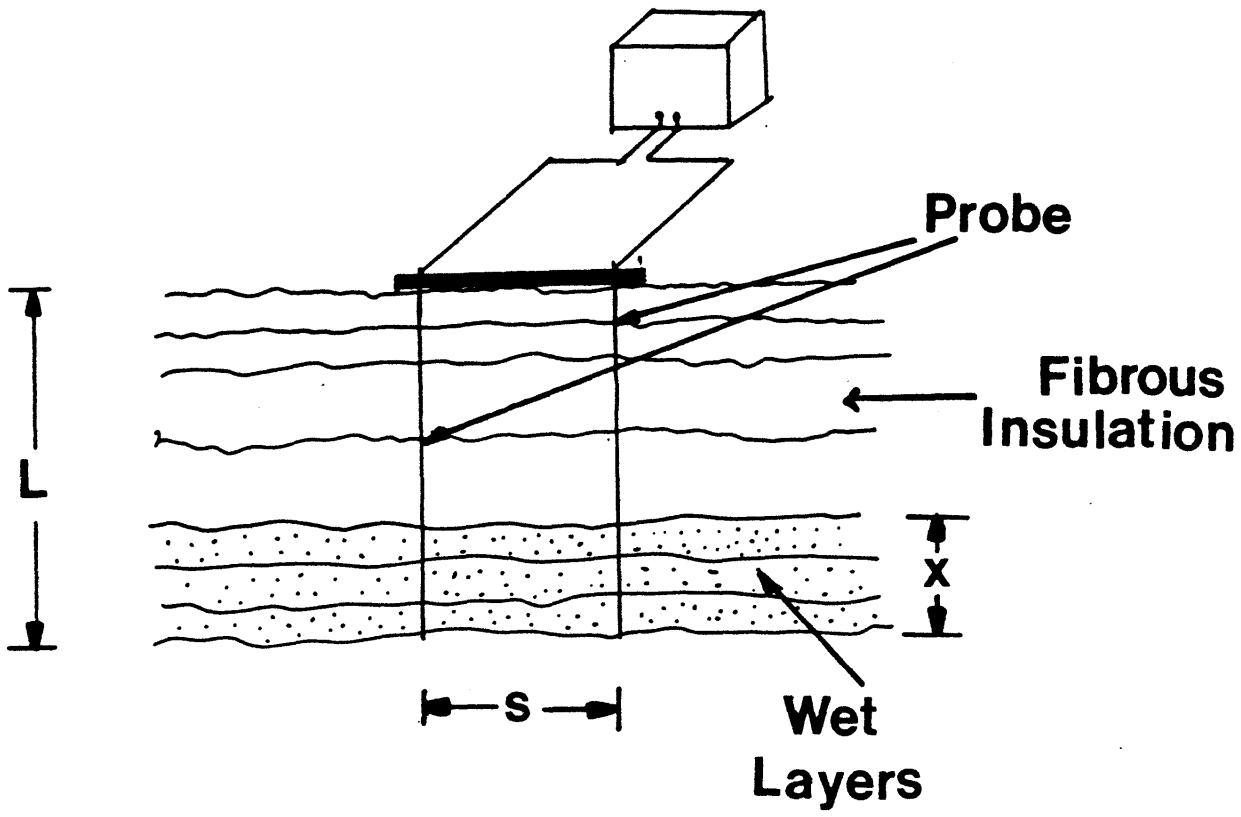

Fig.6.4 Schematic of the Installed Liquid-Content Probes In the Fibrous Media

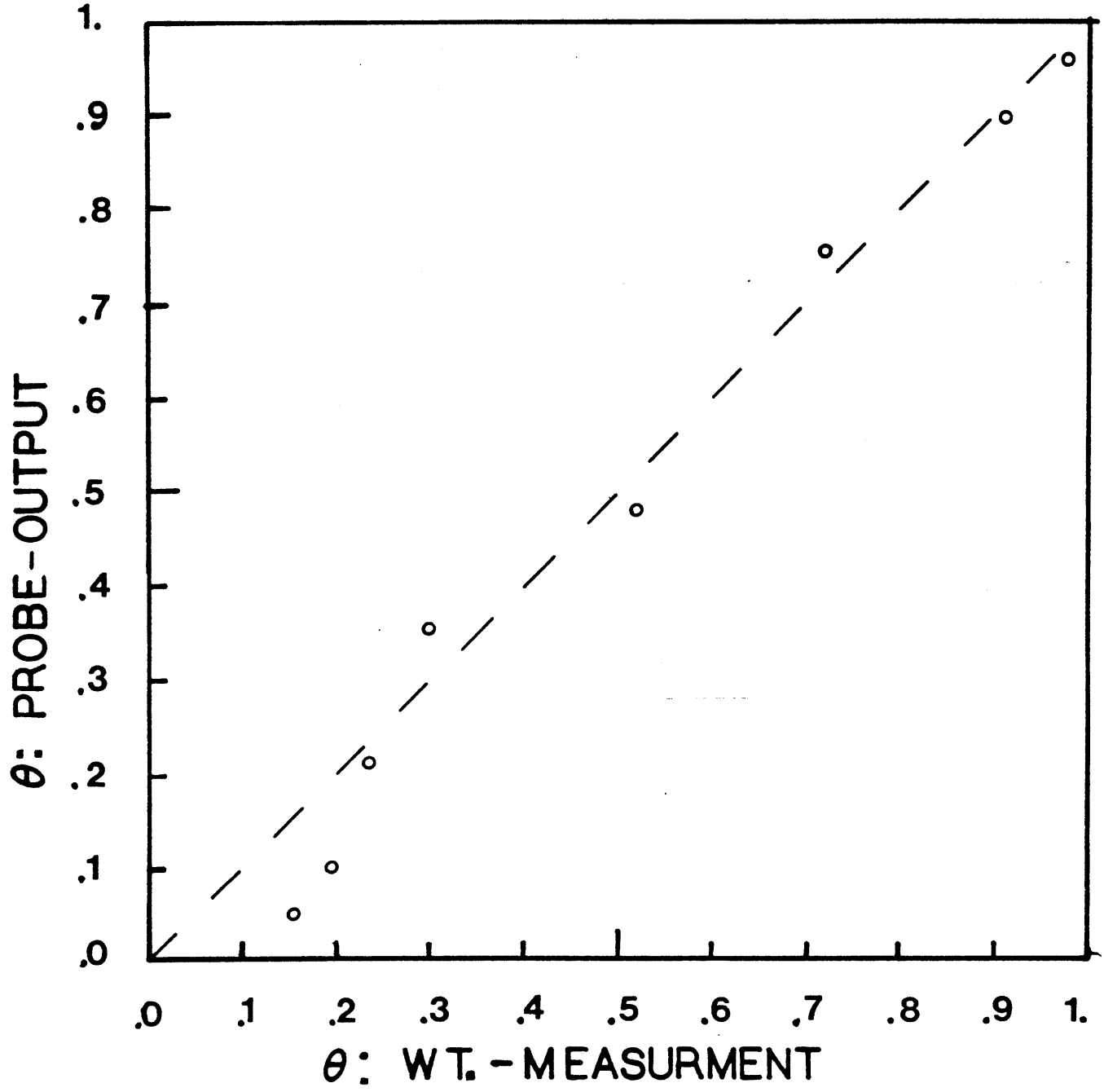

Fig. 6.5 Comparison of Liquid-Content Measurements Obtained from the Probe Output and the eight Measurment Technic.

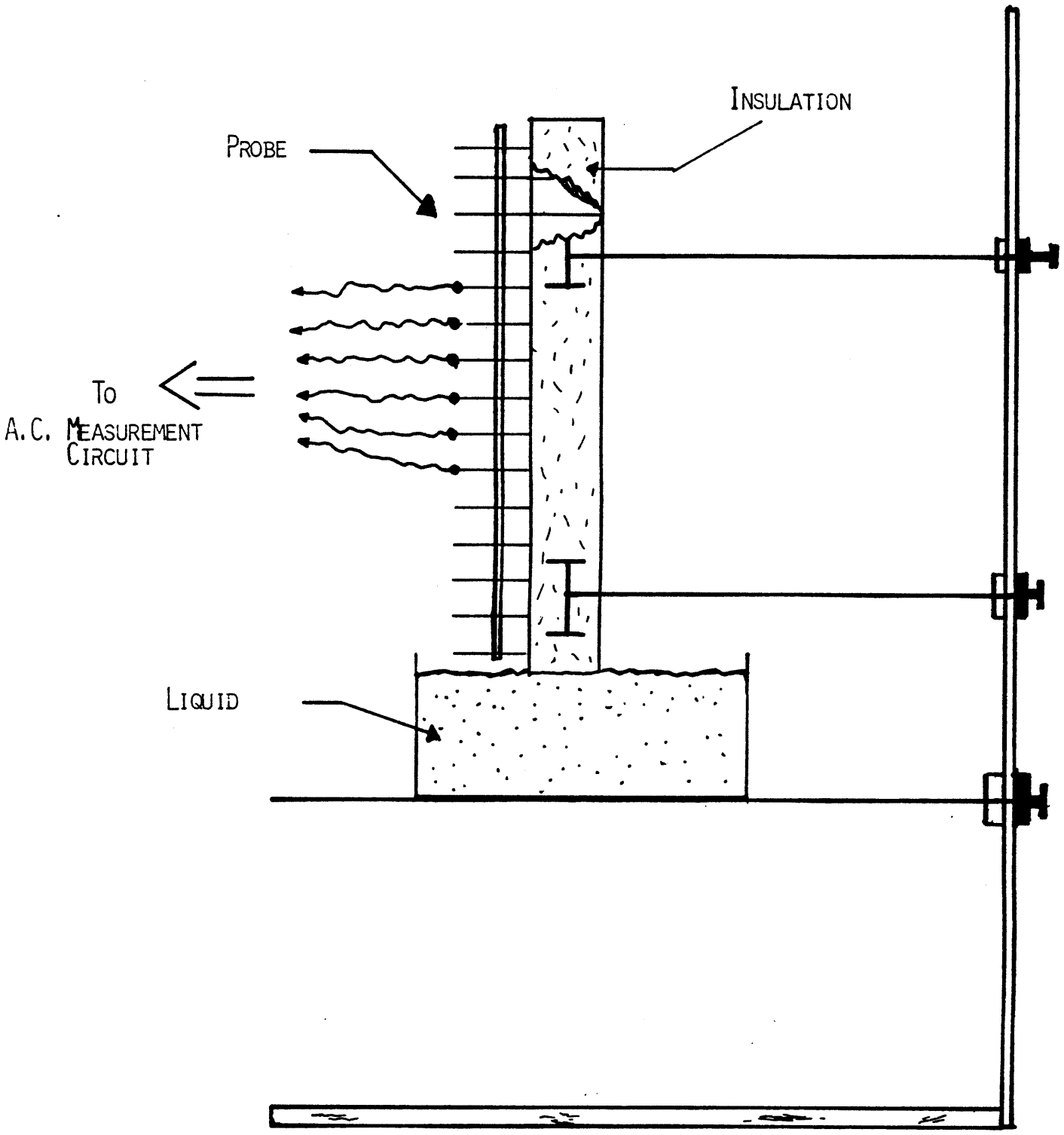

Fig. 6.6 A Schematic Presentation of the Apparatus Used for the Measurement of the Suction-radius Distribution

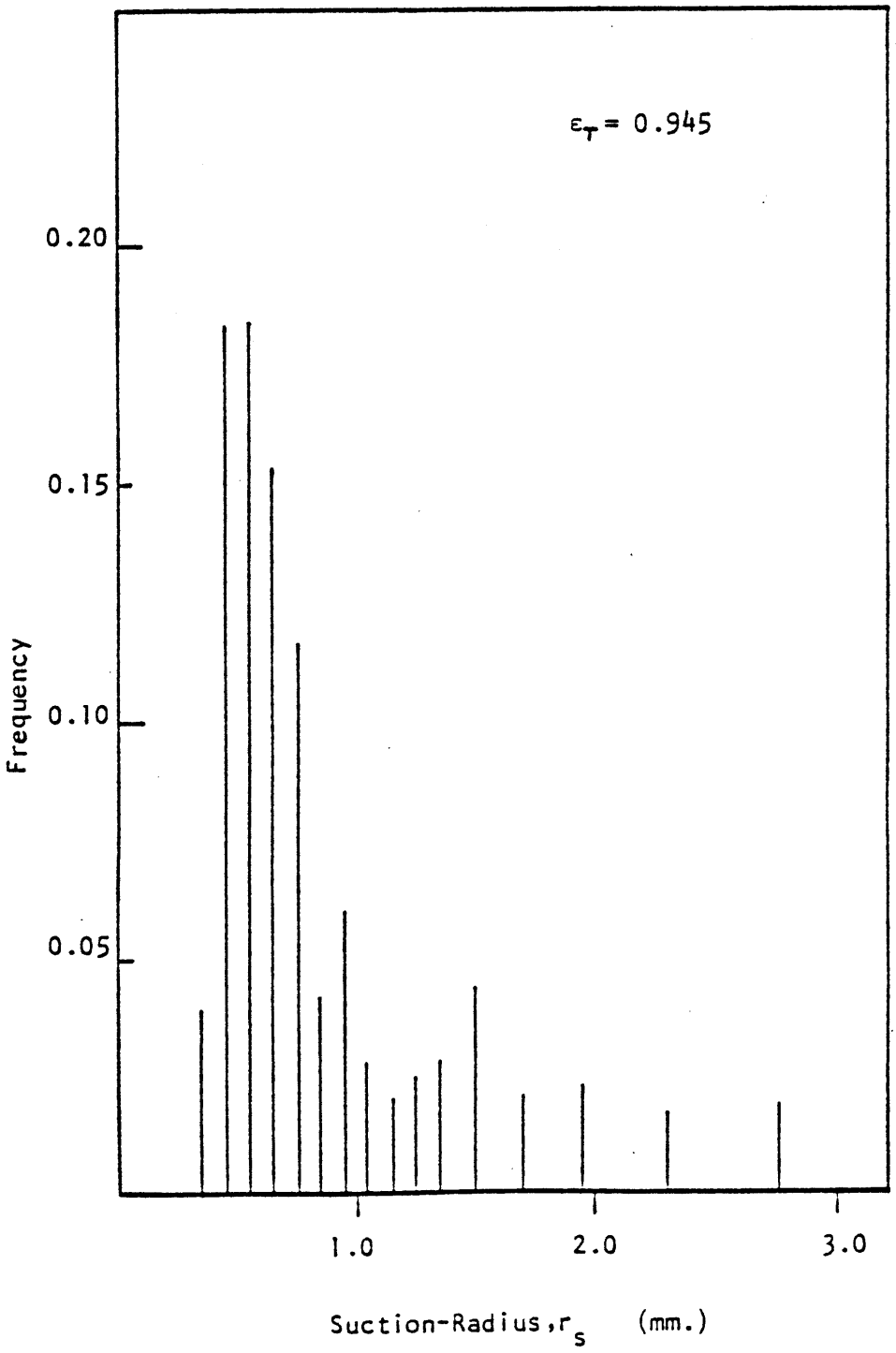

Fig. 6.7 Suction-Radius Distribution

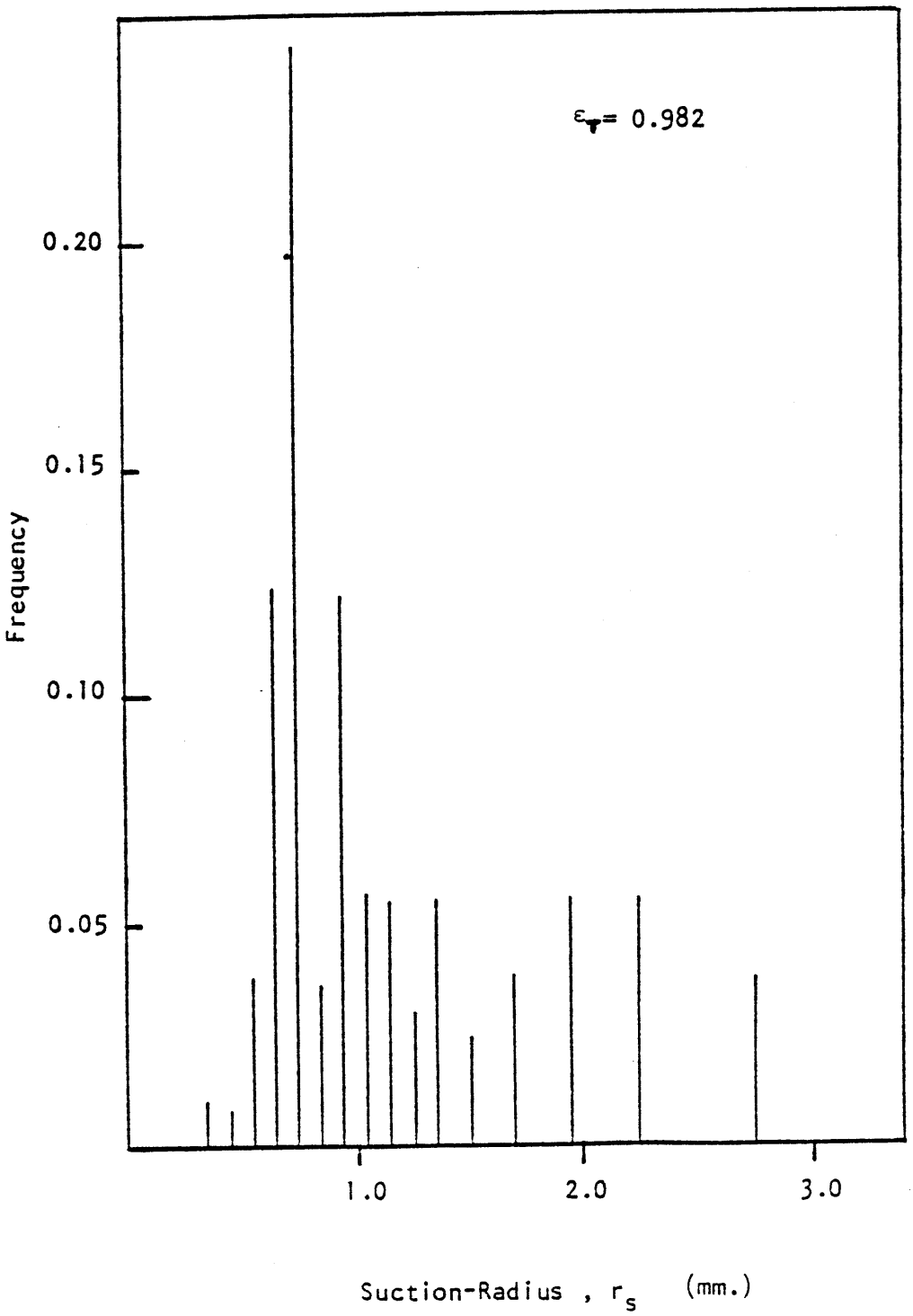

Fig. 6.8 Suction-Radius Distribution

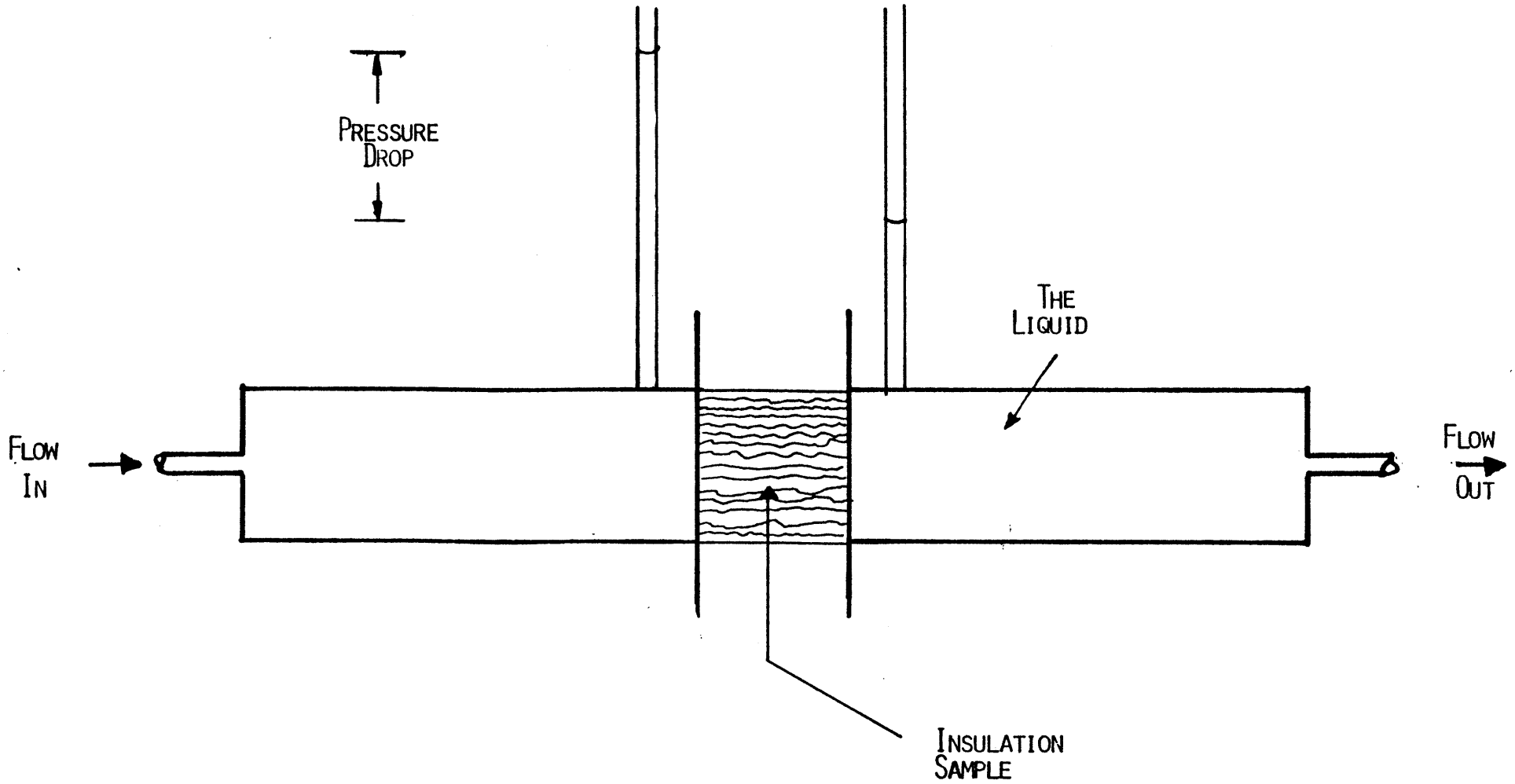

Fig. 6.9 Schematic of the Apparatus Used for Measurement of Pressure-drop/Flow-rate Relation

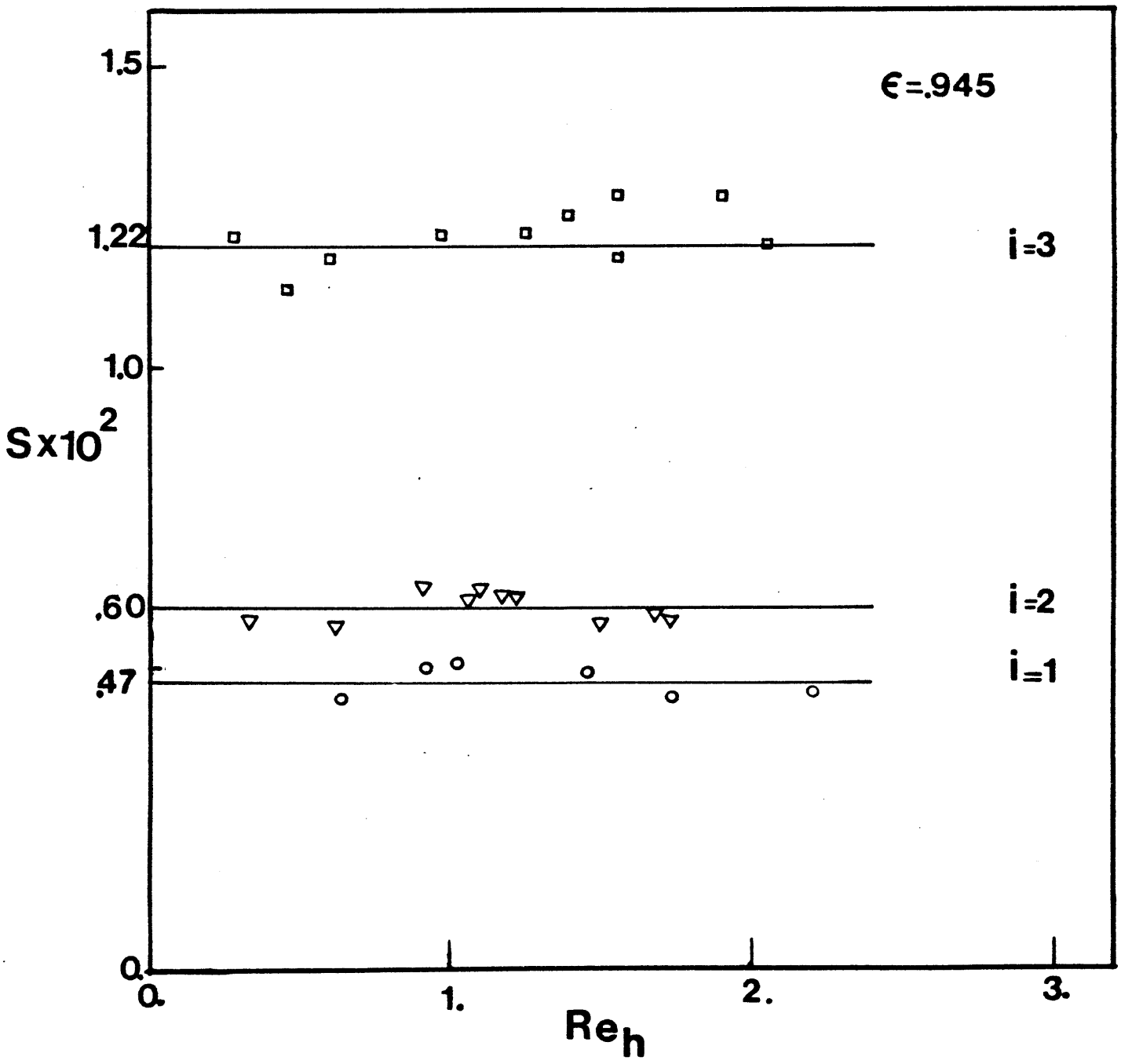

Fig. 6.10 Experimental Values of S versus Reynolds Number

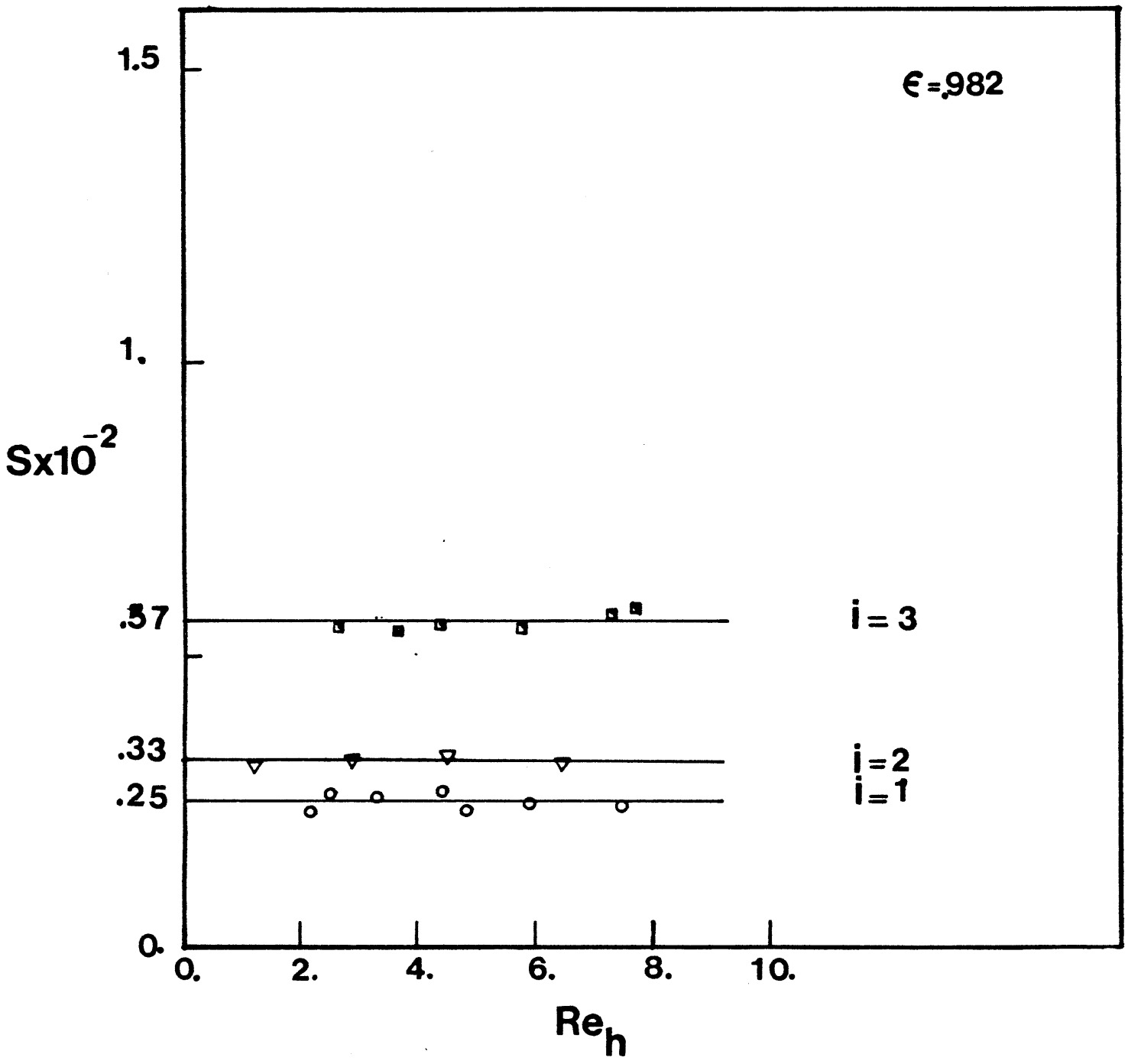

Fig. 6.11 Experimental Values of S versus the Reynolds Number

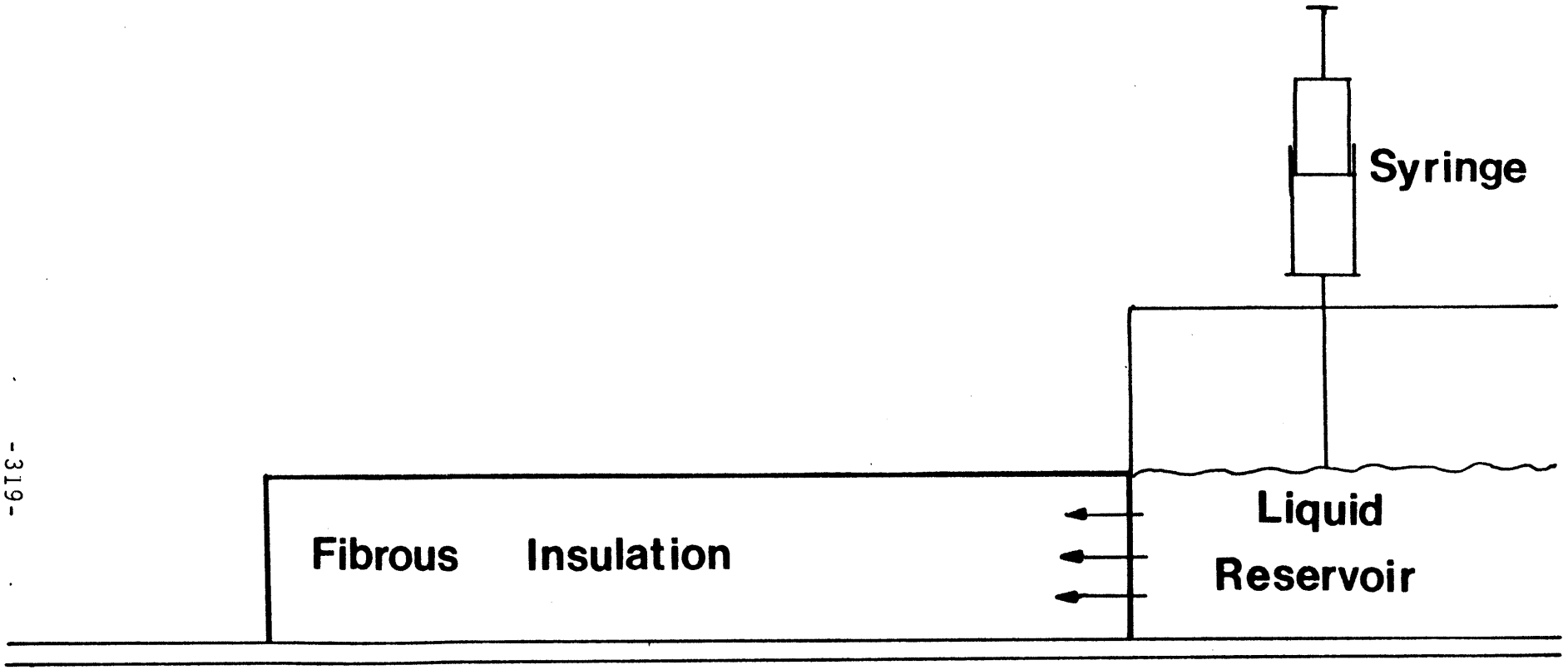

Fig. 6.12 Schematic of the Apparatus Used for the Measurement of Liquid-Diffusion

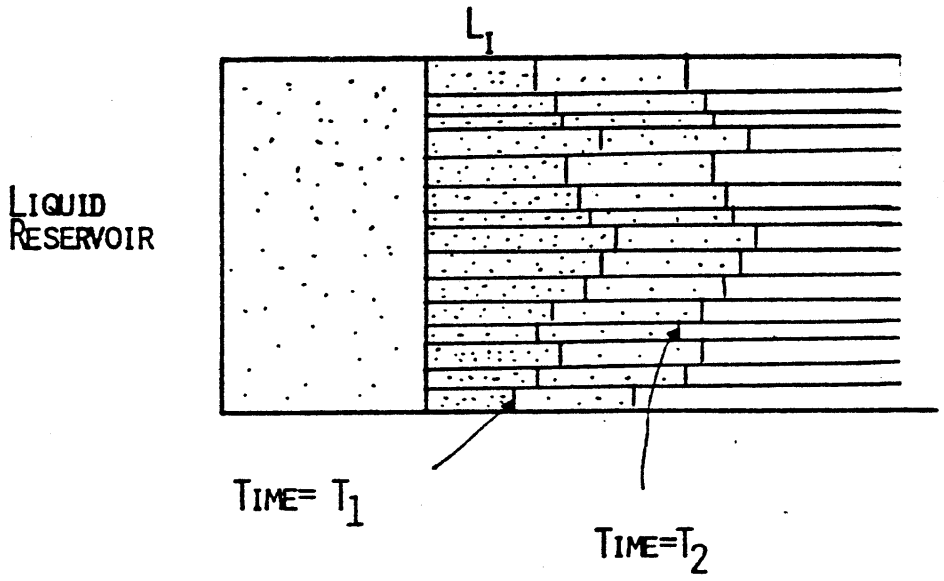

Fig. 6.13 Schematic of the Observed Pattern of Liquid-Diffusion Along the Layers of the Fibrous Insulation

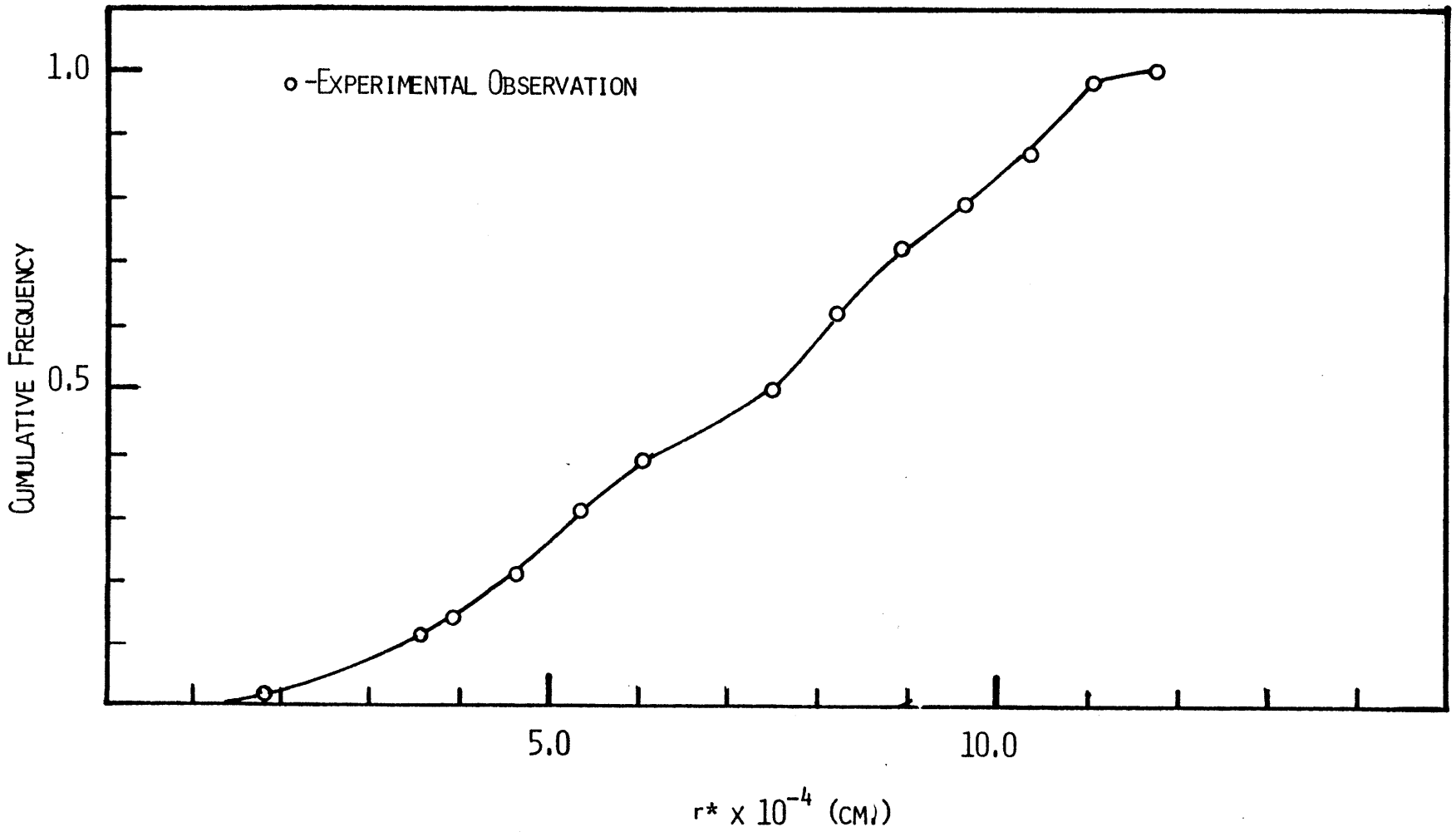

Fig. 6.14 Observed Cumulative Frequency Distribution of Diffusion-Radius in the fiberglass insulation with a void-fraction value of 0.945

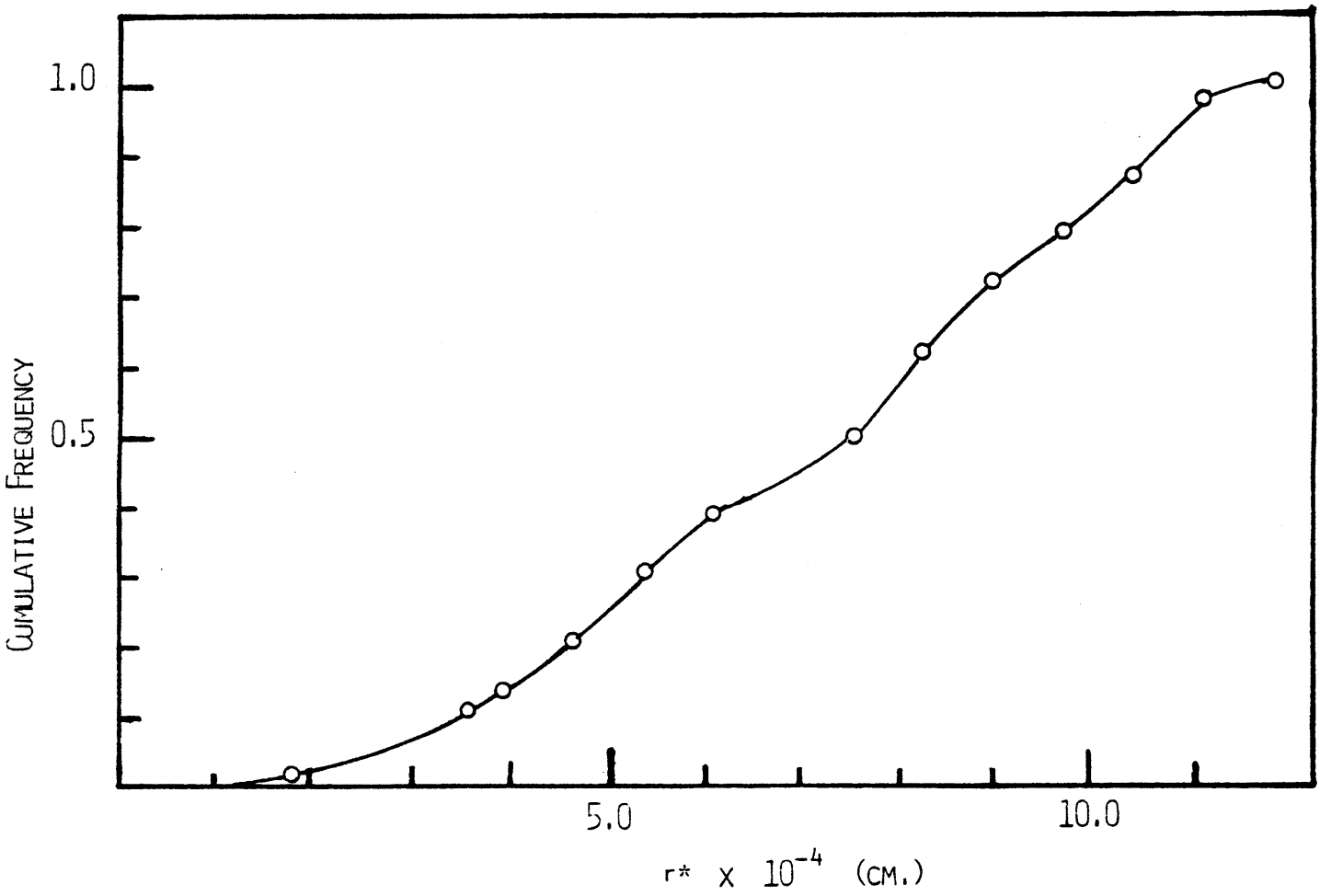

Fig. 6.15 Observed Cumulative Frequency Distribution of the Diffusion-Radius in the Fiberglass Insulation with a void-fraction value of 0.982

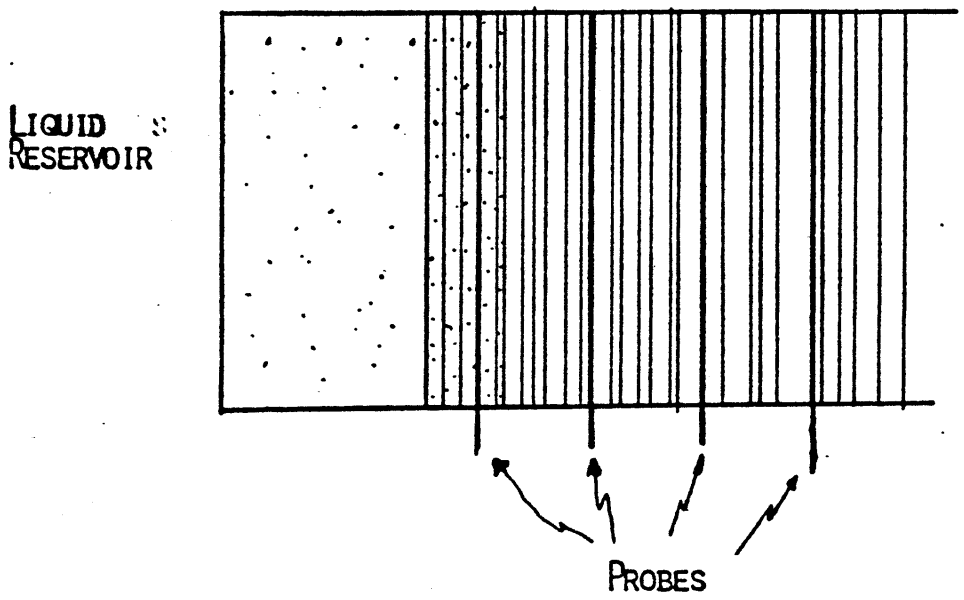

Fig. 6.16 Schematic of the Diffusion Pattern and Measurement Technic for Liquid-Diffusion Through the Layers of a Fiberglass Insulation

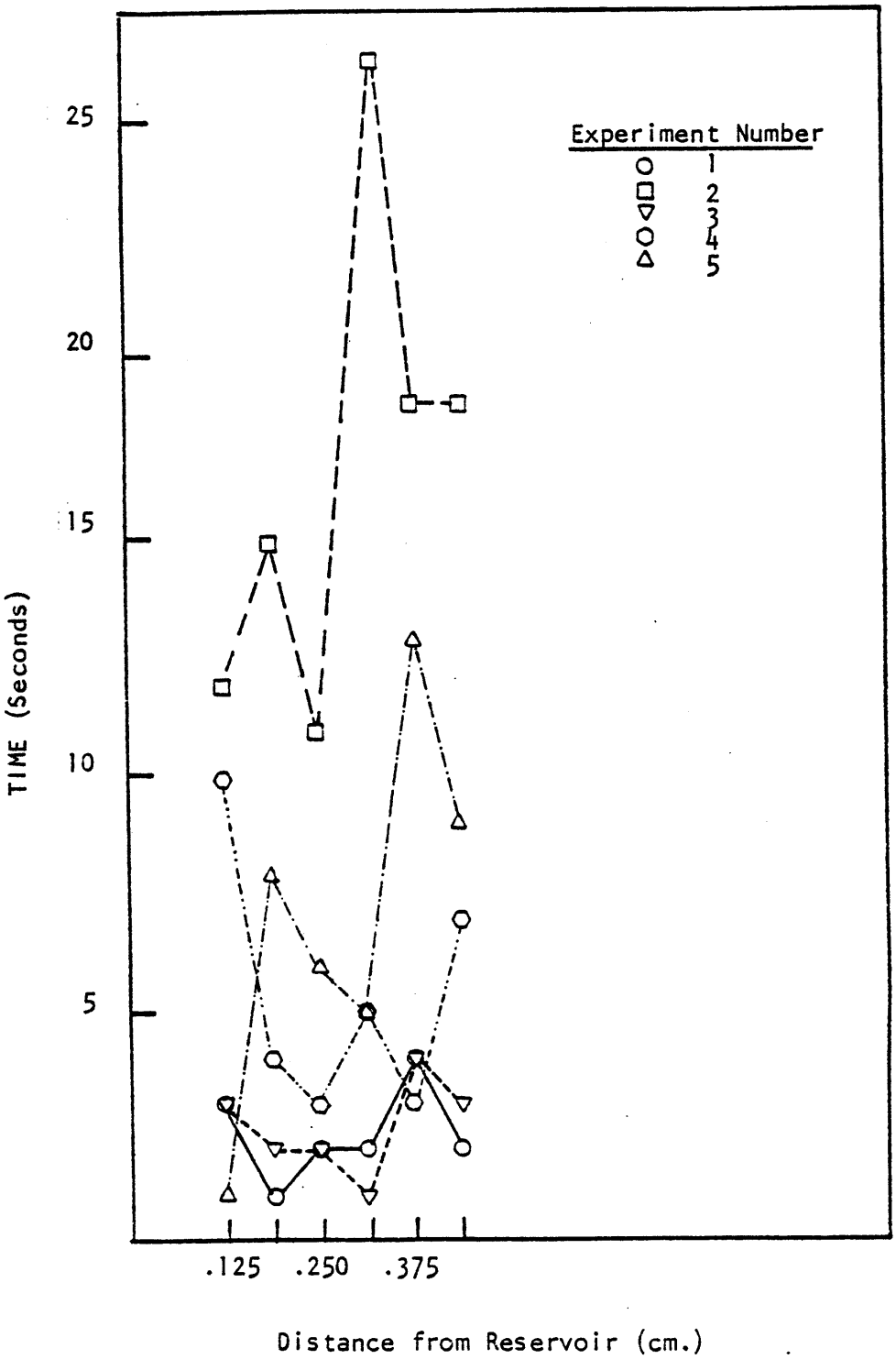

Fig. 6.17 Travel-Time between Succeeding Probes

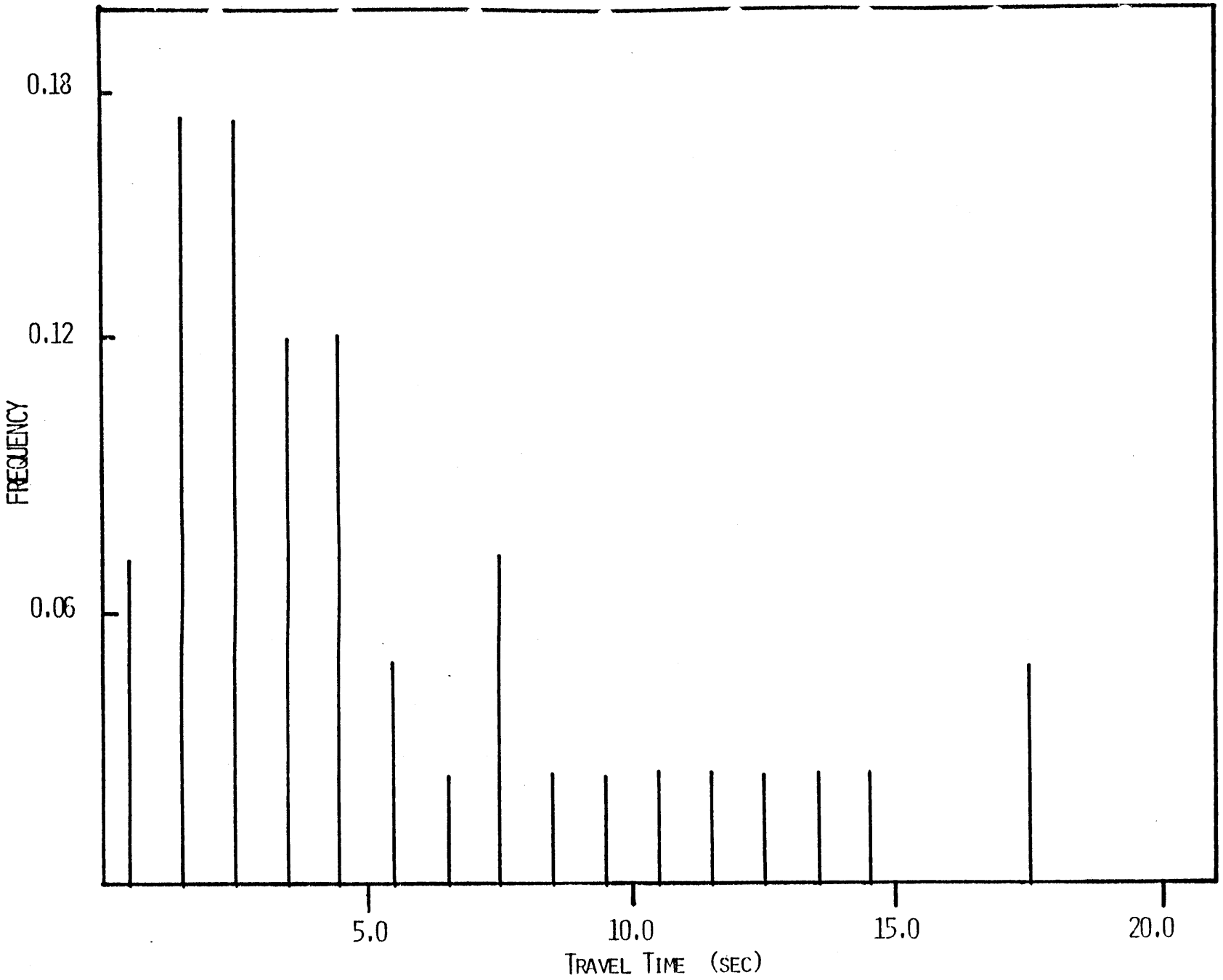

Fig. 6.18 The Frequency-Distribution of Travel Time for the Diffusing Front in Liquid-Diffusion Through the Layers.

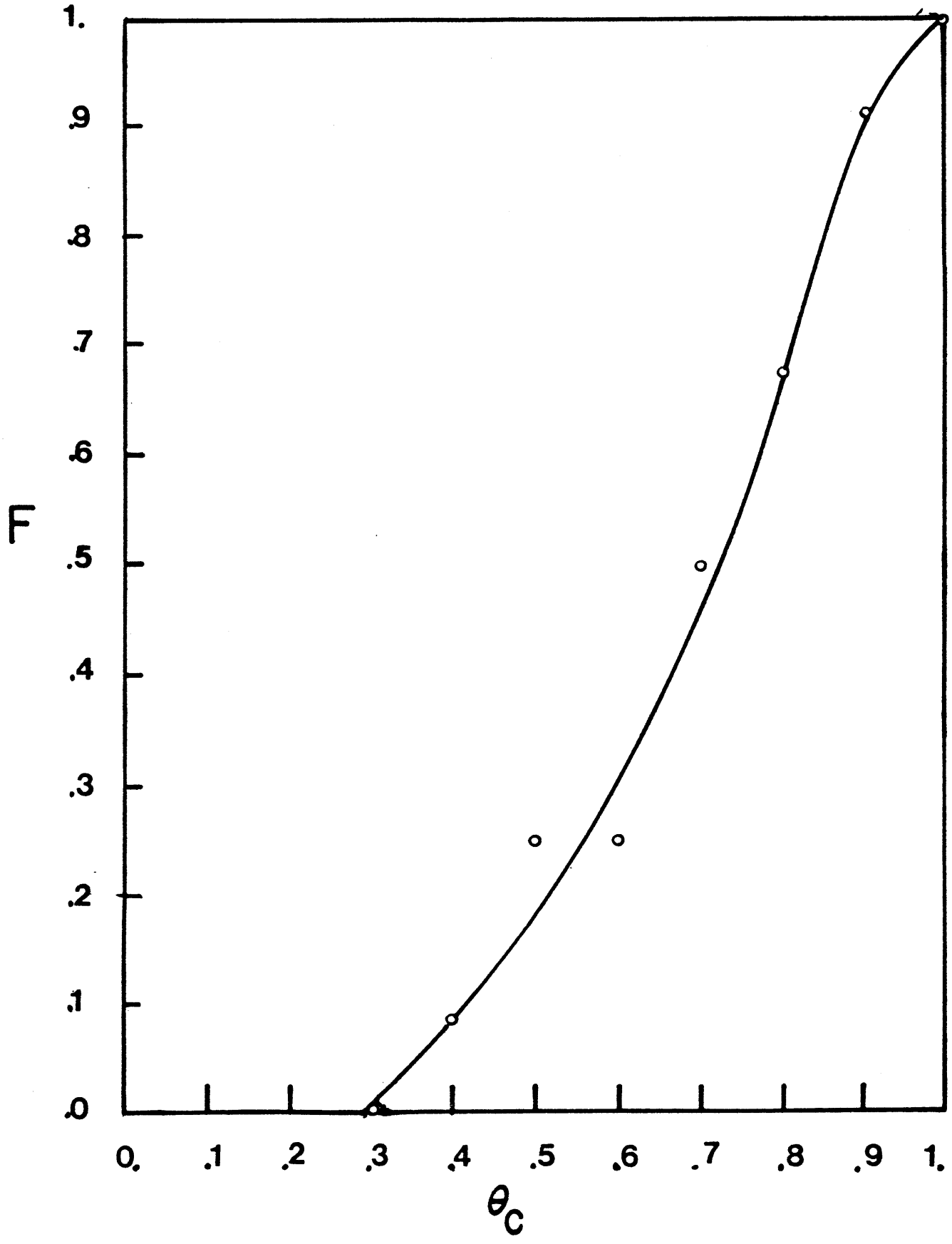

Fig. 6.19 Observed Cumulative Frequency-Distribution of the Critical Liquid-Content.

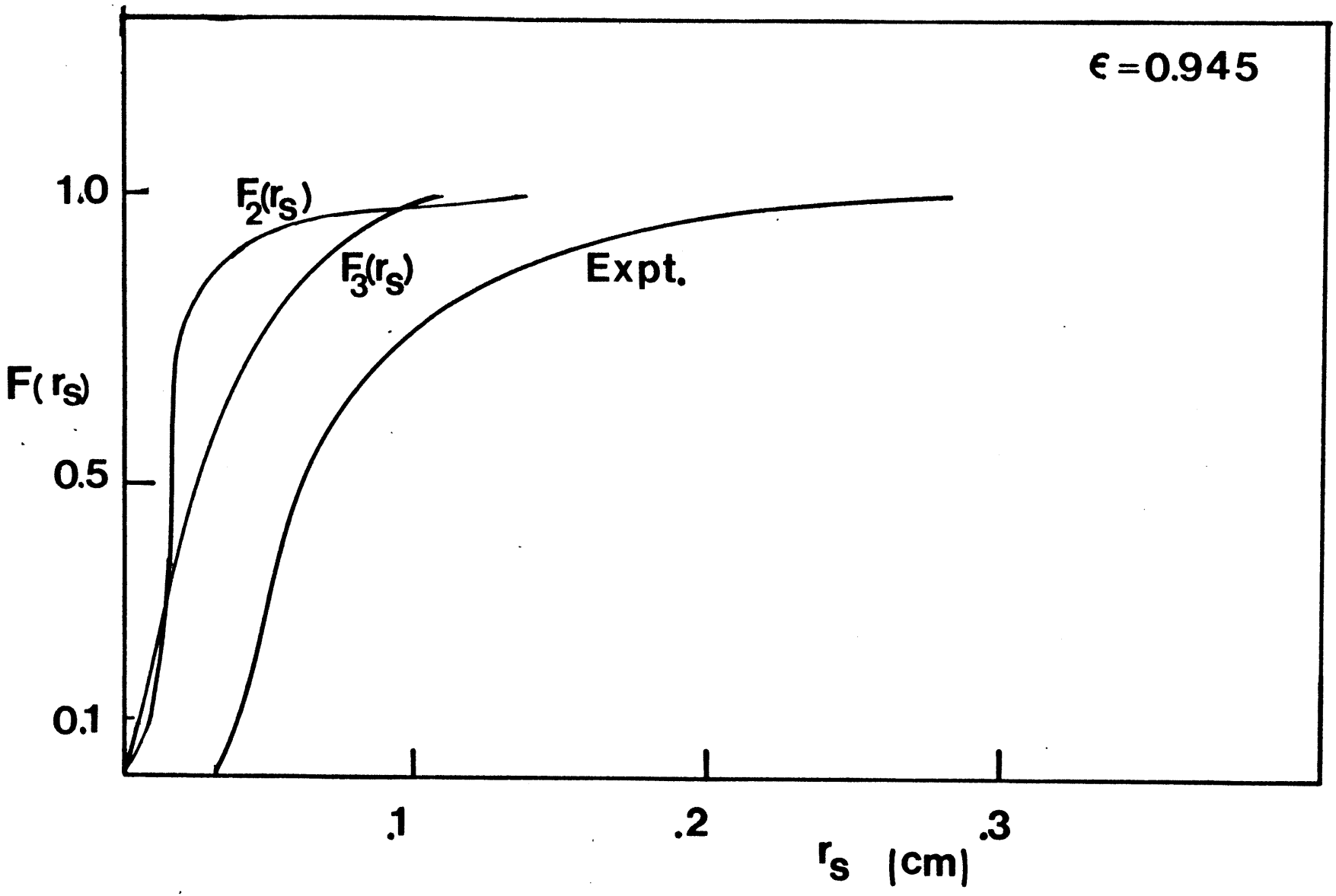

Fig. 6.20 Comparison of the Experimental Observation with the Model-Predictions for the Cumulative Frequency-Distribution of the Suction-Radius for the Fibrous Insulation with a Void-Fraction Value of 0.945

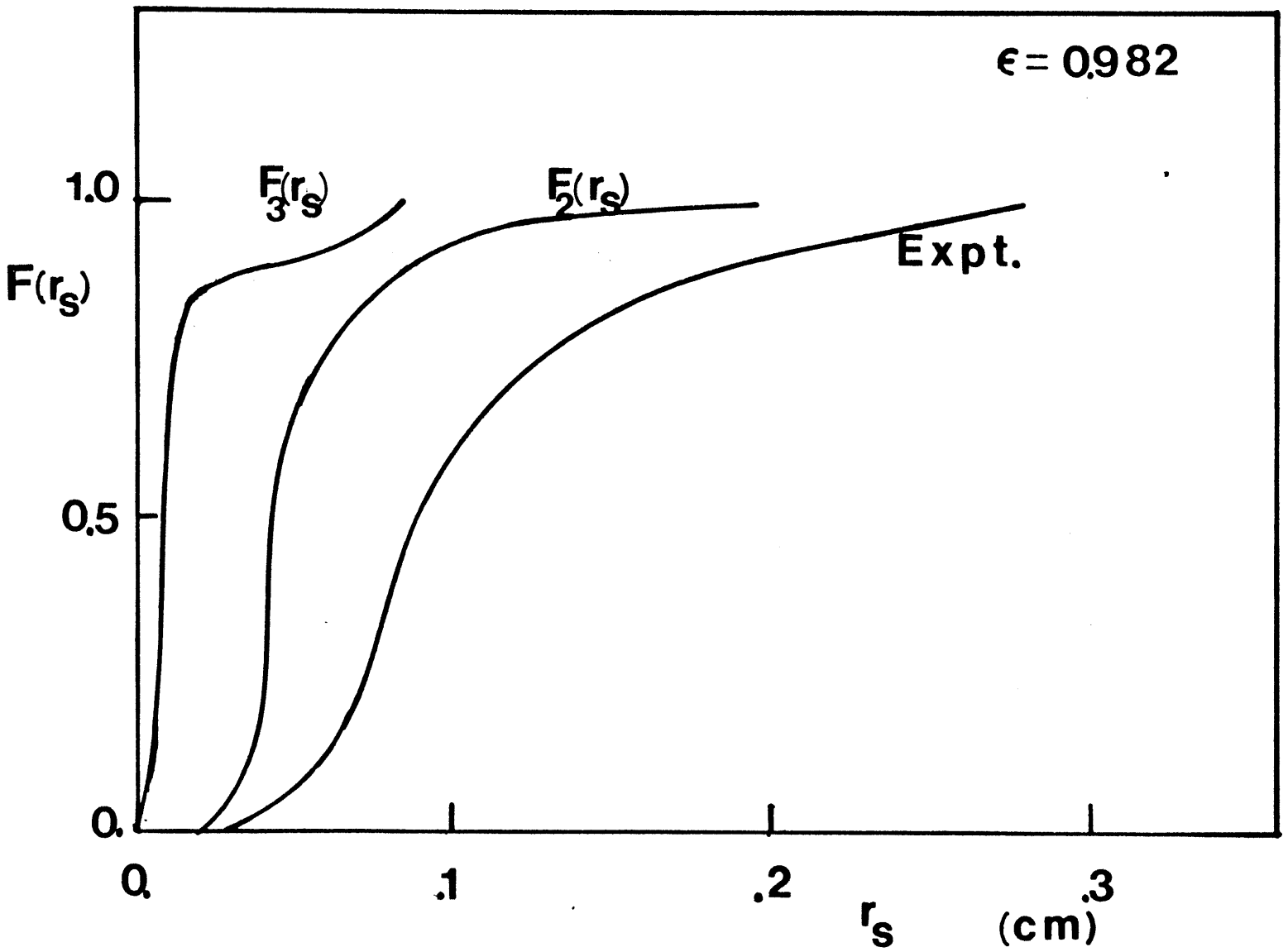

Fig. 6.2 1 Comparison of the Experimentally Observed with the Model-Predictions of Cumulative Frequency Distribution of suction-radius in the Fiberglass Insulation with a void-fraction value of 0.982

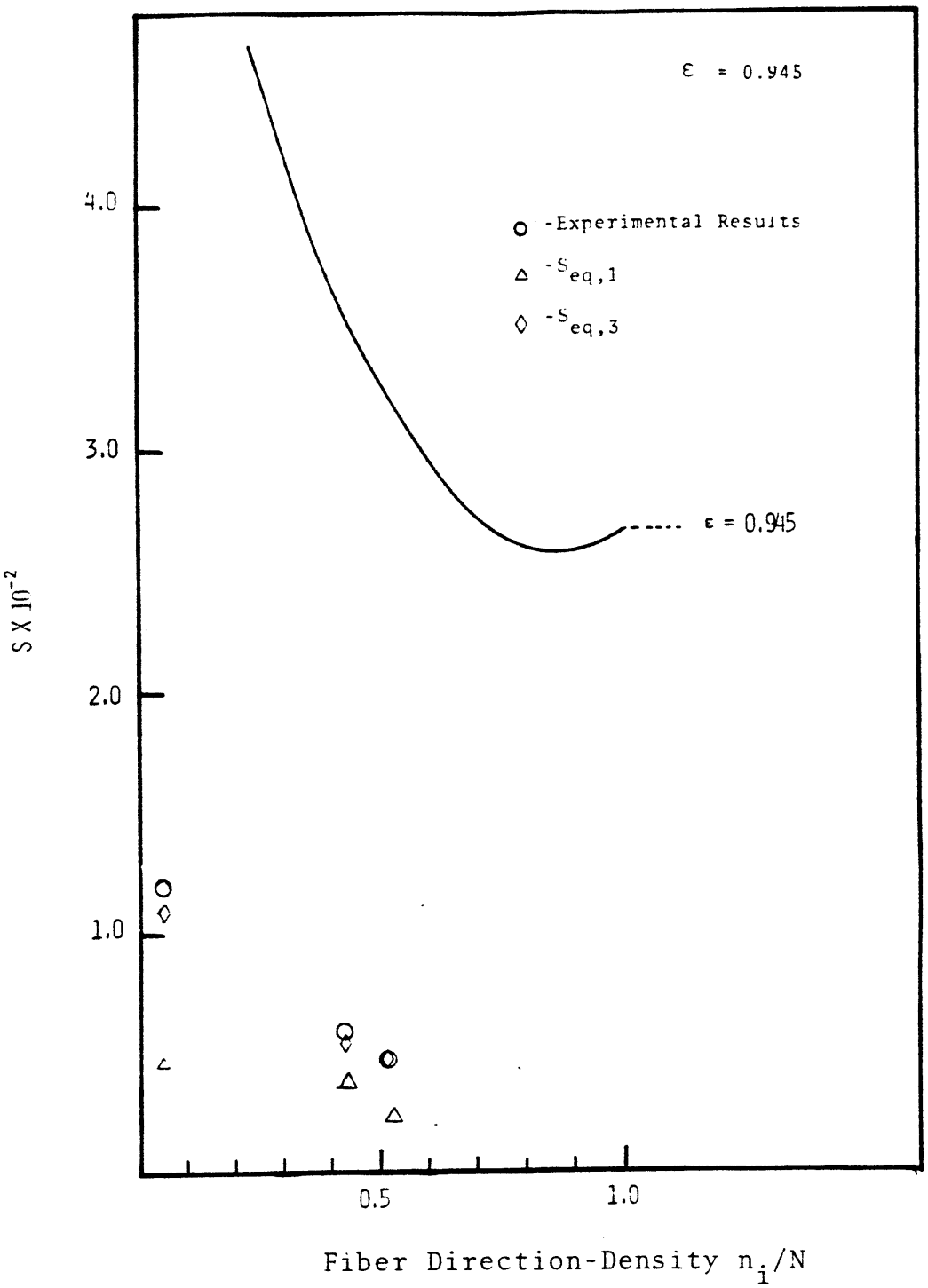

Fig. 6.22 Comparison of the Experimental Observations with the Model Predictions of the S term

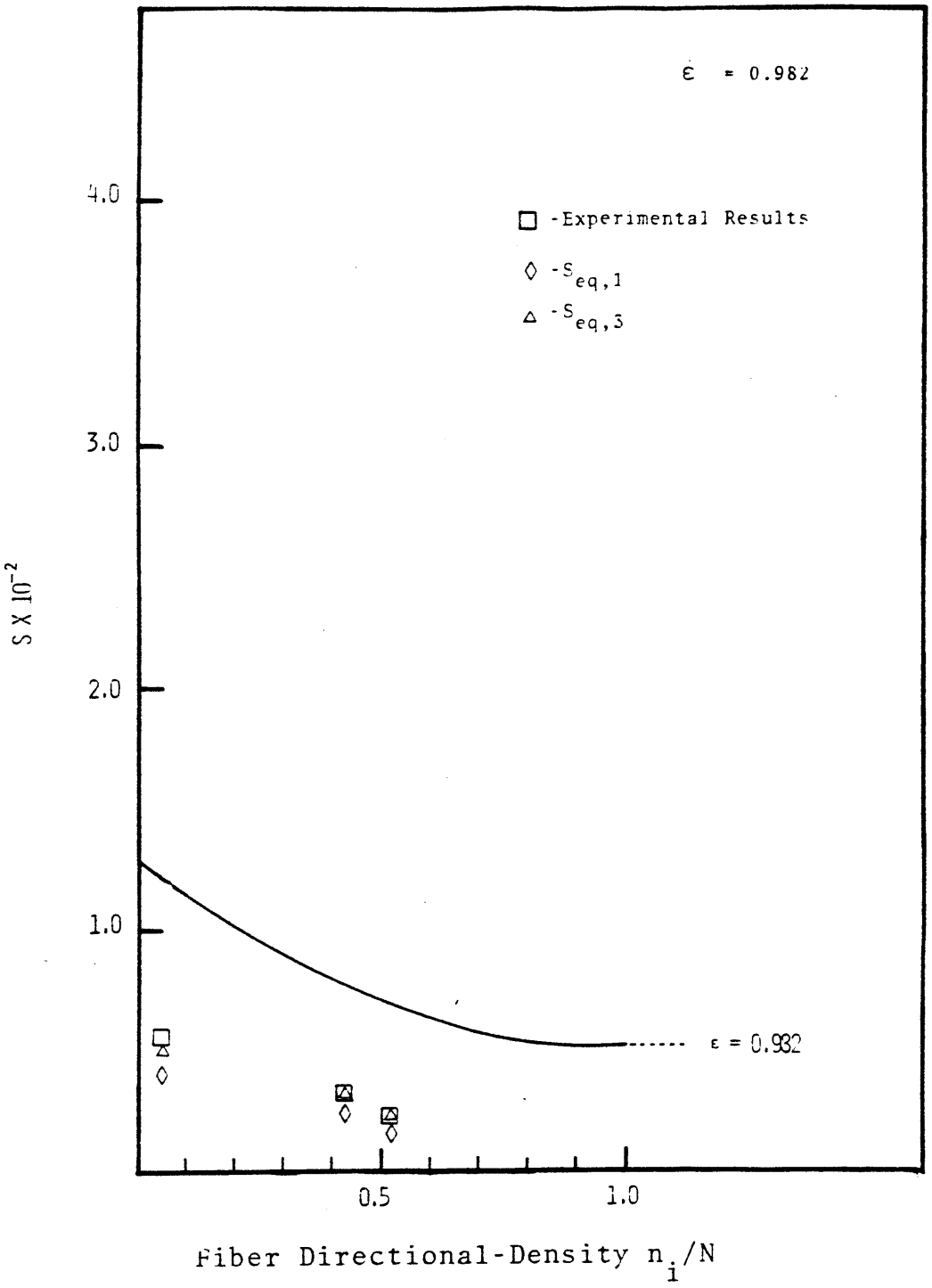

Fig. 6.23 Comparison of the Experimental Observations with the Model Predictions of the S term

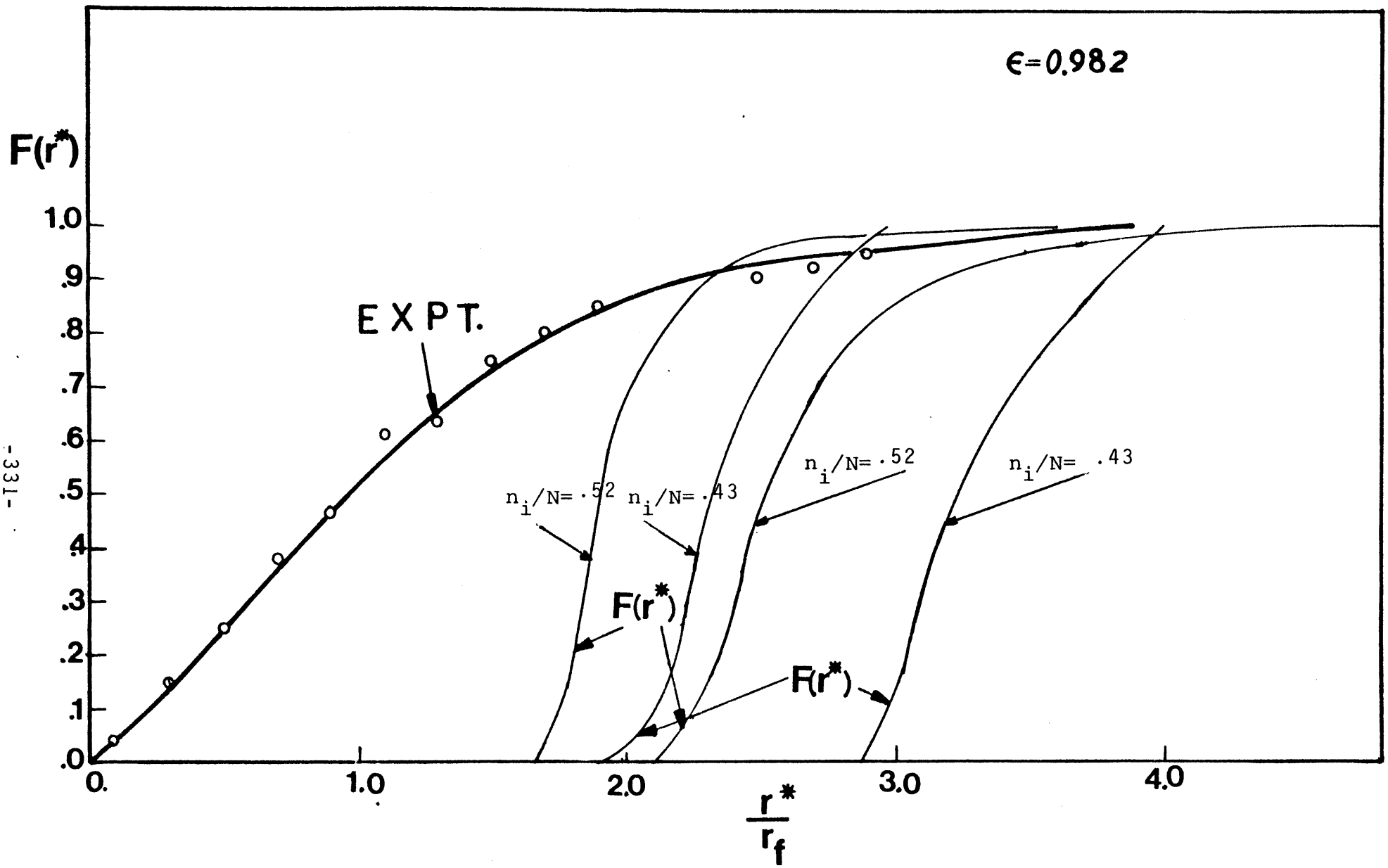

Fig. 6.25 Comparison of The Experimental Observation with the Model Predictions for the Cumulative Frequency-Distribution of Diffusion-Radius in the Fibrous Insulation with a void-fraction value of 0.982

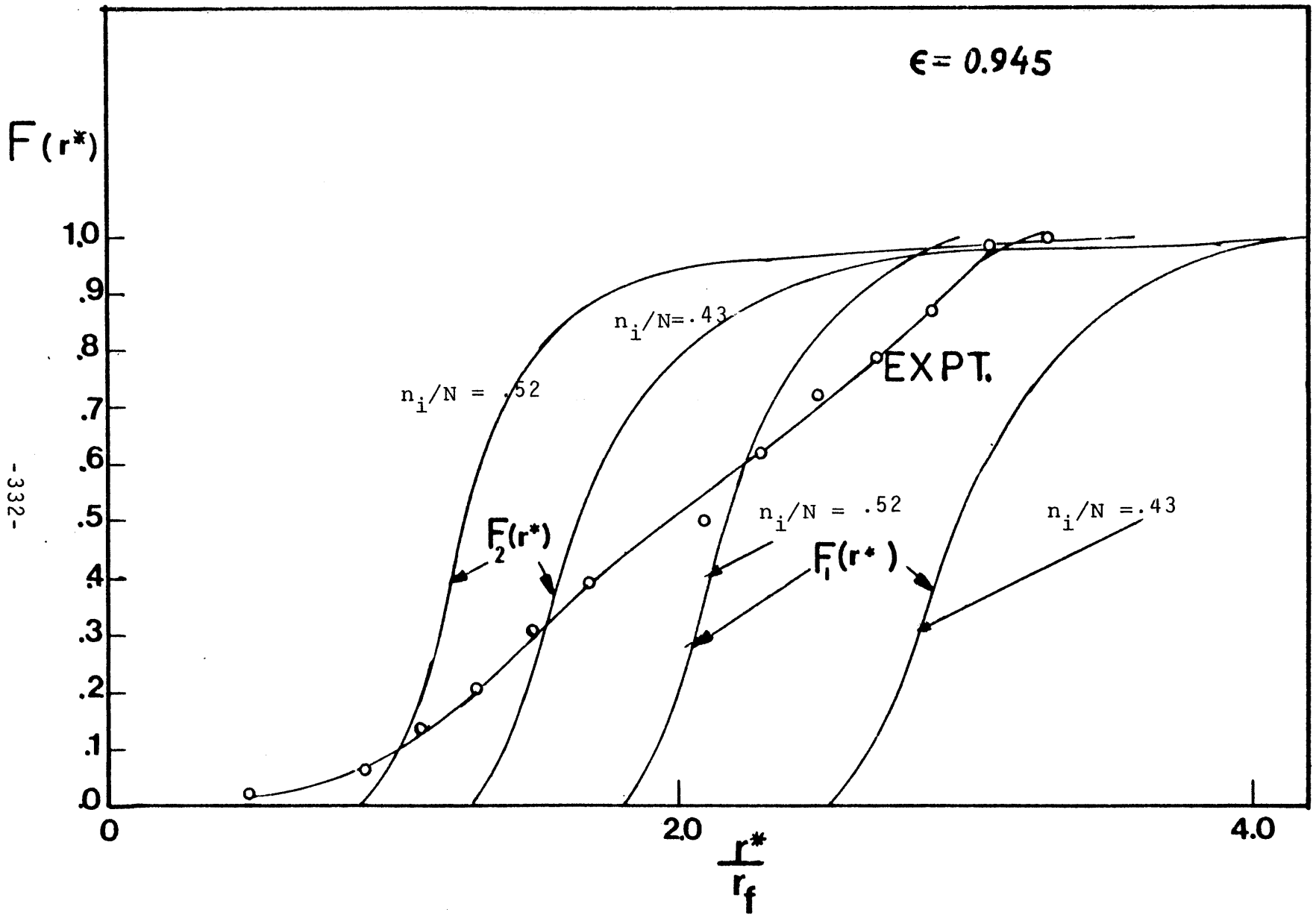

Fig. 6.2 4 Comparison of The Experimental Observation with the Model-Predictions for the Cumulative Frequency-Distribution of Diffusion-Radius in the Fibrous Insulation with a void-fraction value of 0.945

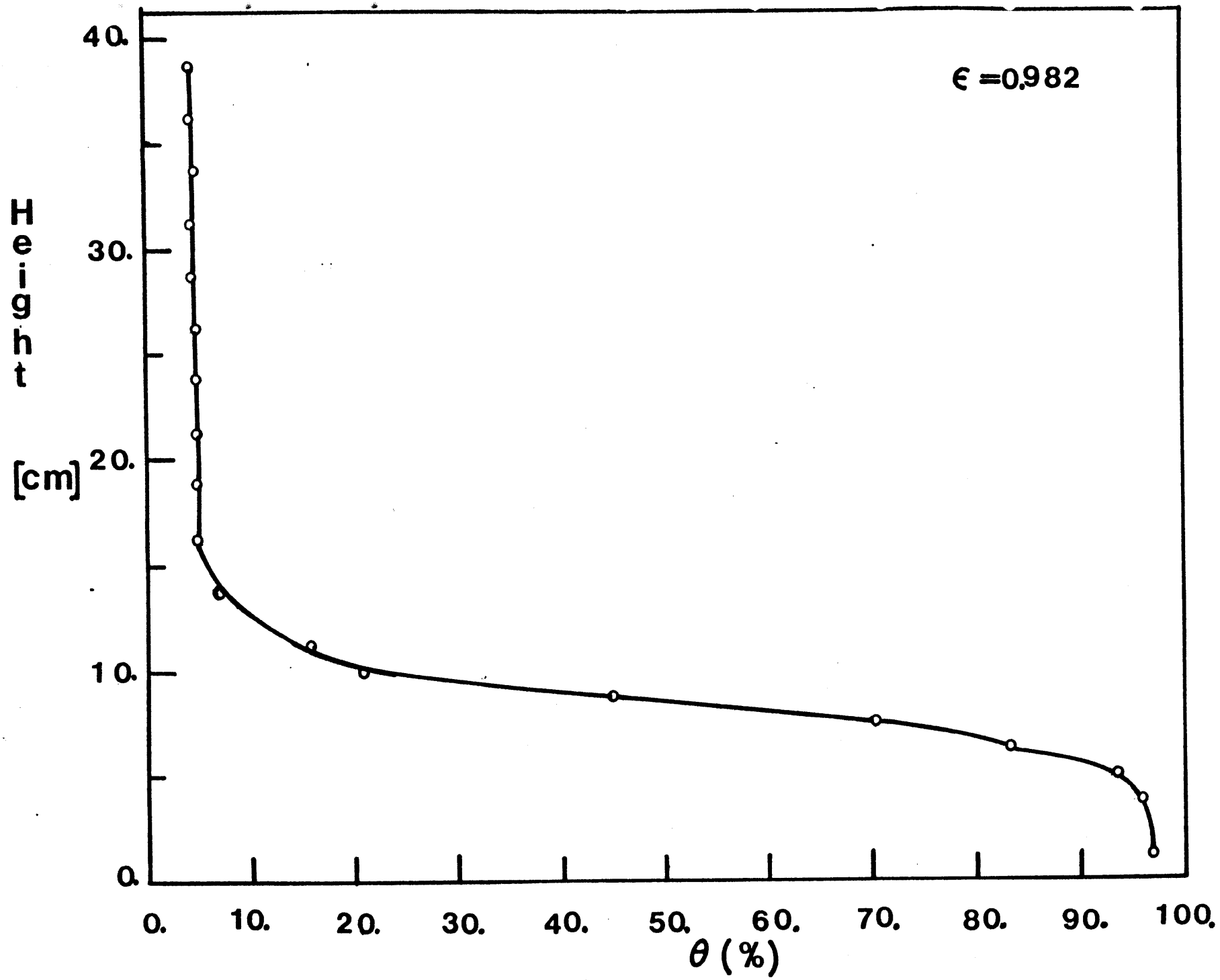

Fig. 6.27 Liquid-Content versus Height Profile Observed in the Drainage Experiment

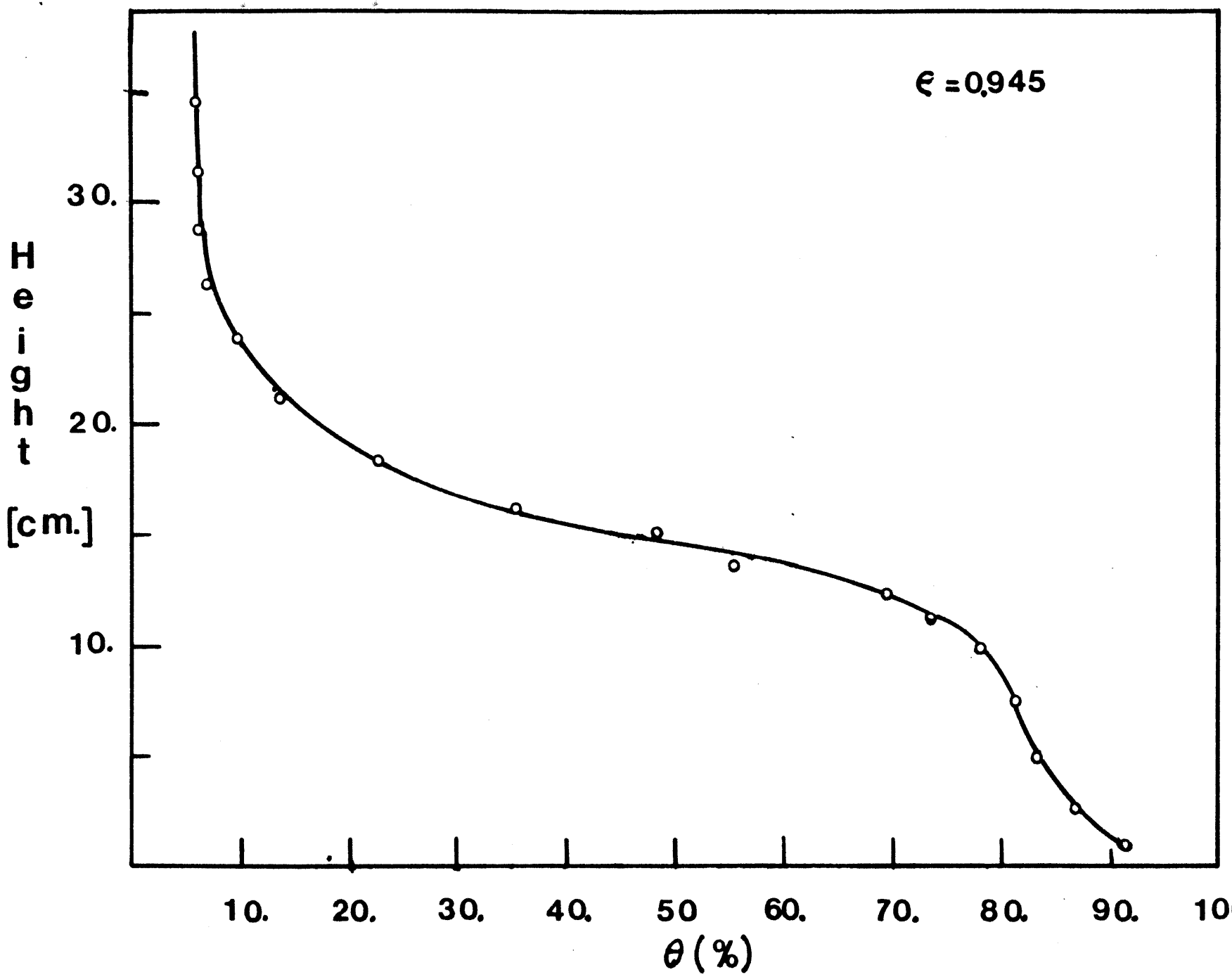

Fig. 6.26 Experimentally Observed Liquid-Content versus Heigth distribution in the Drainage Experiment

CHAPTER 7

CONSIDERATIONS ON THE DESIGN OF INSULATED WALL STRUCTURES

7.1 GENERAL CONSIDERATIONS ON MATERIALS USED IN BUILDING STRUCTURES

In the previous chapters the phenomenon of heat and mass transfer with phase change in composite walls has been exhaustively studied. The analytical results, as well as the experimental results indicate that the behavior of composite walls depends on both the climatic conditions and the properties of the materials used in the construction of the insulated building shells. In this section, the thermal and diffusive properties of the building materials as they relate to heat and

mass transfer across the building shell are discussed. In the next section, two case studies are presented.

In most modern constructions the building structures are insulated. Although closed-pore insulations are receiving increasing attention, in the majority of cases the insulation used is the open-pore fiberglass insulation. The thermal property of the fiberglass insulation bas been the topic of many investigations. The fiberglass insulation has large void-fraction values, e.g. 98%. Therefore, the thermal-conductivity and vapor-diffusivity of the material are closely approximated by those of still-air. The experimental results of this investigation shed light on the mechanisms of liquid-diffusion in fibrous insulation. Liquid-diffusion is a strong function of the orientation of the medium with respect to gravity. It has been found that liquid diffusion from one layer to the next occurs only when liquid-content in a layer reaches a critical-value. This value is found to be approximately 60-70%. However, with the fiberglass layers aligned parallel to the gravity, the suction-sites in the medium cannot hold liquid-contents in excess of 5-10%. In wall constructions, the insulation is placed in such a manner that the layers are parallel to the gravity. Therefore, in wall constructions, liquid does not diffuse from one layer to the other, for the condensate drips to the bottom of the wall before the critical-value of liquid-content necessary for diffusion is reached. On the otherhand, in the roofs, the insulation batt is rolled over the roof and the layers are perpendicular to gravity. In this situation the insulation can sustain liquid-contents of up to 70-80% against gravity. As this value is larger than the critical liquid-content, it is possible to envisage situations where the condensate in the insulation flows towards the dry-regions. The analysis of chapters 2 and 3 for mobile condesates apply to roofs, whereas the analysis for immobile condesates applies to building walls.

In a typical construction, the insulation is sandwiched by various siding layers. The fiberglass insulation has the smallest thermal-conductivity amongst all other materials. As the thickness of the insulation is larger than any other layer in the wall, the major thermal-resistance in a wall is associated with the insulation. The vapor-diffusivity of many building materials is to some extent known. Vapor-diffuses in still-air faster than in any other building material. This implies that the vapor-diffusivity of the insulation is the smallest in a typical wall structure. However, the insulation's width may be one of the largest in the wall. Hence, as it will be shown later, the diffusive resistance of the insulation may be of the same order of magnitude, perhaps even one of the smaller values, in a typical structure. Therefore, the vapor-flux into the structure is strongly controlled by the property of sidings used in the wall-construction.

In sum the thermal and diffusive properties of the wall layers determine the heat and vapor-flux rates through the structure. Condensation-rate, and condensate accumulation in the strucutre depend on, amongst others, on liquid-diffusion in the insulation. In the next section, heat and mass transfer with phase change in a typical wall strucuture for two extreme climatic conditions will be studied.

7.2 CASE STUDIES

In this section the thermal and diffusive properties of a typical wall structure will be studied. Also, vapor condensation in the structure for two climatic conditions will be studied. Of the two cases one corresponds to condensation during the cold-season, and the other during a humid warm-season. The condensation rate, the subsequent evaporation of the condensate for each case and the implications of placing a vapor-barrier will be discussed.

The purpose of the study of thermal and diffusive properties of materials used in a typical wall construction is to investigate the range of effects that the choice of materials has on condensation in insulated structures. A typical wall construction consists of many layers. However, a very basic design is studied in this section. Starting from the outside, the wall consists of the following layers [86]:

1- wood-siding, 0.5 in.x8 in., lapped
2- Sheathing, 0.5 in., vegetable fiber board
3- Fiberglass Insulation
4- Gypsium wallboard, 0.5 in.

The thickness of the insulation is arbitrarily chosen to be 1-ft. The results obtained in this section are not very sensitive to the choice of the insulation's thickness. It is needless to mention that an actual wall structure may be painted or

wall-paperd on the inside. The thermal resistance of these additions are minimal, yet they may offer large resistances to vapor-flux. The air flow patterns on the two sides of the wall structure also effect the flow of heat and vapor through the wall. The value of heat transfer coefficient on the outside is based on a 15mph wind, and that of the inside is based on natural convection [86]. The mass transfer coefficients are calculated using the Colburn analogy, eq. [4.2.8]. The thermal and diffusive conductivities, thickness, and corresponding resistance of each layer are given in Table 7.1. The material properties are assembled from a variety of sources[87,88].

The values of thermal resistances in Table 7.1 indicate that the only significant thermal resistance is provided by the insulation. Hence, it is possible to neglect the presence of all other layers on the heat-flux through the wall. The values of temperature at the boundaries of the insulation are approximately equal to those of the ambient. In the wall structure under study, the thickness of the insulation is taken to be 1-ft. With lower values of insulation-thickness, the error assocaited with the above approximation increases.

On the other hand, the ratio of diffusive resistance of the insulation to the total difffusive resistance is comparable to that of other layers. It may be noted that the wood-siding provides the largest diffusive resistance. This implies that the wall is more vulnerable to vapor-flux from inside the building than from the outside.

The proper location of vapor-barriers was discussed in detail in chapter 4. It was shown there, that vapor-barriers inhibit the flow of vapor into the insulation only during one season. With a a change of season, the vapor-flux changes direction and enters the insulation from the permeable side. A vapor-barrier located on the inner-side of the insulation inhibits vapor-flow and subsequent condensation during the

cold-season, when the interior vapor-concentration is higher than the outside. During the warm-season, if the building is air-conditioned, the temperature of the vapor-barrier is less than the outside temperature. Even without air-conditioning, it is reasonable to assume that the outside-temperature will be higher, perhaps slightly, from inside. With the vapor-barrier's temperature less than the outside temperature, the saturation-concentration corresponding to the vapor-barrier temperature is likely to be less than the outside vapor-concentration. Therefore, a vapor-flux into the insulation is established. Depending, on the specific conditions, condensation may occur in the insulation (for more detail see chapter 4). Condensation during the summer season is investigated in case study 2.

With the vapor-barrier located on the outer-side of the insulation, condensation may occur during the cold-season, and the condensate evaporates into the building during the warm-season. This is the topic of case study I.

The intention of the case studies is to study worst case scenarioes. As indicated in the above vapor-barriers cannot inhibit condensation year-around. We are interested in studying the extent of condensation that occurs during the period other than the one for which the location of the vapor-barrier has been chosen. Steady-state condensation profiles are calculated through a computer program called ADAM. The drying results are obtained using a program called FRANCE. The programs and their associated subroutines, plus the input data files are given in Appendix 7.1.

CASE I:

Consider a wall construction as shown in Fig. 7.1. This is identical to the wall construction discussed before, except that the outer-side of the insulation is covered by a vapor-barrier. The vapor-barrier inhibits moisture migration and condensation during the summer. However, condensation may occur during the cold-season when the vapor-concentration inside is larger than the saturation concentration at the vapor-barrier. To take an extreme view, the outside temperature is taken to be -20°F. It is assumed that the inside is held at 70°F, and 60% relative humidity. The solution scheme for locating the condensation-region has been discussed in chapter 4. The scheme is to find initial estimates of the temperature and vapor-concentration distributions in the wall structure by ignoring condensation. The resulting values of temperature and concentration at the boundary of the insulation are then used to find the condensation-region by the methods of chapter 2. The difference in the thermal properties of solid and liquid condensate is ignored, as the difference has been shown to be negligible in section 2.9. The boundary temperatures and location of the condensation-region are used to calculate the new temperature and concentration values at the insulation boundary. The iteration scheme continues until the solution converges to a final value.

The location of the condensation-region and the values of temperature and concentration are shown in Fig. 7.1. It is interesting to note that the total temperature drop occurs effectively across the insulation. The relative humidity at the

inner boundary of the insulation is reduced from 60% to 37%. This is due to the drop in the vapor-concentration across the gypsium wallboard. The liquid-content profile for a condensation period for 4000 hours is shown in Fig. 7.2. The tempraure-profile is also shown in the same figure. It may be noted that due to the low level of relative humidity at the insulation boundary, the latent heat transport coefficient, λ', is not large. It should be noted that condensation also occurs in the outer-side sidings. However, as the value of vapor-diffusivity of the sidings is low, the volume of the condensate may be assumed to be negligible.

The outside temperature at the end of the cold-season is changed to 80°F. This change causes the vapor-flux to change direction and lead to the evaporation of the condensate. It was found, by the methods of chapter 3, that the condensate evaporated during approximately 4000 hours of warm-season. The time-duration for evaporation is relatively large indicating that under slightly more adverse conditions, e.g. higher inside relative humidity, or workmanship imperfections, the condesate may not evaporate completely over an annual cycle.

The wall structure with the vapor-barrier located at the outside of insulation is suitable for warm and humid environments, where summer condensation is to be avoided. However, when placed in a cold environment condensation occurs in the structure. The condensate may not evaporate during the warm-season, primarily because the temperature difference across the wall is not very large. It must be noted that the results obtained here are not very exact, yet they indicate that the resistance to vapor-flow provided by a single layer of gypsium-board is sufficient to decrease the condensation rate. With infiltration present, the volume of the condensate may increases several fold. Addition of such layers as paint or wall paper on the inside may significantly reduce condensation in the insulation through depressing the humidity at the insulation's

boundary.

The above case may be compared with the case where no vapor-barrier is present. Naturally, condensation may occur during the warm-season. However, we are interested on the effects that the removal of the vapor-barrier may have on condensation during the cold-season. The diffusive resistance of the wood-sidings is so very large that condensation occurs both in the insulation and the fiber-board. This implies that the removal of the vapor-barrier has no positive effects on condensation in the structure. Rather, the significaant diffusive resistance of the wood-sidings creates a pseudo vapor-barrier. The extent of the condensation-region for the case without the vapor-barrier is identical to the case with the vapor-barrier, as shown in Fig. 7.1.

CASE II:

In this study the same wall structure as in case I is under study, except that the vapor-barrier is now located on the inner-side of the insulation, Fig. 7.3. The location of the vapor-barrier insures that no condensation occurs during the cold-season. Of interest is the possibility of condensation during the warm-season. Let the outside ambient conditions represent a hot and humid summer, i.e. a temperature of 90°F and a relative humidty of 80%. As before, the inside conditions are kept at 70°F and 60% relative humidity. The temperature and concentration profiles are obtained by the method discussed for the previous case. The temperature, saturation-concentration and

vapor-concentration values at the layers' boundaries are shown in Fig. 7.3. As before, the significant temperature-drop occurs across the insualtion. The large diffusive resistance of the wood-sidings depresses the humidity at the insulation's boundary to 20%. It was shown in chapter 4 that for a given set of boundary conditions, it is possible to get: (a) no condensation, (b) planar-condensation, (c) regional condensation. For the condensation region to extend into the insulation, the vapor-concentration on the hot-side must be larger than a specific value. In this case, this value of relative humidity is 90%, Fig. 7.4. As the value of humidity is depressed to 20%, condensation occurs only at the plane adjacent to the vapor-barrier. The small vapor-concentration gradient translates to a small condensation-rate. The liquid-content after 4000 hours of condensation is about 0.6%. Needless to mention that this amount of condensation probabaly evaporates during the cold-season, when the temprature drop across the wall is large. If there were no vapor-barriers, condensation would not occur in the insulation, as the relative humidty on the hot-side is rather low. But, of course subsantial condensation would occur during the cold season.

The case studies indicate that the temperature drop takes place primarily across the insulation. On the othr hand, the wood-siding is an effective vapor-retarder. The worst case scenarioes discussed in this section indicate that condensation occurs in the strucuture irregradless of the location of the vapor-barrier. The proper location of the barrier depends on the relative magnitude of the condensation rate. The condensate formed in the cold-season in a structure designed to inhibit condensation during summer, may not evaporate during the warm-season. On the other hand, the large value of diffusive resistance of the wood-siding insures minimal condensation during the warm-season in structures designed to inhibit

condensation during the cold-season.

TABLE 7.1

THERMAL AND DIFFUSIVE PROPERTIES OF THE ELEMENTS IN A TYPICAL WALL STRUCTURE [86]

Description	Thickness (inches)	Thermal Conduct -ivity Btu/hr ft^2 F	Permeab -ility ft^2/hr	R hr F/Btu	R* hr	R/R_T %	R^*/R^*_T %
Outside Air	-----	6	365	.167	.027	.26	.04
Wood Siding Sheathing, Vegetable	0.5	1.234	.0024-.0051	.034	4.17	.054	61.5
Board	0.5	2.4	.025-.058	.017	.72	.027	10.61
Insulation	12	.016	.87	62.5	1.15	98.7	16.9
Gypsium Wallboard	0.5	4.4	.025-.058	.009	.718	.014	10.6
Inside Air	---	1.47	89.35	.68	.012	1.07	.175

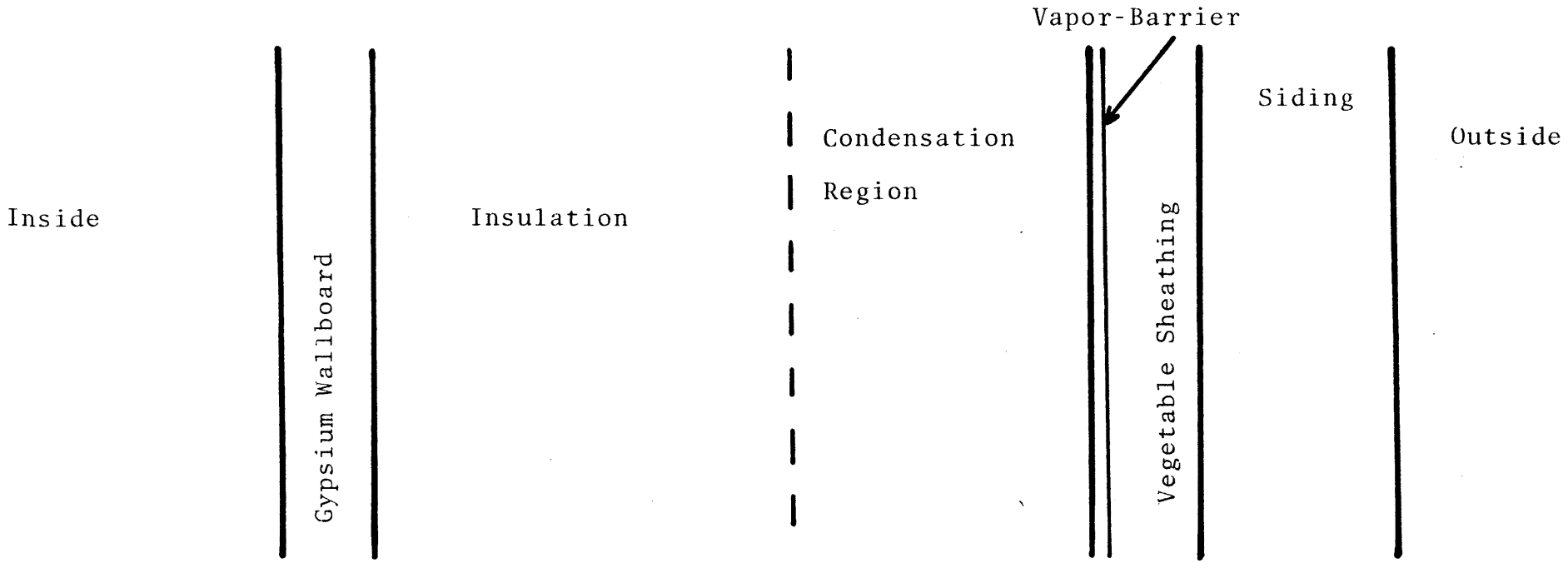

T(°F)	70	69.8	69.1	14.5	-19.8	-20
C*(10^3)	1.15	1.15	1.15	.1425	.0237	.0237
C (10^3)	.69	.69	.415	.1425	.0237	.019
h(%)	60	60	37.1	100	100	80

Fig. 7.1 Wall Construction with the Vapor-Barrier on the outer side

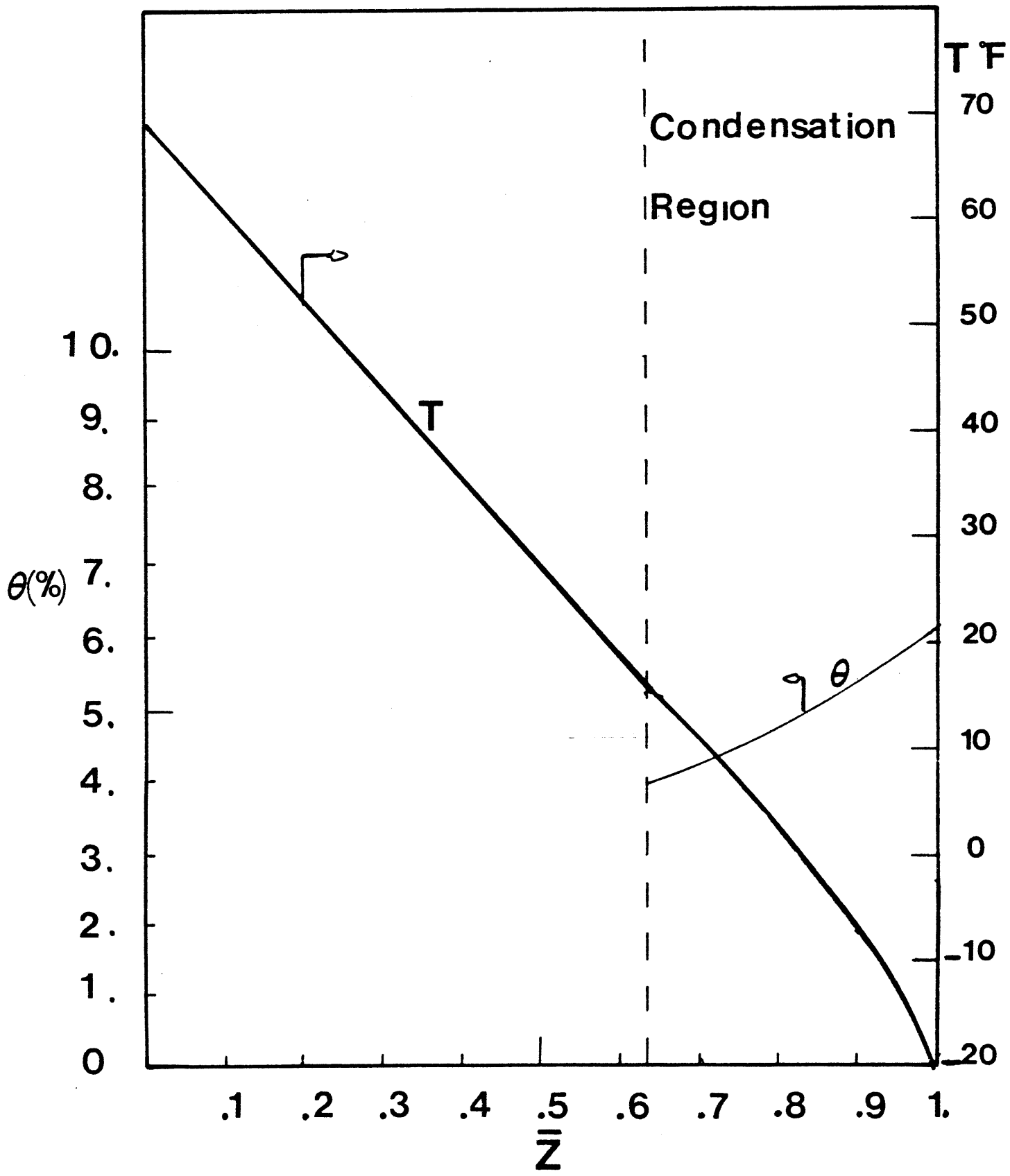

Fig. 7.2 Temperature and Liquid-content Distribution Corresponding to Case I

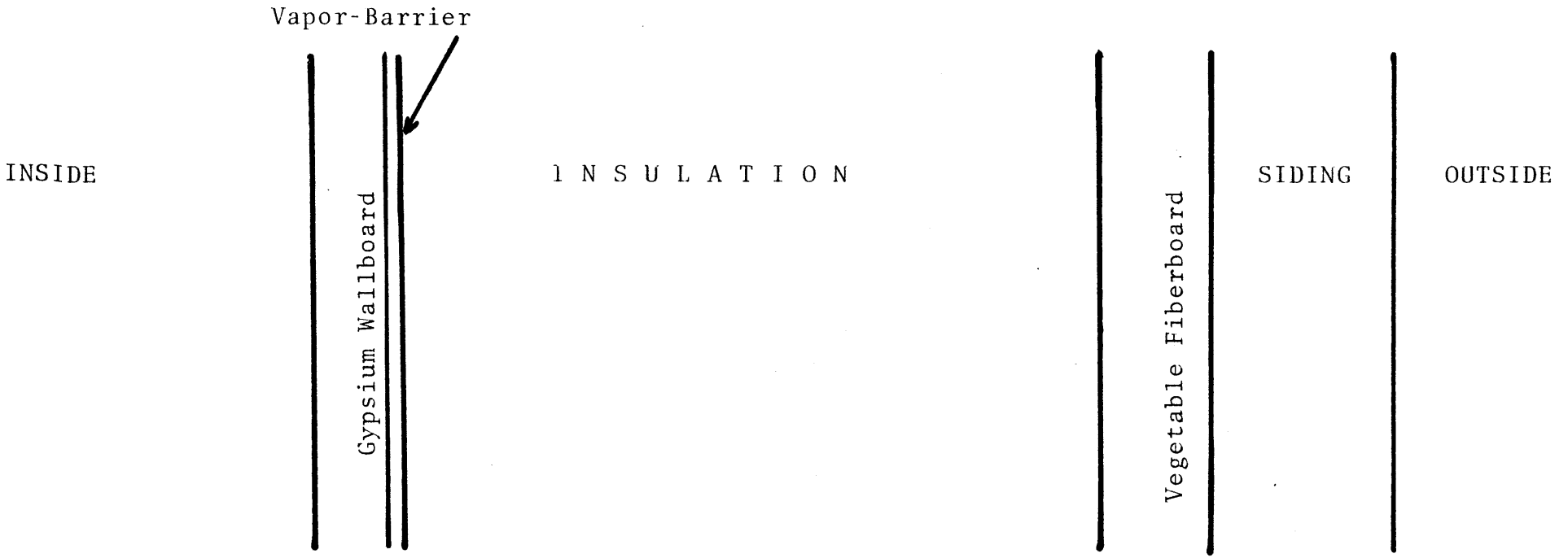

T (°F)	70	70	90	90
C*(10^3)	1.15	1.15	2.138	2.138
C (10^3)	.6912	1.15	.4084	1.71
h (%)	60.	100.	19	80.

Fig. 7.3 Wall Structure With The Vapor-Barrier on the Inner side

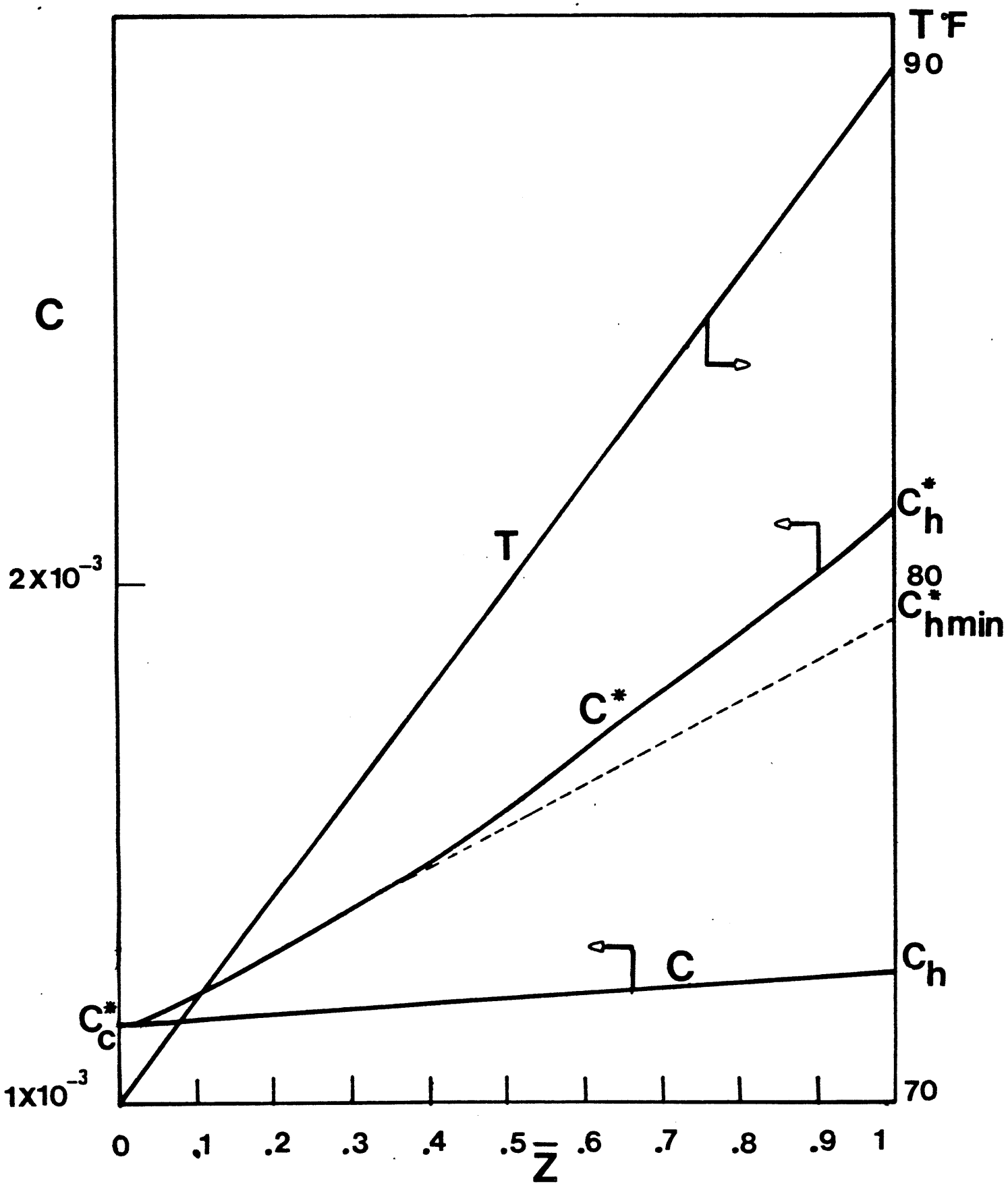

Fig. 7.4 Temperature and Concentration Profiles in the Insulation for Case Study II

CHAPTER 8

CONCLUSIONS

The objective of this study was to investigate the phenomenon of simultaneous transport of heat and mass in an insulated structure. To this end the study was broken up into two tasks. The first task was to develop an analytical model for simultaneous heat and mass transfer with phase change in a porous slab. The second task was to determine the mechanics of liquid-diffusion in fibrous insulation. The results of the two tasks were then combined to study the problem of moisture migration and condensation in insulated building structures.

The analytical model of simultaneous heat and mass transport with phase change in a porous slab was developed for two regimes of liquid-content. At low values of liquid-content the liquid drops are in a pendular state and liquid diffusion is negligible. For values of liquid-content in excess of a critical value the liquid drops coalesce and diffuse towards the drier regions in response to the spatial gradients in liquid-content. During the pendular state, the location of the condensation-region in the porous slab is fixed in space, and liquid-content increases

linearly with time. As the values of liquid-content exceed the critical value, liquid begins to diffuse towards the drier regions. The transition in the diffusive behavior of the condensate causes the boundaries of the condensation-region to move to new locations. After a sufficiently long time-period, the liquid-content profile inside the condensation-region reaches a steady-state distribution, where all of the condensed vapor migrates towards the boundaries of the condensation-region and evaporates into the adjacent dry-regions. It has been discovered that the effect of condensation on the temperature profile in the condensation-region can be represented by a non-dimensional number which is referred to as the latent heat transport coefficient. The location of the condensation-region as well as the condensation rate per unit volume are determined by matching the temperature and concentration profiles of the condensation-region with those of the adjacent dry-regions.

The solution to the case where both solid and liquid condensate are formed in the slab was also developed in this work. However, it has been found that for the instances where the latent heat of condensation and vapor-solidification are not significantly different, the temperature-profile in the condensation-region may be derived by assuming that the only one type of condensate is present. In order for the results obtained for the case where only liquid-condensate is present to be aplicable to this situation, the relevant boundary equations are modified to reflect the immobility of the solid-condensate.

The time-dependant effect of a step change in the values of temperature and/or vapor-concentration at the boundaries of the porous slab were also investigated for both types of diffusive and non-diffusive condensate. A step change in the boundary values leads to a transient motion of the boundaries of the condensation-region. This analysis provides the necessary tools for calculating the time-duration required for the drying of a moist slab.

The effect of placing an impermeable boundary on one side of the condensation-region was found to be two-fold. First, it is found that condensation occurs over a much wider range of boundary values than if there were no impermeable boundaries present. Second, condensation-rate increases significantly with the placement of the impermeable boundary.

The fluid mechanics of flow in an unsaturated fibrous medium was investigated by studying the suction-potential, viscous drag and liquid-diffusion in fibrous insulation. The medium was modelled as an assemblage of layers with each layer consisting of an ordered array of filaments arranged with an unequal number-density in the three orthogonal directions. The parameters that control the fluid-flow are discovered to be the fiber-radius, directionality fiber-density, macroscopic void-fraction, and the spatial distribution of the void-fraction. The experimental results are found to agree with the model-predictions. It was observed that liquid diffusion from one layer to the other is controlled by diffusion along the layers and a factor that represents the tortuous path that the diffusing liquid travels through in going from on layer to the next. Experimental observations indicate that liquid diffusion from one layer to the next take place only when the liquid-content in one layer exceeds a certain value. This value is experimentally estimated to be about 70%. The effect of gravity of liquid-diffusion has been observed to depend on the orientation of the layers with respect to gravity. With the layers parallel to gravity the suction-sites in the fibrous insulation can hold liquid-contents of up to 5-7%. At liquid-contents in excess of this range the liquid drops coalesce and form a continuous column which is driven to the bottom of the layers by the gravitational forces. In commercially available insulations the width of the insulation board is limited to a few inches. With the layers of these types of insulation positioned perpendicularly to gravity, the weight of the liquid columns is not sufficent to overcome the surface tension forces. Therefore,

with gravity perpendicular to the layers, the medium can hold up to 70-80% of liquid by volume.

The phenomenon of condensation in insulated structures is found to be controlled by the climatic conditions, thermal and diffusive properties of the materials used in the wall construction, air infiltration-rates, and the location of the vapor-barrier. The analytical results indicate that condensation rate is largest at the cold-edge of the porous slab. Hence, the placement of a vapor-barrier on the cold-side of a wall leads to large condensation-rates on the vapor-barrier. As most vapor barriers are not capable of absorbing the condensate, the condensed moisture will probably drip to the bottom of a wall structure. The effects of air-infiltration on condesation rate may not be underestimated, for the condensed moisture may consist as much, if not more, of convected vapor as of diffusing vapor. The types of materials used in the shell-construction must be chosen such that the significant resistance to vapor-diffusion takes place in a layer(s) where the temperature drop is not significant. Two worst case scenarios for a typical wall construction with significant insulation were investigated. It is found that the moisture condensed during the cold season in a wall strucutre desgined for the warm climates might not evaporate completely during the warm-season. Over a period of years this may have disastrous implications. On the other hand, moisture condensation during the warm-season in the shell of an air-conditioned building is found to be negligible. These results emphasize the importance of the proper location of vapor-barrier, choice of wall materials, and construction workmanship.

REFERENCES

1. RILEM/CIB Symposium on Moisture Problems in Buildings, Helsinki, August 16-19, 1965

2. RILEM/CIB Symposium on Moisture Problems in Buildings, Rotterdam, 1974

3. "General Report on Physical Effects of Moisture", RILEM/CIB Syposium on Moisture Problesms in Buildings, Helsinki, August16-19, 1965

4. Sneck, T., "General Report: Chemical Effects of Moisture", RILEM/CIB Symposium on Moisture Problems in Building, Helsinki, August 1965

5. Ritchie, T., "Efflorescence on Masonry', RILEM/CIB Syposium on Moisture Problems in Buildings, Rotterdam, 1974

6. Bonne, V., and A. Johnson, "Thermal Efficiency in Non-Modulating Combustion Systems", Conference on Improving Efficiency in HVAC Equipment and Compnonents in Residential and Small Commerical Buildings, Purdue University, October 1974

7. Bonne, V., J. E. Janssen and R.H. Torborg, "Efficiency and Relative Operating Cost of Central Combustion Heating Systems, IV. Oil-Fired Residential Systems", Presented at ASHRAE 1977 Semi-annaul Meeting, Cicago, Illinois, February 1977

8. Janssen, J. E. and V. Bonner, "Improvements of Seasonal Efficiency of Residential Heating Systems", ASME paper 76-WA/FV-7, Trans. of ASME., J. of Engr. For Power

9. Marsh, P., Thermal Insulation and Condensation, The Construction Press, London, 1979

10. Wilson, A. G., and G. K. Garden, "Moisture Accumulation in Walls due to Air Leakage", RILEM/CIB SYmposium on Moisture Problems in Buildings, Helsinki, 1965

11. Holst, P. H., and K. Aziz, "A Theoretical and Experimental Study of Natural Convection in Confined Porous Medium", The Canadian Journal of Chemical Engineering, Vol. 50, p. 232, April 1972

12. Chan, B. K. C., C. M. Ivey, and J. M. Barry, "Natural Convection in Enclosed Porous Media with Rectangular Boundaries", Trans. of ASME, J. of Heat Transfer, Vol. 92, p. 21, February 1970

13. Weber, J.E. "Convection in Porous Medium with Horizontal and Vertical Temperature Gradients", Int. J. Of Heat and Mass Transfer, Vol. 17, p. 241, 1974

14. Brailovskaya, V. A., G. B. Petrazhitsky, and V. I. Polezhaev, "The Effect of Convective Heat Exchange on Thermal Insulating Properties of Permeable Porous Interlayers", Energy Conservation in Heating Cooling, and Ventilating Buildings, Edts. J.C. Hoogendoorn, and N. H. Afgan, Hemisphere Publishing Corp., Washington, 1978

15. Burns, P. J., L. C. Chow and C. L. Tien, "Convection in Verical Slot Filler with Porous Insulation", Int. J. of Heat and Mass Transfer, Vol. 20, p. 919, 1977

16. Kelnhofer, W. J., "Air Infiltration in Buildings Due to Wind Pressures Including some Neighboring Body Effects", Heat Transfer in Energy Conservation, The Winter Annual Meeting of ASME, Atlanta, Nov.-Dec., 1977

17. Tamura, G. T., and A. G. Wilson, "Pressure Differences Caused by Chimney Effect on Three High Buildings", ASHRAE Trans., Vol. 73, Part II, 1967

18. Barrett, R. E. and D. E. Locklin, "Computer Analysis of Stack Effect in High-Rise Buildings", ASHRAE Trans., Vol. 74 Part II, 1968

19. Tamura, G. T., and A. G. Wilson, "Pressure Differences for a Nine-Story Building as a Result of Chimney Effect and Ventilation System Operation", ASHRAE Trans., Vol. 73, Part II, 1967

20. Tamura, G. T., and A. G. Wilson, "Pressure Differences Caused by Wind on Two Tall Buildings", ASHRAE Trans., Vol. 72, Part I

21. Shaw, C. Y., D. M. Sanders, and G. T. Tamura, "Air Leakage Measurements of the Exterior Walls of Tall Buildings", ASHRAE Trans., Vol. 79, Part II, 1973

22. Cermark, J. R., "Determination of Wind Loading on Structural Models in Wind Tunnel Simulated Winds", Proceedings of Symposium on Wind Effects on High Rise Buildings, Northwestern Unviersity, Evanston, Illinois, March 23, 1970

23. Leutheusse, H. J., "Static Wind Loading of Grouped Buildings", Proceedings of the Third International Conference on Wind Effects on Buildings and Structures, Tokyo, Japan, September,1971

24. Kelnhofer, W. J., "Stromungstechnische Utersuchung Uber den Einfluss eines parallel Stehenden Nachbargebaudes auf die Windebelastung eines Gebaudemadells mit Rechteckigen

Grundiss und Flachdach", Bericht Nr. 70/4a, 70/4b, 70/4c, Institut fur Stromungsmechanik, Technische Universitat, Munich, Germany, 1970

25. Ogniewicz, Y., C. L. Tien, "Analysis of Condensation in Porous Insulation", Int. J. of Heat and Mass Transfer, Vol. 24., p. 421, 1981

26. Luikov, A. V., Heat and Mass Transfer in Capillary Porous Bodies, Translated by P. W. B. Harrison, Pergamon Press, Oxford, 1966

27. Luikov, A. V., "Systyem of Differential Equations of Heat and Mass Transfer in Capillary Porous Bodies(Review)", Int. J. of Heat and Mass Transfer, Vol. 18, p. 1, 1975

28 Onsager, L., "Reciprocal Relations in Irreversible Processes", Part I, Phys. Rev., Vol. 37, p. 405, 1931; Part II, Phys. Rev., Vol. 38. p. 2265, 1931

29. Cary, J. W., and S. A. Taylor, "The Interaction of the Simultaneous Diffusion of Heat and Water Vapor", Soil Science Proceedings, p. 413, 1962

30. Cary, J. W., and S. A. Taylor, "Thermally Driven Liquid and Vapor Phase Transfer of Water and Energy in Soils", Soil Science Proceedings, p. 418, 1962

31. De Vries, D. A., "Simultaneous Transfer of Heat and Moisture in Porous Media", Trans. American Geophysical Union, Vol. 39, No. 5, p. 909, 1958

32. Phillip, J. R., and D. A. De Vries, "Moisture Movement in Porous Materials Under Temperature Gradients", Trans. American Geophysical Union, Vol. 38, No. 2, p. 222, 1957

33. Globus, A. M., and S. V. Nerpin, "Thermal Transfer of Moisture in Closed Systems of Aggregates and Granular Ceramics", RILEM/CIB Symposium on Moisture Problems in Building, Helsinki, 1965

34. Vol'fkovich, Y. U. M., et al, "The Physical nature of Mass Transfer Potential and the Potentiometric Curve of Capillary-Porous Media", Heat Transfer - Soviet Research, Vol. 9., No. 1, p. 29, 1977.

35. Huang, C. L. D. ,"Multi-phase moisture Transfer in Porous Media Subjected to Temperature Gradient", Int. J. Heat and Mass Transfer, Vol. 22, p. 1295., 1979

36. Gupta, J. P., and S. W. Churchill, "Moisture Transfer in Porous Medium Under a Temperature Gradient", Energy Conservation in Heating, Cooling, and Ventilating Buildings, edts. C. J. Hoogendoorn, and N. H. Afgan, Hemisphere

Publishing Corp, Washington, 1978

37. Austin, J. W., "Simultaneous Transport of Heat and Moisture Through a Medium Sand, Ph.D. Thesis, University of Wisconsin, August 1973

38. Miller, D. G., "Thermodynamics of Irreversible Processes: The Experimental Verification of the Onsager Reciprocal Relations", Chem. Rev., Vol. 60, p. 15, 1960

39. Edlefsen, N. E., and A. B. C. Anderson, "Thermodynamics of Soil Moisture", Hilgardia, Vol. 15, No. 2, Feb. 1943

40 Luikov, A. V. et al, "Theoretical Investigation of Vapor Transfer Through a Capillary-Porous Body", Int. J. of Heat and Mass Transfer, Vol. 17, p. 961, 1974

41. Romanovsky, S. G., K. D. Lukin, and L. I. Margolin, "The Method of Invariant Groups for Solving the Nonlinear Problem of Heat and Mass Transfer in Capillary-Porous Bodies", Heat Transfer - Soviet Research, Vol. 9, No. 1, 1977

42. McDonald, D. A., "On the Method of the Local Potential as Applied to the Solution of the Equations of Diffusion", Int. J. of Heat and Mass Transfer, Vol. 17, p. 393, 1974

43. Shaw, R. P., "An Integral Equation Approach to Diffusion", Int. J. of Heat and Mass Transfer, Vol. 17, p. 693, 1974

44. Shubin, G.S., "Analysis of Mass and Heat Transfer Accompanied by Movement of the Phase Transition Boundary", Heat Transfer - Soviet Research, Vol. 9, No. 7, 1977

45. Cho, S. H., "An Exact Solution of the Coupled Phase Change Problem in a Porous Medium", Int. J. Heat and Mass Transfer, Vol. 18, p. 1135, 1975

46. Sugiyama, S., et al., "Effects of surface Resistances on Simultaneous Heat and Mass Transfer in Porous Solids with Phase Change"

47. Ginzburg, A. S., "Heat and Mass Tranfer Involved in Phase Seperation (Drying) Upon Interaction of External and Internal Fields", Heat Transfer - Soviet Research, Vol. 9, No. 1, 1977

48. Auracher, W., "Water Vapor Diffusion and Frost in porous Materials", Heat Transmission Measurements in Thermal Insulations, ASTM, STP 544, Philadelphia, April 1973

49. Fagerlund, G., "Critical Moisture Contents at Freezing of Porous Materials", RILEM/CIB Symposium on Moisture Problems in Buildings, Rotterdam, 1974

50. Kudryavtsev, et al., "Moisture Transport and Formation of Segregation (Taber) Ice in Freezing and Thawing Particulate Soils", Heat Transfer - Soviet Research, Vol. 9, No. 1, 1977

51. Christensen, G., "Some Investigation on the Frost Resistance of Insulated Cavity Brick Walls", RILEM/CIB Symposium on Moisture Problems in Buildings, Helsinki, August, 1965

52. Enustun, B. V., H. S. Senturk, and K. Koksal, "Freezing-Melting Behavior of Capillary Water in Porous Materials", RILEM/CIB Symposium on Moisture Problems in Building, Helsinki, August, 1965

53. Bomberg, M. "Moisture Flow Through Porous Building Materials", Lund Institute of Technology, Lund, Sweden, Dec., 1973

54. Nilsson, L., "Hygroscopic Moisture in Concrete- Drying Measurements and Related Material Properties", Lund Institute of Technology, Lund, Sweden, Dec. 1980

55. Huang, C. L., H. H. Siang, and C. H. Best, "Heat and Moisture Transfer in Concrete Slabs", Int. J. of Heat and Mass Transfer, Vol. 22, p. 257, 1979

56. Cammerer, W. F., "The Capillary Motion of Moisture in Building Materials", RILEM/CIB Symposium on Moisture Problems in Buildings, Rotterdam, 1974

57. Bomberg, M., "Usage of Suction Concept in Calculation of Moisture Flow Through Porous Materials', RILEM/CIB Syposium on Moisture Problems in Buildings, Rotterdam, 1974

58. Van der Kooi, J., "Moisture Transport in Cellular Concret Roofs", RILEM/CIB Symposium on Moisture Problems in Buildings, Rotterdam, 1974

59. Van Brakel, J., and P. M. Heertjes, "Anomalies in Capillary Rise in Porous Media", RILEM/CIB Symposium on Moisture Problems in Buildings, Rotterdam, 1974

60. Mujumdar, A. S., edt., 1st International Symposium on Drying, McGill University, Hemishpere Publ. Corp., 1978

61 Mujumdar, A. S., edt., 2nd International Symposium on Drying, McGill University, Hemishpere Publ. Corp., 1980

62 Mujumdar, A. S., edt., Drying '82, McGill University, Hemishpere Publ. Corp., 1982

63. Edenholm, H., "Moisture Movement and Moisture Distribution in the Walls of Buildings", National Research Council of Canada, Technical Translation TT-361, 1952

64. Cold Storage Facilities: A Comprehensive Program For Research, Prepared by an Advisory Committe of the Building Advisory Board, division of Engineering and Industrial Research, National Academy of Science- Material research Council, Washington, D.C. Publication 1099, 1963

65. Bauer, W., "Influence of Holes on Water-vapor Permeability of Vapor- Checking Surface Layers", RILEM/CIB Symposium on Moisture Problems in Buildings, Helsinki, August 1965

66. Wilson, A. G., "Condensation in Insulated Masonry Walls in Summer", RILEM/CIB Symposium on Moisture Problems in Buildings, Helsinki, Aug. 1965

67. Permyakov, S. F., and I. A. Telegina, "The Main factors Governing the Moisture State of Building Construction", RILEM/CIB Symposium on Moisture Problems in Building, Helsinki, Aug. 1965

68. Vos, B. H., "Internal Condensation in Structures", Build Sci, Vol. 3, p. 191, 1969

69. Vos, B. H., "Condensation in Flat Roofs under Non Steady-State Conditions", Build Sci, Vol. 6, p. 7, 1971

70. Vos, B. H., and E. Tammes, "Condensation in Structures (General Aspects)", RILEM/CIB Symposium on Moisture Problems in Buildings, Rotterdam, 1974

71. Tammes, E., and B. H. Vos, "Hygric Aspects of Flat Timber Roofs", RILEM/CIB Sypmosium on Moisture Problems in Buildings, Rotterdam, 1974

72. Scheidegger, A. E., The Physics of Flow Through Porous Media, University of Toronto Press, 1974

73. Hildebrand, F. B., Introduction to Numerical Analysis, Ch. 10, McGraw Hill Book Co., 1974

74. Personal communication with the manufacturer

75. Sparrow, E. M., and A. L. Loeffler Jr., "Longitudinal Laminar flow Between Cylinders Arranged in Regular Array", A.I.Ch.E., Journal, Vol. 5, No. 3, p. 325, 1959

76. Happel, J., "Viscous Flow Relative to Arrays of Cylinders", A.I.Ch.E. Journal, Vol. 5, No. 2, p. 174, 1959

77. Washburn, E. W. "The Dynamics of Capillary Flow", Physical Review, Vol. XVIII, No. 3, p. 273, 1921

78. Kremnev, O. A., et al, "Flow Through Interconnected Capillaries", Fluid Mechanics-Soviet Research, Vol. 5, No. 1, p. 17, 1976

79. Bender, C. M. and S. A. Orzag, Advanced Mathematical Methods for Scientists and Engineers, Ch. 4, McGraw Hill Bokk Co., 1978

80. Paquet, J., "Application des Methodes Electriques a la Mesure de la Teneur en Eau des Materiaux", RILEM/CIB Symposium on Moisture Problems in Buildings, Helsinki, Aug. 1965

81. Cermak, H. "Moisture Determination in concrete Sands by Means of High-Speed Neutrons", RILEM/CIB Symposium on Moisture Problems in Buildings, Helsinki, Aug. 1965

82. Hartman, H., "Notes on Moisture Testing of Wall Structures Using Fast Neutrons", RILEM/CIB Symposium on Moisture Problems in Buildings, Helsinki, Aug. 1965

83. Kasi, S., and H. Koskinen, "Analysis, Calculations and Measurements Concerning the Moisture Measuring by the Neutron Method", RILEM/CIB Symposium on Moisture in Buildings, Helsinki, Aug. 1965

84. Watson, A., "Measurement of Moisture Content in some Structures and Materials by Microwave Absorption", RILEM/CIB Symposium on Moisture Problems in Buildings, Helsinki, Aug. 1965

85. Vos, B. H., "Measurement of Moisture Content in Building Structures in-Situ", RILEM/CIB Symposium on Moisture Problems in Buildings, Helsinki, Aug. 1965

86. ASHRAE Handbook of Fundamentals, 1978

APPENDIX A

LISTING OF COMPUTER PROGRAMS ADAM AND FRANC AND THE ASSOCIATED SUBROUTINES

```
CC*************************************************************************
C       SIMULTANEOUS HEAT AND MASS TRANSPORT WITH PHASE CHANGE IN A
C       COMPOSITE SLAB
C       SPATIALLY-STEADY SOLUTION
C*************************************************************************
        PROGRAM ADAM
        CHARACTER Z*70
        REAL LEWIS
        DIMENSION T(100),F(100),A(100,100),X(100),TR(100)
        1, CF(100),D1CR(100),D2CR(100),DTDX(100),D2TDX2(100),DTHDRT(100)
        2,CFR(100),ZL(100),ETA(100),ETAP(100),ARG(100),VAL(100),ZLL(100)
        3,DTHDFUR(100),U2(100),U1(100)
        COMMON/TRMPT/CND(20),VD(20),THCK(20),TL(20),CL(20),HL(20),
        1 CNDINS,VDINS,THCKINS,THO,TCO,HHO,HCO,CHO,CCO,ICNT,NLH,NLC,
        2 HXFRH,HXFRC,MXFRH,MXFRC,TO,T1
        COMMON/BN/ALANDA
        COMMON/BC/GAMA,BETA
        COMMON/BCF/TAU
C*************************************************************************
C       INPUT FROM THE INPUT.DAT FILE
C*************************************************************************
        OPEN(UNIT=2,NAME='INPUT.DAT',TYPE='OLD')
        OPEN(UNIT=60,NAME='ADAM.DAT',TYPE='NEW')
        OPEN(UNIT=70,NAME='LQCNT.DAT',TYPE='NEW')
        READ(2,*)Z,N
        READ(2,*)Z,NLH
        READ(2,*)Z,NLC
        READ(2,*)Z,THO
        READ(2,*)  Z,HHO
        READ(2,*)Z,HXFRH
        READ(2,*)Z,MXFRH
        READ(2,*)Z,TCO
        READ(2,*)Z,HCO
        READ(2,*)Z,HXFRC
        READ(2,*)Z,MXFRC
        READ(2,*)Z,THCKINS
        READ(2,*)Z,CNDINS
        READ(2,*)Z,CAPINS
        READ(2,*)Z,VDINS
        READ(2,*)Z,DNSTYINS
        READ(2,*)Z,VDFRCTN
        READ(2,*)Z
        DO 1 I=1,NLH
1       READ(2,*)J,CND(I),VD(I),THCK(I)
        READ(2,*)Z
        DO 2 I=NLH+1, NLH+NLC
2       READ(2,*)J,CND(I),VD(I),THCK(I)
        READ(2,*)Z,ERL
        READ(2,*)Z,ERLIMIT
        READ(2,*)Z,ERL3
        READ(2,*)Z,DNSTYRTO
        READ(2,*)Z,PE
        READ(2,*)Z,LEWIS
        CLOSE(UNIT=2)
C*************************************************************
C       DEFINING SOME TERMS
C*************************************************************
        THO=THO+459.6
        TCO=TCO+459.6
        ELTOTAL=THCKINS
```

```
        DXDZ=1./THCKINS
        DELX=1./(N-1)
        CALL CONC(THO-459.6,CHO)
        CHO=CHO*HHO
        CALL CONC(TCO-459.6,CCO)
        CCO=CCO*HCO
C*************************************************************************
C       USING THE CHARACTERISITICS OF THE WALLS AND INSIDE AND OUTSIDE
C       TEMPERATURE AND HUMIDITY,THE SUBROUTINE JERRICO CALCULATES THE
C       TMEPRATURE ON THE TWO SIDES OF THE INSULATION.
C*************************************************************************
        CALL JERRICO(EL0,EL1,THOT,HH,TCOLD,HC,CHS,CCS,CH,CC)
        ICNT=1
C***************************
C       DEFINING SOME TERMS:
C***************************
950     CONTINUE
        TYPE *,'ITERATING  TO GET THE RIGHT WALL TEMPS.'
        DELT=THOT-TCOLD
        DELC=CHS-CCS
        TREF=((THOT+TCOLD)/2.)
        BETA=DELT/TREF
        ETAH=(THOT-TREF)/DELT
        ETAC=(TCOLD-TREF)/DELT
        CALL CONC(TREF-459.6,CREF)
        GAMA=1070./(.1103*TREF)
        OMEGA=(CREF*1070.)/(CAPINS*DNSTYINS*TREF)
        ALANDA=((GAMA**2.)*2.*BETA*OMEGA)/(LEWIS+(OMEGA*GAMA))
C*********************************************************
C       Solving the boundary condition equations
C*************************8************************
        CALL MOSES(HH,UH,ET0)
        TYPE *,'TAU=',TAU
        CALL JONAS(HC,UC,ET1)
        TYPE *,'TAU=',TAU
        T0=ET0*DELT+TREF
        T1=ET1*DELT+TREF
C*************************************************************
C       Locating the boundaries of the condensing region
C*************************************************************
        DELTP=(ET0-ET1)*DELT
        TREFP=((ET0+ET1)*DELT/2.)+TREF
        BETAP=DELTP/TREFP
        GAMAP=1070./(.1103*TREFP)
        CALL CONC(TREFP-459.6,CREFP)
        OMEGAP=(CREFP*1070.)/(.0763*.24*TREFP)
        ETAHP=(ETAH*DELT+TREF-TREFP)/DELTP
        ETACP=(ETAC*DELT+TREF-TREFP)/DELTP
        ALANDAP=((GAMAP**2.)*2.*BETAP*OMEGAP)/(LEWIS+(OMEGAP*GAMAP))
        TERM=-0.5*((ALANDAP/(EXP(ALANDAP)-1.))+1.)
        TERM=(0.5-ETAHP)/TERM
        TRM=-0.5*(((ALANDAP*EXP(ALANDAP))/(EXP(ALANDAP)-1.))+1.)
        TRM=(ETACP+0.5)/TRM
        DXDZ=TERM+TRM+1.
        DZDX=1./DXDZ
        EL0=TERM*DZDX
        EL1=1.-(TRM*DZDX)
        TYPE *,'ET0=',ET0,'ET1=',ET1,'T0=',T0,'T1=',T1
        TYPE *, 'EL0=',EL0,'EL1=',EL1
        ER0=ABS(EL00-EL0)/EL0
```

```
      ER1=ABS(EL1O-EL1)/EL1
      IF(ERO.LT.ERL3.AND.ER1.LT.ERL3) GO TO 970
C*****************************************************************
C     Iterating in finding the two temps and c's on the cold and
C     hot sides using the values of EL0 and EL1
C*****************************************************************
      CALL JERRICO(EL0,EL1,THOT,HH,TCOLD,HC,CHS,CCS,CH,CC)
      EL0O=EL0
      EL1O=EL1
      GO TO 950
970   CONTINUE
      ICNT=2
      DO 500 I=1,N
      X(I)=(I-1.)/(N-1.)
      ZL(I)=EL0+DZDX*(I-1)/(N-1.)
      U2(I)=-0.5*((ALANDAP**2.)*(EXP(ALANDAP*X(I)))/(EXP(ALANDAP)-1.))
      U1(I)=-0.5*((U2(I)/((-0.5)*ALANDAP))+1.)
      TT=U2(I)+(GAMAP*BETAP*(U1(I)**2.))
      TERM=(EXP(ALANDAP*(X(I)))-1.)/(EXP(ALANDAP)-1.)
      ETAP(I)=0.5*(1-X(I)-TERM)
      ETA(I)=(ETAP(I)*DELTP+TREFP-TREF)/DELT
      T(I)=ETA(I)*DELT+TREF
      U3=EXP(GAMAP*BETAP*ETAP(I)/(1.+BETAP*ETAP(I)))
      U2(I)=U2(I)*BETAP*U3*GAMAP*DXDZ*DXDZ*CREFP
      U1(I)=(U1(I)*GAMAP*BETAP*DXDZ)**2.*U3*CREFP
      U=U1(I)+U2(I)
      DTHDRT(I)=U/(VDFRCTN*62.2)
      WRITE(70,*) X(I),DTHDRT(I)
500   IF(T(I).LT.491.6)DTHDRT(I)=DTHDRT(I)*DNSTYRTO
      NDIM=8
      WRITE(70,*) EL0,EL1
      DO 600 I=1,N
      ZLL(I)=(I-1)/(N-1.)
      IF(ZLL(I).LT.EL0.OR.ZLL(I).GT.EL1) GO TO 600
      CALL ATSM(ZLL(I),ZL,DTHDRT,N,1,ARG,VAL,NDIM)
      CALL ALI(ZLL(I),ARG,VAL,DTHDFUR(I),NDIM,ERL,IER)
600   WRITE(70,*)ZLL(I),DTHDFUR(I)
      Z0=ELTOTAL*EL0
      Z1=ELTOTAL*EL1
************************************************
C     OUTPUT:
C************************************************
      WRITE(60,601) THO,HHO,CHO,TCO,HCO,CCO,TREF,DELT
      WRITE(60,602) N,DELX,DZDX
      WRITE(60,603) PE,LEWIS,BETA, GAMA,OMEGA,ALANDA
      WRITE(60,607) TREFP,DELTP,BETAP,GAMAP,OMEGAP,ALANDAP
      WRITE(60,604) Z0,Z1
      WRITE(60,609) T0,T1
      CALL JERRICO(EL0,EL1,THOT,HH,TCOLD,HC,CHS,CCS,CH,CC)
      WRITE(60,605)
      DO 690 I=1,NLC+NLH+2
690   WRITE(60,606) I,TL(I),CL(I),HL(I)
      WRITE(60,610)
      DO 2000 I=1,N
      WRITE(60,620)
      CALL CONC(T(I)-459.6,CF(I))
      CFR(I)=(CF(I)-CCS)/DELC
      WRITE(60,613) X(I),ETA(I),CF(I)
      WRITE(60,613) ZL(I),T(I),DTHDRT(I)
2000  CONTINUE
```

```
601     FORMAT(3X,'TEMP. ON HOT SIDE=',2X,E10.4,3X,'HUMIDITY ON HOT SIDE=',
        1 2X,E10.4,/,2X,'VAPOR CONC. ON HOT SIDE=',2X,E10.4,/,3X,'TEMP. ON COLD
        2 SIDE=',2X,E10.4,3X,'HUMIDITY ON COLD SIDE=',2X,E10.4,/,2X,'VAPOR
        3 CONC. ON COLD SIDE=',2X,E10.4,/,3X,'TREF=',2X,E10.4,2X,'DELT='2X
        4 ,E10.4)
602     FORMAT(3X,'NUMBER OF NODES=',3X,I5,2X,'DELTA X=',2X,E10.4,2X,'DZDX=',2X
        1,E10.4)
603     FORMAT(/,2X,'PE=',E10.4,2X,'LEWIS=',E10.4,/,2X,'BETA=',E10.4
        1,2X,'GAMA=',E10.4,2X,'OMEGA=',E10.4,2X,'LANDA=',2X,E10.4)
604     FORMAT(3X,'Z0 =',2X,E10.4,3X'Z1 =',2X,E10.4)
605     FORMAT(3X,'LAYER #',5X,'TEMP.',6X,'CONC.',6X,'HUMIDITY')
606     FORMAT(3X,I4,5X,E10.4,2X,E10.4,2X,E10.4)
607     FORMAT(3X,'TREFP=',2X,E10.4,3X,'DELTP=',2X,E10.4,3X,'BETAP=',2X,
        1 E10.4,/,3X,'GAMAP=',E10.4,2X,'OMEGAP=',E10.4,2X,'LANDAP=',E10.4)
609     FORMAT(3X,'T0=',E10.4,3X,'T1=',E10.4)
610     FORMAT(3X,'LOCATION',3X,'ETA',13X,'SAT. CON.',/,3X,'LOCATION',
        1 3X,'ACTUAL TEMP.',3X,'DTHDRT')
613     FORMAT(2X,3(E10.4,2X))
620     FORMAT(1X,'************************************************')
675     FORMAT(3X,'N O  C O N D E N S A T I O N')
        GO TO 976
975     TYPE *,'CONDENSATION DOES NOT TAKE PLACE'
        WRITE(60,675)
976     CONTINUE
        CLOSE(UNIT=60)
        CLOSE(UNIT=70)
        STOP
        END
```

There is no text material missing here.
Pages have been incorrectly numbered.

p. 367

```
      SUBROUTINE MOSES(H,U,ETA)
      COMMON/BCF/TAU
      COMMON/BC/GAMA,BETA
      TAU=1.
      TAUO=0.
1     CONTINUE
      ERL=.0005
      U3=0.
10    U3=U3+.05
      R=FU(U3,H)/FU(0.,H)
      IF(R.GT.0.) GO TO 10
      IF(R.EQ.0.) GO TO 100
      U1=U3-0.05
      U2=U3
11    U3=U2-((U2-U1)/(FU(U2,H)-FU(U1,H)))*FU(U2,H)
      IF(ABS(FU(U3,H)).LT.ERL) GO TO 100
      IF(R)20,100,30
20    U1=U3
      GO TO 11
30    U2=U3
      GO TO 11
100   U=U3
      ETA=.5-(U/(GAMA*BETA))
      TAU=.5*BETA*(.5+ETA)+1.
      TAU=1./TAU
      ER=ABS(TAU-TAUO)/TAU
      TAUO=TAU
      IF(ER.GT..01) GO TO 1
      RETURN
      END
```

```
      SUBROUTINE JONAS(H,U,ETA)
      COMMON/BCF/TAU
      COMMON/BC/GAMA,BETA
      TAU=1.
      TAUO=0.
1     ERL=.0005
      U3=0.
10    U3=U3-.05
      R=FU(U3,H)/FU(0.,H)
      IF(R.GT.0.) GO TO 10
      IF(R.EQ.0.) GO TO 100
      U1=U3+0.05
      U2=U3
11    U3=U2-((U2-U1)/(FU(U2,H)-FU(U1,H)))*FU(U2,H)
      IF(ABS(FU(U3,H)).LT.ERL) GO TO 100
      IF(R)20,100,30
20    U1=U3
      GO TO 11
30    U2=U3
      GO TO 11
100   U=U3
      ETA=-0.5-(U/(GAMA*BETA))
      TAU=0.5*BETA*(-0.5+ETA)+1.
      TAU=1./TAU
      ER=ABS(TAUO-TAU)/TAU
      TAUO=TAU
      IF(ER.GT..01) GO TO 1
      RETURN
      END
```

```
FUNCTION FU(U,H)
COMMON/BCF/TAU
FU=1.-H*EXP(U*TAU)+U
RETURN
END
```

```
FUNCTION BEN(X,ETA)
COMMON/BN/ALANDA
T=(EXP(ALANDA*X)-1.)/(EXP(ALANDA)-1.)
T=(-T-X+1.)*.5
BEN=ETA-T
RETURN
END
```

```
C*********************************************************************
C       SIMULTANEOUS HEAT AND MASS TRANSPORT WITH PHASE CHANGE IN A
C       COMPOSITE SLAB
C       SPATIALLY UNSTEADY SOLUTION
C       DATA INPUT FILE: UINPUT.DAT;
C       THIS PROGRAM CALCULATES THE MOVEMENT OF THE BOUNDARIES OF THE
C       WET REGIION  IN A COMPOSITE WALL
C*********************************************************************

        PROGRAM FRANCE
        CHARACTER ZZ*70
        REAL LEWIS
        DIMENSION ETAX(11),ETAY(11),THIN(11),ANX(11),Y(11),Z(11),
        1 DTHDRTX(11),DTHDRTY(11),THETA(11),THETAY(11),ARG(11),VAL(11),
        2 DTHDFUR(11)
        COMMON/WZFN/LEWIS,EL0,EL1,TH,TC,HH,HC,S
        COMMON/T/TR0,TR1
        COMMON/PS/TRS
        COMMON/TRMPT/CND(20),VD(20),THCK(20),TL(20),CL(20),HL(20),
        1 CNDINS,VDINS,THCKINS,THO,TCO,HHO,HCO,CHO,CCO,ICNT,NLH,NLC,
        2 HXFRH,HXFRC,MXFRH,MXFRC,T0,T1
C*********************************************************************
C       DATA INPUT, THIN =  INITIAL LIQUID-CONTENT (THETA):
C*********************************************************************
        OPEN(UNIT=2,NAME='UINPUT.DAT',TYPE='OLD')
        OPEN(UNIT=11,NAME='USA.DAT',TYPE='NEW')
        OPEN(UNIT=70,NAME='LQCNT.DAT',TYPE='OLD')
        READ(2,*)ZZ,N
        WRITE(11,*)'TOTAL NUMBER OF NODES IN THE CONDENSING REGION',N
        READ(2,*)ZZ,NLH
        WRITE(11,*)'NUMBER OF WALL LAYERS ON THE HOT SIDE',NLH
        READ(2,*)ZZ,NLC
        WRITE(11,*)'NUMBER OF WALL LAYERS ON THE COLD SIDE',NLC
        READ(2,*)ZZ,THO
        WRITE(11,*)'HOT SIDE TEMPERATURE',THO
        READ(2,*)ZZ,HHO
        WRITE(11,*)'HOT SIDE HUMIDITY',HHO
        READ(2,*)ZZ,HXFRH
        WRITE(11,*)ZZ,HXFRH
        READ(2,*)ZZ,MXFRH
        WRITE(11,*)ZZ,MXFRH
        READ(2,*)ZZ,TCO
        WRITE(11,*)ZZ,TCO
        READ(2,*)ZZ,HCO
        WRITE(11,*)ZZ,HCO
        READ(2,*)ZZ,HXFRC
        WRITE(11,*)ZZ,HXFRC
        READ(2,*)ZZ,MXFRC
        WRITE(11,*)ZZ,MXFRC
        READ(2,*)ZZ,THCKINS
        WRITE(11,*)ZZ,THCKINS
        READ(2,*)ZZ,CNDINS
        WRITE(11,*)ZZ,CNDINS
        READ(2,*)ZZ,CAPINS
        WRITE(11,*)ZZ,CAPINS
        READ(2,*)ZZ,VDINS
        WRITE(11,*)ZZ,VDINS
        READ(2,*)ZZ,DNSTYINS
        WRITE(11,*)ZZ,DNSTYINS
        READ(2,*)ZZ,VDFRCTN
```

```
      WRITE(11,*)ZZ,VDFRCTN
      READ(2,*)ZZ
      WRITE(11,*)ZZ
      DO 1 I=1,NLH
      READ(2,*)J,CND(I),VD(I),THCK(I)
1     WRITE(11,*)J,CND(I),VD(I),THCK(I)
      READ(2,*)ZZ
      WRITE(11,*)ZZ
      DO 2 I=NLH+1,NLH+NLC
      READ(2,*)J,CND(I),VD(I),THCK(I)
2     WRITE(11,*)J,CND(I),VD(I),THCK(I)
      READ(2,*)ZZ,ERL
      WRITE(11,*)ZZ,ERL
      READ(2,*)ZZ,ERLIMIT
      WRITE(11,*)ZZ,ERLIMIT
      READ(2,*)ZZ,ERL3
      WRITE(11,*)ZZ,ERL3
      READ(2,*)ZZ,DNSTYRTO
      WRITE(11,*)ZZ,DNSTYRTO
      READ(2,*),ZZ,PE
      WRITE(11,*)ZZ,PE
      READ(2,*)ZZ,LEWIS
      WRITE(11,*)ZZ,LEWIS
      READ(2,*)ZZ,DELTME
      WRITE(11,*)ZZ,DELTIME
      READ(2,*)ZZ,PERIOD1
      WRITE(11,*)ZZ,PERIOD1
      READ(2,*)ZZ,TIMELIMT
      WRITE(11,*)ZZ,TIMELIMIT
      CLOSE(UNIT=2)
      READ(70,*) EL0,EL1
      THO=THO+459.6
      TCO=TCO+459.6
      S=EL0-EL1
      NDIM=8
      TIME=0.0
      PERIOD1=PERIOD1*VDINS
C*********************************************************************
C     CONVERTING THE INPUT DTHETADT TO LIQUID-CONTENT
C*********************************************************************
      WRITE(11,904)
      DZ=Z(2)-Z(1)
      DO 21 I=1,11
      READ(70,*)Z(I),DTHDFUR(I)
      THETA(I)=DTHDFUR(I)*PERIOD1
      THINTL=THINTL+THETA(I)*DZ
      WRITE(11,905) Z(I),THETA(I)
21    CONTINUE
      WRITE(11,906)THINTL
      CLOSE(UNIT=70)
      CALL CONC(THO-459.6,CHO)
      CALL CONC(TCO-459.6,CCO)
      CHO=CHO*HHO
      CCO=CCO*HCO
      CALL JERRICO(EL0,EL1,TH,HH,TC,HC,CHS,CCS,CH,CC)
      DTS=(TH-TC)*(EL1-EL0)
      TRS=(TH+TC)/2.

C*********************************************************************
C     CALCULATING THE TEMPERATURE OF THE TWO SIDES OF THE INSULATION
```

```
C*****************************************************************
7       CONTINUE
        CALL JERRICO(EL0,EL1,TH,HH,TC,HC,CHS,CCS,CH,CC) -
        ICNT=1
C*****************************************************************
C       CALCULATING THE VALUES OF DT AND TR FOR THE GIVEN EL0 AND EL1
C*****************************************************************

        CALL FINDZ(DTS,1.,.01,DT,FZERO)

C*****************************************************************
C       CALCULATING THE RELEVANT PARAMETERS
C*****************************************************************
        TR=(TR0+TR1)/2.
        BETA=DT/TR
        T0=-0.5*DT+TR
        T1=0.5*DT+TR
        GAMA=1070./(.1103*TR)
        RT=TR-459.6
        CALL CONC(RT,CR)
        OMEGAP=(1070.*CR)/(.0763*.24*TR)
        OMLE=OMEGAP/LEWIS
        ALANDA=(2.*(GAMA**2.)*BETA*OMEGAP)/(LEWIS+(OMEGAP*GAMA))
        DELTIME=DELTME*VDINS*CR/(62.2*VDFRCTN*THCKINS*THCKINS)
        TIMELIMIT=TIMELIMT*VDINS*CR/(62.2*VDFRCTN*THCKINS*THCKINS)
        TYPE *,DT,TR0,TR1,FZERO,EL0,EL1
        WRITE(11,17)
        WRITE(11,11) TIME
        WRITE(11,12) S,TIME1
        WRITE(11,13) TR,CR,DT
        WRITE(11,20) GAMA,OMEGAP,ALANDA
C*****************************************************************
C       GENERATING THE ETA AND LIQUID CONTENT DISTRIBUTIOON IN THE
C       CONDENSING REGION
C*****************************************************************
        DELX=1/10.
        DO 90 I=1,11
        ANX(I)=DELX*(I-1)
        ETAX(I)=.5-(ANX(I)/2.)-.5*((EXP(ALANDA*ANX(I))-1.)/(EXP(ALANDA)-1.))
        TERM=(ALANDA*EXP(ALANDA*ANX(I)))/(EXP(ALANDA)-1.)
        DETDX=-.5*(TERM+1.)
        DETDX2=DETDX**2.
        D2ETDX2=-.5*(ALANDA*ALANDA*EXP(ALANDA*ANX(I)))/(EXP(ALANDA)-1.)
        TERM=DETDX2*GAMA*BETA
        TERM=TERM+D2ETDX2
        TERM1=EXP((GAMA*BETA*ETAX(I))/(1.+(BETA*ETAX(I))))
        TERM1=DETDX2*GAMA*BETA
        DTHDRTX(I)=TERM1*TERM*S*S
90      CONTINUE
        WRITE(13,17)
        WRITE(13,11)
C*****************************************************************
C       CHANGINNG THE AXIS AND REDEFINING THE LQIUID CONTENT AND
C       ETA VALUES
C*****************************************************************
        DO 95 J=1,11
        I=12-J
        Y(J)=EL0+(ANX(J))*(EL1-EL0)
        ETAY(J)=ETAX(I)
        DTHDRTY(J)=DTHDRTX(I)
```

```
        CALL ATSM(Y(J),Z,THETA,11,1,ARG,VAL,NDIM)
        CALL ALI(Y(J),ARG,VAL,THETAY(J),8,.0001,IER)
        THETA(J)=THETAY(J)+(DELTIME*DTHDRTY(J))
        Z(J)=Y(J)
        WRITE(13,*) J, Y(J),ETAY(J),THETAY(J),DTHDRTY(J)
95      CONTINUE
C*****************************************************************************
C       CALCULATING THE RATE OF MOVEMENT OF THE BOUNDARIES
C*****************************************************************************
C       EL1:

        ETAH=(TH-TR)/DT
        TERMH=(GAMA*BETA*ETAH)/(1.+(BETA*ETAH))
        TERM=(GAMA*BETA)/(2+BETA)
        TOP=EXP(TERM)-HH*EXP(TERMH)+(BETA*GAMA*EXP(TERM)*(ETAH-.5))
        BOT=1.+(OMLE*EXP(TERM)*GAMA)
        A1=2*TOP/BOT
        A1=A1/THETA(11)

C       EL0:

        ETAC=(TC-TR)/DT
        TERMC=(GAMA*BETA*ETAC)/(1.+(BETA*ETAC))
        TERM=(GAMA*BETA)/(BETA-2.)
        TOP=EXP(TERM)-HC*EXP(TERMC)-(BETA*GAMA*EXP(TERM)*(-.5-ETAC))
        BOT=1.+(OMLE*GAMA*EXP(TERM))
        A0=2*TOP/BOT
        A0=A0/THETA(1)
        WRITE(11,909) ETAH,ETAC,THETA(1),THETA(11)
        WRITE(11,3)A0,A1
C*****************************************************************************
C       GENERATING THE NEW EL0 AND EL1
C*****************************************************************************
        EL0=((EL0**2.)+(A0*DELTIME))**.5
        EL1=1-((1-EL1)**2.+(A1*DELTIME))**.5
        WRITE(11,4) EL0, EL1
        TIME1=TIME1+(DELTIME*62.2*VDFRCTN/CR)
        TIME=TIME+DELTIME
        IF(EL0.GE.EL1) GO TO 1000
        IF(TIME. GE. TIMELIMIT) GO TO 1000
        DTS=DT
        TRS=TR
        S=EL0-EL1
        GO TO 7
1000    CLOSE(UNIT=11)
        STOP
17      FORMAT(/,'*************************************************************')
11      FORMAT(10X,'T I M E =', 2X,E10.4)
12      FORMAT(3X,'SCALE FACTOR=',E10.4,2X,'TIME1=',E10.4)
13      FORMAT(3X,'TR=',E10.4,2X,'CR=',E10.4,2X,'DT=',E10.4)
20      FORMAT(3X,'GAMAP=',E10.4,2X,'OMEGAP=',E10.4,2X,'ALANDAP=',E10.4)
904     FORMAT(/,10X,' I N I T I A L  LIQUID-CONTENT DISTRIBUTION',/,
        1 4X,'POSITION',15X,'LIQUID-CONTENT')
905     FORMAT(3X,E10.4,6X,E10.4)
906     FORMAT(3X,'INITIAL TOTAL LIQUID CONTENT=',2X,E10.4)
909     FORMAT(3X,'ETA HOT=',E10.4,2X,'ETA COLD=',E10.4,/,3X,'THETA AT EL0=',
        1 E10.4,2X,'THETA AT EL1=',E10.4)
3       FORMAT(3X,'A0=',2X,E10.4,'A1=',2X,E10.4)
4       FORMAT(3X,'EL0=',2X,E10.4,'EL1=',2X,E10.4)
        END
```

```
'*****************************************************
NUMBER OF NODES, N='                                    11
'NUMBER OF LAYERS IN THE WALL ON THE HOT SIDE='          0
'NUMBER OF LAYERS IN THE WALL ON THE COLD SIDE='         0
'
AMBIENT CONDITIONS:

 TEMPERATURE ON THE HOT SIDE(DEG.F)='                   69.1
'REALTIVE HUMIDITY ON THE HOT SIDE='                     .371
'HEAT TRANSFER COEFFICENT ON THE HOT SIDE='            60000000.
'MASS TRANSFER COEFFICIENT ON THE HTO SIDE='           365000000.
'


 TEMPERATURE ON THE COLD SIDE(DEG. F)='                 -19.8
'RELATIVE HUMIDITY ON THE COLD SIDE='                   .9999999
'HEAT TRANSFER COEFFICIENT ON THE COLD SIDE='          14700000.
'MASS TRANSFER COEFFICIENT ON THE COLD SIDE='          8900000.
'
 I N S U L A T I O N   P R O P E R T I E S :

THICKNES(FT)='                                          .5
'THERMAL CONDUCTIVITY='                                 .014
'THERMAL CAPACITANCE='                                  .24
'VAPOR DIFFUSIVITY='                                    .85
'MASS DENSITY='                                        .0763
'VOID FRACTION='                                        .99
'
PROPERTIES OF THE WALL LAYERS:

HOT SIDE:
# OF LAYERS            CNDCTVTY       V.DFFSVTY       THCKNSS'
'
COLD SIDE:
#OF LAYERS             CNDCTVTY       V.DFFSVTY       THCKNSS'
'
E R R O R   L I M I T S:
        ERRORLIMIT IN GETTING LO&L1='      .00001
        'ERRORLIMIT FOR CONVERGENCE='       .00001
        'ERL3='                            .01
'MISC:
        DENSITY RATIO OF ICE/WATER='        .9
        'PECLET NUMBER='                   0.
        'LEWIS NUMBER='                    1.
```